Design optimisation and experimental evaluation of a grain vibration screen

J Bloem

22113657

Dissertation submitted in fulfilment of the requirements for the degree *Magister* in Mechanical Engineering at the Potchefstroom Campus of the North-West University

Supervisor: Dr CB Nel

May 2016

Abstract

Mechanical screening is an important process which is used in a wide range of industries. This study focused on screens in the agricultural industry used for cleaning and classifying of grain.

Mathematical models were developed and also implemented in computer programs used for design analysis of a vibration screen. This was regarded as necessary to investigate effective screening of maize in order to remove unwanted larger and smaller particles, and also to provide acceptable service life from a fatigue point of view. A three degree of freedom mathematical model was developed and used for prediction of static and dynamic displacements, static and dynamic forces, and also system natural frequencies. Another mathematical model was formulated and implemented in a computer program and used for fatigue analysis.

All the input parameters required for the computer programs were characterised. Different mathematical models were also developed for characterisation of the screen rubber mount vertical and also horizontal stiffness and damping coefficients. Different measured data obtained from different test set-ups were used as input data for these programs respectively. Mount static stiffness coefficients were also experimentally determined. The required amplitude and frequency for a certain layer of maize was also characterised with electrodynamic Shaker tests, and two different feasible sieve apertures identified.

Three different design goals for an optimisation approach were identified. Firstly, the criteria for vibration isolation an objective function based on the transmission of dynamic forces to the fixed foundation was formulated. Secondly, two different constraints that also influenced vibration isolation were also formulated. These constraints were regarded as necessary to ensure enough movement for effective sieving, but also to limit the horizontal and vertical mount displacements during transient conditions. Three-dimensional graphical representations and contour plots were constructed in a Matlab environment, and used to determine vertical and horizontal mount stiffness coefficients chosen as design variables, for an optimum design according to the criteria formulated.

A Finite Element Analysis (FEA) approach was followed to investigate possible structural resonance of the elastic screen, and also to evaluate the structure's vertical stiffness coefficient at the point of investigation. An FEA approach was also used to determine static and dynamic material stresses used for fatigue analysis to investigate the screen structure service life.

The optimised design parameters were used to build and then test the vibration screen. Effective sieving was evaluated to remove the larger and smaller unwanted particles such as weed seeds, sand, small broken maize kernels, stalks, and maize plant stems as typically present, from harvested maize. Sufficient maize mass flow rates were also evaluated for different screen angles, and with two different sieves simultaneously used. The underlying three degree of freedom mathematical model for the vibration screen was experimentally validated. The predicted responses, dynamic forces, and also the system natural frequencies were compared to the corresponding measured values respectively. This was done for several operational conditions (transient and steady state), at an empty and fully loaded screen respectively. Transient conditions include start-up and shut-down of the screen.

The grain vibration screen was designed to mainly sieve maize, but other grain such as sunflower, soybean, canola, groundnuts, wheat, barley, oats and sorghum could also be sieved.

Keywords: Optimisation, objective function, constraints, grain vibration screen, sieving, flow rate, fatigue, service life, vibration isolation, Finite Element Analysis, resonance, evaluation, response, dynamic forces.

Samevatting

Meganiese sifting is 'n belangrike proses wat gebruik word in 'n wye verskeidenheid nywerhede. Hierdie studie fokus op siwwe wat gebruik word in die landboubedryf vir die skoonmaak en klassifisering van graan.

Wiskundige modelle is ontwikkel en ook geïmplementeer in rekenaarprogramme wat gebruik is vir die ontwerpanalise van ‘n vibrasiesif. Dit was nodig geag om effektiewe sifting van mielies te ondersoek om sodoende ongewenste groter en kleiner deeltjies te verwyder, en ook om aanvaarbare dienslewe te voorsien vanuit 'n vermoeidheidoogpunt. 'n Drievryheidgraad wiskundige model is ontwikkel en gebruik vir die voorspelling van statiese en dinamiese verplasings, statiese en dinamiese kragte, en ook die sisteem natuurlike frekwensies. Nog ‘n wiskundige model is geformuleer en in 'n rekenaarprogram geïmplementeer wat gebruik is vir vermoeidheidsanalise.

Al die insetparameters wat nodig is vir die rekenaarprogramme is gekarakteriseer. Verskillende wiskundige modelle is ook ontwikkel vir die karakterisering van die vibrasiesif se rubber monteerstukke se vertikale en ook horisontale styfheid en demping koëffisiënte. Verskillende gemete data verkry uit verskillende toetsopstellings is gebruik as insetdata vir hierdie programme onderskeidelik. Monteerstuk statiese styfheidkoëffisiënte is ook eksperimenteel bepaal. Die vereiste amplitude en frekwensie vir 'n sekere laag mielies is ook gekarakteriseer met elektrodinamiese skudapparaattoetse en twee verskillende geskikte sifopeninge is geïdentifiseer.

Drie verskillende ontwerpdoelwitte vir 'n optimeringsbenadering is geïdentifiseer. Eerstens, as kriteria vir vibrasie isolasie is ‘n doelfunksie gebaseer op die oordrag van dinamiese kragte na die vaste fondasie geformuleer. Tweedens, was twee verskillende beperkings wat vibrasie isolasie beïnvloed ook geformuleer. Hierdie beperkings was nodig geag om genoegsame beweging vir effektiewe sifting te verseker, maar ook om die horisontale en vertikale monteerstukverplasings te beperk tydens oorgangsgedrag. Driedimensionele grafiese voorstellings en kontoergrafieke is in 'n Matlab omgewing gekonstrueer, en is gebruik om vertikale en horisontale

monteerstukstyfheidkoëffisiënte wat as ontwerpveranderlikes gekies is te bepaal, vir ‘n optimum ontwerp volgens die geformuleerde kriteria.

'n Eindige Element Analise (EEA) benadering is gevolg om moontlike strukturele resonansie van die elastiese vibrasie sif te ondersoek, en ook om die strukturele styfheid van die vibrasiesif by die punt van ondersoek te evalueer. ‘n EEA benadering is ook gebruik om statiese en dinamiese materiaalspannings te bepaal wat gebruik is vir vermoeidheidsanalise om die dienslewe van die vibrasiesif te ondersoek.

Die geoptimeerde ontwerpparameters is gebruik om ‘n vibrasiesif te bou en dan te toets. Effektiewe sifting is geëvalueer om die groter en kleiner ongewenste deeltjies soos onkruidsade, sand, klein gebreekte mieliepitte, stronke, en mielieplantstamme soos tipies teenwoordig is by gestroopte mielies te verwyder. Voldoende mieliemassa vloeitempo is ook geëvalueer deur verskillende vibrasiesifhoeke te verstel, en met twee verskillende siwwe wat gelyktydig gebruik is. Die onderliggende drievryheidsgraad wiskundige model vir die vibrasiesif is eksperimenteel gevalideer. Die voorspelde respons, dinamiese kragte, en ook die stelsel natuurlike frekwensies is vergelyk met die ooreenstemmende gemete waardes onderskeidelik. Dit is gedoen vir verskeie operasionele toestande (oorgangsgedrag en bestendige toestand), vir 'n leë en volgelaaide vibrasiesif onderskeidelik. Oorgangsgedragtoestande sluit in aansit en afsit van die vibrasiesif.

Die graanvibrasiesif is ontwerp om hoofsaaklik mielies te sif, maar ander graan soos sonneblom, sojabone, canola, grondboontjies, koring, gars, hawer en sorghum kan ook gesif word.

Sleutelwoorde: Optimering, doelfunksie, beperkings, graanvibrasiesif, sifting, vloeitempo, vermoeidheid, dienslewe, vibrasie isolasie, Eindige Element Analise, resonansie, evaluering, respons, dinamiese kragte.

Declaration

I, Johann Bloem, hereby declare that the material used in this study is my own original work, except where specifically referred to by name, or in the form of a reference. This work has not been submitted to any other university.

Johann Bloem
Student number: 22113657
Identity number: 9106055027086

Acknowledgements

- God Almighty for everything.
- My father Albie and mother Karen for their support.
- Dr Carl Nel for all his advice, guidance and support during this study.
- Mr Bartlo and Mr André for the manufacturing of parts.
- Mr Sarel Naudé for the use of the laboratory.
- Mr Willem van Tonder and Mr Thabo Diobe for their help in the laboratory.
- Mr Stephan Grobler and Mr Lourens Pretorius for their help.
- Mr Terence Kent and Mr Cleo Enslin for their help in the laboratory
- Prof Annette Combrink for the language-editing of this dissertation.
- Family and friends for their support.

Table of contents

List of tables

List of figures

Nomenclature

Capital letters

A	Excitation amplitude	m
F_{01}	Static vertical reaction force at Mount 1	N
F_{02}	Static vertical reaction force at Mount 2	N
F_e	Dynamic force of exciter motors	N
F_{ex}	Dynamic force of exciter motors x direction force component	N
F_{ez}	Dynamic force of exciter motors z direction force component	N
J_{yy}	Effective Mass Moment of Inertia of vibration screen	kgm^2
K	Stiffness matrix	$-$
M	Mass matrix	$-$
M_{ey}	Dynamic moment caused by exciter motors	Nm
M_u	Equivalent unbalance product of exciter motors	kgm
S_e	Modified material endurance limit	MPa
S_e'	Material endurance limit	MPa
S_{ut}	Material ultimate tensile strength	MPa
W	Effective weight of vibration screen	N
ΔU_c	Maximum allowable dynamic displacement amplitude matrix	m
ΔU_d	Dynamic displacement amplitude matrix	m
ΔU_s	Static displacement matrix	m
$\Delta \overline{U}$	Vertical and horizontal displacement amplitude vector	m
ΔX	Dynamic horizontal displacement amplitude of center of mass	m

ΔX_1	Dynamic horizontal displacement amplitude at Mount 1	m
ΔX_2	Dynamic horizontal displacement amplitude at Mount 2	m
ΔZ	Dynamic vertical displacement amplitude of center of mass	m
ΔZ_{01}	Static vertical displacement at Mount 1	m
ΔZ_{02}	Static vertical displacement at Mount 2	m
ΔZ_1	Dynamic vertical displacement amplitude at Mount 1	m
ΔZ_2	Dynamic vertical displacement amplitude at Mount 2	m
ΔZ_c	Minimum allowable dynamic displacement amplitude	m
ΔZ_{s1}	Displacement amplitude of moving mass on electrodynamic Shaker	m
ΔZ_{s2}	Displacement amplitude of base of electrodynamic Shaker	m

Lower-case letters

a	Factor used in fatigue analysis	MPa
b	Exponent used in fatigue analysis	$-$
$c_{c_{sz}}$	Critical viscous damping coefficient used for characterisation	Ns/m
c_{sz}	Viscous damping coefficient used for characterisation	Ns/m
c_{x1}	Equivalent horizontal damping coefficient of Mount 1	Ns/m
c_{x2}	Equivalent horizontal damping coefficient of Mount 2	Ns/m
c_{z1}	Equivalent vertical damping coefficient of Mount 1	Ns/m
c_{z2}	Equivalent vertical damping coefficient of Mount 2	Ns/m
d	Equivalent diameter used for fatigue analysis	mm
f_n	Natural frequency	Hz

f_{sn}	Natural frequency used for characterisation	Hz
g	Gravitational acceleration	m/s^2
k_a	Surface factor used for fatigue analysis	$-$
k_b	Size factor used for fatigue analysis	$-$
k_c	Loading factor used for fatigue analysis	$-$
k_d	Temperature factor used for fatigue analysis	$-$
k_e	Reliability factor used for fatigue analysis	$-$
k_f	Miscellaneous effects factor used in fatigue analysis	$-$
k_{sz}	Dynamic stiffness coefficient used for characterisation	N/m
k_{x1}	Equivalent horizontal stiffness coefficient of Mount 1	N/m
k_{x2}	Equivalent horizontal stiffness coefficient of Mount 2	N/m
k_{z1}	Equivalent vertical stiffness coefficient of Mount 1	N/m
k_{z2}	Equivalent vertical stiffness coefficient of Mount 2	N/m
m	Effective mass of vibration screen	kg
m_e	Equivalent mass used for characterization	kg
n_{sf}	Safety factor against fatigue failure	$-$
r_u	Unbalance radius of exciter motors	m
t	Time	s
Δx	Horizontal displacement of centre of mass	m
Δx_1	Dynamic horizontal displacement at Mount 1	m
Δx_2	Dynamic horizontal displacement at Mount 2	m
x_1	x coordinate of Mount 1	m
x_2	x coordinate of Mount 2	m
x_3	x coordinate of exciter motors	m

$\Delta\ddot{x}_{g1}$	Acceleration at centre of mass used for characterisation.	m/s^2
$\Delta\ddot{x}_{g2}$	Acceleration at centre of mass used for characterisation.	m/s^2
Δz	Vertical displacement of centre of mass	m
Δz_1	Dynamic vertical displacement at Mount 1	m
Δz_2	Dynamic vertical displacement at Mount 2	m
Δz_{s1}	Acceleration of moving mass	m/s^2
Δz_{s2}	Acceleration of Shaker base	m/s^2
z_1	z coordinate of Mount 1	m
z_2	z coordinate of Mount 2	m
z_3	z coordinate of exciter motors	m

Greek symbols

α	Vibration screen angle	rad
β	Angle of attachment of exciter motors	rad
ζ_x	Damping ratio in x direction	$-$
ζ_z	Damping ratio in z direction	$-$
$\Delta\theta_y$	Angular displacement about y axis	rad
σ_a	Alternating stress	MPa
σ_m	Mean stress	MPa
τ_{dx}	Periodic time of the damped vibration used for characterisation	sec
ϕ	Phase angle used for characterisation	rad
ω	Forced frequency	rad/s
ω_{dx}	Damped natural frequency	rad/s
ω_{nx}	Natural frequency used for characterisation	rad/s

ω_s	Forced frequency used for characterisation	rad/s
ω_{sn}	Natural frequency used for characterisation	rad/s
ω_n	Natural frequency	rad/s

Abbreviations

DEM	Discrete Element Method
FEA	Finite Element Analysis
FEM	Finite Element Method
FFT	Fast Fourier Transform

1 Introduction and literature Overview

1.1 Introduction

Mechanical screening is defined as the practice of taking granulated ore material and separating it into multiple grades by particle size (MGLEngineering, 2014). Mechanical screening is a very important process which is used in a number of industries which include Mining, Mineral Processing, Agriculture, Pharmaceutical, Food, Plastics and Recycling (MGLEngineering, 2014). In this study the focus will be on screens used in agricultural industries. In the agricultural industry, screens are mainly used for cleaning and classifying of grain.

Grain is typically cleaned by making use of a sieve with a specific aperture size which allows specific size particles to pass through. Vibration of the screen causes smaller particles to move to the bottom and penetrate the mesh; this is known as stratification (Xiao & Tong, 2012). A vibration screen consists of five main components which are a screen box (structure), exciter motor(s), isolators, sieves and a support frame. Vibrations can be generated by either unbalance motors (exciter motors) or by using irregular movement cams.

The most common movements of screens are linear, circular and elliptical (Xiao & Tong, 2012). When using exciter motors, these movements are obtained by specific position and relative rotation of the motor(s).

The purpose of the isolators is to reduce the dynamic forces caused by the vibration. The dynamic properties of the isolators (damping capacity and stiffness) determine the magnitude of the dynamic forces transmitted and also the magnitude of the maximum displacement of the screen (Nel, 2007; Nel, 2009). For a given screen mass, the stiffness of the isolators determines the natural frequency of the screen.

In the literature, many studies have been done for vibration screens and the effect of different parameters on the screening process. A common method used to simulate a screening process is the Discrete Element Method (DEM). The Discrete Element Method is a numerical method used to simulate the dynamic behaviour of a large number of particles. Various studies done on vibration screens used this method to

simulate the screening process with great accuracy. The dynamics of the particles is simulated by solving differential equations that describe the motion of the particles. The motion of each particle is then determined by the forces acting on it. This method can lead to a large number of differential equations which require a lot of computer processing power to be solved.

1.2 Vibration screens

A typical schematic of a vibration screen is shown in Figure 1.1 with the most important components indicated by the arrows.

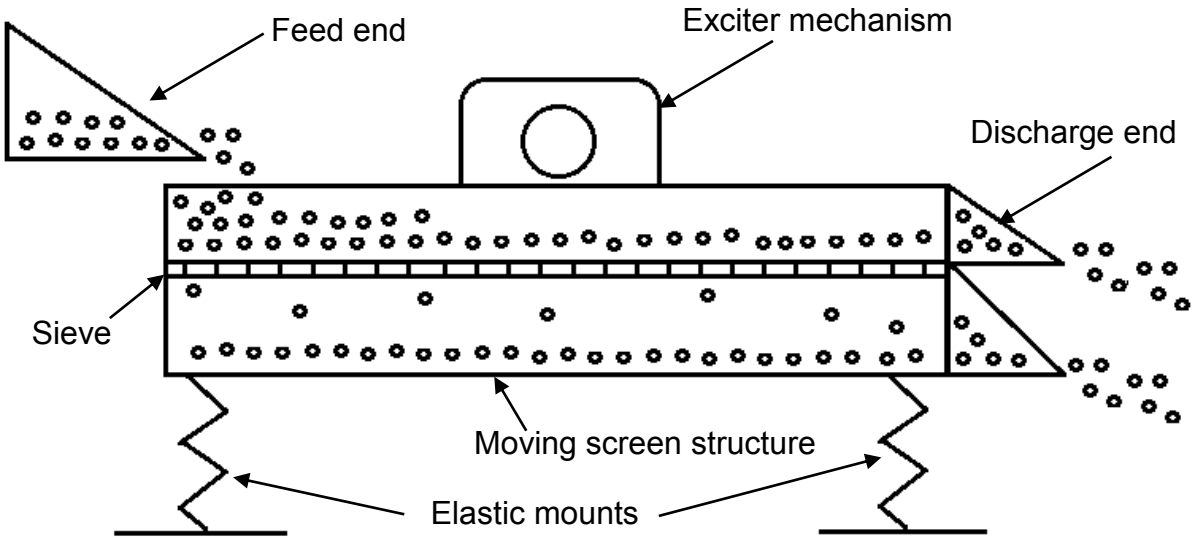

Figure 1.1: Typical vibration screen box

1.2.1 Exciter motors

There are mainly two types of exciter mechanisms used on vibration screens. The first mechanism consist of a crank shaft which is connected to the vibration screen which is driven by a motor. The screen is then forced to move in a circular pattern with the crank shaft. The second type of exciter mechanism makes use of inertia force from unbalance masses. The unbalance masses can either be located directly on the shafts of electric motors or driven separately by an electric motor via a belt mechanism. As the shaft rotates, a harmonic force is generated which is proportional to the unbalance mass, frequency of the motor and radius of eccentricity. The frequency of the electrical motor is a function of the input AC voltage frequency and the number of poles of the

motor. The power of an exciter motor is related to the maximum force that the motor can generate.

1.2.2 Vibration screen mounts

Vibration screens are generally supported by mounts at each corner of the screen. One of the disadvantages of vibration screens is that they transmit large dynamic forces (van Wyk *et al.*, 1994). In vibration screens, mounts must be selected as soft as possible in order for them to act as isolators and reduce dynamic forces transmitted. An isolator is characterised by two very important properties which are stiffness and damping coefficients (Rao, 2011). There are mainly two types of materials used for isolators which are elastomers and steel. Elastomers provide a larger damping coefficient than steel, which is favourable when operating at or near resonance. Steel isolators are preferred when the vibration frequency is far above resonance (BarryControls, 2014). Steel isolators are generally used in the form of coiled springs.

In vibration screens, the stiffness of the isolators plays a very important role as it determines the displacements of the screen and also the dynamic forces transmitted. The dynamic forces transmitted should ideally be as small as possible and displacements should be within acceptable limits for good vibration isolation (Nel, 2007; Nel, 2009), but sufficient movement is necessary to ensure the screen is working effectively. The position of isolators also plays a very important role in terms of dynamic forces transmitted. In a study on the position of isolators at vibratory conveyors, it was found that the improved position of isolators can reduce forces transmitted by up to 20 % (van Wyk *et al.*, 1994).

Limited work could be found regarding optimal or feasible dynamic mount properties for vibration screens.

1.2.3 Resonance state

The natural frequency of a system is determined by the equivalent mass and stiffness of a system (Rao, 2011). The resonance state of a vibration screen is thus directly influenced by the stiffness of the mounts that support it, and the mass of the moving structure of the screen here considered as a rigid body. When the excited force frequency coincides with a system natural frequency, then resonance takes places and this leads to amplitude amplification. When a machine experiences resonance, most of the force required to vibrate the system is stored and released in the mounts (Harris, 1988). The exciter motors of a screen therefore only need to make up the losses due to damping under steady state conditions (Harris, 1988). This can lead to more efficient movement, as a smaller dynamic force is required to achieve the desired displacement amplitude. It should, however, be kept in mind that at resonance the maximum force is transmitted to the foundation through the mounts, and this could negatively influence the fatigue life of the structure (Rao, 2011).

Although the moving mass of the screen could be considered as a rigid body for simulation when its stiffness is large enough, it should, however, be kept in mind that the screen moving structure is actually elastic and therefore natural frequencies of this structure that could also experience resonance problems when the structure is not stiff enough (Yue-min *et al.*, 2009; Du, 2012; Zhou, 2015).

1.2.4 Vibration screen sieves

Vibration screens are generally fitted with one or more sieves which allow material to be separated with multiple particle sizes simultaneously. Most recent vibration screens are fitted with sieves that allow then to be tensioned. These sieves are commonly called overhook sieves due to the hooks installed on them so that they can be tensioned. There are mainly two types of overhook sieve configurations (GKD, 2015). The first configuration is side tension sieves, and these sieves are fitted with two hooks each at the side of the screen. The second configuration is end tension sieves and these sieves are fitted with hooks at the discharge and feed ends of the sieve. If the sieve is correctly tensioned, resonance of the sieve could be avoided with a longer service life, and also better sieving then obtained.

1.3 The sieving process

Mechanical screening is a complex process where particles move by throwing, rolling or sliding motions (He & Liu, 2009). From the literature, it is evident that various factors have an influence on the sieving process (Chen & Tong, 2010; Xiao & Tong, 2012; Dong *et al*, 2013). These factors include:

- Mode shape of the screen
- Vibration frequency
- Vibration amplitude
- Screen mesh size
- Screen wire diameter
- Screen deck inclination angle
- Vibration force direction angle

1.3.1 Forced operational mode shapes of vibration screens

A study was done by several researchers to investigate the effect of different screen motions (Dong *et al*, 2013). The motion of a vibration screen can be classified into three categories which include, linear, circular and elliptical. Under the same conditions, linear screens cause particles to travel faster along the screen (flow rate), compared to circular and elliptical screens. This also leads to a thinner material layer. Circular screens have the slowest travel velocity along the screen, which results in a thickness gradient along the screen. Elliptical screens have a thickness gradient and particle velocity that falls between that of a circular and linear screen. Linear screens have the lowest sieving efficiency, and circular screens have the highest efficiency. Elliptical screens have a sieving efficiency that is between that of a linear and circular screen. Elliptical motion vibration screens combine the basic advantages of linear and circular screens (He & Liu, 2009).

1.3.2 Particle stratification and penetration

Stratification and penetration are the two main processes that occur during sieving (Xiao & Tong, 2012). Stratification is defined as the fine particles passing through the big particles to form particle segregation layers (Xiao & Tong, 2012). Penetration is defined as the fine particles passing through the sieve apertures. Inclination angle of a screen positively influence stratification, but negatively influence penetration. Increasing sieve wire diameter has a positive effect on stratification rate, but has negligible effect on penetration (Xiao & Tong, 2012). It is not obvious how sieve aperture size and sieve width affect stratification and penetration (Xiao & Tong, 2012).

1.3.3 Screen throwing coefficient

The throwing coefficient is one of the most important properties of a sieve. The throwing coefficient is defined as the ratio of the acceleration capable to throw up a particle from the screen surface, and the gravity of the particle (Dinu *et al.*, 2009). The throwing coefficient is defined as

$$c_t = \frac{A\,\omega^2}{g\,cos(\alpha)} \qquad (1.1)$$

where A is the vibration amplitude, omega is the vibration frequency, α is the screen inclination angle and g is the gravitational constant (Dinu *et al.*, 2009). If the throwing coefficient is less than unity, it would result in the particles never leaving the screen surface. If the motion of the screen is assumed to be sinusoidal, the maximum flight time of a particle above the screen is achieved when the throwing coefficient equals 3.3 (Winkler, 1979). In most vibration screens, a throwing motion is adopted, which implies a throwing coefficient larger than unity. The throwing motion provides good segregation performance, good sieving with a higher efficiency and productivity (Zhoa *et al.*, 2010). In order for a screen to obtain best dynamic behaviour, the following must be satisfied (Winkler, 1979):

- The jump of each particle must be higher than the diameter of the sieve wire.
- The length of the particle jump must be big enough to reach at least the next eye (aperture) of the sieve.

1.3.4 The ideal screen surface motion

The ideal screen surface motion can be summarized as follows (He & Liu, 2009):

1. The feed end of the screen should have a bigger throwing coefficient and a higher material delivery velocity. This ensures that bulk material penetrates quickly, which leads to rapid delaminating. Earlier lamination of the material increases the probability of fine grained material penetrating the mesh.
2. In the middle of the screen the throwing index should be lower and the material delivery velocity should be higher. This helps to stabilize fine-grained material and ensures uniform penetration along the screen length.
3. At the end of the screen, the throwing coefficient and material delivery velocity should be lower. This causes the material to stay longer on the mesh, and leads to more complete penetration of the mesh.

1.3.5 Linear motion sieving

Linear sieving is one of the most common types of screening. The term linear refers to the motion of the screen deck, which means that the screen deck follows linear up and down movement. This type of movement is generated by two exciter motors. For linear vibration, the exciter motors must be synchronized and connected to a common beam with their shafts perfectly aligned (Fuchs, 1984). The starting torque, which is at least two times the nominal torque, provides for immediate synchronization of the two motors (Fuchs, 1984). When two exciter motors are mounted at the sides of the screen, synchronized and rotating in opposite directions, then the resultant horizontal unbalance force component is cancelled out, and this leads to linear vibration. The result is that linear vibration is then obtained for any magnitude for angle of attachment of the two motors, but with the angle of attachment the same for each motor. When this angle of attachment is however larger than zero degrees, then the vertical component of the unbalance force will provide a horizontal force component at the screen which allows flow of material on the screen.

Studies have been done on linear vibration screens, in order to determine the effect of various kinematic parameters. These parameters include vibration frequency,

vibration amplitude, inclination angle of screen, and angle of attachment of exciter motor (Chen & Tong, 2010; Zhoa *et al.*, 2010).

1.3.5.1 Vibration frequency

Frequency has some effect on the average throw height of the particles. The average velocity of a particle is not much affected by the vibration frequency. The highest average velocity and throw height are obtained at a frequency of 13 Hz (Zhoa *et al.*, 2010). These researchers found that for frequencies lower than 19.9 Hz, sieving efficiency increases with increasing frequency (Chen & Tong, 2010). For frequencies larger than 19.9 Hz, screening efficiency decreases with increasing frequency. They found that a frequency of 19.9 Hz was the optimum for maximum sieving efficiency (Chen & Tong, 2010).

1.3.5.2 Vibration amplitude

Vibration amplitude has a large influence on the average throw height of the particles (Zhoa *et al.*, 2010). Vibration amplitude also has some influence on the average velocity of the particles (Zhoa *et al.*, 2010). This indicates that amplitude should be selected according to the properties of the screened material. For materials difficult to screen, relatively large amplitude is needed to ensure higher average velocities and thrown heights. They found for their specific application that the particle average velocity and thrown height increase rapidly when the amplitude is 6.5 mm (Zhoa *et al.*, 2010). They also found for amplitudes smaller than 2.55 mm, the screening efficiency increases and starts to decrease after 2.55 mm. Amplitude is thus a sensitive parameter for effective sieving.

1.3.5.3 Screen deck inclination

When the deck inclination angle is increased, the average particle velocity is increased but the average thrown height then decreased. It was found when the inclination angle is between 3 and 6 degrees, high average velocity and thrown height can be obtained for a specific application studied (Zhoa *et al.*, 2010). The magnitude of the screen deck inclination is thus important regarding material flow.

1.3.5.4 Angle of attachment of exciter motor

The average particle velocity and thrown height are influenced by the angle of attachment of exciter motors (Zhoa *et al.*, 2010). These researchers found that a high average velocity and thrown height may be simultaneously obtained at a vibration angle of 40° for a specific application studied (Zhoa *et al.*, 2010). Other researchers found that the maximum screening efficiency is achieved at an angle of 20° in their application (Chen & Tong, 2010).

To obtain optimal sieving effect of material that are difficult to screen, the frequency, amplitude, inclination angle and angle of attachment of exciter motors must be set to 13 Hz, 6.6 mm, 6° and 40° respectively for another specific application (Zhoa *et al.*, 2010).

The magnitude of the angle of attachment of an exciter motor is thus important regarding sufficient material flow and also effective sieving.

1.3.6 Variable elliptic motion screening

Variable elliptic motion sieving was studied (He & Liu, 2009). Most screens such as linear, circular and elliptical screens have a simple translational motion. This means that each point on the screen follows the same path and thus the screen has constant transport velocity and throwing index. These researchers found that this led to low screening efficiency, but sieving efficiency can be enhanced by forcing the screen to have a variable elliptic motion along the screen surface. The position of the exciter motor shaft axis relative to the centre of gravity is then extremely important for efficient sieving. They report that by proper adjustment of the position of the rotating unbalance axis relative to the centre of gravity of the screen, variable elliptic motion can be obtained. They found that properly adjusted variable motion caused the screen to approach ideal motion as described in Paragraph 1.3.4.

1.4 Seeds in South Africa

1.4.1 Grain seeds

The main types of grain cultivated in South Africa are classified as (SAGIS, 2015)

- Maize (white and yellow)
- Oilseeds (sunflower, soybean, canola and groundnuts)
- Winter grain (wheat, barley and oats)
- Sorghum

1.4.2 Weed seeds

Weed seeds can be classified as toxic and non-toxic. In South Africa there are mainly three types of toxic weed seeds that have to be removed from grain. These three types are the Thorn Apple (Olieboom), Scenecio spp (Sprinkaanbos) and Mielie Crotalaria (Wilde lusern) seeds. These seeds contain toxins and it is important that these seeds should not be ingested by human beings in large quantities. In South Africa there is zero tolerance for weed seeds that contain toxins. Any shipment of grain that contains the slightest amount of toxic material will be fully rejected (GrainSA, 2014). Thus it is very important that these three toxic weed seeds be removed effectively from grain. Figure 1.2 shows a picture of these three different toxic plants.

Figure 1.2: Toxic Plants Thorn apple (left), Scenecio spp (middle) and Mielie Crotalaria (right); (GrainSA, 2014; Ispot, 2014)

Other types of non-toxic weeds are the Common Cocklebur (Kankerroos) and Sklerotinia. The latter is not a seed, but a type of fungus that grows on sunflower. Figure 1.3 shows the Klerotinia fungus (left) and Common Cocklebur (Right).

Figure 1.3: Non-Toxic unwanted material Klerotinia fungus (left) and Common Cocklebur (right); (von Beesten, 2014; Hurst, 2014)

1.5 Fatigue failures at vibration screens

Due to the nature of a vibration screen, it is normally subjected to fluctuating forces when operational. A typical vibration screen can be subjected to about 10 million cycles in just 185 hours (Steyn, 1995). The magnitude of the fluctuating forces can significantly influence the fatigue life of the screen. Fatigue failures at vibration screens were reported and investigated by numerous researchers (Steyn, 1995; Yue-min *et al.*, 2009; Zhang & Zhong, 2009; Du, 2012; Hou *et al.*, 2012; Cheng *et al.*, 2013; Patel & Prajapati, 2013; Zhang & Xu, 2013; Zhang *et al*., 2014; Peng *et al.*, 2015; Zhou, 2015). These reported failures and analysis done for vibration screens are proof that most of these screens are traditionally designed without consideration of possible fatigue failures.

1.5.1 Factors that influence fatigue failures at vibration screens

The main reason for most reported fatigue failures is high stresses generated by forces acting on the screen structure. Despite the large dynamic forces acting on the screen, there are other factors that can contribute to fatigue failures.

Structural changes: Changing the structural design of a vibration screen can highly influence the fatigue strength. Proof of this is an ore-processing screen that failed due to changes made to the structure which led to high dynamic bending stresses and ultimately fatigue failure (Steyn, 1995).

Welding: The type and quality of a weld can highly influence fatigue strength. To increase the fatigue strength of welds on vibration screens, the following are proposed by (Steyn, 1995):

1. Use full penetration welds.
2. Welds should be dressed and defects must be ground out.
3. Do magnetic particle inspection to ensure no surface weld defects.

Surface finish: The surface finish of a component of a vibration screen can highly influence the fatigue strength. Increased surface roughness of a vibration screen part can highly influence the fatigue strength (Zhang & Xu, 2013).

Corrosive environments: It is generally accepted that components operating in corrosive environments, with inadequate surface protection, have a finite life. Most vibration screens in mining industries commonly operate in highly corrosive environments where water is continuously sprayed onto these screens. Although the screen components are normally protected against corrosion, the material handled often damage the protection and reduce the fatigue life significantly (Steyn, 1995).

Structural stiffness: The stiffness of a vibration screen structure can highly influence the structural strength. Low structural stiffness can lead to resonance and cause fatigue failures (Du, 2012). Damage due to resonance often occurs at vibration screen components (Du, 2012). To increase the fatigue strength of a vibration screen, it is important that the screen frame structure be designed to have a high structural stiffness. This will ensure that the natural modal frequencies of the screen are far above the working frequency and avoid resonance. Studies have been done on existing vibration screens to analyse the modal frequencies of the structure (Yue-min *et al.*, 2009; Du, 2012; Zhou, 2015). In these studies it was found that at least one of the modal frequencies was close to the forced frequency and resonance occurred (not stiff enough).

1.5.2 Fatigue analysis tools

The complex structural shapes of typical vibration screens make it difficult to compute stress with traditional strength calculations (Hou *et al.*, 2012). A common analysis tool used for strength analysis of complex structures is the Finite Element Method (FEM). The frequent failure of vibration screen components encouraged researchers to thoroughly investigate the reasons for the failures. As a tool for failure analysis, the Finite Element Method was used with great success in several studies (Yue-min *et al.*, 2009; Zhang & Zhong, 2009; Cheng *et al.*, 2013; Hou, 2012; Zhou, 2015). The results from the Finite Element Analysis done on existing vibration screens indicated that vibration screens are in general highly susceptible to fatigue failures. The Finite Element Analysis (FEA) done typically indicated possible fatigue failure as a result of high dynamic stresses as well as low structural stiffness of components that lead to resonance. The results reveal that screen designers in general do not do the necessary calculations to prevent fatigue failures. The Finite Element Method allowed

designers to perform stress analysis, as well as modal analysis to avoid local structural resonance of screen components.

1.5.3 Fatigue failure criteria

The cyclic forces acting on a vibration screen can generate a complex stress pattern. Research showed that the complex stress pattern can be simplified by defining two stress components namely midrange and alternating stress (Budynas & Nisbett, 2011). The two stress components can be calculated mathematically if the maximum and minimum stress are known. Various researchers used these two stress components to derive criteria to prevent fatigue failure. The four criteria that are generally used for fatigue analysis are the Soderberg criteria, Goodman criteria, Gerber criteria and ASME-elliptic criteria (Budynas & Nisbett, 2011).

1.6 Optimisation of a vibration screen

Limited work could be found regarding optimisation studies for vibration screens. Optimisation involves minimizing an objective function by changing one or more design variables. Work reported regarding optimisation is next described.

1.6.1 Optimisation criteria of different researchers

Before optimisation can be performed, a reliable objective function must be formulated. The objective function can either be constrained by constraint equations or unconstrained. In a study “Optimisation studies on vibratory conveyors” (Hota & Karmakar, 1988), a conveyor was optimized. Maximization of the mean transport velocity described as objective function was the goal of the optimisation problem. The vibratory conveyor deck (also referred to as trough) was excited in two directions by two separate exciter mechanisms which provided out of phase vibrations. The design variables used were vibration frequency, amplitude and phase difference of trough vibrations. The design variables were constrained between certain upper and lower limits and was thus a constraint problem.

In another study “Dynamic design theory and application of a large vibrating screen” (Yue-min *et al*, 2009), the strength and mass of the side plates of a vibration screen were optimized. Stiffener beams were used to increase the fatigue strength of a vibration screen’s side plates. In order to reduce manufacturing costs, the mass of the

screen was used as optimisation aim. The sizes of the stiffeners were taken as design variables and were constrained between certain upper and lower limits. The modal frequencies of the screen body were also constrained to ensure that it is far above the operation frequency. A similar study was done on a different vibration screen where the objective was to reduce weight of the side plate described in an objective function, and frequency constrains were also added to avoid resonance (Zhou, 2015). In both studies the frequency constraints were set to ensure that the lowest natural frequency is above the operational frequency. An objective function was also formulated in both studies to express the mass as function of the design variables.

The position of isolators on a vibratory conveyor was optimised in a study "Optimization of a vibratory conveyor for reduced support reaction forces" (van Wyk *et al.*, 1994). In this study, an accurate mathematical model of a vibratory conveyor was developed. The model was used to predict the dynamic forces transmitted by the isolators. The positions of the isolators were chosen as design variables and the optimisation objective was to minimize reaction forces. An objective function was formulated to express the total force transmitted as a function of the design variables. Constraints were used to limit the isolator positions between certain upper and lower limits. Another constraint was used to limit the maximum peak to peak vibration amplitude of the conveyor between certain upper and lower limits.

1.6.2 Optimisation algorithms

A common mathematical method for optimisation is the conjugate gradient method. In a paper "Function minimization by conjugate gradients" this method is discussed in detail (Fletcher & Reeves, 1964). This method is used for unconstrained minimisation of a function of several variables.

In a study on the optimisation of vibratory conveyors, Powell's method was successfully implemented (Hota & Karmakar, 1988). Powell's method involves an iterative process to find the minimum value of an objective function subject to several variables. This method is generally used for unconstrained minimisation. In this study, a penalty function was formulated to account for the constraints. A penalty function

involves adjustment of the objective function to less feasible values when the constraints are violated.

The Leapfrog algorithm was used with great success for optimisation of isolator position on vibratory conveyors (Snyman, 1982). In this study, the Leapfrog algorithm was successful to converge, while other standard optimisation techniques such as quasi-newton and the conjugate gradient method have failed to converge. The leapfrog algorithm is normally used for unconstrained minimisation. A penalty function was also formulated in this study to account for the constraints. The Leapfrog algorithm is described in detail (Snyman, 1982).

The use of a so-called genetic algorithm is also a common optimisation method. A genetic algorithm was used with great success in an optimisation study on a vibration screen (Zhou, 2015). This method was used for constrained minimisation of the mass of side plates on a vibration screen. An objective function was formulated with certain frequency constraint equations.

1.7 Conclusions

The literature study indicated that vibration screening is a very important process used in a wide range of different industries. The effects of important vibration parameters such as forced operational mode shape, frequency, amplitude, screen inclination angle, and also angle of attachment of exciter motors on the screening process were reported in several studies. Some of these parameters influenced the sieving efficiency, while others influenced the material flow rate through the screen.

Three types of toxic weed seeds commonly found in South Africa were identified namely, the Thorn Apple (Olieboom), Scenecio spp (Sprinkaanbos) and Mielie Crotalaria (Wilde lusern). Other types of non-toxic weeds identified were the Common Cocklebur (Kankerroos) and Sklerotinia. The latter is not a seed, but a type of fungus that mainly grows on sunflowers. These unwanted material particles which are typically present in harvested grain should be removed, and this could be done by screening. The choice of sieve is also important to allow effective sieving. Sieve tension, aperture and wire diameter are important for a feasible screen design.

Several researchers mentioned that fatigue problems occurred frequently at vibration screens, mainly because of cyclic overloading. The choice of mount properties plays a major role in the service life of a typical vibration screen structure. Resonance, or a near resonance condition, could lead to amplitude amplification, but very large dynamic forces then transmitted to the foundation and the screen structure as a result. These forces generate cyclic stresses which could limit the service life of the screen structure.

A few researchers reported the results of Finite Element Analysis (FEA) that were used for screens. Although they mentioned that this is unfortunately not often used, it is regarded as a powerful approach which should be used during the design stage of a screen. The advantages of results obtained with the FEA are accurate material stress magnitudes especially at local stress concertation points such as holes, and also that the stiffness of the moving screen structure could be evaluated. The screen structure as a moving mass could be considered as a rigid body for computer simulations when its stiffness is enough. It should, however, be kept in mind that the screen moving

structure is actually elastic and therefore natural frequencies of this structure that could also experience resonance problems when the structure is not stiff enough.

Limited work could be found regarding fatigue strength and optimisation of the vibration screen structure. Although a few optimisation studies for vibration screens could be found, very little work could be found regarding the optimal properties of mounts to be used for screens.

1.7.1 Scope of the work

The problem statement is that unwanted particles such as weed seeds, maize plant stems of various sizes, broken maize kernels, and small stone particles must be removed from harvested maize by screening. A vibration screen should be designed and optimised to ensure effective sieving with sufficient flow rate, and also to provide a long service life. The grain vibration screen must be built, tested and experimentally evaluated.

Chapter 2 describes the mathematical models that were regarded as necessary to achieve a feasible design.

2 Mathematical models

2.1 Introduction

For this study four mathematical models were developed. The first model is developed for computation of the static and dynamic displacements and rigid body natural frequencies of a linear vibration screen. The second model is developed for fatigue stress analysis of the vibration screen structure. The third and fourth models are developed for characterisation of the vertical and horizontal dynamic properties of the rubber mounts respectively.

2.2 Three degree of freedom mathematical model

For this study a three degree of freedom (3 DOF) model is developed to predict the response under different loading conditions and also the natural frequencies of a linear vibration screen. The vibration screen is idealized as a rigid body with mass m and Mass Moment of Inertia J_{yy} attached to a rigid support structure by means of two equivalent elastic screen mounts with arbitrary positions relative to the vibration screen global coordinate system. The origin of the fixed orthogonal global coordinate system xyz is located at g, the centre of gravity of the vibration screen as shown in Figure 2.1. The rigid body mass is positioned at a screen angle α relative to the x axis, which is aligned with the horizontal. The three modes considered are two translational modes for movements as vertical displacement Δz and horizontal displacement Δx respectively, and also one rotational mode for movement as rotational displacement $\Delta\theta_y$ about the y axis. The rigid body mass is supported by two screen mounts with vertical stiffness coefficients $k_{z1}$and k_{z2} and also horizontal stiffness coefficients $k_{x1}$and k_{x2} respectively. It is assumed that the vertical and horizontal stiffness coefficients are independent of each other in the two coordinate directions if the rotational stiffness of the mounts are neglected (Nel, 2009). A viscous damping model is used to describe the damping characteristics of the two screen mounts. The vertical viscous damping coefficients of the two screen mounts are c_{z1} and c_{z2} and the horizontal damping coefficients are c_{x1} and c_{x2} respectively.

The rigid body mass is subjected to fluctuating forces produced by two identical exciter motors attached to opposite sides of the vibration screen structure, in order to obtain

linear motion (see Chapter 1, Paragraph 1.3.5). These two electrical motors rotate in opposite directions relative to each other which then produce no resultant force in the y direction as a result. The centre of gravity of each of the two motors is also aligned with the same x and z coordinates and located at point e, which is the acting point of the unbalance shaking force as shown in Figure 2.1. The result is that the moments produced by each motor about the x and z axis are cancelled. Both exciter motors are mounted such that the centre lines of the rotors are parallel and at an angle β relative to the x axis of the global coordinate system. It is thus evident that the motion of the screen is fully described with the three modes. The resultant shaking forces F_{ex} and F_{ez} and moment M_{ey} cause movements in three directions respectively.

The resultant force produced by the two exciter motors can be described as a force $F_e(t)$ with force components F_{ex} and F_{ez} in the direction of the x and z axis respectively. The magnitude of the resultant shaking force at time t is

$$F_e = M_u \omega^2 \sin(\omega t) \tag{2.1}$$

with x direction force component

$$F_{ex} = F_e \sin(\beta) \tag{2.2}$$

and z direction force component

$$F_{ez} = F_e \cos(\beta) \tag{2.3}$$

The rotational speed of the motors is defined as ω and M_u is defined as the equivalent unbalance product of the two exciter motors. The unbalance product is related to the unbalance mass m_u at the exciter motors positioned at the radius r_u. This product can be described as

$$M_u = m_u r_u \tag{2.4}$$

The force components acting at point e produce a resultant moment M_{ey} about the y axis. The resultant moment is

$$M_{ey} = F_{ex}z_3 - F_{ez}x_3 \tag{2.5}$$

where x_3 and z_3 are the coordinates of point e.

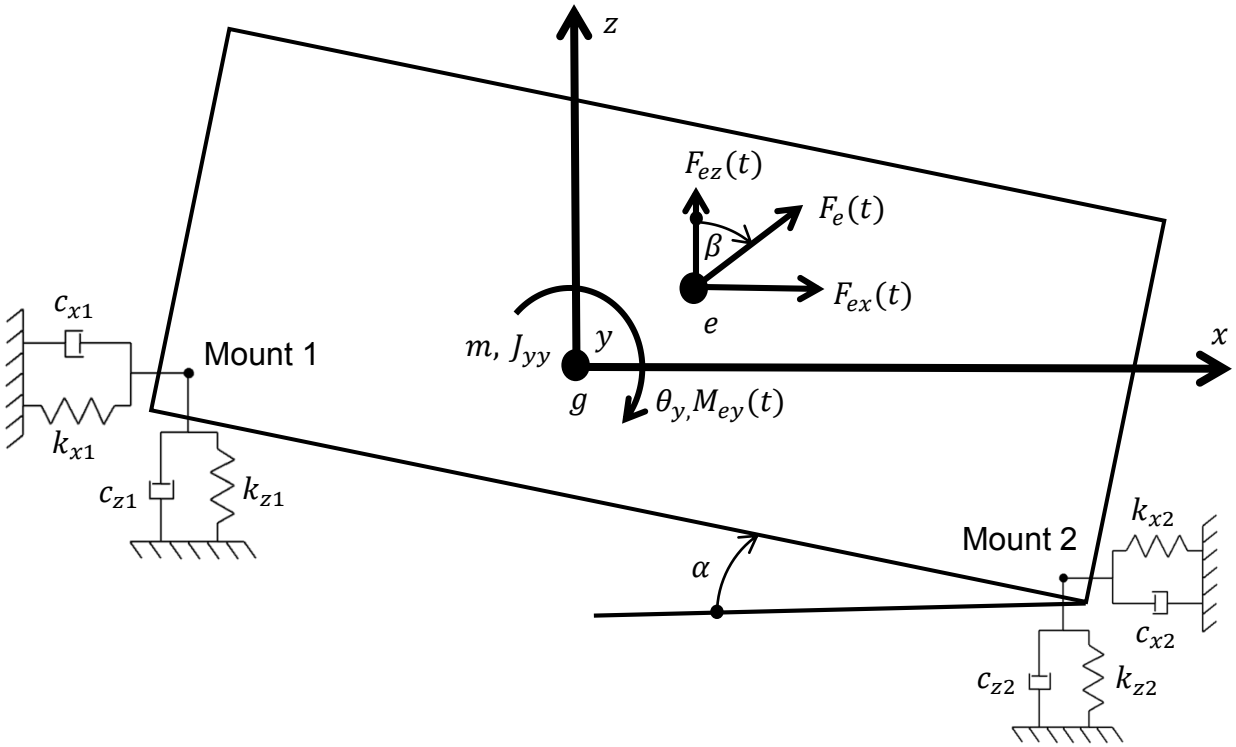

Figure 2.1: Vibration screen in three degree of freedom

With reference to Figure 2.1, and according to Newton's second law, three differential equations of motion are herewith derived. Firstly, for equilibrium, the dynamic forces in the x direction are

$$\begin{aligned} m\Delta\ddot{x} = (-k_{x1} - k_{x2})\Delta x \; + \; (-k_{x1}z_1 - k_{x2}z_2)\Delta\theta_y \; + \; (-c_{x1} - c_{x2})\Delta\dot{x} \\ + \; (-c_{x1}z_1 - c_{x2}z_2)\Delta\dot{\theta}_y + \; F_{ex} \end{aligned} \tag{2.6}$$

Where Δx, $\Delta \dot{x}$ and $\Delta \ddot{x}$ are the displacement, velocity and acceleration in the x direction, and $\Delta\theta$ and $\Delta\dot{\theta}$ are the rotational displacement and rotational velocity about the y axis, at time t. The coordinates of Mount 1 is z_1 and of Mount 2 is z_2 in the z direction respectively.

Secondly, for equilibrium, the dynamic forces in the z direction are

$$\begin{aligned} m\Delta\ddot{z} = {} & (-k_{z1} - k_{z2})\Delta z + (k_{z1}x_1 + k_{z2}x_2)\Delta\theta_y + (-c_{z1} - c_{z2})\Delta\dot{z} \\ & + (c_{z1}x_1 + c_{z2}x_2)\Delta\dot{\theta}_y + F_{ez} \end{aligned} \tag{2.7}$$

Where Δz, $\Delta \dot{z}$ and $\Delta \ddot{z}$ are the displacement, velocity and acceleration in the z direction at time t. The coordinates of Mount 1 is x_1 and of Mount 2 is x_2 in the x direction respectively.

Thirdly, for equilibrium, the dynamic moments about the y axis are

$$\begin{aligned} J_{yy}\Delta\ddot{\theta} = {} & (-k_{x1}z_1 - k_{x2}z_2)\Delta x + (k_{z1}x_1 + k_{z2}x_2)\Delta z \\ & + (-k_{x1}z_1^2 - k_{x2}z_2^2 - k_{z1}x_1^2 - k_{z2}x_2^2)\Delta\theta_y \\ & + (-c_{x1}z_1 - c_{x2}z_2)\Delta\dot{x} + (c_{z1}x_1 + c_{z2}x_2)\Delta\dot{z} \\ & + (-c_{x1}z_1^2 - c_{x2}z_2^2 - c_{z1}x_1^2 - c_{z2}x_2^2)\Delta\dot{\theta}_y + M_{ey}(t) \end{aligned} \tag{2.8}$$

where $\Delta\ddot{\theta}$ is the rotational acceleration about the y axis at time t.

The dynamic displacement Δx and Δz at time t can also be expressed in terms of corresponding amplitudes ΔX and ΔZ and expressed as

$$\Delta x(t) = \Delta X \sin(\omega t) \tag{2.9}$$

and

$$\Delta z(t) = \Delta Z \sin(\omega t) \tag{2.10}$$

2.2.1 Natural frequencies and mode shapes of screen as rigid body supported by elastic mounts

The three natural frequencies with corresponding rigid body mode shapes of the vibration screen as a rigid body supported by elastic mounts as a system can be determined by solving the Eigenvalue problem. This requires that the system stiffness and mass matrices be known (Rao, 2011). The system stiffness and mass matrices are determined by using the equations of motion for the system as described by Equations (2.6) to (2.8), but with all the damping coefficients and the external force here then disregarded to consider natural frequencies. The result is that the stiffness matrix

$$\mathrm{K} = \begin{bmatrix} (-k_{x1} - k_{x2}) & 0 & (-k_{x1}z_1 - k_{x2}z_2) \\ 0 & (-k_{z1} - k_{z2}) & (k_{z1}x_1 + k_{z2}x_2) \\ (-k_{x1}z_1 - k_{x2}z_2) & (k_{z1}x_1 + k_{z2}x_2) & (-k_{x1}z_1^2 - k_{x2}z_2^2 - k_{z1}x_1^2 - k_{z2}x_2^2) \end{bmatrix} \quad (2.11)$$

and the mass matrix

$$\mathrm{M} = \begin{bmatrix} m & 0 & 0 \\ 0 & m & 0 \\ 0 & 0 & J_{yy} \end{bmatrix} \quad (2.12)$$

These stiffness and mass matrices are related to a displacement vector $\Delta\bar{U}$ comprising the three eigenvectors (mode shapes), and the three system eigenvalues (natural frequencies) ω_n (Ewins, 1984), as follows:

$$\left[[K] - \omega_n^2[M]\right][\Delta\bar{U}] = \bar{0} \quad (2.13)$$

For each mode shape, each of these three corresponding natural frequencies ω_n can also be expressed as

$$f_n = \frac{\omega_n}{2\pi} \quad (2.14)$$

2.2.2 Static vertical deflection and reaction forces

The static vertical reaction forces at the two screen mount coordinates are described by two static equilibrium equations. The weight W of the vibration screen is expressed as

$$W = mg \tag{2.15}$$

with g the gravitational acceleration and m the mass of the vibration screen.

For static equilibrium, and with reference to Figure 2.1, the vertical reaction force at Mount 1 is related to the global coordinates and is

$$F_{01} = \frac{-Wx_2}{x_1 - x_2} \tag{2.16}$$

and the vertical reaction force at Mount 2 is

$$F_{02} = W + \frac{Wx_2}{x_1 - x_2} \tag{2.17}$$

The static vertical deflection at Mount 1 is

$$\Delta Z_{01} = \frac{-F_1}{k_{z1}} \tag{2.18}$$

and the static vertical deflection at Mount 2 is

$$\Delta Z_{02} = \frac{-F_2}{k_{z2}} \tag{2.19}$$

2.3 Fatigue stress

Fatigue stress calculations are needed to ensure that the vibration screen has an infinite service life. The static and dynamic forces described in Paragraph 2.2 generate material stresses (static and dynamic) related to the specific geometry of the screen structure, which influence the fatigue strength and service life of the vibration screen structure. In this study Goodman's criteria is also used for fatigue analysis. Goodman's criteria based on different stresses (Budynas & Nisbett, 2011) are expressed as follows:

$$\frac{\sigma_a}{S_e} + \frac{\sigma_m}{S_{ut}} = \frac{1}{n_{sf}} \tag{2.20}$$

with the alternating (dynamic) stress σ_a and the midrange (static) stress σ_m which is thus mathematically related to the material ultimate tensile stress S_{ut} and the endurance stress limit S_e at the critical point of interest of the structural part, with the safety factor against fatigue failure defined as n_{sf}.

2.3.1 The Marin equation

The Marin equation is used to mathematically express the actual endurance stress limit at the point of interest of the particular part. This equation consists of certain modification factors which are used to adjust the endurance stress limit S_e' for the material, at a critical position of the part. The Marin equation (Budynas & Nisbett, 2011) is

$$S_e = k_a k_b k_c k_d k_e k_f S_e' \tag{2.21}$$

where the modification factors $k_a, k_b, k_c, k_d, k_e, k_f$ are used to adjust the endurance stress limit for the material, to become S_e at the point of interest for the structural part.

The endurance stress limit for the material S_e' which is a constant for the specific steel alloy is defined as the endurance limit of a rotating test specimen under ideal test conditions (Budynas & Nisbett, 2011). These six modification factors are described in the next few paragraphs.

2.3.1.1 Surface factor

The surface finish of the part can significantly influence the fatigue strength. To account for this, the surface modification factor

$$k_a = aS_{ut}^b \tag{2.22}$$

where the values for a and b depend on the type of surface finish typically caused during manufacturing as listed in a table (Budynas & Nisbett, 2011).

2.3.1.2 Size factor

The value of the size factor k_b is determined by the cross-sectional area of the geometry under concern. The size factor is expressed in terms of a rotating shaft diameter. The size factor

$$k_b = \begin{Bmatrix} 1.24d^{-0.107} & 2.79 \leq d \geq 51\ mm \\ 1.51d^{-0.157} & 51\ \leq d \geq 254\ mm \end{Bmatrix} \tag{2.23}$$

where d is the diameter of a circular rotating shaft between the limits as indicated. In the case of a non-circular mechanical part (for example structural steel sections which is the case for the structure of the screen), subject to cyclic loading, an equivalent diameter should be determined (Budynas & Nisbett, 2011).

2.3.1.3 Loading factor

The loading factor k_c is determined by the type of loading applied (Budynas & Nisbett, 2011), with three possible values as indicated:

$$k_c = \begin{Bmatrix} 1 & bending \\ 0.85 & axial \\ 0.59 & torsion \end{Bmatrix} \tag{2.24}$$

2.3.1.4 Temperature factor

The temperature factor is defined as k_d and its value is determined by the operational temperature of the relevant part. The possible values for k_d as function of temperature are listed in a table (Budynas & Nisbett, 2011).

2.3.1.5 Reliability factor

When the exact value for the material endurance stress limit S'_e is unknown, but with the ultimate tensile strength known, the material endurance stress is expressed as

$$S'_e = \begin{cases} 0.5S_{ut} & S_{ut} \leq 1400\ MPa \\ 700\ MPa & S_{ut} > 1400\ MPa \end{cases} \quad (2.25)$$

and thus related to a threshold magnitude for S_{ut}. The reliability factor k_e is introduced to account for the scatter in empirical test data for S_{ut} of many tensile test specimens, and values are given in a table (Budynas & Nisbett, 2011).

2.3.1.6 Miscellaneous-effects factor

The miscellaneous-effects factor is defined as k_f and is introduced to account for all other effects that may influence fatigue strength (Budynas & Nisbett, 2011). This factor is also used to account for stress concentration due to the geometry of a part. The magnitude of k_f is taken as unity when stress magnitudes obtained from FEA is used.

2.4 Characterisation of dynamic mount properties

This section consists of two mathematical models that were used to characterise the dynamic properties of the mounts. The first model is the electrodynamic Shaker model which was used to characterise the vertical dynamic properties. The horizontal dynamic properties were characterised *in situ* at the screen with a Bump test approach. Paragraph 2.4.2 describes the mathematical Bump test model.

2.4.1 Electrodynamic Shaker model

A rigid body mass, m_e which is supported by a stiffness element k_{sz} and viscous damping element c_{sz} which represents the equivalent mount as bolted to the base of an electrodynamic Shaker is considered as shown in Figure 2.2. It is assumed that the

screen angle α is small, and the difference in distances between the centre of mass of this vibration screen and Mount 1 and Mount 2 are also small, which is indeed the case for this design (see Figure 2.1). The mass m_e represents the equivalent mass carried by one of the four mounts at the vibration screen, and with this assumption the result is that m_e is 25 % of the mass m. The spring and damping elements represent the equivalent dynamic properties of one of the four mounts. If four identical mounts are selected, the stiffness and damping elements can be expressed in terms of the properties of Mount 1 and Mount 2 (screen mounts, see Figure 2.1) as follows:

$$k_{z1} = k_{z2} = 2k_{sz} \tag{2.26}$$

and

$$\mathrm{c_{z1}} = c_{z2} = 2c_{sz} \tag{2.27}$$

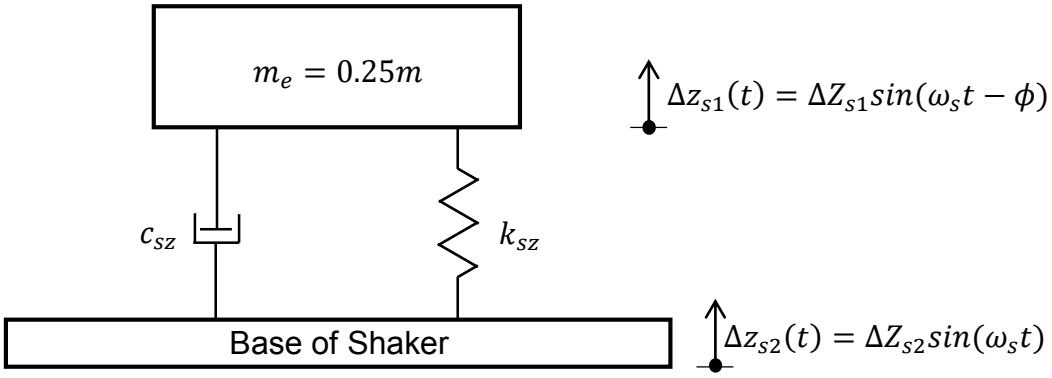

Figure 2.2: Base excitation

When $\Delta z_{s2}(t)$ denotes the displacement of the base of the Shaker table, and $\Delta z_{s1}(t)$ the moving rigid body mass displacement from equilibrium position at time t, then the relative displacement of the stiffness element will be $(\Delta z_{s1} - \Delta z_{s2})$ and the relative velocity of the two ends at the damper $(\Delta \dot{z}_{s1} - \Delta \dot{z}_{s2})$. The response of a viscous damped system under harmonic motion of the base (Rao, 2011), can be described by the equation of motion as

$$m_e\Delta\ddot{z}_{s1} + c_{sz}(\Delta\dot{z}_{s1} - \Delta\dot{z}_{s2}) + k_{sz}(\Delta z_{s1} - \Delta z_{s2}) = 0 \tag{2.28}$$

With ΔZ_{s_1} the displacement amplitude of the Shaker base and ω_s the forced frequency

$$\Delta z_{s2}(t) = \Delta Z_{s2} sin(\omega_s t) \tag{2.29}$$

Equation (2.28) becomes

$$m_e\Delta\ddot{z}_{s1} + c_{sz}\Delta\dot{z}_{s1} + k_{s1}\Delta z_{s1} = k_{sz}\Delta Z_{s2}\sin(\omega_s t) + c_{sz}\omega_s\Delta Z_{s2}\cos(\omega_s t) \tag{2.30}$$

also

$$\Delta z_{s1}(t) = \Delta Z_{s1} sin(\omega_s t - \phi) \tag{2.31}$$

where the amplitude ratio is given by

$$\frac{\Delta Z_{s1}}{\Delta Z_{s2}} = \left[\frac{k_{sz}^2 + (c_{sz}\omega_s)^2}{(k_{sz} - m_e\omega_s^2)^2 + (c_{sz}\omega_s)^2}\right]^{1/2} \tag{2.32}$$

and the phase angle

$$\phi = \tan^{-1}\left[\frac{m_e c_{sz}\omega_s^3}{k_{sz}(k_{sz} - m_e\omega_s^2) + (c_{sz}\omega_s)^2}\right] \tag{2.33}$$

The response ΔZ_{s1} represents the excitation amplitude, and ϕ represents the phase angle between these ΔZ_{s1} and ΔZ_{s2} displacement vectors.

The displacement amplitudes ΔZ_{s1} and ΔZ_{s2} can also be written as

$$\Delta Z_{s1} = \frac{\Delta\ddot{Z}_{s1}}{\omega_s^2} \tag{2.34}$$

and

$$\Delta Z_{s2} = \frac{\Delta \ddot{Z}_{s2}}{\omega_s^2} \tag{2.35}$$

where $\Delta \ddot{Z}_{s1}$ and $\Delta \ddot{Z}_{s2}$ are the corresponding acceleration amplitudes.

The critical damping coefficient is defined as

$$c_{c_{sz}} = 2\sqrt{k_{sz} m_e} \tag{2.36}$$

The damping ratio ζ_z is defined as the ratio between the actual damping coefficient c_{sz} and the critical damping coefficient $c_{c_{sz}}$as

$$\zeta_z = \frac{c_{sz}}{c_{c_{sz}}} \tag{2.37}$$

The natural frequency for this system is defined as

$$\omega_{sn} = \sqrt{\frac{k_{sz}}{m_e}} \tag{2.38}$$

and

$$f_{sn} = \frac{\omega_{s_n}}{2\pi} \tag{2.39}$$

2.4.2 Bump test model (*in situ*)

Figure 2.1 represents the screen model which was also used to characterise the horizontal dynamic properties of the screen mounts *in situ* as installed at the screen. If the input force F_e is disregarded and $\Delta\ddot{x}_g$ denotes the horizontal acceleration response at the centre of gravity of the rigid body mass at time t. This is due to an impact mallet load applied at an initial static equilibrium position, with the system's horizontal mode of the damped vibration ω_{dx} then excited. This frequency of free vibration can be described as

$$\omega_{dx} = \frac{1}{\tau_{dx}} \tag{2.40}$$

Where τ_{dx} denotes the periodic time of the damped vibration between two successive acceleration amplitudes $\Delta\ddot{x}_{g1}$ and $\Delta\ddot{x}_{g2}$ at the centre of gravity of the screen for one complete cycle in the time domain response signal. Also the acceleration ratio in the logarithmic decrement time domain response signal (Rao, 2011) is expressed as

$$\frac{\Delta\ddot{x}_{g1}}{\Delta\ddot{x}_{g2}} = e^{\zeta_x \omega_{nx} \tau_{dx}} \tag{2.41}$$

with the natural frequency

$$\omega_{nx} = \frac{\omega_{dx}}{\sqrt{1-\zeta_x^2}} \tag{2.42}$$

By solving Equations (2.41) and (2.42) simultaneously, the damping ratio ζ_x as well as the natural frequency of the horizontal mode ω_{nx} can be determined. The dynamic horizontal stiffness at Mount 1 and Mount 2 is

$$k_{x1} = k_{x2} = 0.5 m \omega_{nx}^2 \tag{2.43}$$

when preload dependency of stiffness and damping is regarded very small and thus neglected. This is regarded valid, because it is assumed that the screen angle α is

small, and the difference in distances between the centre of mass of this vibration screen and Mount 1 and Mount 2 are also small, which is indeed the case for this design (see Figure 2.1).

2.5 Conclusions

Four different mathematical models were formulated in order to describe the response of the vibration screen, the fatigue strength of the screen structure, and also to characterise the screen mount vertical and horizontal dynamic properties. These mathematical models were implemented in different computer programs in a Matlab environment for simulation purposes. The computer implementation is described in Chapter 3.

3 Computer implementation

3.1 Introduction

The four different mathematical models discussed in Chapter 2 were implemented as computer programs in a Matlab environment. The first model was implemented to compute the static and dynamic displacements and rigid body system natural frequencies of the vibration screen. The second model was implemented to compute the safety factor against fatigue failure for the vibration screen structure. The third and fourth models were implemented to compute vertical and horizontal dynamic properties of the rubber screen mounts respectively.

3.2 Vibration screen model

The flow chart in Figure 3.1 describes the computer program which was used to predict the response (acceleration, velocity and displacement), static and dynamic forces and natural frequencies of the vibration screen. The input can be divided into three groups namely:

- Screen effective mass and Mass Moment of Inertia.
- Excitation force characteristics, coordinates of the acting point e and forced frequency.
- Mount dynamic properties and mount coordinates.

The three second order differential Equations (2.6) to (2.8) were converted to six first-order differential equations. These equations were then implemented into a Matlab environment and solved by numerical integration with *ode23.m*. The same computer program was used to compute the magnitude of the objective function (Equation (5.1)) and constraints (Equations (5.2) and (5.3)), but the dynamic properties of the screen mounts were chosen as design variables. The detail of the optimisation is discussed in Chapter 5.

The Eigen values and Eigen vectors (natural frequencies and mode shapes) were also computed by using Matlab's built in algorithm *eig.m.*

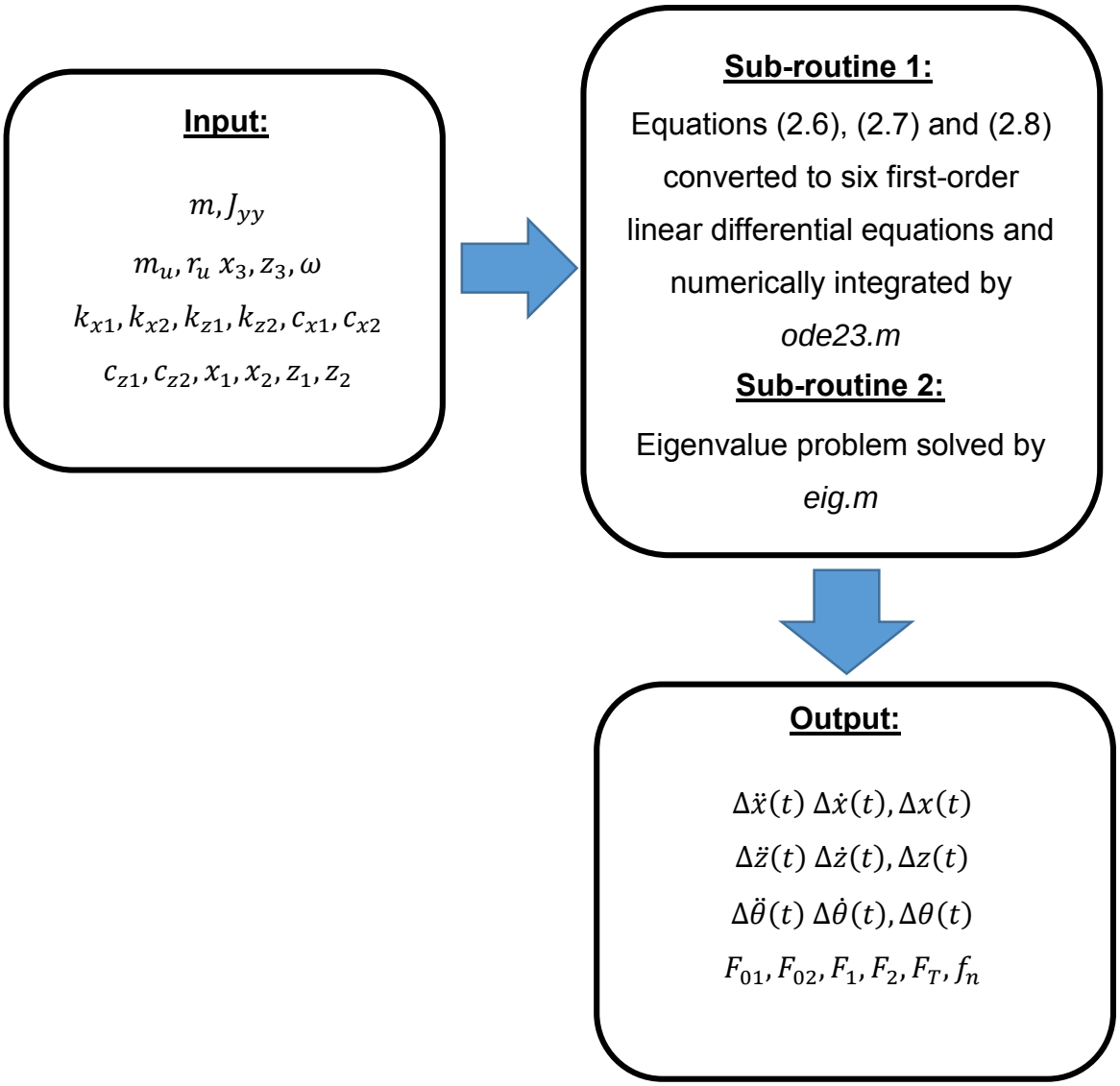

Figure 3.1: Vibration screen computer program flow chart

3.3 Fatigue stress analysis

Some of the output data (static and dynamic forces) of the vibration screen program was used as input values in the Finite Element Analysis (FEA) regarding material stresses induced. The FEA results were used in conjunction with this computer program which is based on the mathematical model described in Paragraph 2.3. This computer program was implemented in a Matlab environment to compute the safety factor against possible fatigue failure. The flow chart for this computer program is shown in Figure 3.2.

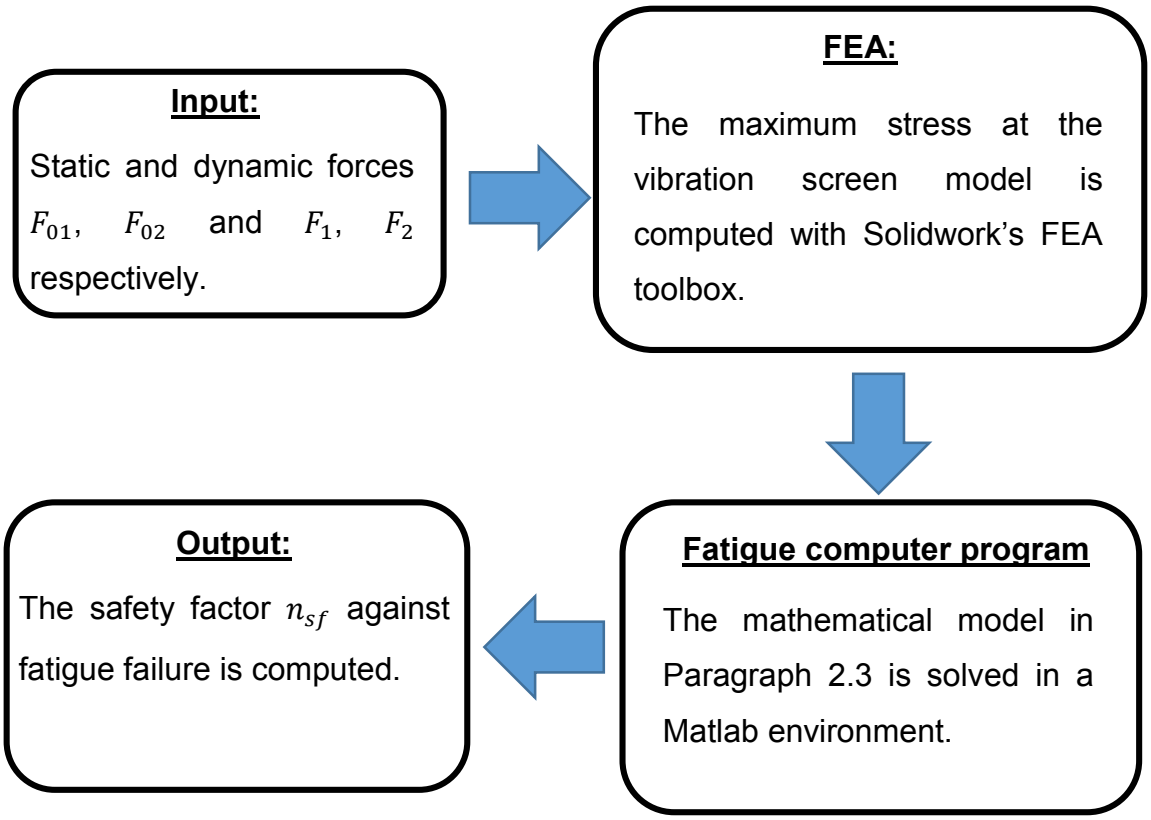

Figure 3.2: Fatigue analysis flow chart

3.4 Characterisation of mount dynamic properties

3.4.1 Vertical dynamic properties

The flow chart in Figure 3.3 describes the computer program based on the mathematical model described in Paragraph 2.4.1. The input data consists of the equivalent mass carried by the mount and also two measured time domain acceleration signals at the mass and the base of the test assembly respectively. The two time domain signals were passed through a filter which removed noise generated by the electrodynamic Shaker. The filter process involves conversion of this measured time domain data into corresponding frequency domain data, with phase angles then also determined. The Fourier coefficients were then determined in order to remove the unwanted noise in the signals. The filtered data was then used in conjunction with the equivalent mass to determine the dynamic stiffness and damping coefficients of the rubber screen mount. This process was repeated for different excitation amplitudes and also different preload magnitudes. More detail regarding the characterization process is given in Chapter 4.

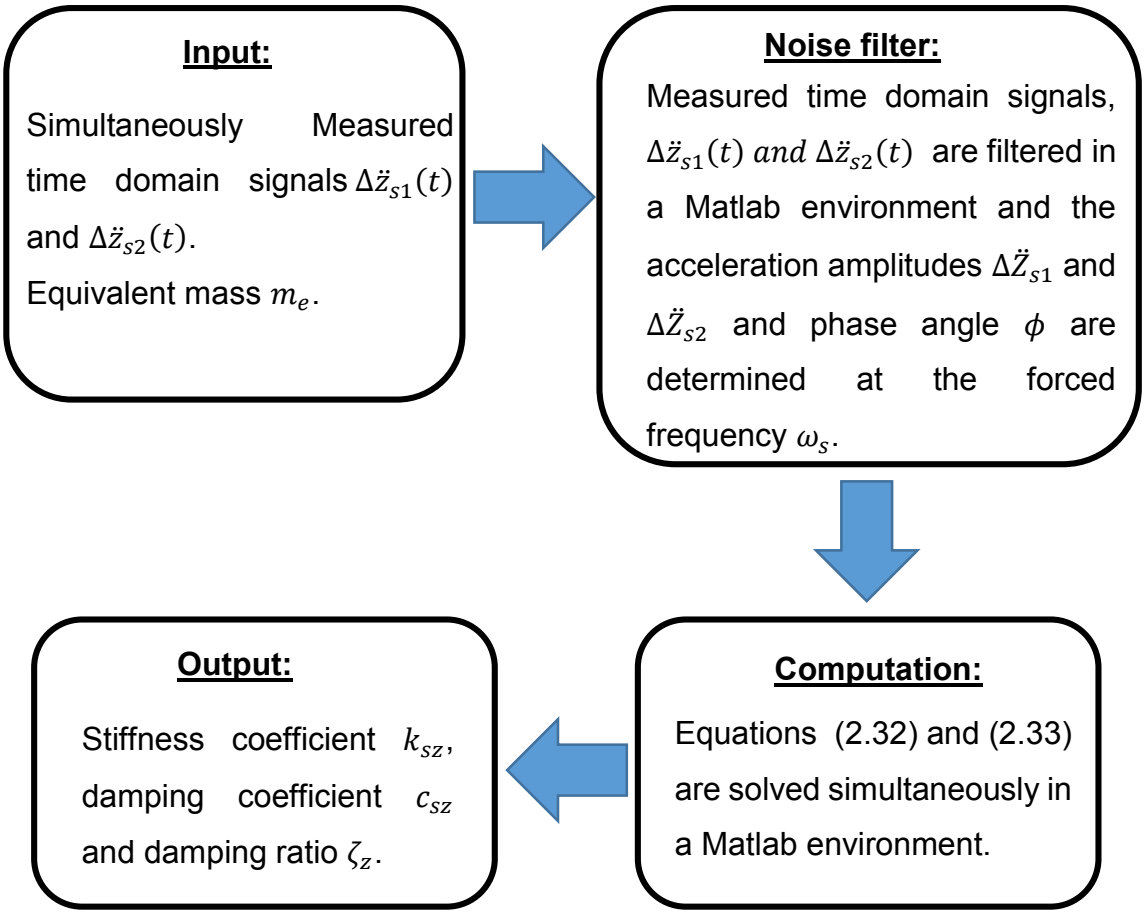

Figure 3.3: Vertical mount properties computer program flow chart

3.4.2 Horizontal dynamic properties

The horizontal dynamic properties were characterised *in situ* at the screen with a Bump test approach. The mathematical model described in Paragraph 2.4.2 was implemented in a Matlab environment to compute the dynamic horizontal stiffness and damping coefficients of the screen mounts. The flow chart for this computer program is shown in Figure 3.4.

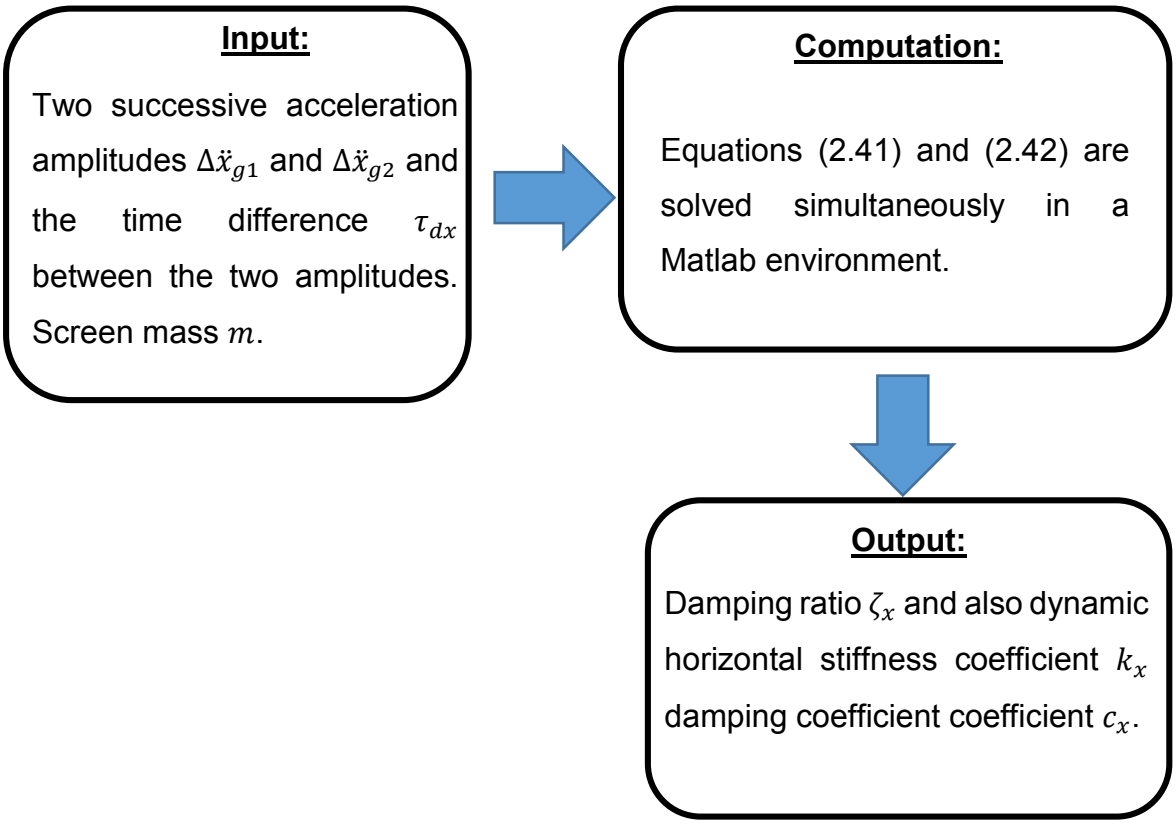

Figure 3.4: Horizontal mount properties computer program flow chart

3.5 Conclusions

The four different mathematical models were successfully implemented as separate computer programs respectively in a Matlab environment. The characteristics of some of the parameters used as input values at the first two programs were characterised and are described in detail in Chapter 4. The last two programs were used for characterisation and the implementation of these two programs are also discussed in detail in Chapter 4. More detail on the implementation of the first two programs is given in Chapters 5 and 6.

4 Experimental characterisation

4.1 Introduction

The design of a grain vibration screen requires that the characteristics of grain be known. The grain characteristics determined the required sieve aperture dimensions, as well as the size of the vibration screen. The required sieving amplitude for effective removal of weed seeds and other unwanted particles is another important characteristic that was determined experimentally. These characteristics were determined before the vibration screen structure was designed. After these characteristics had been determined, the body of the vibration screen was designed and computer simulations were done to determine the optimal dynamic properties of the screen mounts. More detail regarding the optimisation process is described in Chapter 5. The dynamic properties of the rubber mounts were characterised with the use of an electrodynamic Shaker. The effect of preload on the dynamic properties were also investigated. This was done to determine the influence of different loading conditions such as when the vibration screen was empty or fully loaded with grain.

4.2 Required sieving amplitude

An electrodynamic Shaker was used to determine the minimum required sieving amplitude for effective removal of weed seeds and other unwanted particles. This empirical method was chosen because the Shaker was available in the laboratory, and used as alternative method to the theoretical Discrete Element Method as described in Chapter 1, Paragraph 1.1. This test was only performed for maize, as this type of grain is the main focus of the study. A test setup was designed and built from clear Perspex tube which allowed a good visual representation of the sieving process. The setup was bolted to the base of the electrodynamic Shaker and a wire mesh installed to act as a preliminary sieve. Contaminated maize was tested at different amplitudes as well as different forced frequencies. The amplitudes and forced frequencies were measured with an accelerometer attached to the base of the test setup. The accelerometer was coupled to a Diagnostics Instrument 2200 FFT Analyser which was configured to provide measured displacement as output. A picture of this test setup is shown in Figure 4.1.

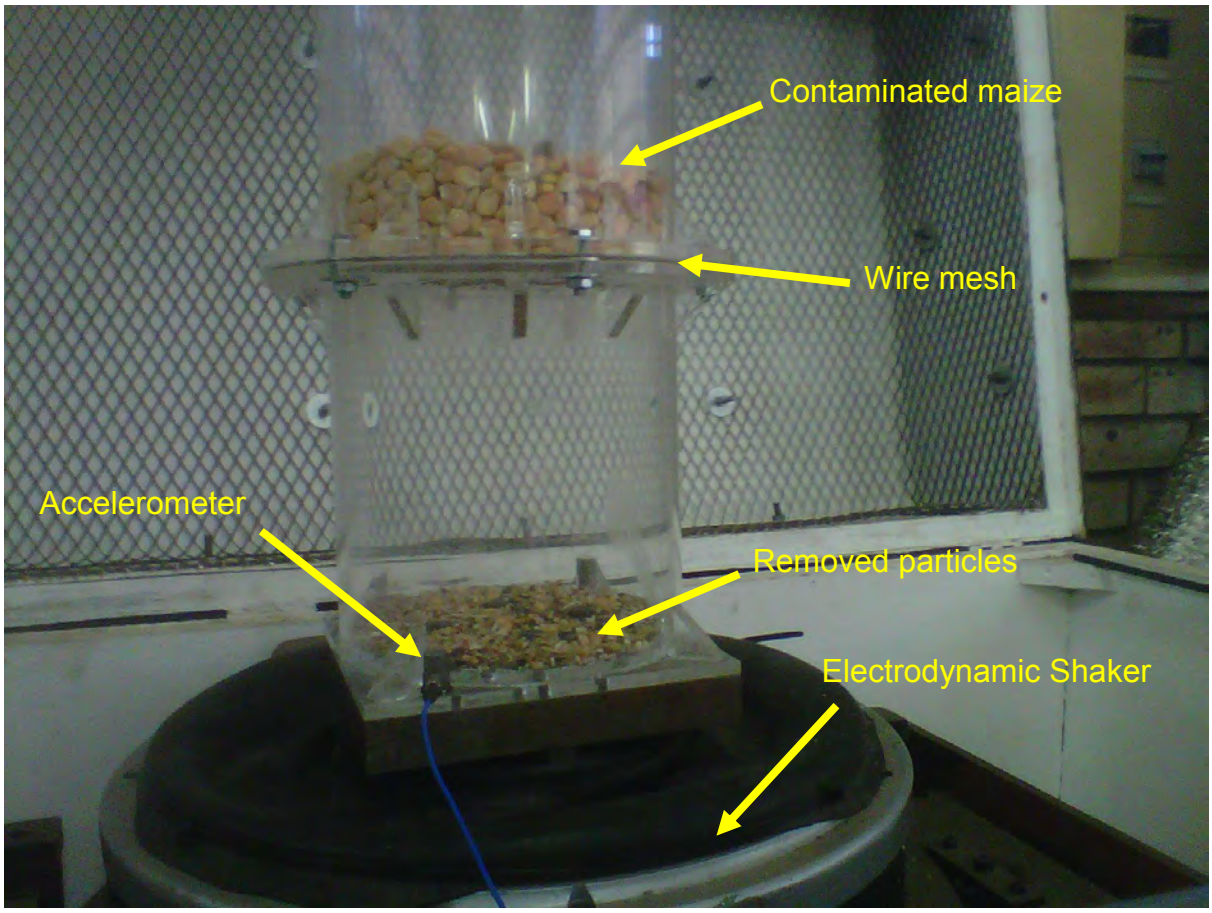

Figure 4.1: Electrodynamic Shaker test setup for sieving tests

The tests indicated that the best sieving frequency was between 16 and 25 Hz. This is also the range of commercially available exciter motors. The effects of different maize layers thicknesses were also investigated. It was found that a layer of approximately 50 mm provided the best sieving results. The required sieving amplitude was determined to be 1.4 mm at a forced frequency of 25 Hz for a 50 mm maize layer. The tests indicated that larger amplitudes were required at lower forced frequencies. The required sieving amplitude at 16.75 Hz forced frequency for a 50 mm maize layer was determined as 2.3 mm. The frequencies of 16.75 and 25 Hz correlate to the synchronous frequency of a 6 pole and a 4 pole induction motor respectively, and hence the decision to use it for these tests. A final decision for motor speed was taken as 25 Hz for this design, and thus a required sieving amplitude at 1.4 mm.

Figures 4.2 and 4.3 show the measured response (time domain acceleration and frequency domain peak displacement) at 16.75 and 25 Hz respectively for a maize layer of 50 mm.

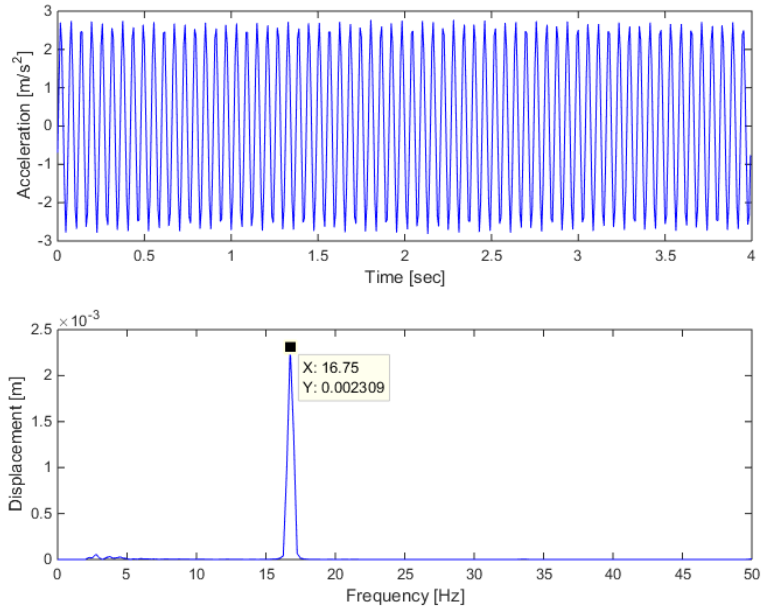

Figure 4.2: Measured required sieving amplitude at 16.75 Hz

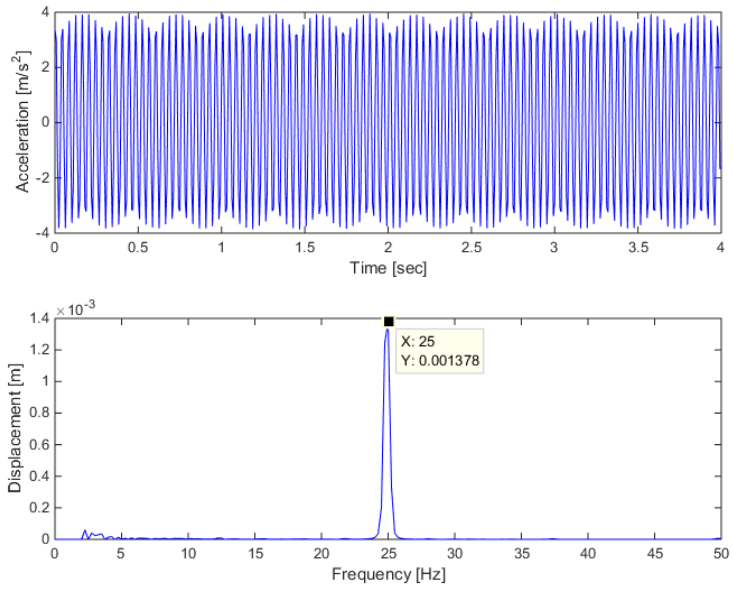

Figure 4.3: Measured required sieving amplitude at 25 Hz

4.3 Density of maize

The tests described in Paragraph 4.2 indicated that the maximum maize layer thickness for effective sieving was approximately 50 mm. The design of the vibration screen structure required that the mass of the maize at the screen must be known. The bulk density of the maize was determined which in turn was used in conjunction with this layer thickness and vibration screen dimensions to compute the theoretical mass of the maize on the vibration screen. To determine the bulk density, a calibrated scale was used to measure the mass of maize added to a bucket of known volume as shown in Figure 4.4. The maize was obtained from the Senwes Silos located in Potchefstroom. The density of the maize sample was approximately 830 kg/m^3.

Figure 4.4: Bucket filled with maize on scale

4.4 Typical dimensions of grain seeds

4.4.1 Maize kernels

The dimensions of typical maize kernels were measured with a digital Vernier calliper and the results of one maize kernel as example are shown in Figure 4.5. This sample was obtained from a local farmer for the 2014 harvest.

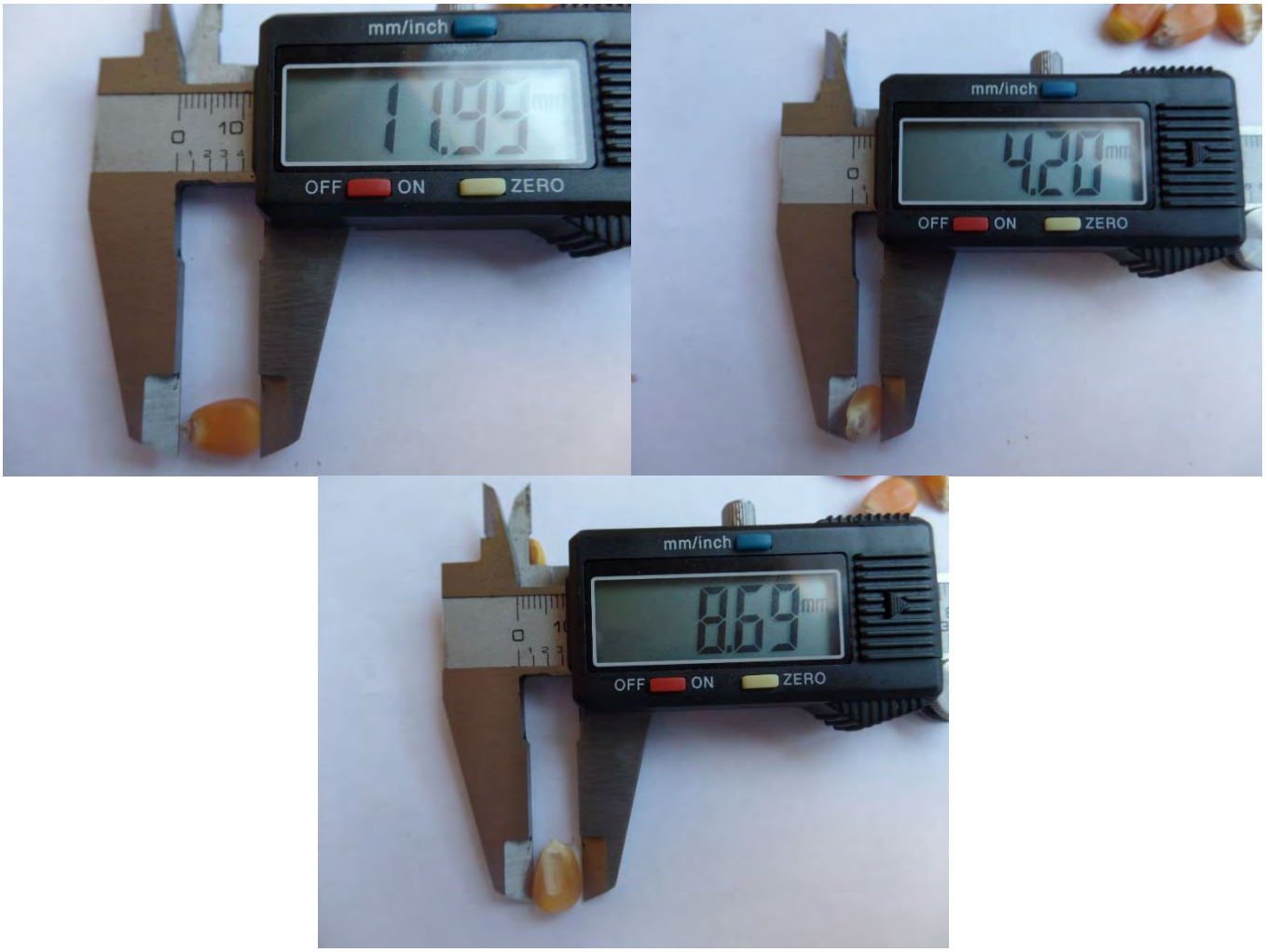

Figure 4.5: Dimensions of a maize kernel

4.4.2 Sunflower seeds

Figure 4.6 shows as an example the dimensions of typical sunflower seed. This sample was also obtained from a local farmer from the 2015 harvest.

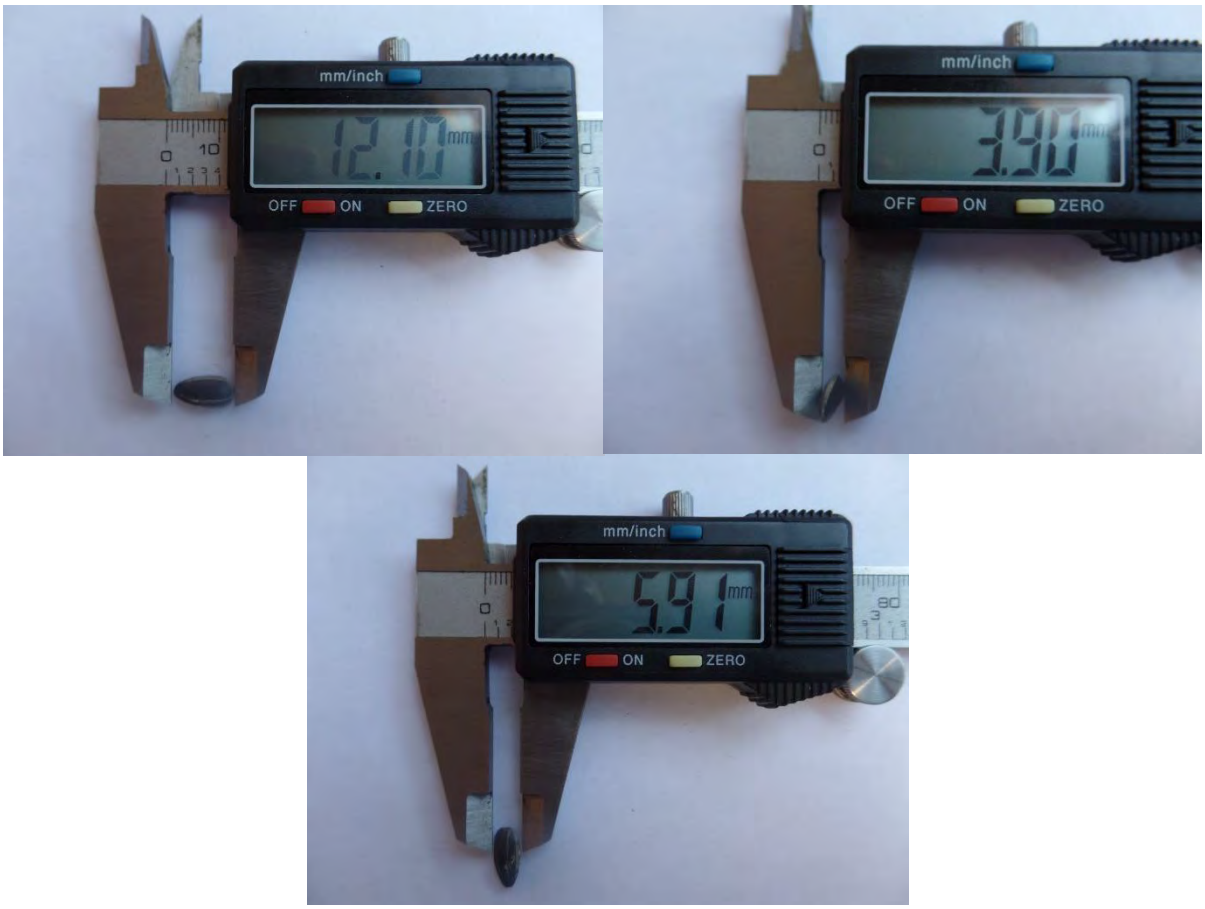

Figure 4.6: Dimensions of a sunflower seed

4.4.3 Summary of typical grain dimensions

Table 4.1 summarizes the experimental average dimensions of several maize kernels and sunflower seeds respectively.

Table 4.1: Summary of typical grain dimensions

Type of Grain	Length [mm]	Width [mm]	Height [mm]
Maize	12.0	4.2	8.7
Sunflower	12.0	4.0	6.0

4.5 Sieve characteristics

4.5.1 Sieve aperture dimensions

A few sieves were selected based on the average size of maize, sunflower, weed seeds and also other unwanted particles to be removed. The vibration screen was designed to be fitted with two different sieves, a coarse one at the top and a finer one at the bottom. This allowed the grain to pass through the coarse sieve, but larger weed seeds and other unwanted particles were then removed. The fine sieve allowed smaller weed seeds and other small unwanted particles to pass through, but the grain remained on the fine sieve and then exited at the discharge end of the vibration screen. The sieves were manufactured from 1.6 mm galvanized mild steel wire and standard available over hook sieves in an “s” type configuration were used. This allowed the sieves to be tensioned when fitted at the vibration screen. Figure 4.7 shows the four different sieves that could be fitted to the vibration screen. The sieves are arranged from coarse (left) to fine (right). Figure 4.8 shows close-up photos of the different sieve apertures. The aperture dimensions are 10x10 mm (top left), 8x10mm (top right), 6x6 mm (bottom left) and 3.15 x 3.15 mm (bottom right). These are standard aperture sizes that were available from the supplier (Vibra-Tech). More information is included in Appendix D. For the application to screen maize, the 6x6 mm sieve was used as a fine sieve, and the 8x10 mm sieve was used as a coarse sieve. The other two sieves were selected to clean other types of grain such as sunflower and groundnuts.

Figure 4.7 Four different screen sieves

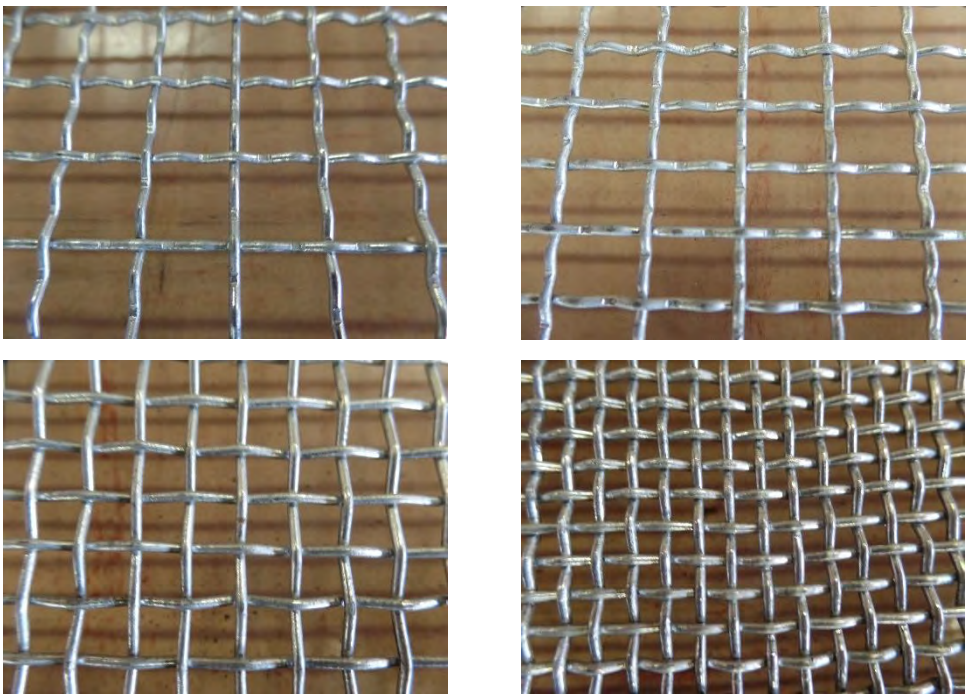

Figure 4.8: Sieve apertures

4.5.2 Sieve mass

The mass of each sieve was measured to accurately compute the position of the centre of mass and also the magnitude of the Mass Moment of Inertia with Solidworks. Each sieve was suspended from a small scale which provided a digital readout of the mass. Figure 4.9 shows a photo of one sieve and the scale. The mass of the different sieves is summarized in Table 4.2.

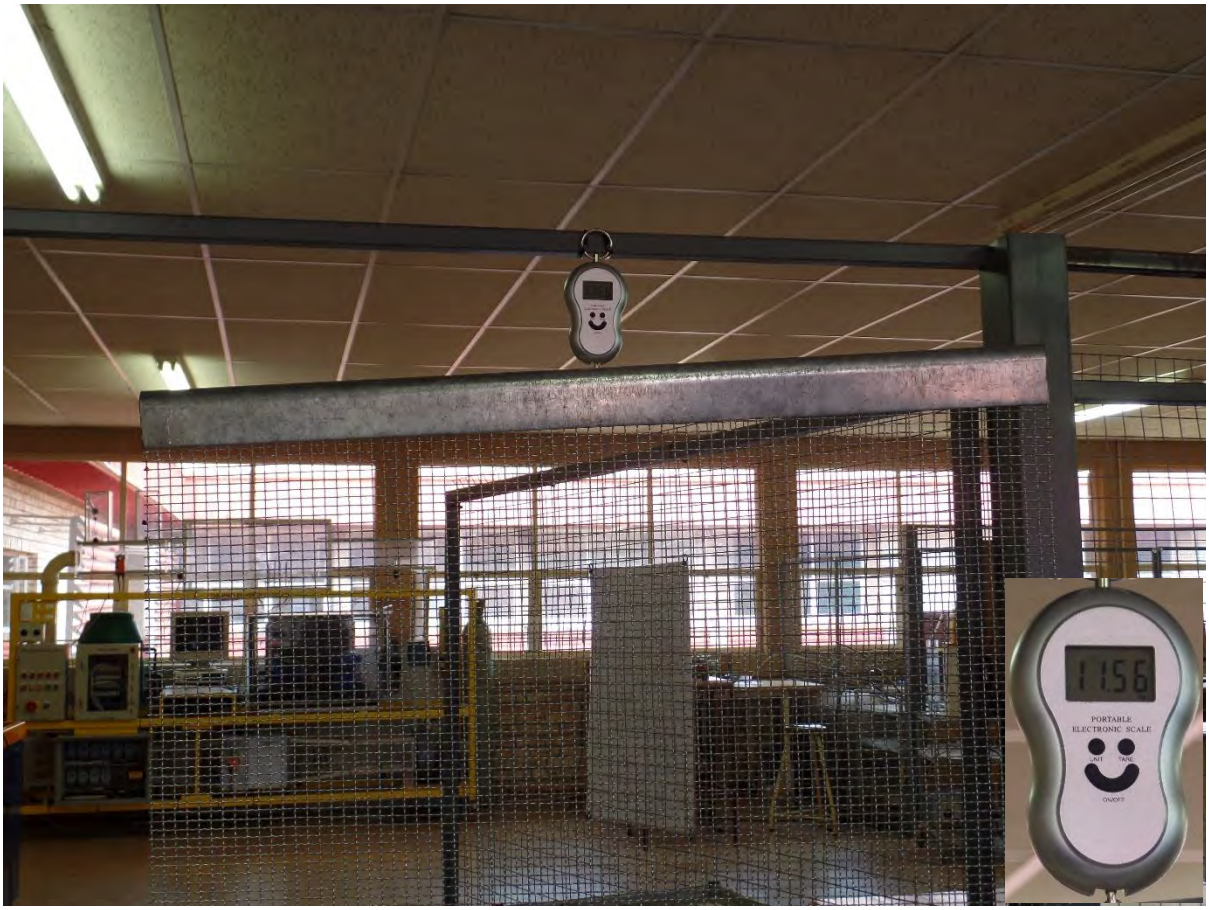

Figure 4.9: Sieve mass measurements with scale

Table 4.2: Summary of different sieve mass

Sieve aperture size	Sieve mass $[kg]$
10 x 10 mm	10.83
8 x 10 mm	11.56
6 x 6 mm	13.82
3.15 x 3.15 mm	17.67

4.6 Dynamic properties of rubber mounts

The dynamic properties of the rubber mounts were characterised to verify the supplier's values and also to investigate the influence of different operational conditions on the mount properties. Based on properties obtained from the mount supplier, it was found that two mounts have to be connected in series as one of four sets at the screen to provide optimal stiffness. More detail regarding the selection of the mounts is described in Chapter 5. Standard manufactured Novibra type M 400-40 mounts were chosen for this application. The technical specifications of these mounts are listed in Appendix C. The vibration screen is supported by four sets of these mounts located at each corner of the screen. One set of series connected mounts was used to characterise the dynamic properties. The vertical dynamic properties were characterised for different preload conditions and also different excitation amplitudes. This was done to make provision for an empty and fully loaded vibration screen. Static tests were also done to characterize the static mount stiffness properties. The horizontal dynamic properties were characterised *in situ* with a Bump test approach.

4.6.1 Instrumentation

The vertical dynamic properties of the mounts were characterised with the use of a Ling Dynamic Systems V724 electrodynamic Shaker connected to a DPA4 Amplifier and SPC4 Signal Controller which allowed different excitation amplitudes. Linear polished shafts guided a moving mass with minimal friction. One set of mounts was bolted between this mass and the base of the test assembly. The test assembly was then firmly bolted to the base of the electrodynamic Shaker. The test assembly and electrodynamic Shaker are shown in Figure 4.10. The Amplifier and Signal Controller are shown in Figure 4.11. Two 100 mv/g PCB accelerometers coupled to a Diagnostics Instruments 2200 FFT Analyser were used to measure the acceleration signals simultaneously at the base and moving mass of the test assembly. The data recorded on the Analyser were downloaded to a Laptop for further analysis. The same accelerometers and FFT Analyser were used to characterise the horizontal dynamic mount properties as an *in situ* approach at the screen.

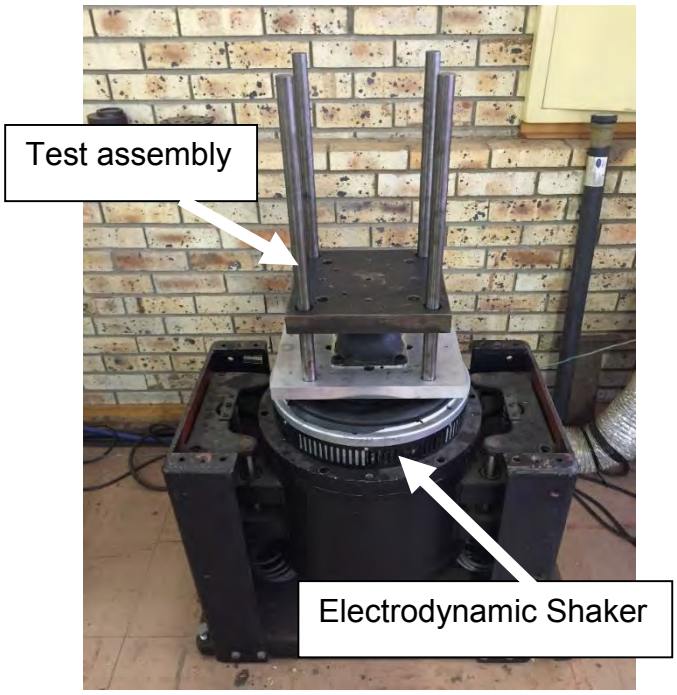

Figure 4.10: Electrodynamic Shaker with test assembly

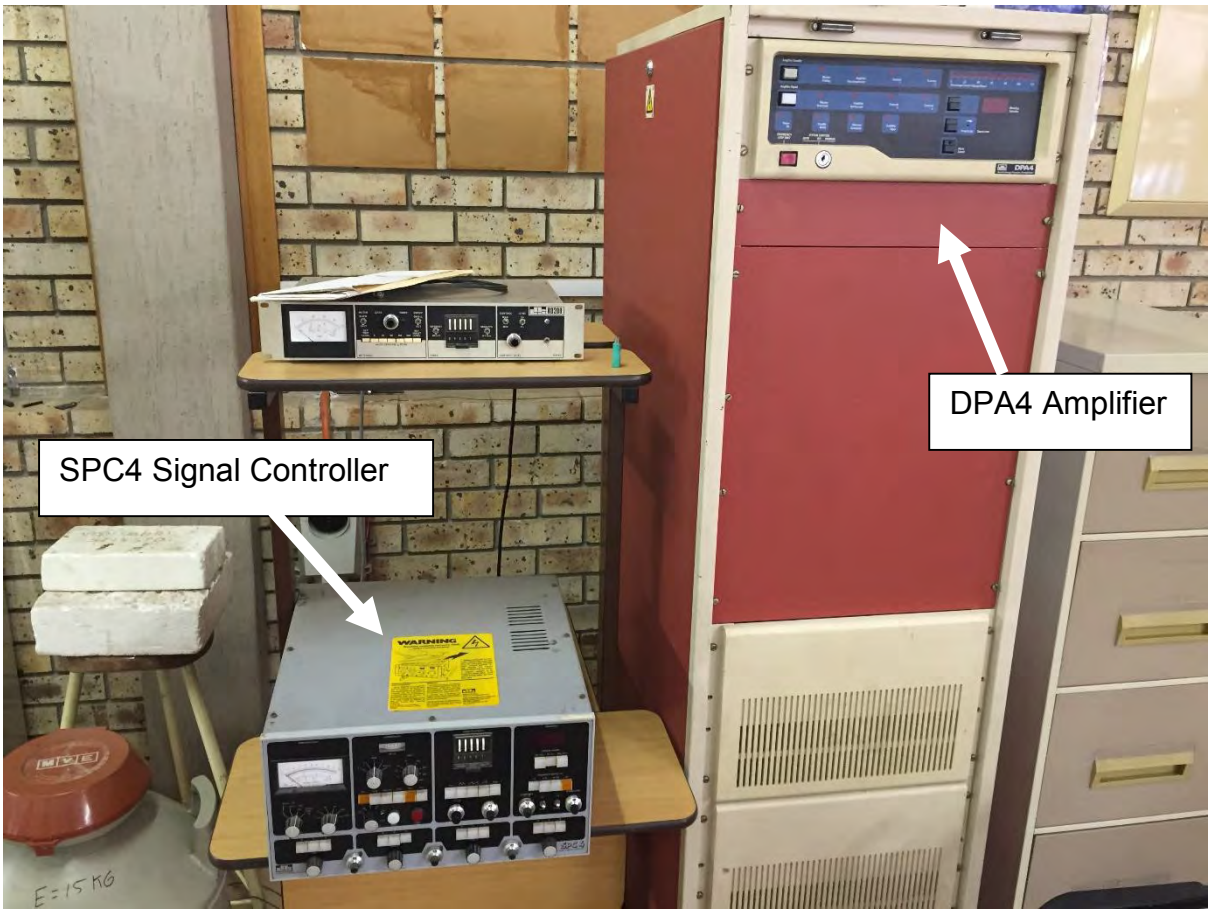

Figure 4.11: DPA4 Amplifier and SPC4 Signal Controller

4.6.2 Test setup

Figures 4.12 and 4.13 show the test setup for the characterisation of the vertical dynamic properties of a rubber mount set, comprising two standard mounts coupled in series. A total of four of these mount sets were used at the screen.

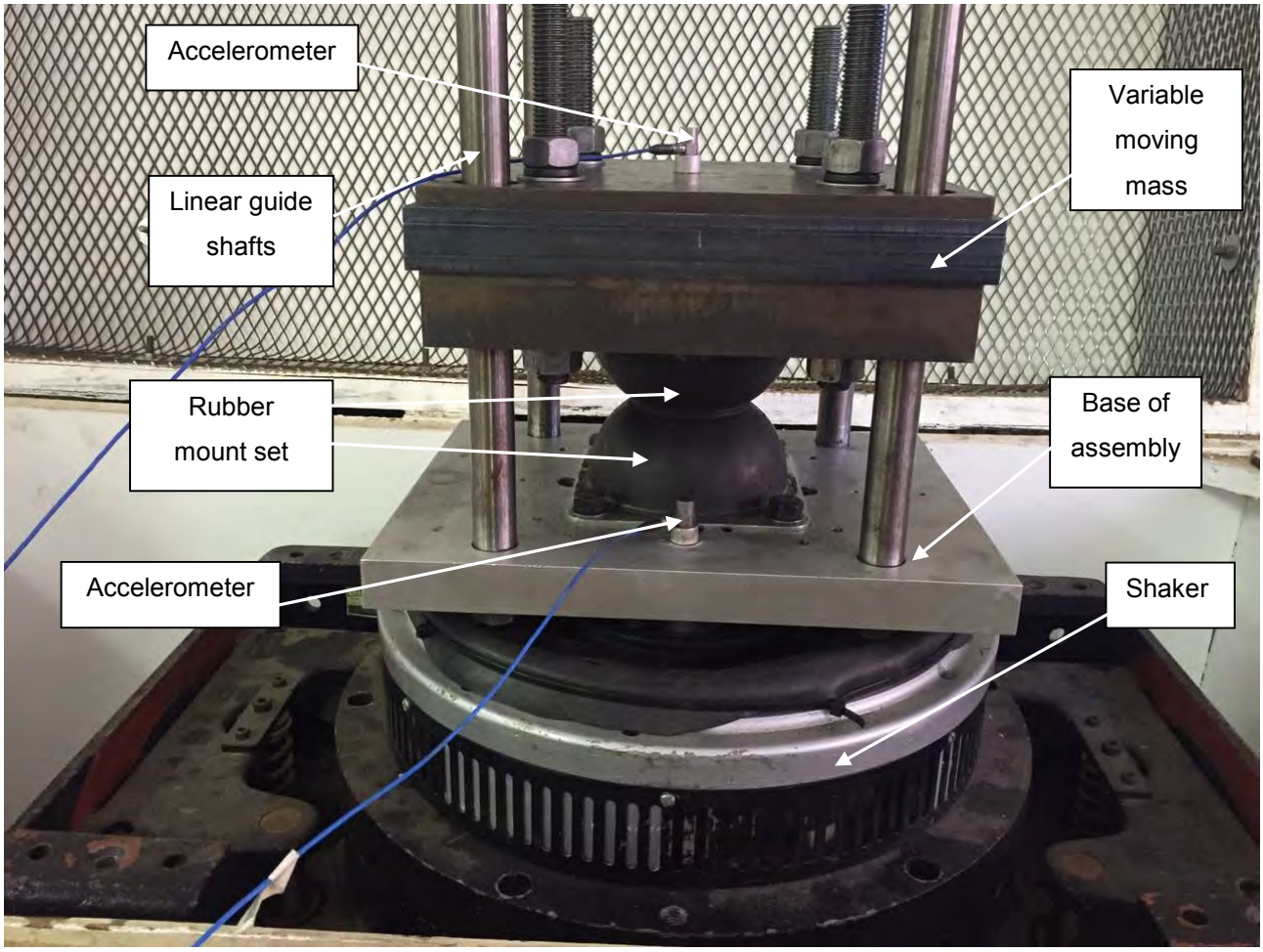

Figure 4.12: Shaker test setup

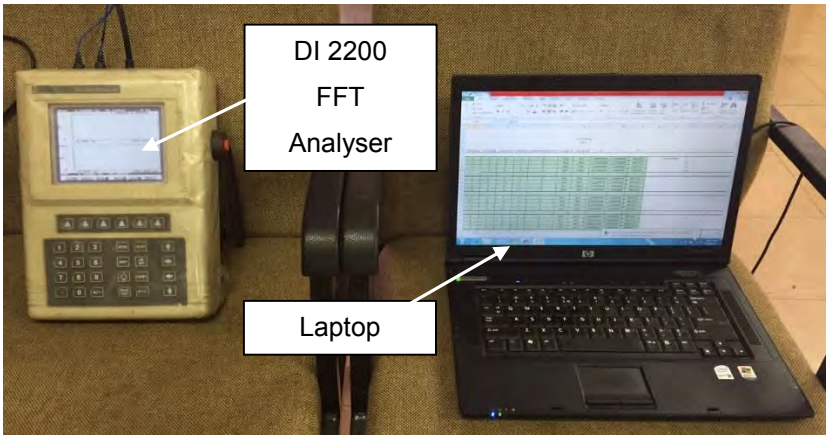

Figure 4.13: DI 2200 and Laptop computer

4.6.3 Experimental measurement procedure

The vertical dynamic properties of the rubber mount set were characterised for different excitation amplitudes as well as different preload conditions. This allowed both preload and amplitude dependency to be investigated. The excitation amplitudes were varied between 0.1 and 1.4 mm and the preload varied between 30 and 70 kg for each excitation amplitude. This was chosen to provide for the different loading conditions (empty and fully-loaded screen). The preload was increased with the addition of different 8 mm thick steel plates of approximately 5 kg each at the test assembly. These plates were successively bolted with four 20 mm diameter threaded rods and nuts. Calculations were done to ensure that the threaded rods were stiff enough such that the mass can be regarded as rigid. The excitation amplitudes were varied with adjustments made at the SPC4 Signal Controller. All the tests were performed at a fixed frequency of 45 Hz. This frequency allowed the best results to avoid resonance regarding possible excitation of rotational modes at the test assembly. The dynamic properties of rubber mounts are not appreciably affected by frequency in the low frequency range between 5 and 50 Hz (Nel, 2000). Although the test frequency is slightly larger compared to the operational frequency of approximately 24.5 Hz at the vibration screen, it was thus regarded as valid, because it is in this low frequency range.

Two 100 mV/g PCB accelerometers were attached to the base and the moving mass of the test assembly. The time and frequency domain signals for each preload condition and excitation amplitude were recorded at the Diagnostic Instruments 2200 FFT Analyser. These measured signals were then downloaded to a laptop. This measured data was then used by a computer program as described in Chapter 3, Paragraph 3.4.1, with the program code included in Appendix A. This program as implemented in a Matlab environment was used for computations, in order to determine the mount set stiffness and damping properties. This program was also used to filter out the noise at the measured signals generated at 50 Hz by the electrodynamic Shaker. Assembly drawings of the test assembly are shown in Figures 4.14 and 4.15.

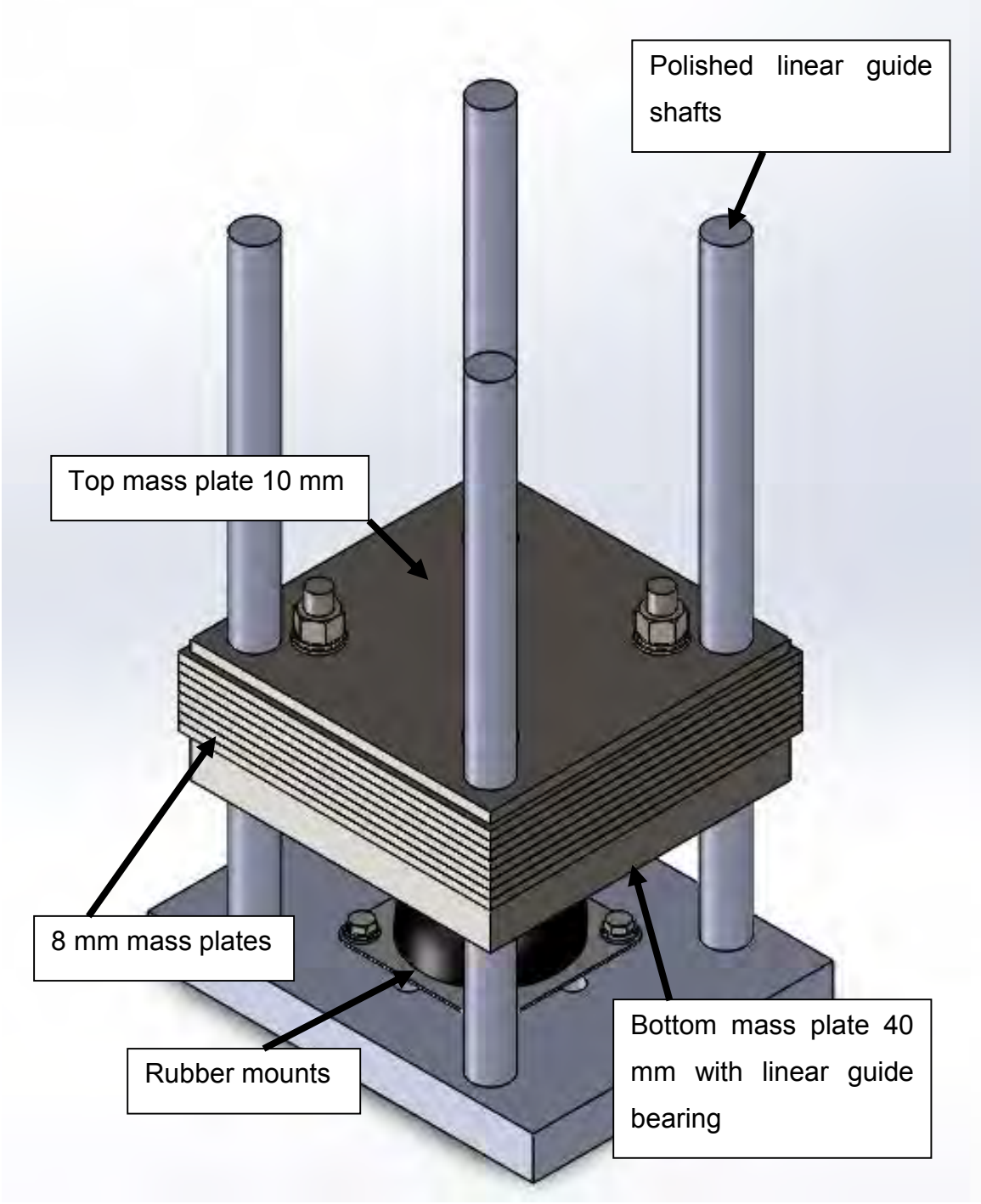

Figure 4.14: Test assembly for mount characterisation

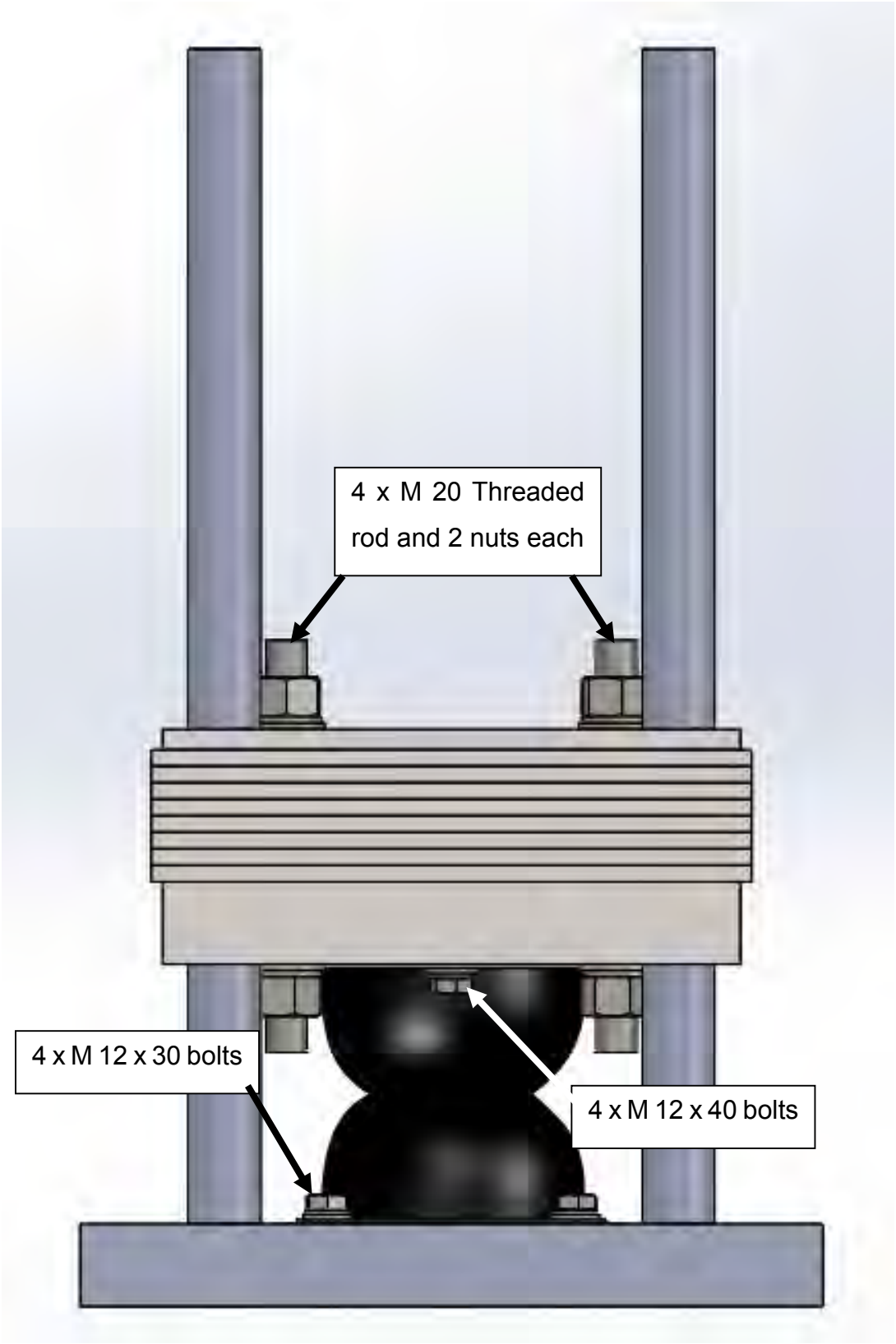

Figure 4.15: Test assembly for mount characterisation

4.6.4 Results of mount vertical stiffness and damping properties with Shaker tests

Figures 4.16 and 4.17 show the two simultaneously measured and filtered time domain signals respectively with 30 kg preload and also 0.1 mm relative excitation amplitude. It should be kept in mind that this is an example of one measurement condition, thus one point at Figures 4.18 and 4.19 respectively. The computer program as described in Paragraph 3.4.1 then converted this measured time domain data into corresponding frequency domain signals, with phase angles. These Fourier coefficients (peak amplitude at corresponding frequency and phase angle) of the measured signals are shown graphically in Figure 4.17. The dynamic stiffness and damping coefficients were then computed with this data. Similar computations were done for all the other measurement conditions, thus for all the points as indicated in Figures 4.18 and 4.19 respectively.

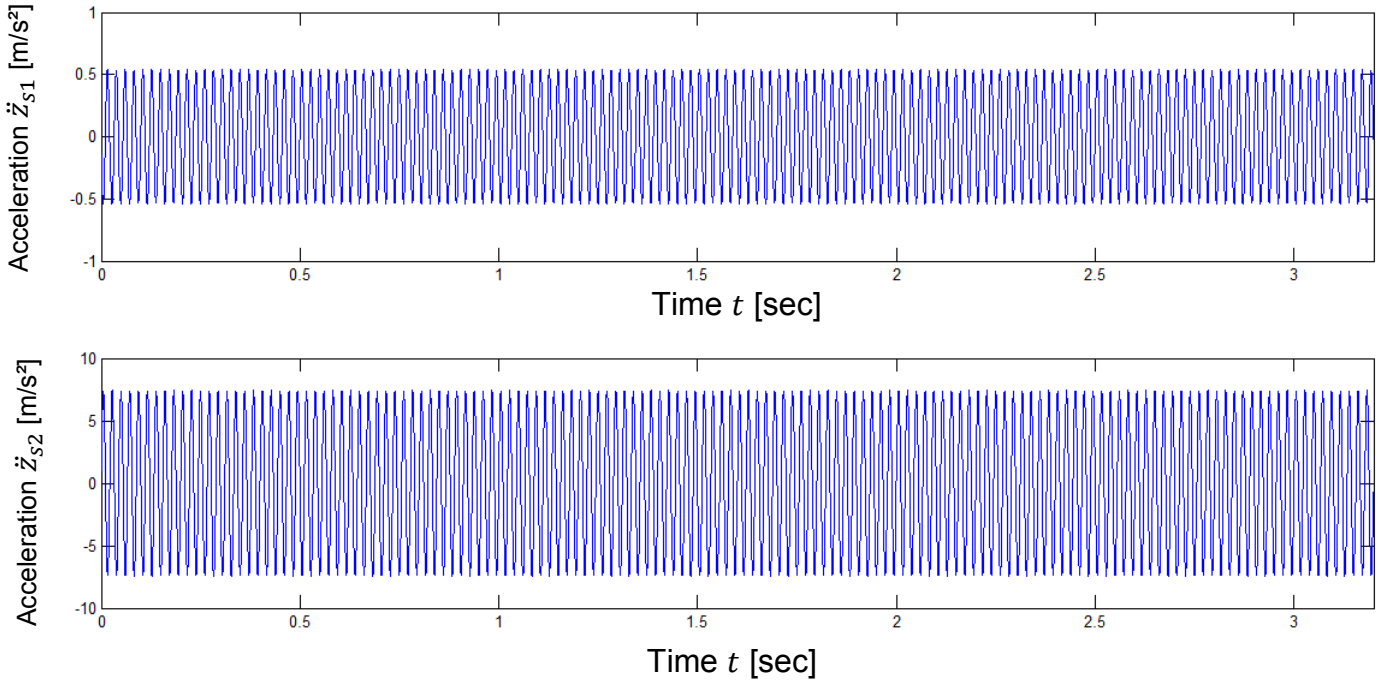

Figure 4.16: Filtered time domain acceleration signals

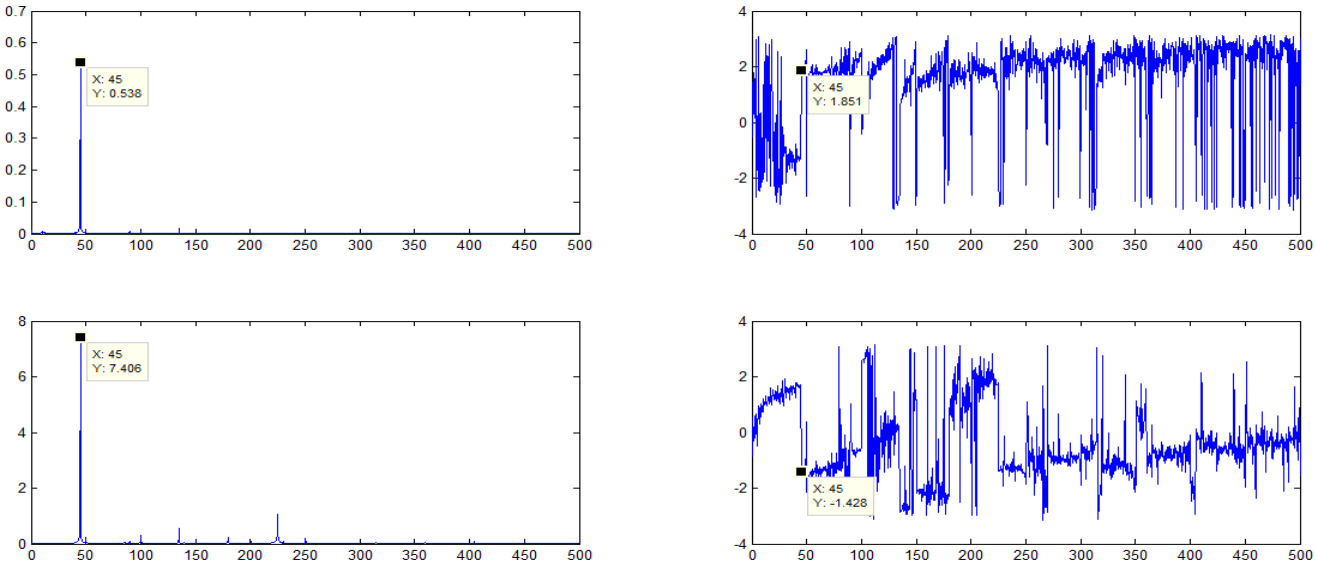

Figure 4.17: Graphic representation of Fourier coefficients

The graphs in Figures 4.18 and 4.19 show graphic representations of the mount dynamic properties as characterised. The dynamic properties were computed with the Matlab program as described in Chapter 3, Paragraph 3.4.1.

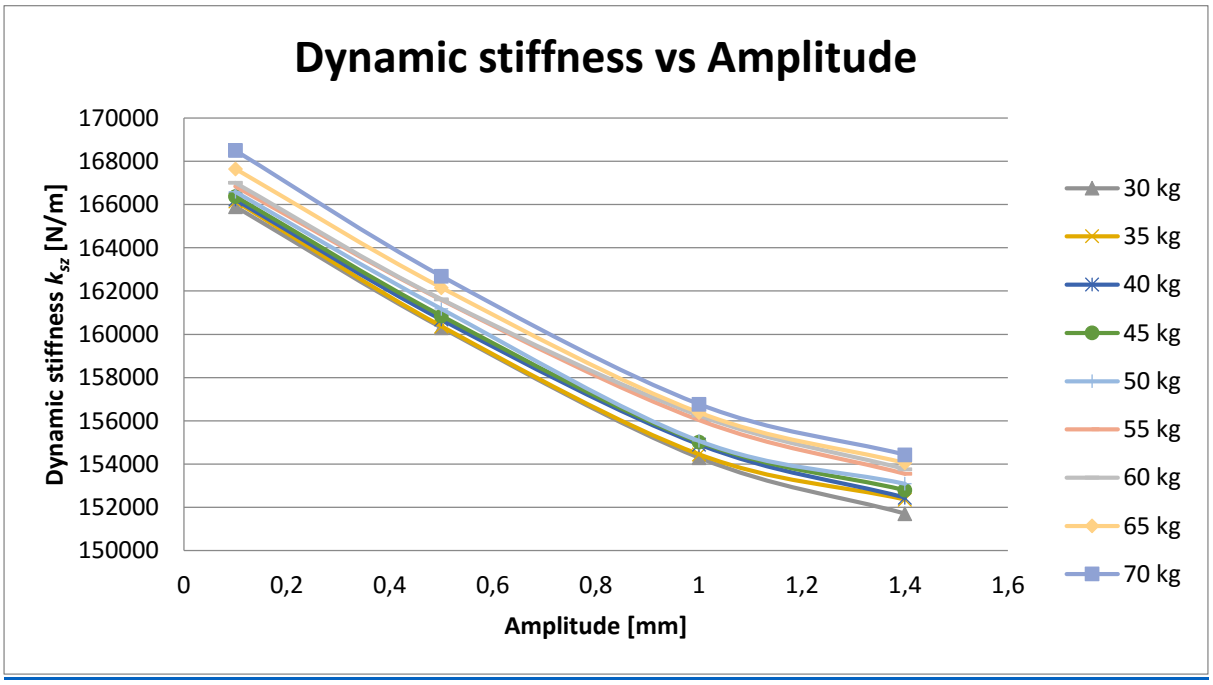

Figure 4.18: Measured vertical dynamic stiffness

Figure 4.18 shows a graphic representation of the rubber mount dynamic stiffness k_{sz} obtained from the different Shaker tests performed. The graph shows that the dynamic stiffness is a maximum for the lowest excitation amplitude of 0.1 mm and also with largest preload of 70 kg. For all the different preload conditions, the dynamic stiffness magnitudes decreased with an increase in excitation amplitude. Strong amplitude dependency was obtained for this 0.1 to 1 mm amplitude range, with a smaller amplitude dependency between 1 to 1.4 mm. The dynamic stiffness also increased slightly with an increase in preload. The maximum dynamic stiffness as characterised is approximately 15 % larger than the nominal stiffness value at 145 000 N/m obtained from the mount supplier. The lowest dynamic stiffness as characterised is approximately 5% higher than the corresponding magnitude obtained from the mount supplier.

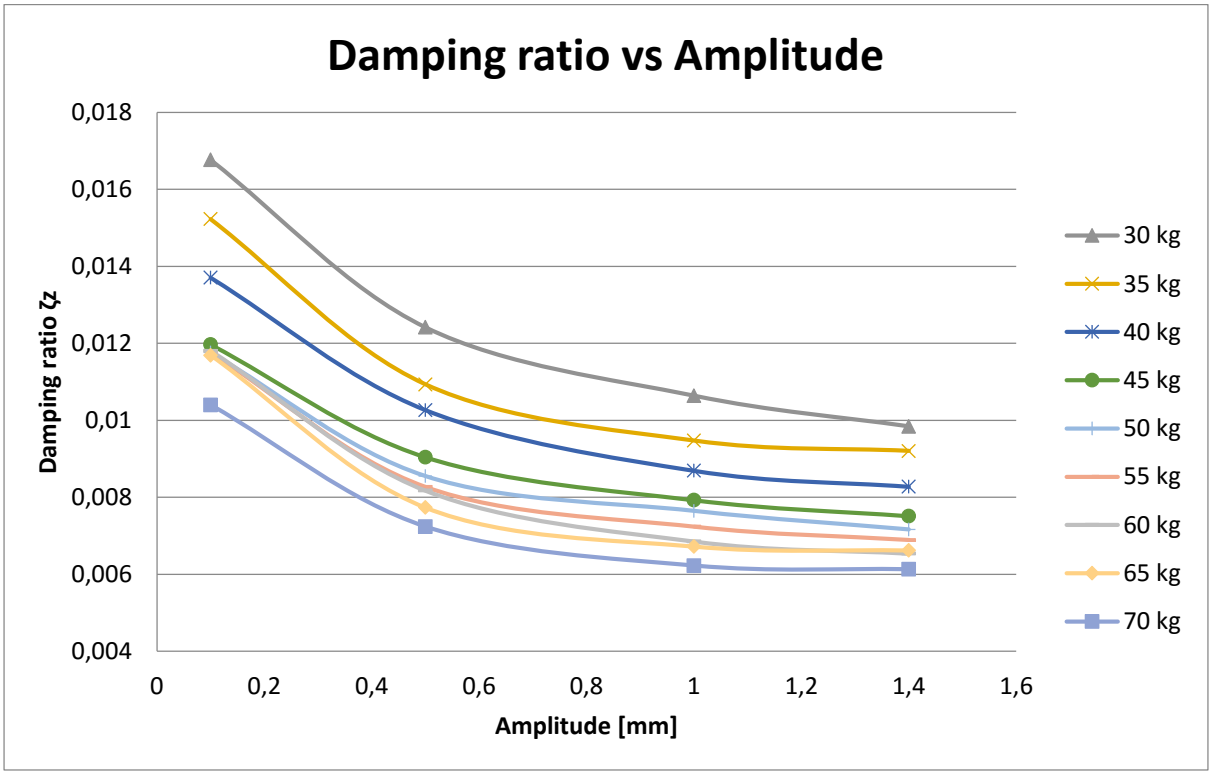

Figure 4.19: Measured vertical damping properties

A graphic representation of the damping ratio ζ_z is shown in Figure 4.19. Low magnitudes for damping ratio were obtained. The damping ratio is a maximum for the smallest excitation amplitude of 0.1 mm and also with smallest preload of 30 kg. The damping ratio decreased with an increase in preload and also an increase in excitation amplitude.

4.6.5 Vector representation of dynamic forces

As an example of one measurement condition, thus one point at Figures 4.18 and 4.19 respectively, the magnitudes of the dynamic forces and the phase angle ϕ were computed with the output from the computer program described in Paragraph 3.4.1. The force magnitudes and phase angle were then used to construct a vector diagram as shown in Figure 4.20. This vector diagram comprises the four different dynamic force vectors and the phase angle ϕ for a 30 kg preload with 0.1 mm excitation amplitude (see also Chapter 2, Equation 2.28). Similar vector diagrams were constructed for all the other measurement conditions, thus for all the points as indicated in Figures 4.18 and 4.19 respectively. These dynamic forces which are in equilibrium proved the validity of the mathematical model.

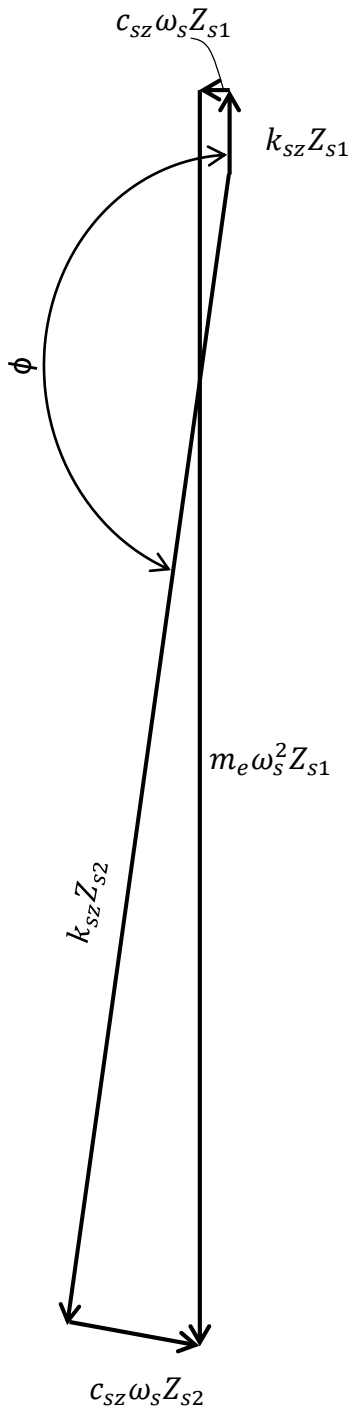

Figure 4.20: Vector representation of dynamic force amplitudes and phase angle ϕ

4.6.6 Results of mount horizontal stiffness and damping properties with Bump tests

The horizontal dynamic properties were characterised *in situ* at the screen with a Bump test approach. The computer program used for computations is described in Paragraph 3.4.2. The vibration screen was loaded with 65 kg of maize, and a Bump test then done. An impact load was applied and response signals then recorded with a Diagnostics Instruments 2200 FFT Analyser as shown in Figure 4.22. The mass of the maize was measured with a load cell connected to an Amplifier as described in Paragraph 4.7.

Figure 4.21: Maize mass (65 kg) measurement

Figure 4.22: Bump test approach *in situ* for horizontal dynamic properties

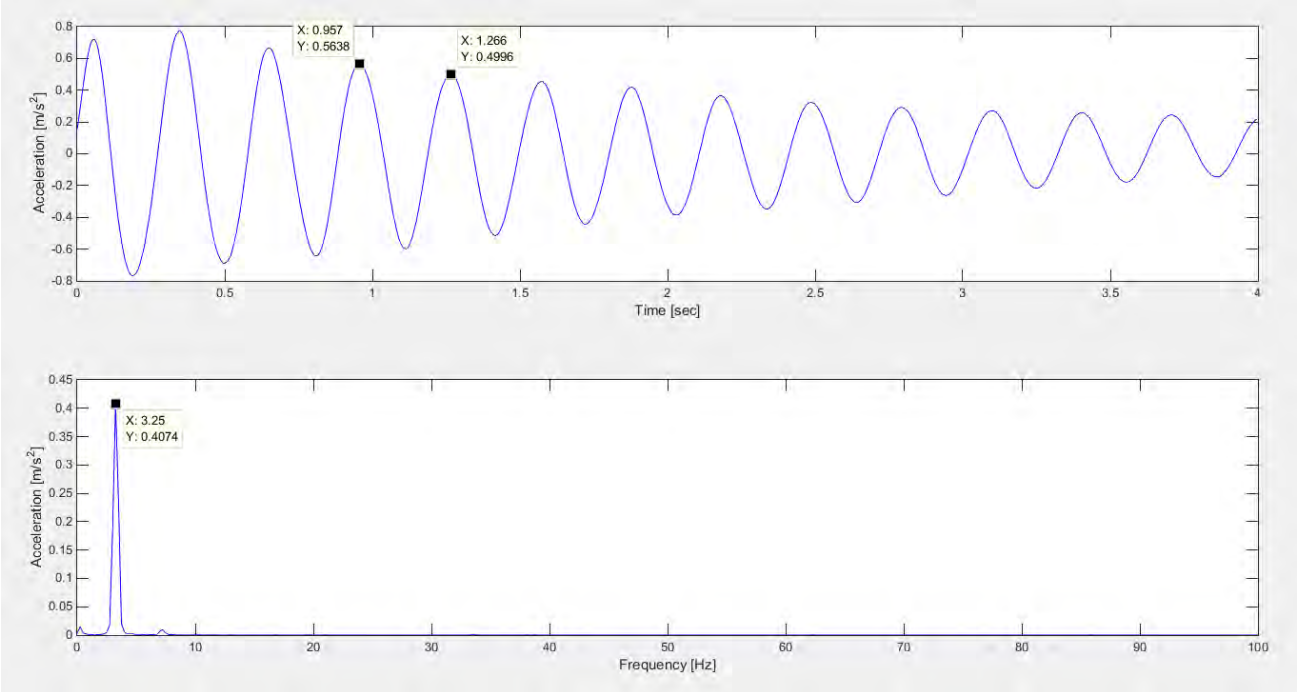

Figure 4.23: Bump test time and frequency domain acceleration signals

The time and frequency domain signals of the Bump test are shown in Figure 4.23. The Matlab program as described in Paragraph 3.4.2 (see also Appendix A) was used to compute the dynamic stiffness coefficient, damping coefficient, and damping ratio. For one typical screen mount the dynamic stiffness $k_{x1} = k_{x2}$ was computed as 67 600 N/m, and damping ratio ζ_x computed as 1.9 %. The damping coefficient $c_{x1} = c_{x2}$ was determined as 127.9 Ns/m. The equivalent horizontal dynamic stiffness coefficient specified by the supplier is 80 000 N/m, which is in the same range compared to the measured magnitude. The difference between these values as observed could be caused by different preload conditions.

4.7 Static stiffness

The same mass plates and test assembly as described in Paragraph 3.6.3 were used for static tests. The static stiffness was then characterised. A clock gauge was used to measure deflections for corresponding static loads applied. The mass plates were successively added to allow different static loads applied. Figure 4.24 shows the load vs deflection graph as obtained for the load range tested. The average static stiffness of the mount was then determined as 125 300 N/m with the measured data. The nominal static stiffness as obtained from the supplier was 100 000 N/m. The static stiffness is also approximately 30% lower compared to the maximum dynamic stiffness (see Figure 4.18).

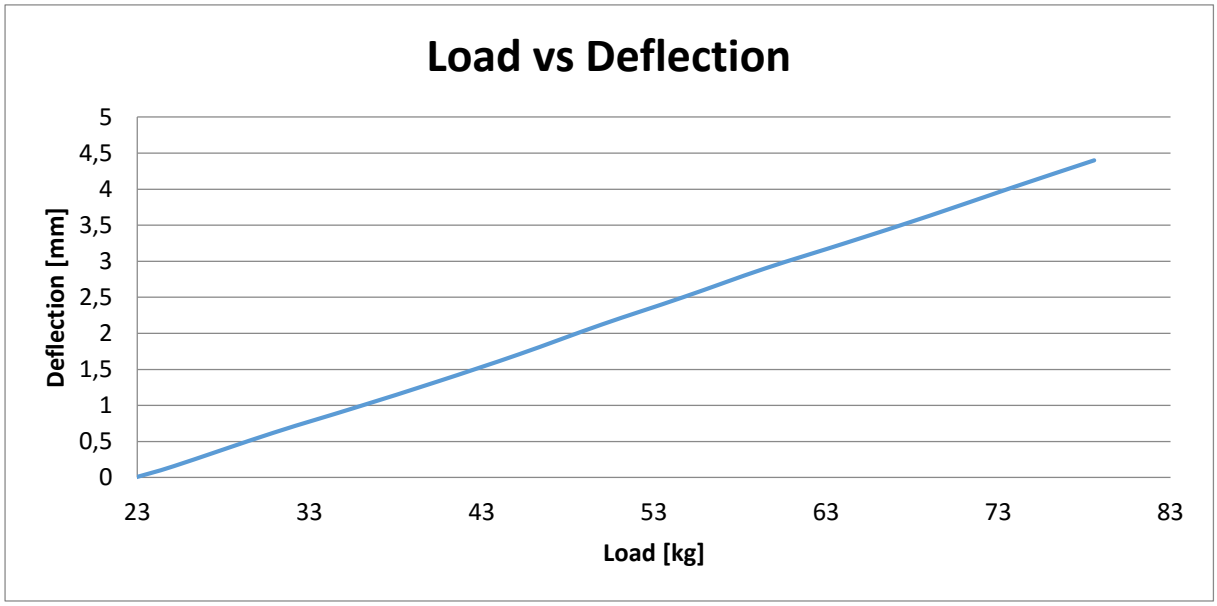

Figure 4.24: Load vs deflection graph for static stiffness

4.8 Vibration screen mass

The mass of the vibration screen was characterised with the use of a load cell coupled to an Amplifier. The Amplifier was connected to a computer through a USB port. A Matlab program (see Appendix A) was written which provided a visual readout on the laptop. The vibration screen was lifted by a hydraulic jack with the load cell attached. Figure 4.25 shows the vibration screen in the lifted position.

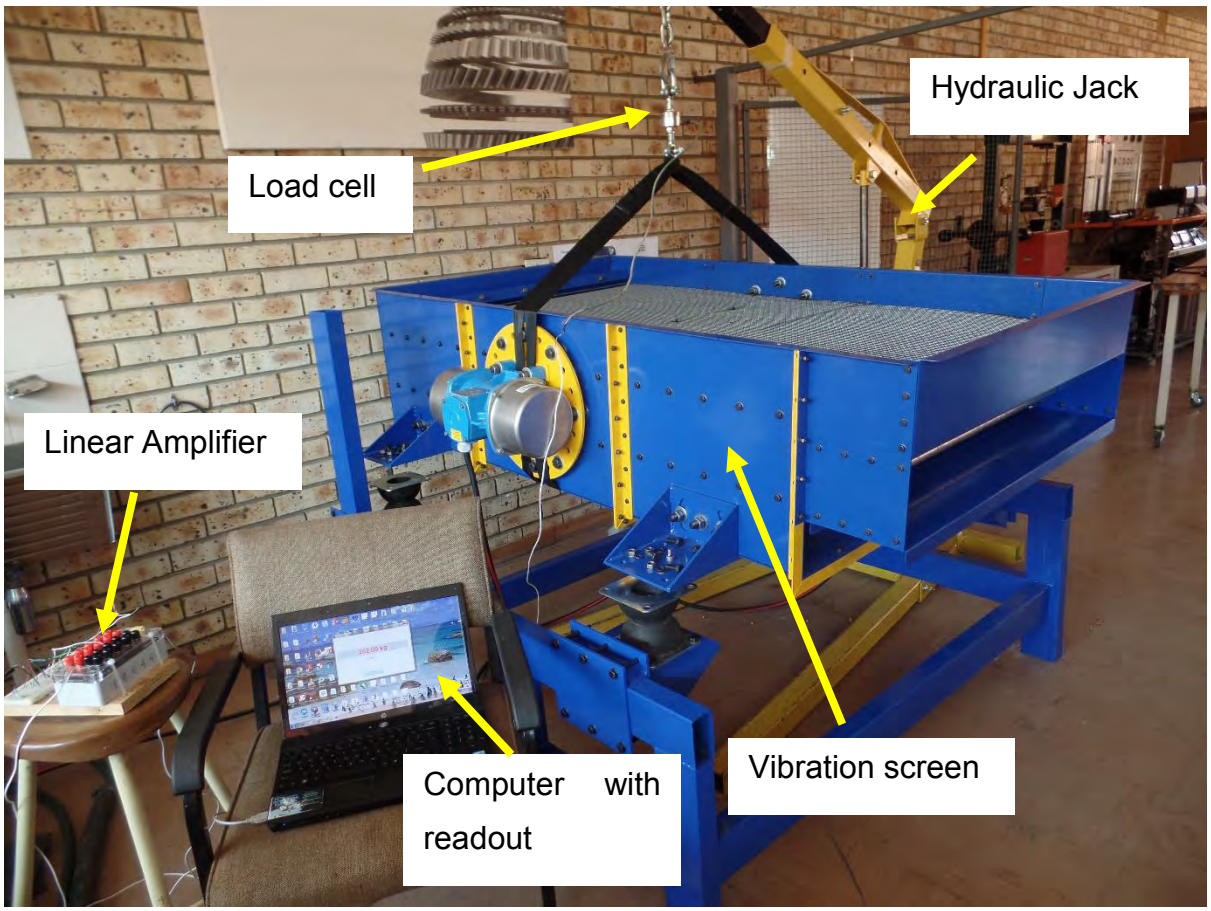

Figure 4.25: Empty mass of vibration screen

The mass of the empty vibration screen was measured as 262 kg, which was almost the same as the corresponding magnitude determined by Solidworks. The radius of gyration about the y axis (see also Figure 2.1) of the screen was then determined with Solidworks as 0.49 m based on the measured mass. The Mass Moment of Inertia of the screen about the y axis (see also Figure 2.1) was then computed and is 62.9 kgm^2 for the empty screen based on the measured mass. The Mass Moment of Inertia of the fully loaded screen about the y axis (see also Figure 2.1) was then also computed and is 78.5 kgm^2.

4.9 Exciter motor power and shaking force magnitudes

Two exciter motors are required to obtain linear motion at the vibration screen (see also Chapter 1, Paragraph 1.3.5). The shaking force was produced by two identical exciter motors mounted on opposite sides of the vibration screen structure. The two motors rotate in opposite directions relative to each other which then produce no resultant force in the y direction as a result (see also Figure 2.1). The required dynamic force amplitude of the two exciter motors was computed to provide a steady state displacement amplitude of 1.4 mm for a fully loaded screen. This was done with the computer program described in Chapter 3, Paragraph 3.2 (see also Appendix A). This dynamic force magnitude was then used to select standard exciter motors capable to produce the force with a safety factor of 1.5. Two Venanzetti VV30B/4 exciter motors were chosen for this design. These motors operate at 25 Hz (4 Pole) and can deliver a maximum shaking force of 7.36 kN each. The technical specifications of these motors are listed in Appendix C. The shaking force of an exciter motor could be changed by the adjustment of two unbalanced masses located on the shafts at opposite sides of the rotor. Increments at 5% each can be used for accurate shaking force magnitude adjustments. Figure 4.26 shows one of the exciter motors mounted on the side of the screen, but with the protection caps here removed. Figure 4.27 shows the unbalance masses currently set at 65 % that provide a total resultant force of about 9.57 kN for both motors simultaneously. The operational force at each unbalance setting could thus be easily obtained as the product of the percentage setting and the maximum force.

Figure 4.26: Exciter motor with protection caps removed

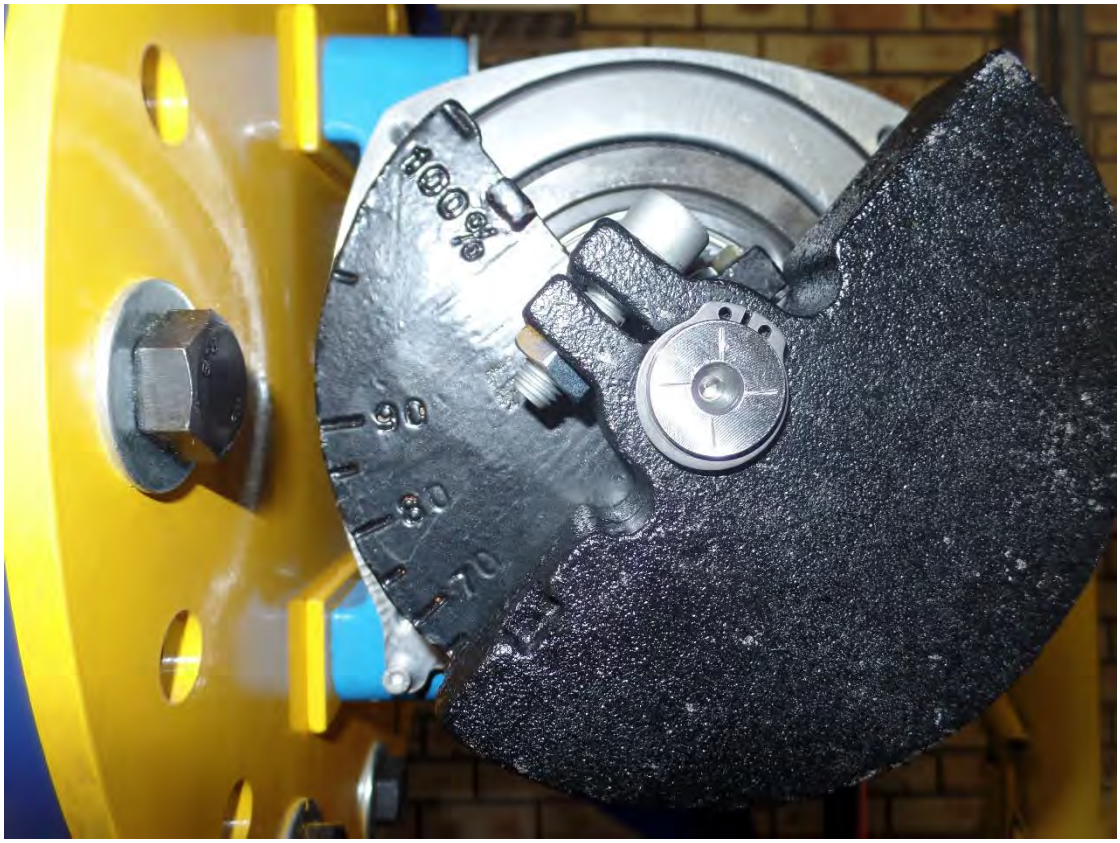

Figure 4.27: Exciter motor unbalance mass with percentage setting

4.10 Vibration screen angle and angle of attachment of exciter motors

The angle of the vibration screen α and also the angle of attachment β of the exciter motors were designed to be adjustable. The vibration screen angle can be adjusted from -5^0 (uphill sieving) to $+30^0$ (downhill sieving). Figure 4.28 shows the angle of the vibration screen currently set to 5^0 downhill. The exciter motor angle can be adjusted through 360^0 with increments of 18^0. The angle of attachment of the exciter motors to the screen is currently set at 0^0. The angle adjustments are illustrated in Figure 4.28. With the angle of the vibration screen set at 5 degrees downhill, a horizontal force component provided by the exciter motors and transmitted to the screen was obtained. This was experimentally determined to allow sufficient flow rate of maize through the screen.

Figure 4.28: Vibration screen and exciter motor attachment angle adjustments

4.11 Conclusions

The required sieving amplitude for effective sieving of maize was determined with an electrodynamic Shaker. The average typical dimensions and density of maize kernels were characterised. The dynamic vertical properties of the rubber mounts were successfully characterised with an electrodynamic Shaker approach and the values corresponded well to magnitudes obtained from the supplier. The Shaker tests showed that the mount dynamic properties are dependent on both amplitude and static preload. The horizontal dynamic properties of the rubber mounts were successfully characterised *in situ* at the screen with a Bump test approach, and is in the same range compared to the magnitude obtained from the supplier. The exciter motor force magnitude, vibration screen mass, screen sieving angle and the angle of attachment of the exciter motors were successfully characterised. The next Chapter describes the optimisation of the screen.

5 Optimisation

5.1 Introduction

This chapter describes the process followed to determine the optimal dynamic stiffness properties for the rubber mounts of the screen chosen as design variables. The optimisation criteria are described and an objective function is defined. A Finite Element Analysis is also included in this chapter and it was regarded as necessary to evaluate the screen structural stiffness and fatigue life.

5.2 Optimisation criteria

As criteria for vibration isolation, a similar, but more simplified objective function based on the sum of dynamic forces transmitted to the foundation through all the mounts as formulated (Heyns et al., 1994; Nel, 2000; Nel, 2007; Nel, 2009) is here defined. The simplified objective function is

$$F_T = \sqrt{(k_{x1}\Delta X_1)^2 + (c_{x1}\omega\Delta X_1)^2} + \sqrt{(k_{x2}\Delta X_2)^2 + (c_{x2}\omega\Delta X_2)^2} + \sqrt{(k_{z1}\Delta Z_1)^2 + (c_{z1}\omega\Delta Z_1)^2} + \sqrt{(k_{z2}\Delta Z_2)^2 + (c_{z2}\omega\Delta Z_2)^2} \quad (5.1)$$

where F_T represents the combined amplitude based on all the dynamic forces transmitted to the foundation, with a similar force amplitude transmitted back into the screen structure. The objective function is thus related to vertical and horizontal mount stiffness and damping coefficients, and also to screen responses at the mounts, in both the vertical and horizontal directions. Each of these parameters is explained and included in the mathematical model as described in Chapter 2, Paragraph 2.2. A single magnitude of the objective function F_T could be used as an indication of vibration isolation obtained, and is clearly dependent on mount stiffness properties chosen as the design variables. The better the vibration isolation, the smaller the magnitude of the objective function.

It is required to minimize F_T with respect to the design variables, subject to certain inequality constraints. The first constraint

$$w_1 = (\Delta Z_1 + \Delta Z_2)/2 - \Delta Z_c \geq 0 \tag{5.2}$$

involves the required minimum dynamic steady state vertical translational displacement amplitude of the vibration screen, expressed here in terms of the average of the two vertical mount responses ΔZ_1 and ΔZ_2 at Mount 1 and Mount 2 respectively (see also Figure 2.1). The specified required movement of the screen as an amplitude ΔZ_c and is regarded necessary to insure effective sieving in order to remove unwanted material.

The second constraint equation involves maximum allowable translational displacement of the vibration screen. This constraint

$$w_2 = |\Delta \mathrm{U_s} + \max(\Delta \mathrm{U_d})| - \Delta \mathrm{U_c} \leq 0 \tag{5.3}$$

where ΔU_s and ΔU_d represents the static and dynamic translational displacement matrices of the two screen mounts respectively. The dynamic displacement amplitude of the element in the dynamic matrix must be in the same direction as the static displacement amplitude of the corresponding element in the static displacement matrix. The maximum allowable translational mount displacement matrix is represented by ΔU_c that could be specified.

The static displacement matrix is

$$\Delta U_s = \begin{bmatrix} \Delta X_{01} \\ \Delta X_{02} \\ \Delta Z_{01} \\ \Delta Z_{02} \end{bmatrix}$$

and the dynamic displacement matrix is

$$\Delta U_d = \begin{bmatrix} \Delta X_1 \\ \Delta X_2 \\ \Delta Z_1 \\ \Delta Z_2 \end{bmatrix}$$

The equations for the objective function and the two different constraints were also implemented in the computer program described in Chapter 3, Paragraph 3.2, and they form then part of the three degree of freedom mathematical model described in Chapter 2, Paragraph 2.2.

5.3 Graphic optimisation

A graphic optimisation approach was used to identify feasible design regions regarding vertical and horizontal mount stiffness coefficients. The extensive graphic capabilities of Matlab were used to construct three-dimensional graphs of different parameters as a function of vertical and horizontal mount stiffness coefficients. Most of the parameters characterised as described in Chapter 4 were used in the computer program as described in Chapter 3, Paragraph 3.2 to solve equations of motion as described in Chapter 2, Paragraph 2.2. This entailed a numerical integration procedure as described in Chapter 3, Paragraph 3.2, and as a result screen mount responses computed for different rubber screen mount stiffness coefficients used as input parameters. The magnitudes of the objective function and the two different constraints were then also computed by this computer program. It is assumed that the vertical and horizontal mount stiffness coefficients are the same for the two screen mounts respectively, thus with Mount 1 and Mount 2 identical (see Figure 2.1).

Figure 5.1 shows the graphical representation for different objective function magnitudes computed by Equation (5.1) for steady state behaviour, and plotted as a function of the vertical and horizontal stiffness of a screen mount. It should be kept in mind that the unbalance force provided by the exciter motors are constant at all the different graphs used here for optimisation.

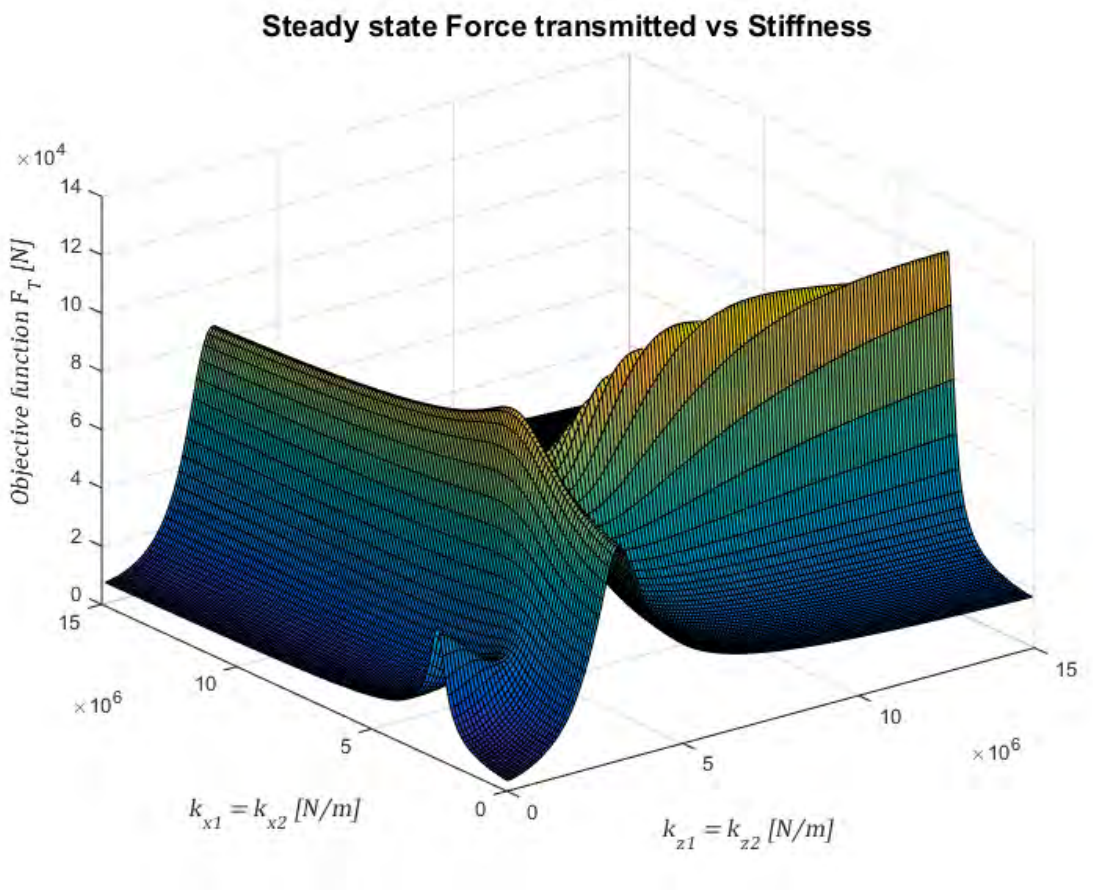

Figure 5.1: Steady state force transmitted vs stiffness

Figure 5.1 clearly indicates that both the vertical and horizontal mount stiffness coefficients play a major role in the magnitude of the objective function. As an alternative view, a contour plot as top view of Figure 5.1 was constructed as graph shown in Figure 5.2.

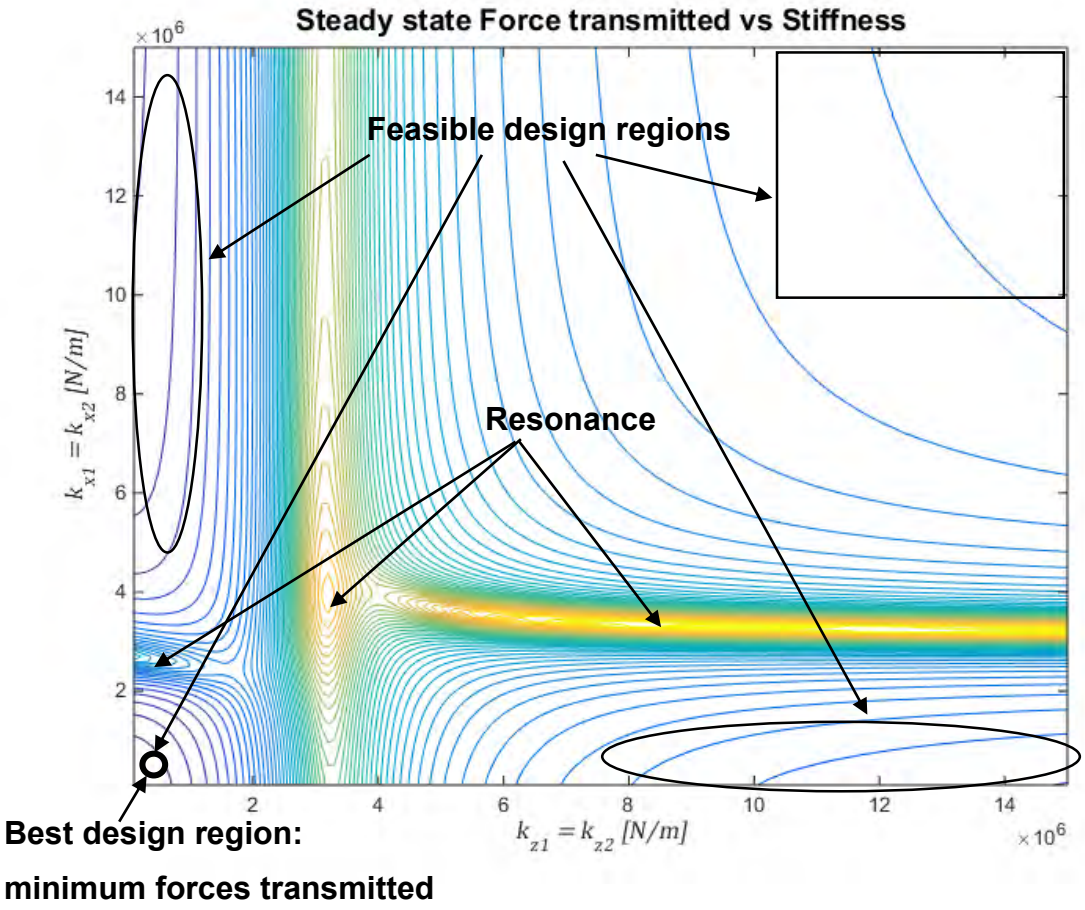

Figure 5.2: Steady state forces transmitted vs stiffness – contour plot

Figures 5.1 and 5.2 show that both the horizontal and vertical stiffness of the mounts have an enormous influence on the magnitude of the objective function. An interesting observation was made, because the higher peaks at these graphs correspond to resonance, with one or more of the three modes excited.

The same process was followed to compute the values for the objective function during transient conditions (starting and stopping), and similar graphs as Figures 5.1 and 5.2 were obtained, but with larger objective function magnitudes.

Figure 5.3 shows the average dynamic vertical mount displacement amplitudes computed for steady state behaviour, and plotted as a function of the vertical and horizontal stiffness of a screen mount.

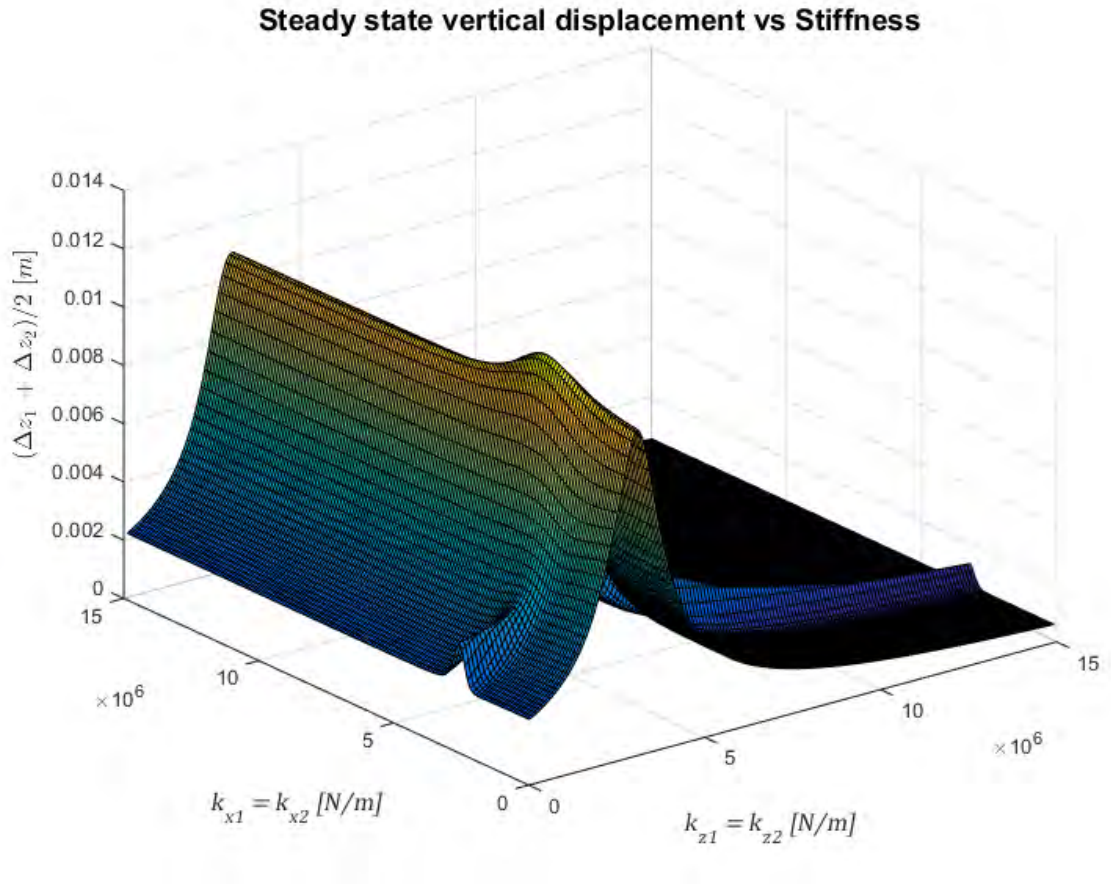

Figure 5.3: Steady state average vertical displacement vs stiffness

The choice of horizontal and vertical stiffness coefficients is critical to ensure acceptable movement of the screen for effective sieving, with feasible design regions clearly observed in Figure 5.3. With reference to Chapter 4, an amplitude of 1.4 mm at 25 Hz for the screen was determined in order to effectively remove the unwanted particles from the maize kernels. As an alternative view, a contour plot as top view of Figure 5.3 was constructed as graph shown in Figure 5.4.

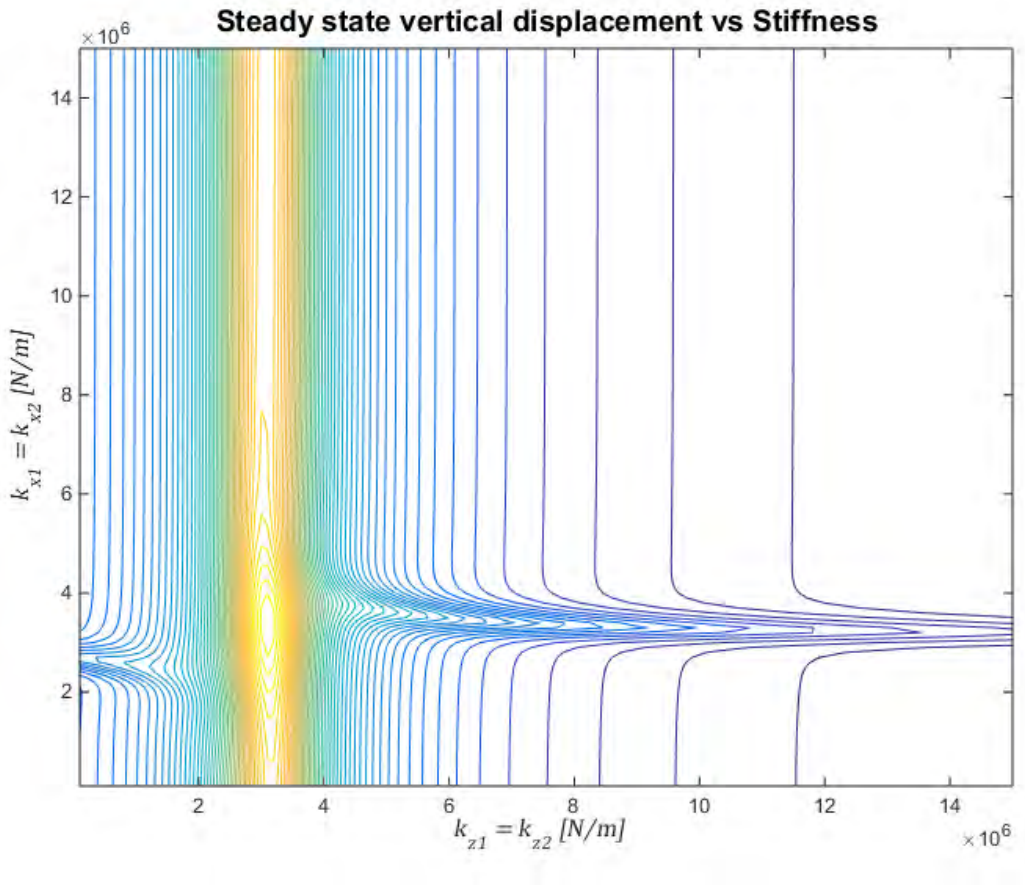

Figure 5.4: Steady state average displacement vs stiffness – contour plot

It is observed that the screen mount vertical displacement (sum of static and dynamic displacements) is significantly larger, compared to the screen mount horizontal displacement (sum of static and dynamic displacements) as expected. Figure 5.5 shows the maximum vertical displacement as the sum of static and dynamic displacements computed for transient behaviour (starting and stopping), and plotted as a function of the vertical and horizontal stiffness of a screen mount. This was regarded necessary because the movements are significantly larger during transient behaviour, compared to steady state behaviour. A maximum allowable vertical displacement (sum of static and dynamic displacements) of 20 mm for the screen was specified and used at one of the constraints in the optimisation approach (see Equation (5.3)).

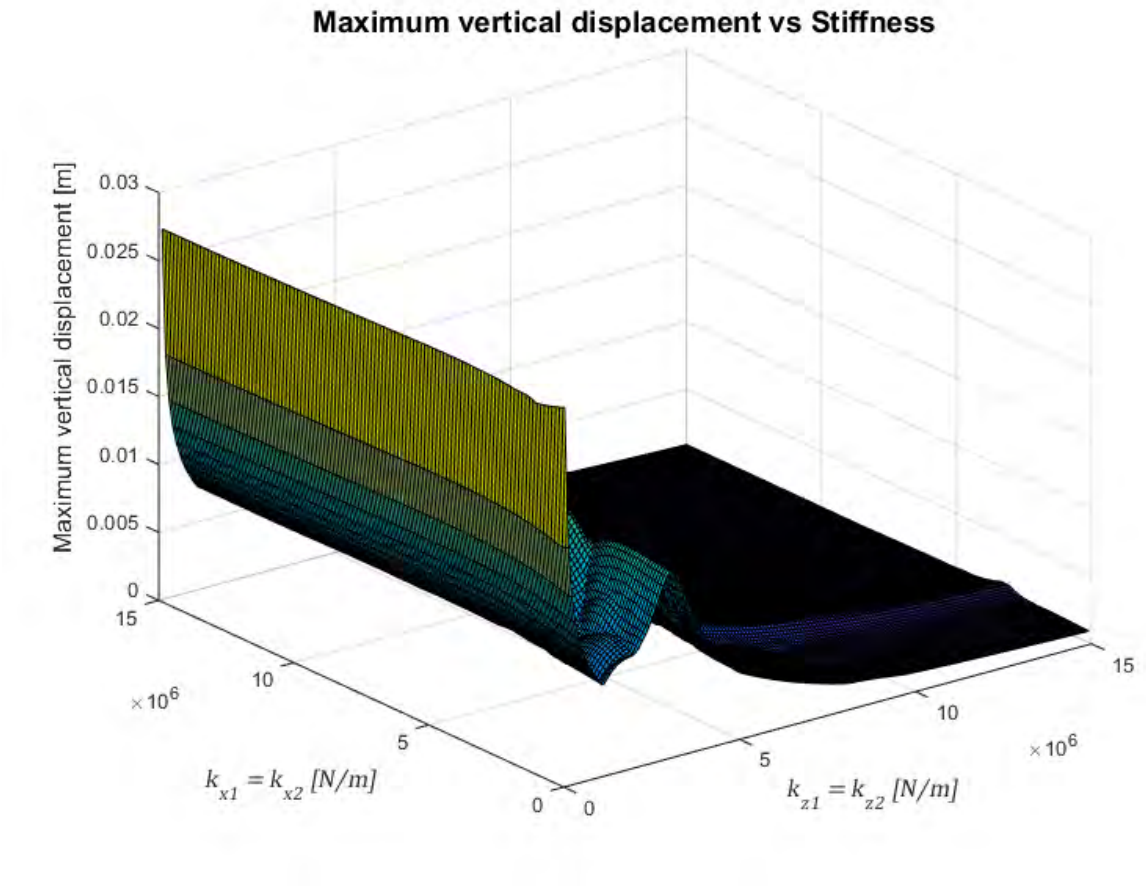

Figure 5.5: Maximum vertical displacement vs stiffness

The choice of horizontal and vertical stiffness coefficients is also critical to ensure that a screen mount can withstand the maximum vertical displacement (sum of static and dynamic displacements) without failure, with feasible design regions clearly observed

in Figure 5.5. This vertical displacement is thus a limit (constraint indicated in Equation (5.3)). As an alternative view, a contour plot as top view of Figure 5.5 was constructed as graph shown in Figure 5.6.

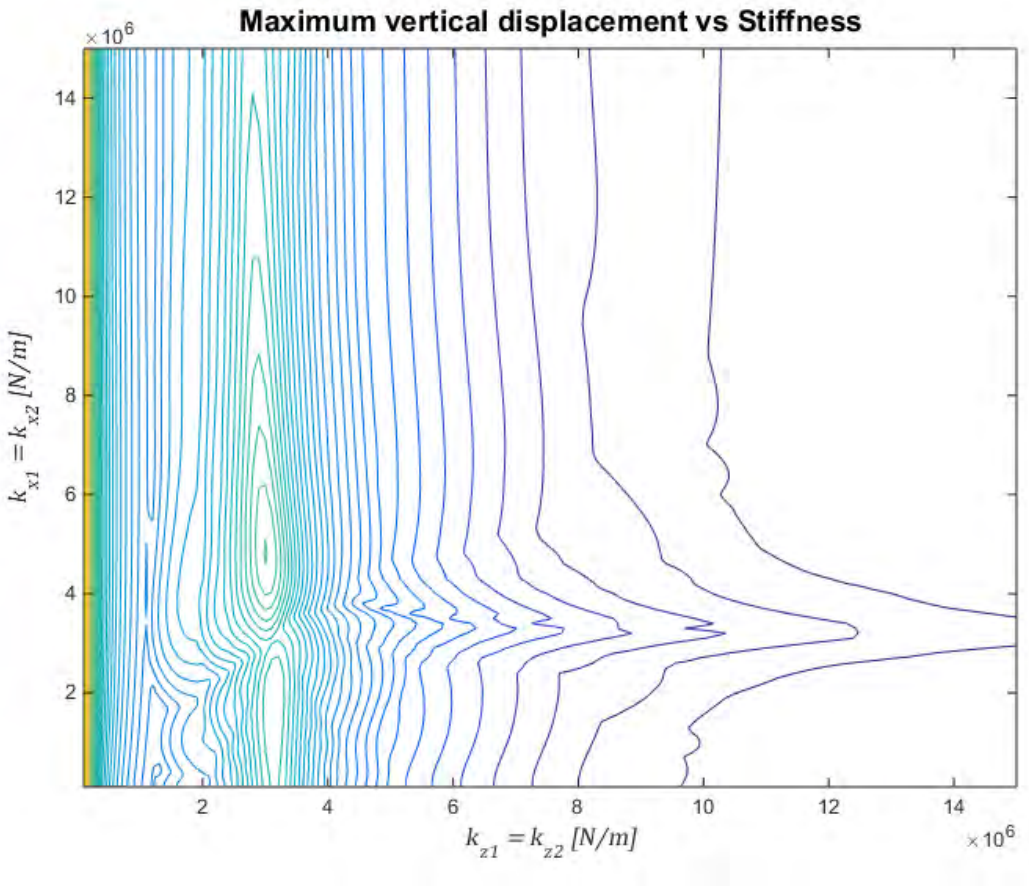

Figure 5.6: Maximum vertical displacement vs stiffness – contour plot

Figure 5.7 shows the maximum horizontal displacement as the sum of static and dynamic displacements computed for transient behaviour (starting and stopping), and plotted as a function of the vertical and horizontal stiffness of a screen mount.

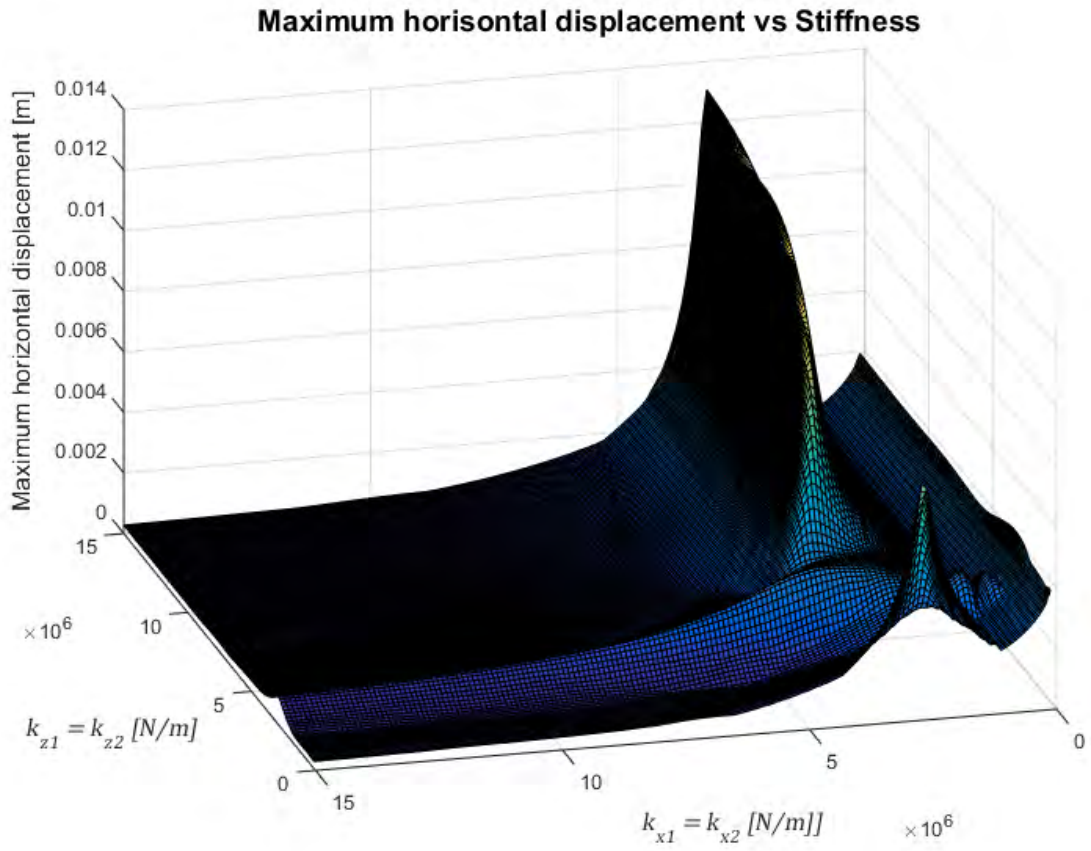

Figure 5.7: Maximum horizontal displacement vs stiffness

A maximum allowable horizontal displacement (sum of static and dynamic displacements) of 1.6 mm for the screen was specified and used as another constraint in the optimisation approach (see Equation (5.3)). This allowable displacement was chosen conservatively to make provision for possible adjustments of the exciter motor mount angle β to obtain a feasible maize flow rate. As an alternative view, a contour plot as top view of Figure 5.7 was constructed as graph shown in Figure 5.8.

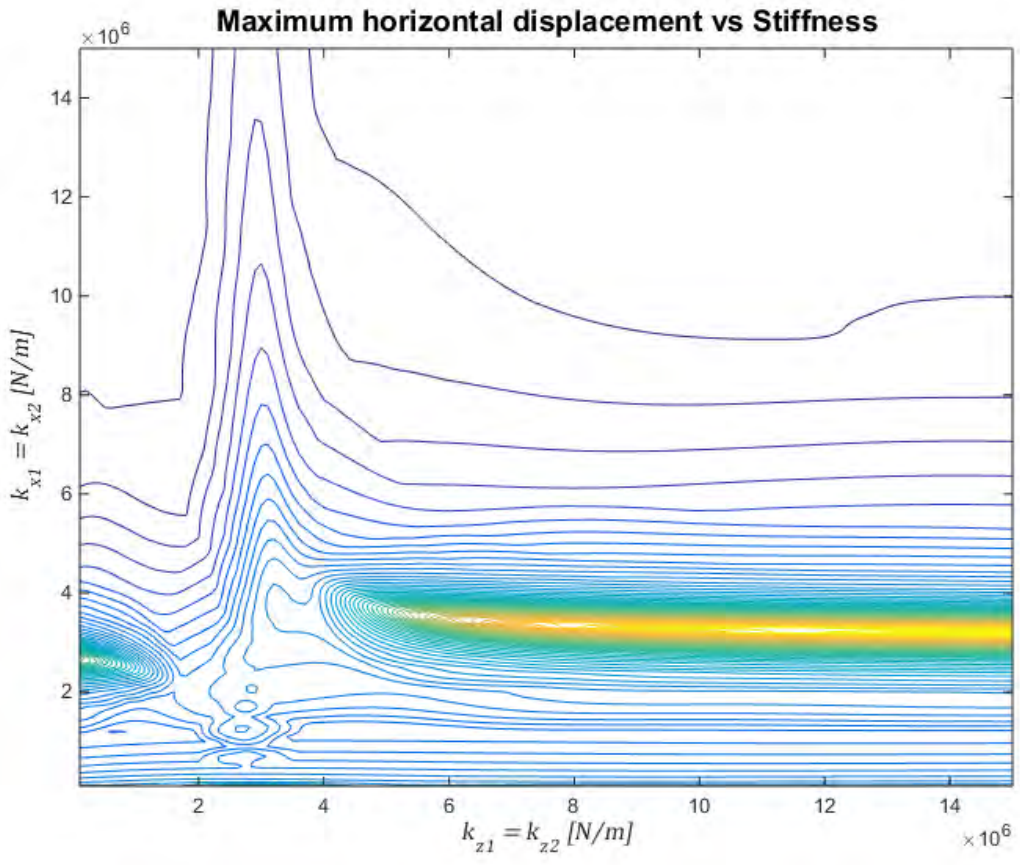

Figure 5.8: Maximum horizontal displacement vs stiffness – contour plot

It should be noted that for a close to vertical resonance design, a significantly smaller unbalance force could also provide the same vertical response as required for effective sieving, but this will however result in significantly larger vertical stiffness coefficients and therefore significantly larger dynamic forces transmitted. This clearly reveals that a resonance condition should be avoided during steady state conditions.

5.4 Optimisation process

The graphs in Paragraph 5.3 were used to determine ideal horizontal and vertical screen mount stiffness coefficients for feasible design regions. For stiffness coefficients chosen, three different design goals should be achieved namely:

- Reduced magnitude for the objective function based on the transmission of dynamic forces to the foundation, to achieve good vibration isolation and to provide a long fatigue service life (ideally infinite).
- Acceptable vertical steady state dynamic motion, to ensure effective sieving for removal of unwanted particles from the maize kernels.
- Limit the maximum vertical and horizontal screen mount displacements (sum of static and dynamic displacements) during the transient condition respectively, to avoid failure of the screen mounts. The horizontal allowable displacement should be chosen conservatively, to make provision for possible adjustments of the exciter motor mount angle β and screen angle α to obtain a feasible maize flow rate.

The contour graphs shown in Figures 5.2, 5.4 and 5.6 were used for the final decision regarding optimal stiffness coefficients. This was done by superimposing all four these different contour graphs. The final optimal design region was then identified to satisfy all three design goals simultaneously. It is clear that to achieve good vibration isolation, a compromise for best screen mount stiffness properties is obtained between two contradictory design goals as constraints, namely acceptable vertical dynamic motion and maximum vertical and horizontal screen mount displacement (sum of static and dynamic displacements). Figure 5.9 shows a contour plot as a graph similar to Figure 5.2, but the optimal design point here indicated, and with the superimposing of the other two contour plots, was also taken into account.

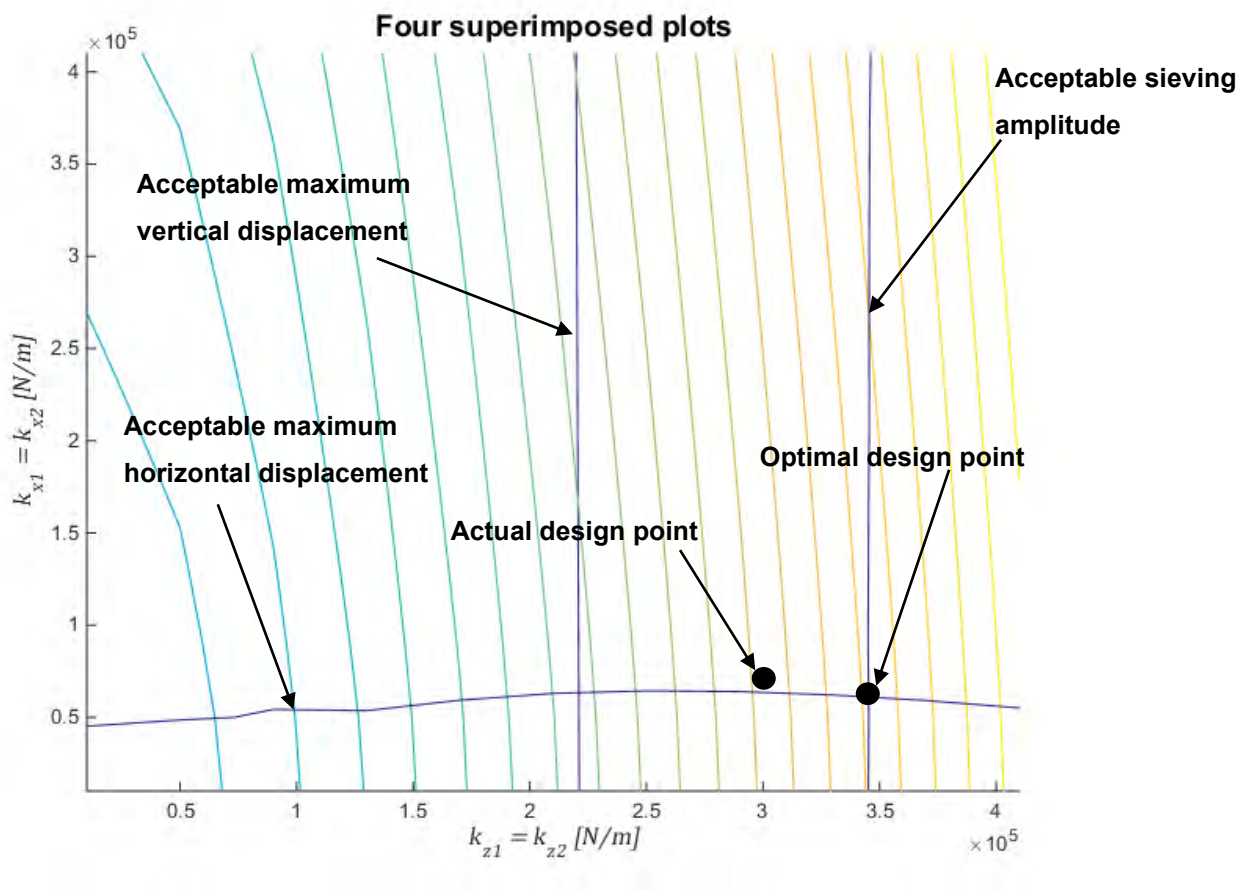

Figure 5.9: Four superimposed contour plots for the best design region

For this design, the optimal mount stiffness coefficients identified were used for the selection of standard rubber mounts that are commercially available. A single standard rubber mount as a screen mount within the required stiffness requirements could provide good vibration isolation, but resulted in the nominal displacement then being exceeded during transient behaviour at the screen. It was necessary for the combination of two standard rubber mounts to be arranged in series (a screen mount), which then closely provided the required horizontal and vertical screen mount stiffness coefficients. The nominal safe static vertical and horizontal displacement of a screen mount specified by the mount manufacturer is 27.4 mm and 32 mm respectively. This screen mount could thus withstand the required vertical and horizontal screen mount displacements (sum of static and dynamic displacements) of approximately 18.2 mm and 1.5 mm respectively during the transient condition as obtained from computer simulation. The two Novibra type M400-40 standard rubber mounts arranged in series were used as a screen mount. This then resulted in the equivalent horizontal stiffness coefficient being then 67 600 N/m and the equivalent vertical stiffness coefficient being 308 870 N/m for a screen mount. This corresponds to a point in the optimal design region as shown in Figure 5.9. The results for two different possible designs are indicated in Table 5.1. These possible designs are the optimised design which rendered the lower objective function value, and a resonance design with the undesired larger objective function value. The optimised design therefore resulted in approximately 22 times smaller objective function value.

Table 5.1: Example optimisation iterations

Design	Mount vertical stiffness $\boldsymbol{k_{z1} = k_{z2}}$ $[\boldsymbol{N/m}]$	Mount horizontal stiffness $\boldsymbol{k_{x1} = k_{x2}}$ $[\boldsymbol{N/m}]$	Maximum steady state force transmitted $\boldsymbol{F_T}$ $[\boldsymbol{N}]$
Optimal	308 870	67 600	1 260.5
Resonance	308 870	3190 000	27 859.0

5.5 Finite element analysis

Finite Element Analysis (FEA) was used to analyse the structural stiffness and fatigue strength of the vibration screen. The vibration screen detailed structure was designed in a Solidworks version 2015 environment and the CAD model was used to perform the necessary Finite Element Analysis. To simplify the analysis, the detail regarding fasteners and the sieves was neglected. The model was simulated as if all screen components in the assembly were bonded together. Solidworks provides a special type of contact set known as bonded contact which was used for all the simulations. A solid mesh was selected for the Finite Element Analysis regarding strength (material stresses), and also dynamics (natural frequencies and mode shapes).

5.5.1 Screen modal analysis

A Modal Analysis with finite elements was performed for the vibration screen to investigate whether the detailed elastic screen structure was stiff enough. This was regarded as necessary because the screen structure was assumed to be a rigid body mass as supported by soft rubber mounts, in the three degree of freedom mathematical model described in Chapter 2, Paragraph 2.2. In the Finite Element Model the rubber mounts were replaced by equivalent cylindrical shaped mounts of a different material. The geometry and elasticity modulus for an equivalent mount provided the same corresponding vertical and horizontal stiffness magnitudes as a rubber mount. The lower ends of these equivalent mounts were then attached to a rigid foundation as constraints. This analysis was used to clarify whether the natural frequencies provided by the elastic screen structure (natural frequencies mainly provided by the relatively much softer elastic mounts here excluded), are above the exciter motor speed at 25 Hz to prevent structural resonance. The design was an iterative process and several different structural components as stiffeners were added to the model, to eventually obtain a feasible design. Various different stiffener designs were considered to increase the structural natural frequencies, without adding too much mass. The design which provided feasible natural frequencies with the minimal mass added was selected. The simulation results computed for this design are shown in Figures 5.10 to 5.21 for the first 12 mode shapes at corresponding frequencies. The magnitudes of the frequencies for the first six mode shapes in the FEA mainly provided by the relatively much softer mounts are shown in Figures 5.10 to 5.15. These

frequency magnitudes correspond well to the magnitudes obtained where the elasticity of the screen structure was disregarded and thus assumed to be a rigid body supported by soft elastic mounts, as modelled in a Matlab environment (see Paragraph 2.2, Figure 2.1, Paragraph 3.2 and Paragraph 6.7.3). Slight differences in magnitudes are mainly caused by the detail of fasteners and sieves that were neglected, and thus reduced the mass to 206 kg in the FEA model. The next six mode shapes at corresponding frequencies are shown in Figures 5.16 to 5.21 and are mainly provided by the elasticity of the screen structure. The seventh, and most important mode shape is shown in Figure 5.16 with the natural frequency at 39.4 Hz which is above the forced frequency at 25 Hz (exciter motor speed). This analysis was done for an empty screen and it is regarded that this natural frequency value will not significantly shift lower for a loaded screen with maize, because the mass of the maize is only 65 kg and the actual mass of the screen structure is 262 kg. Calculations indicate that the natural frequency of the seventh mode at 39.4 Hz is still regarded as safe in spite of the larger magnitude in mass (actual screen structure mass and mass of maize).

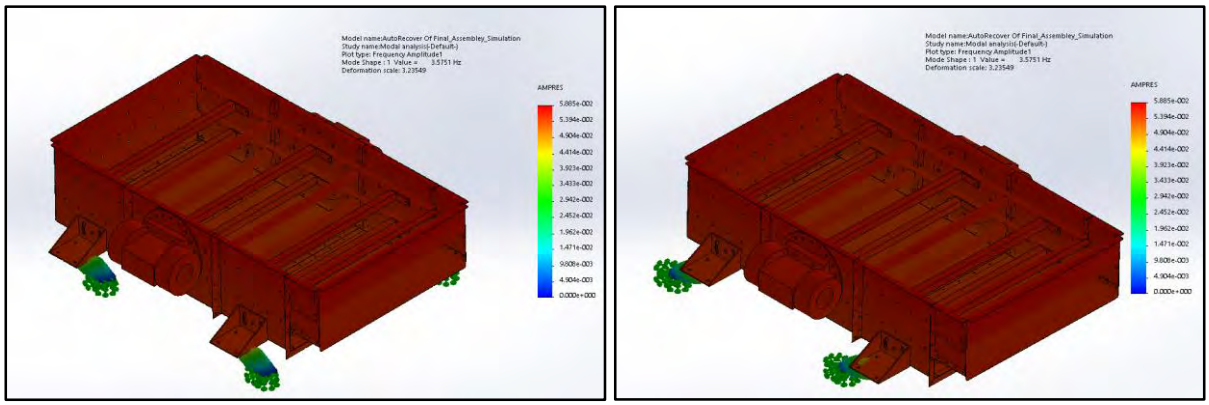

Figure 5.10: Mode shape 1 at 3.6 Hz

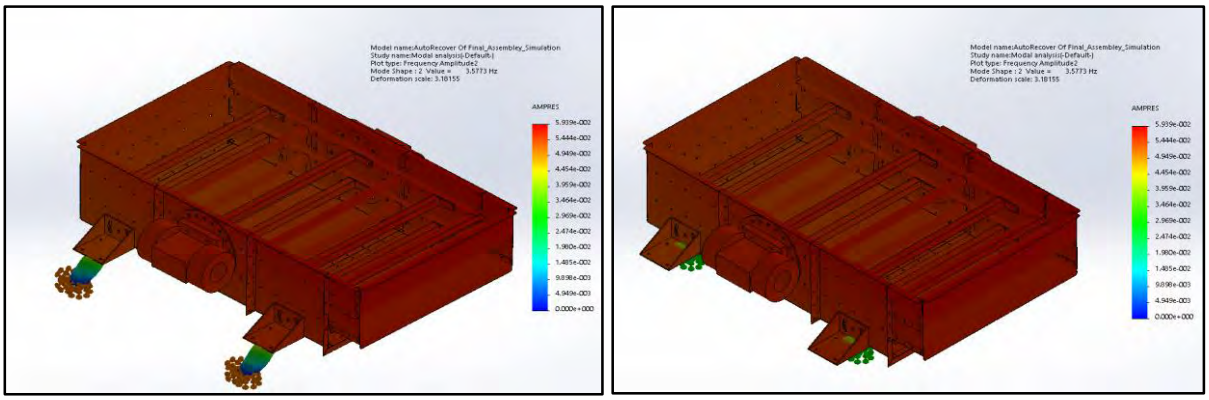

Figure 5.11: Mode shape 2 at 3.6 Hz

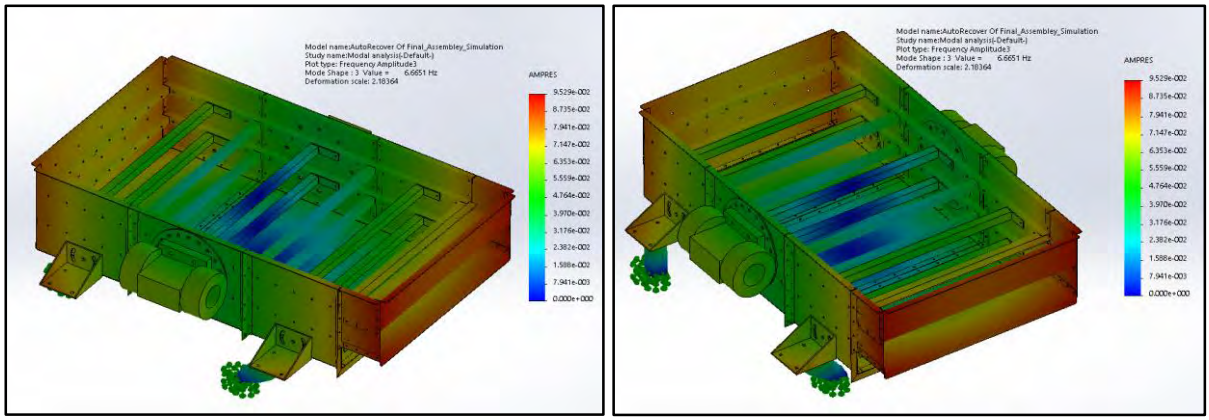

Figure 5.12 Mode shape 3 at 6.7 Hz

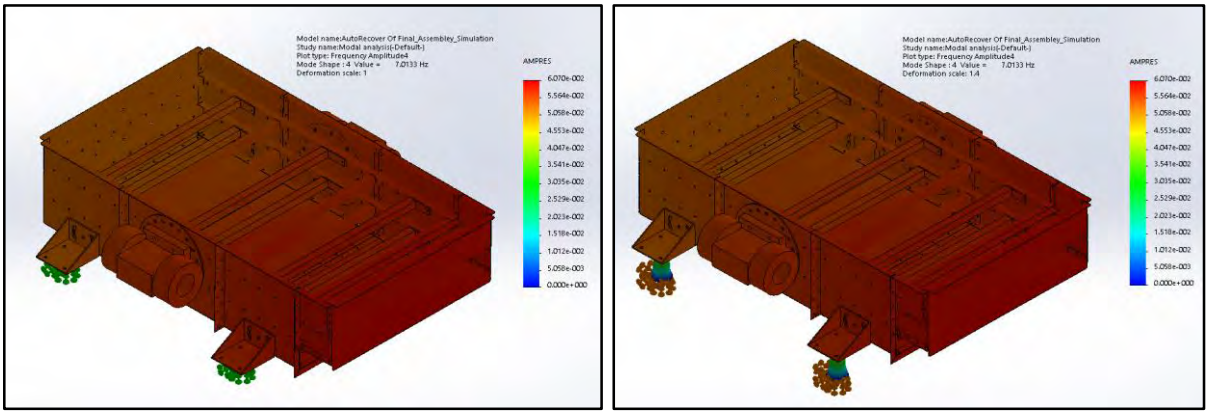

Figure 5.13: Mode shape 4 at 7 Hz

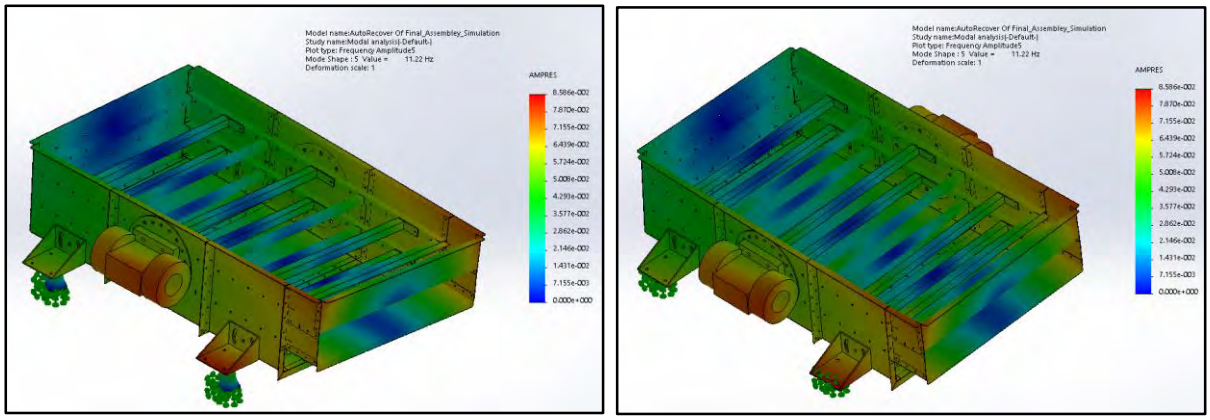

Figure 5.14: Mode shape 5 at 11.2 Hz

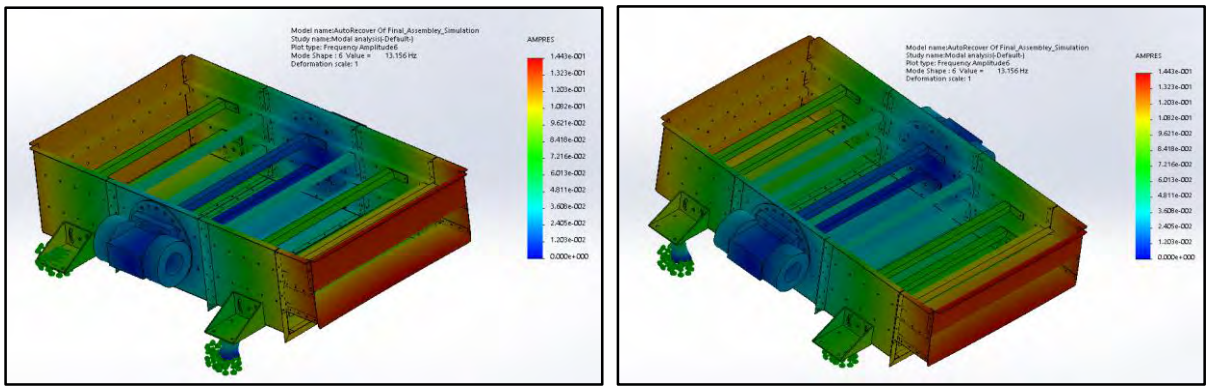

Figure 5.15: Mode shape 6 at 13.2 Hz

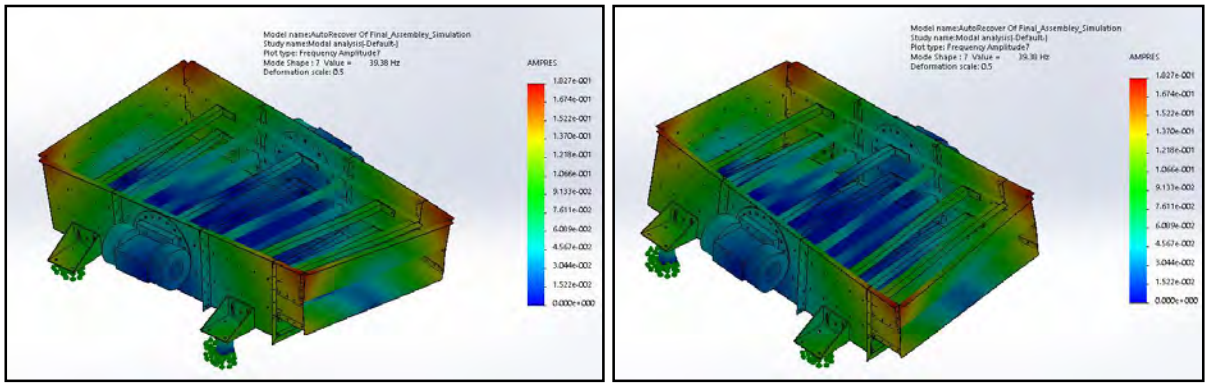

Figure 5.16: Mode shape 7 at 39.4 Hz

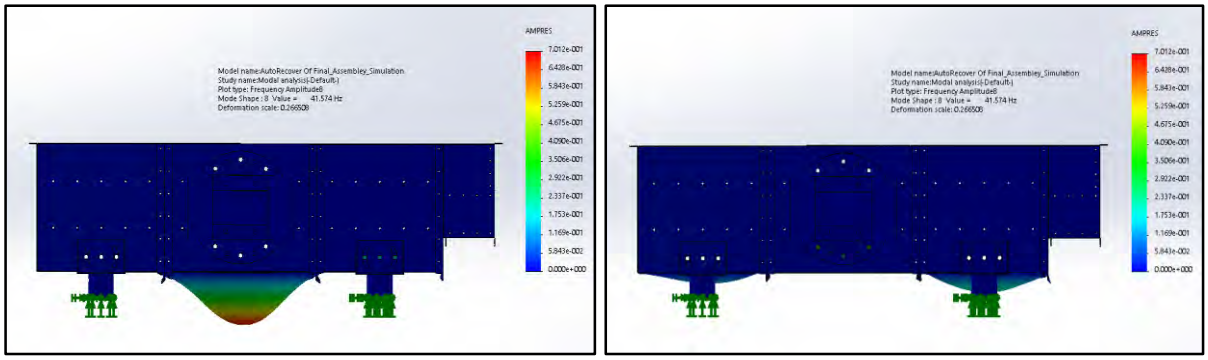

Figure 5.17: Mode shape 8 at 41.6 Hz

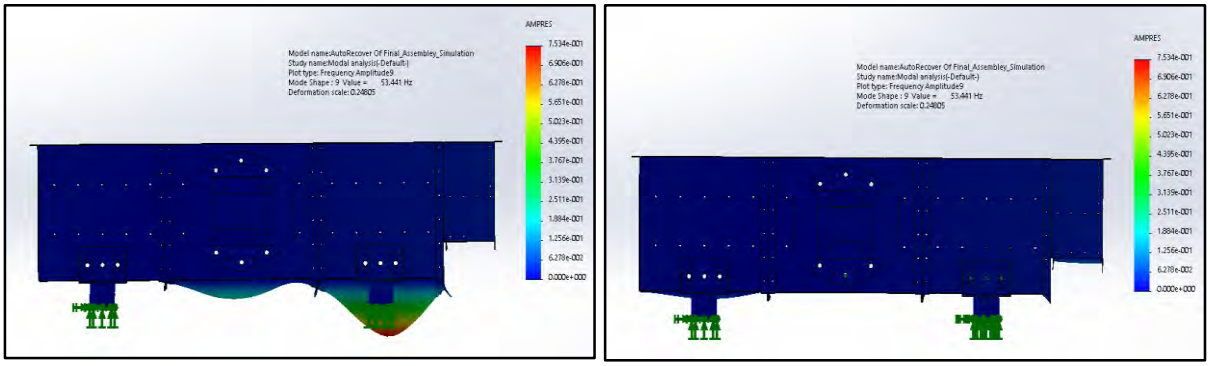

Figure 5.18: Mode shape 9 at 53.4 Hz

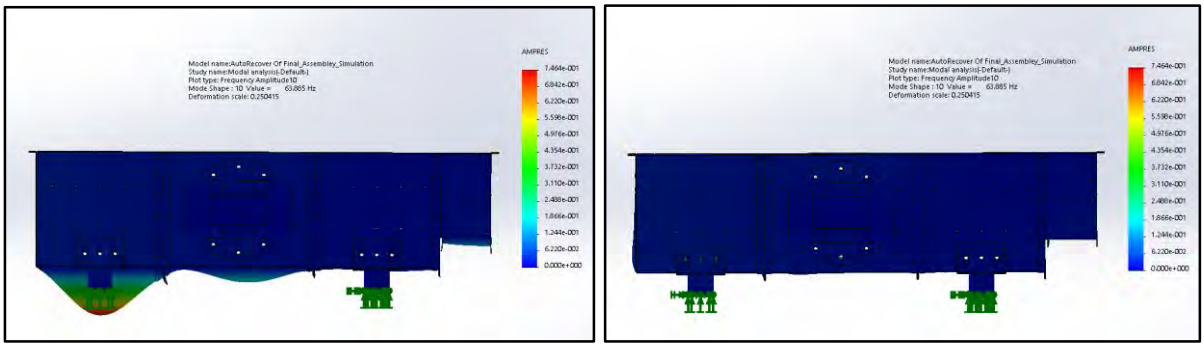

Figure 5.19: Mode shape 10 at 63.9 Hz

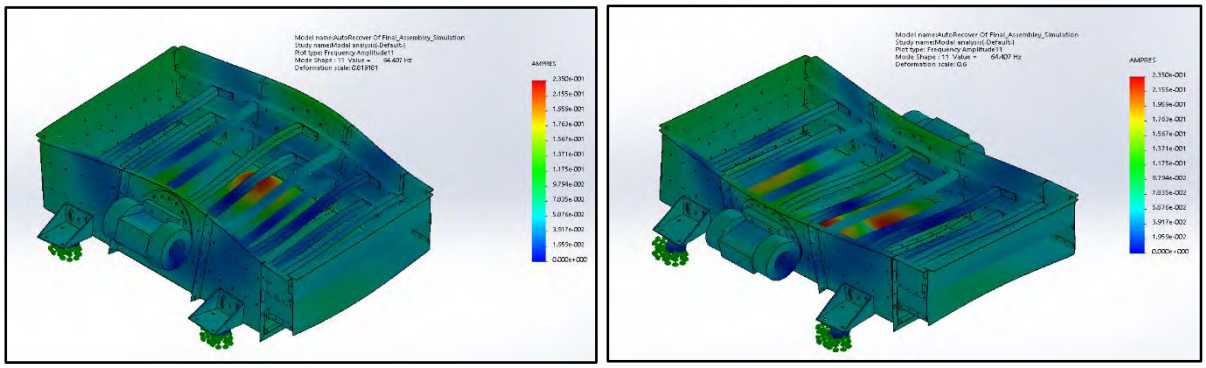

Figure 5.20: Mode shape 11 at 64.4 Hz

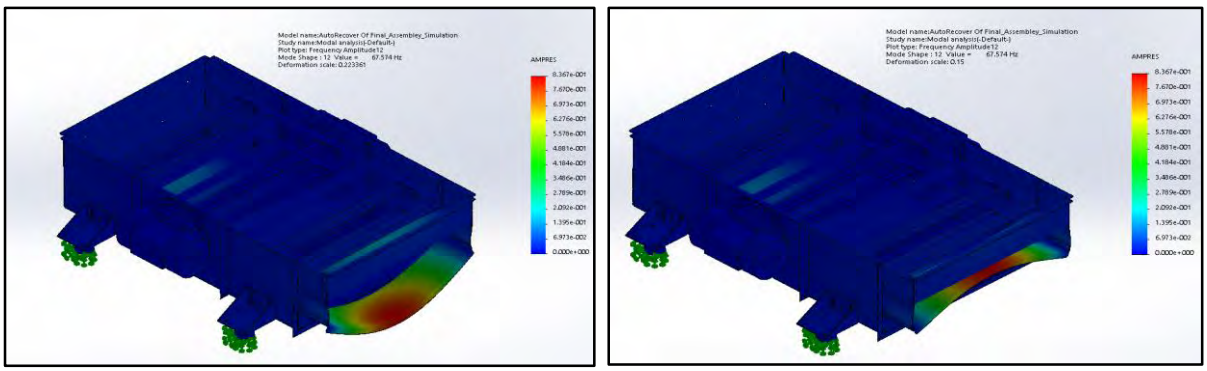

Figure 5.21: Mode shape 12 at 67.6 Hz

5.5.2 Screen stiffness analysis

The same FEA model described in Paragraph 5.5.1 was also used to determine the vertical stiffness of the elastic screen. This was regarded as necessary to further investigate whether the detailed elastic screen structure was stiff enough. This additional approach was regarded as necessary to clarify relative stiffness. The screen structure was assumed to be a rigid body mass as supported by soft rubber mounts, in the three degree of freedom mathematical model described in Chapter 2, Paragraph 2.2. The elastic mounts were deliberately removed from the screen structure in the FEA and replaced by a rigid platform at the original mount locations. To quantify the bending stiffness of the screen, two different distributed loads were applied and the corresponding deflections at the centre of the screen then computed. The bending stiffness was then quantified with the difference in these distributed loads and the corresponding difference in deflections at the centre of the screen. Figure 5.22 shows the elastic screen model with a distributed proof-load applied to the screen structure in the vertical direction as indicated with the arrows.

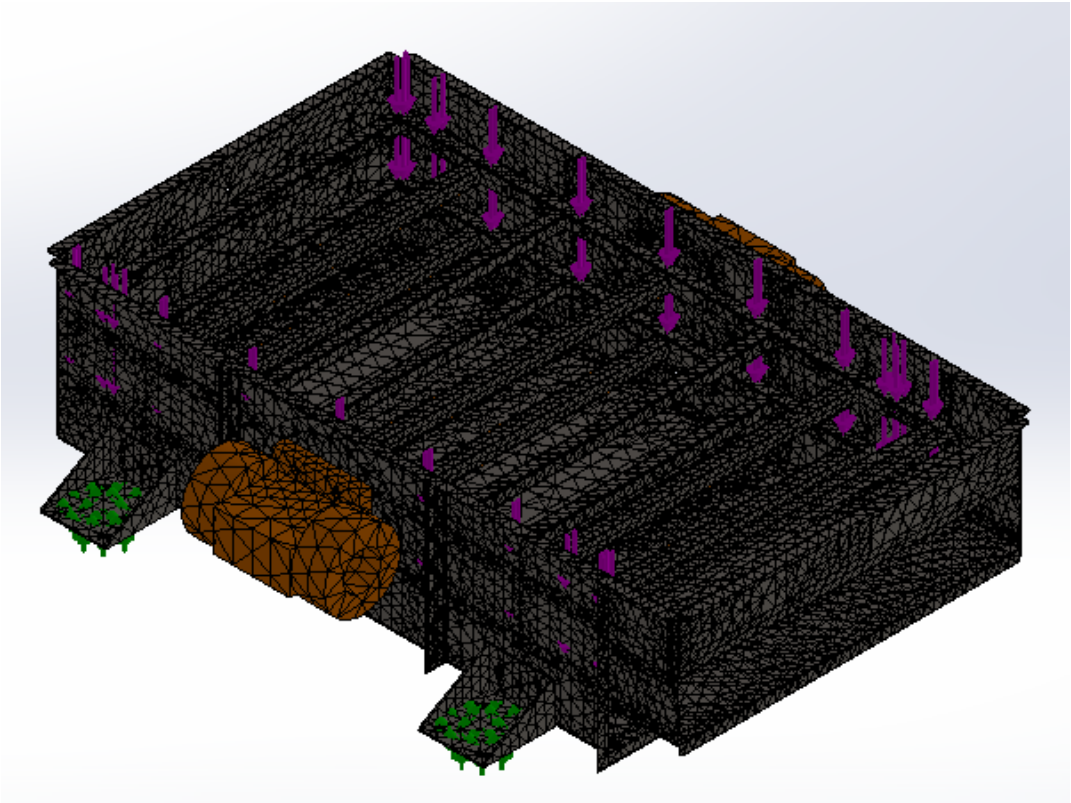

Figure 5.22: Vibration screen Finite Element mesh and proof load

The deflections at the centre of the screen structure as a result of 1 kN and 2 kN distributed proof-loads applied were computed, and found to be 6.9 μm and 13.9 μm respectively as shown in Figures 5.23 and 5.24. The vertical stiffness was calculated with Hook's law and compared to the equivalent vertical stiffness provided by all the rubber screen mounts (see also Figure 2.1). The vertical stiffness of the elastic screen is 143 kN/mm, and this is about 120 times more than the equivalent vertical mount stiffness as provided by all the rubber screen mounts (see also Figure 2.1; and Chapter 4, Paragraph 4.6.5). The assumption made of a rigid body mass in Chapter 2 (mathematical model), is thus regaded as valid.

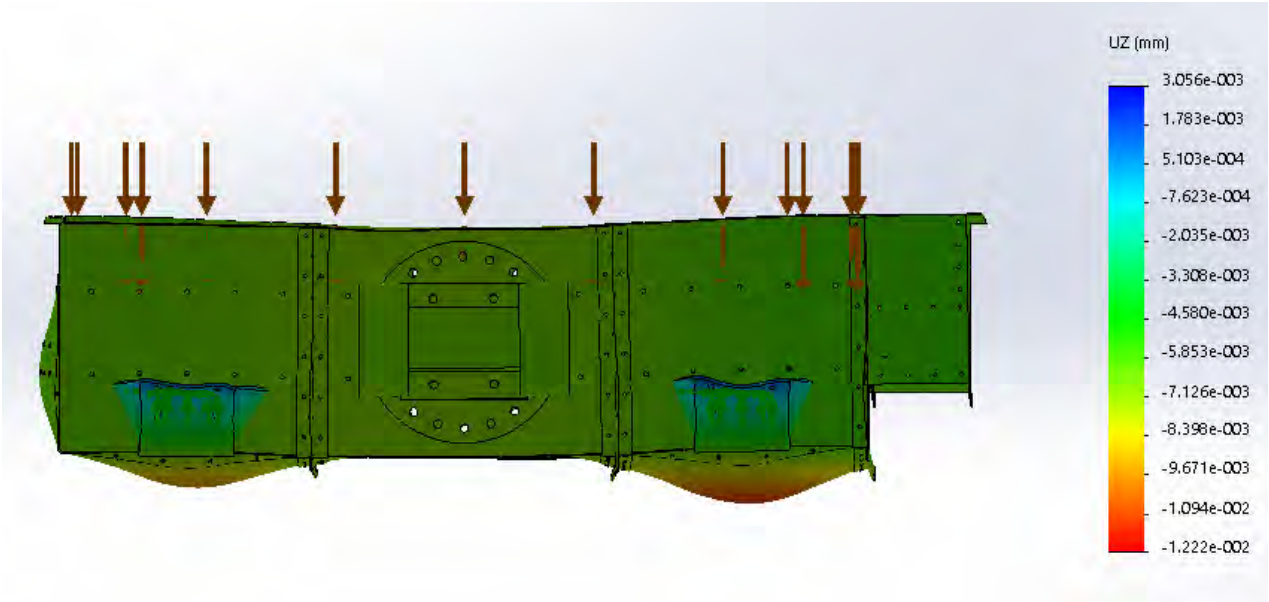

Figure 5.23: Vertical deflection plot of vibration screen (1 kN load)

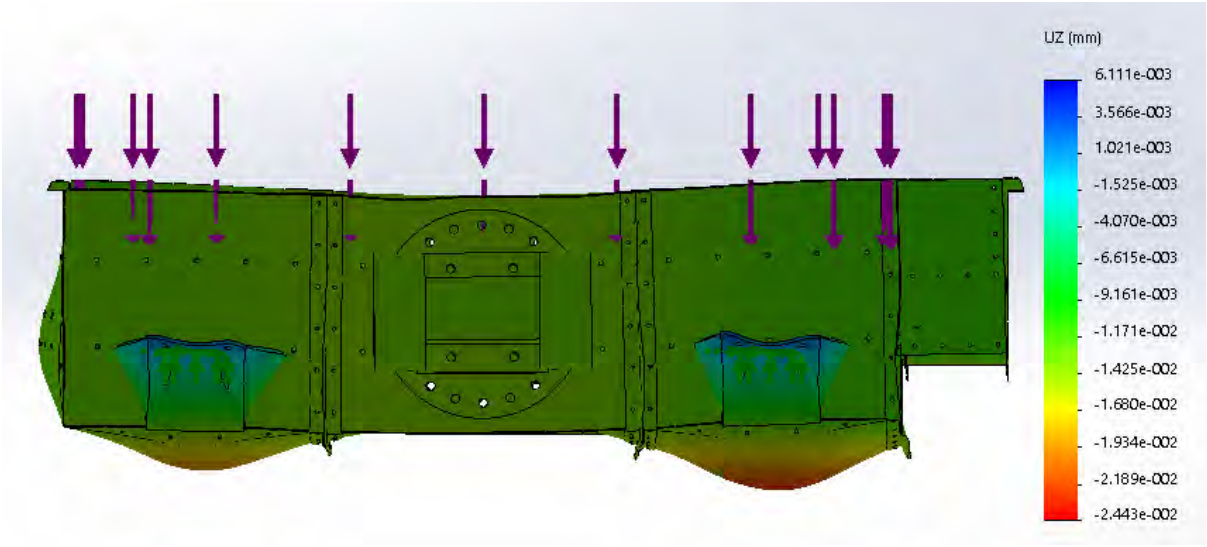

Figure 5.24: Vertical deflection plot of vibration screen (2 kN load)

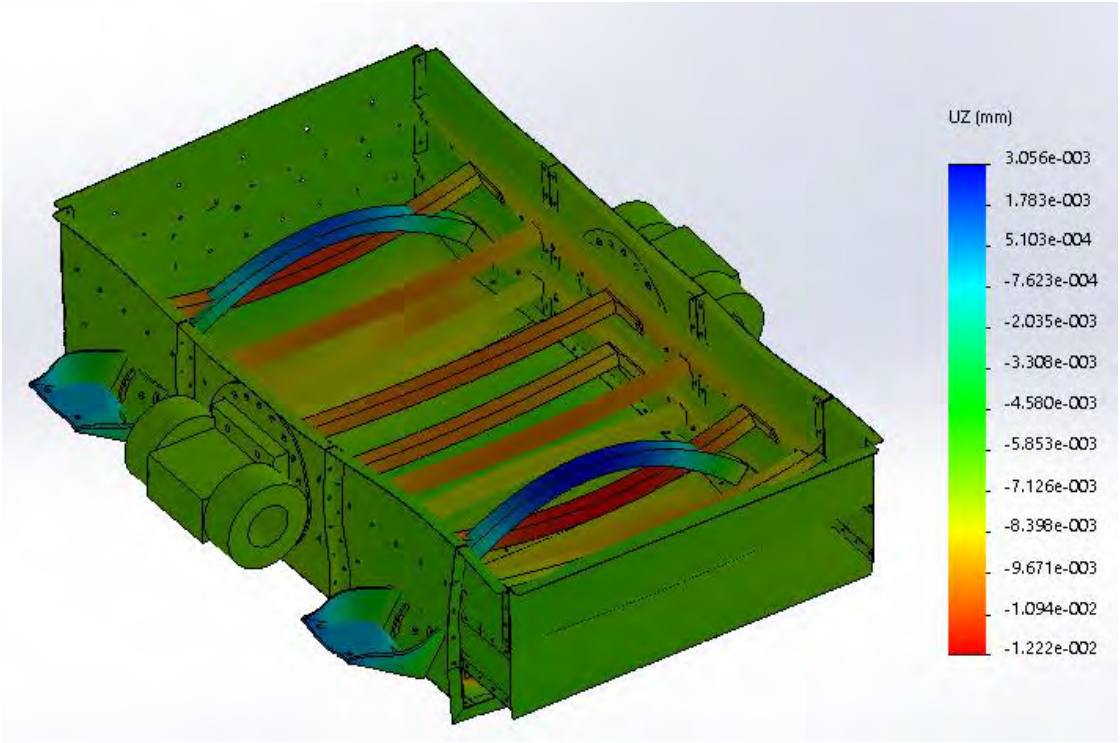

Figure 5.25: Vertical deflection plot of vibration screen (alternative view)

5.5.3 Screen fatigue analysis

With reference to the literature study, it is clear that fatigue failures at vibration screens are a major problem. Fatigue analysis was done for the screen structure to determine whether the screen design will provide a long service life, and preferably an infinite fatigue life. Solidworks was also used to compute the static (midrange) and dynamic (alternating) stresses as described in Paragraph 2.3. The midrange and alternating stress were computed for both a fully loaded and empty grain vibration screen. It was found that maximum force magnitudes were transmitted through the rubber mounts to the vibration screen structure during transient conditions. These transient force magnitudes transmitted for the two loading conditions (empty and fully loaded) were used to compute the material stresses at the screen structure respectively. These stresses were then used as input data at the computer program for fatigue analysis as described in Paragraph 3.3 in order to compute the safety factor regarding fatigue failure. In addition, fatigue analysis was however also performed according to the EN 1993-1-9 code as developed for fatigue consideration in the standard design of steel structures. The fatigue safety factors were compared for these two different approaches.

5.5.3.1 Midrange (static) stress

The midrange (static) stress was calculated with an equivalent gravitational acceleration acting on the screen in the vertical direction as shown in Figure 5.26. The mass of the screen as modelled was slightly lower than the actual screen mass mainly due to the fasteners and the sieves that were neglected to simplify the model. To account for this difference, an equivalent gravitational acceleration constant was calculated to provide for the larger static force. The mass of the vibration screen as modelled is 206 kg and the actual mass is 262 kg for an empty vibration screen. The equivalent gravitation constant calculated to compensate for this difference was 12.47 m/s^2. A similar procedure was followed for a fully loaded screen, thus with maize added.

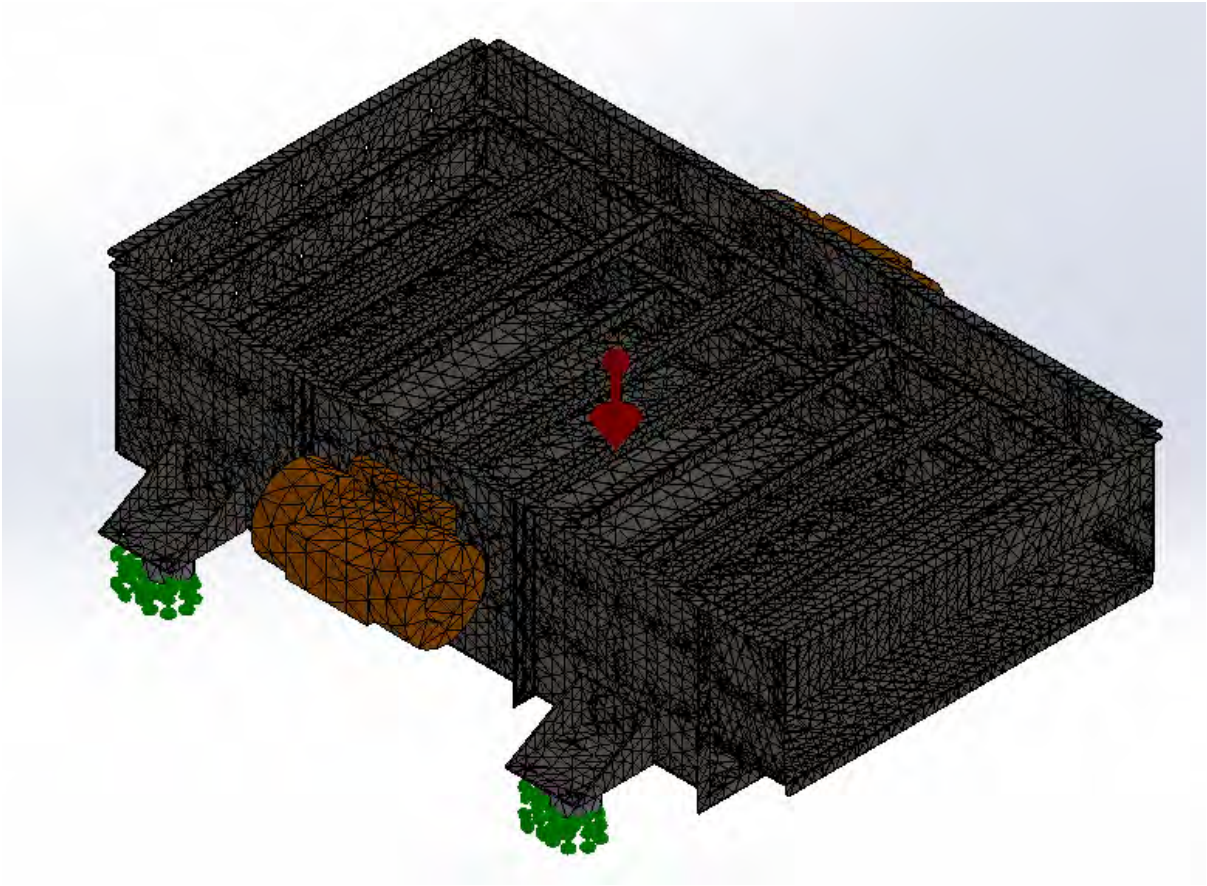

Figure 5.26: Vibration screen FEA mesh with static load for empty screen

The midrange stress for both the fully loaded and empty vibration screen were computed. Figure 5.27 shows the FEA results for the empty vibration screen midrange stress.

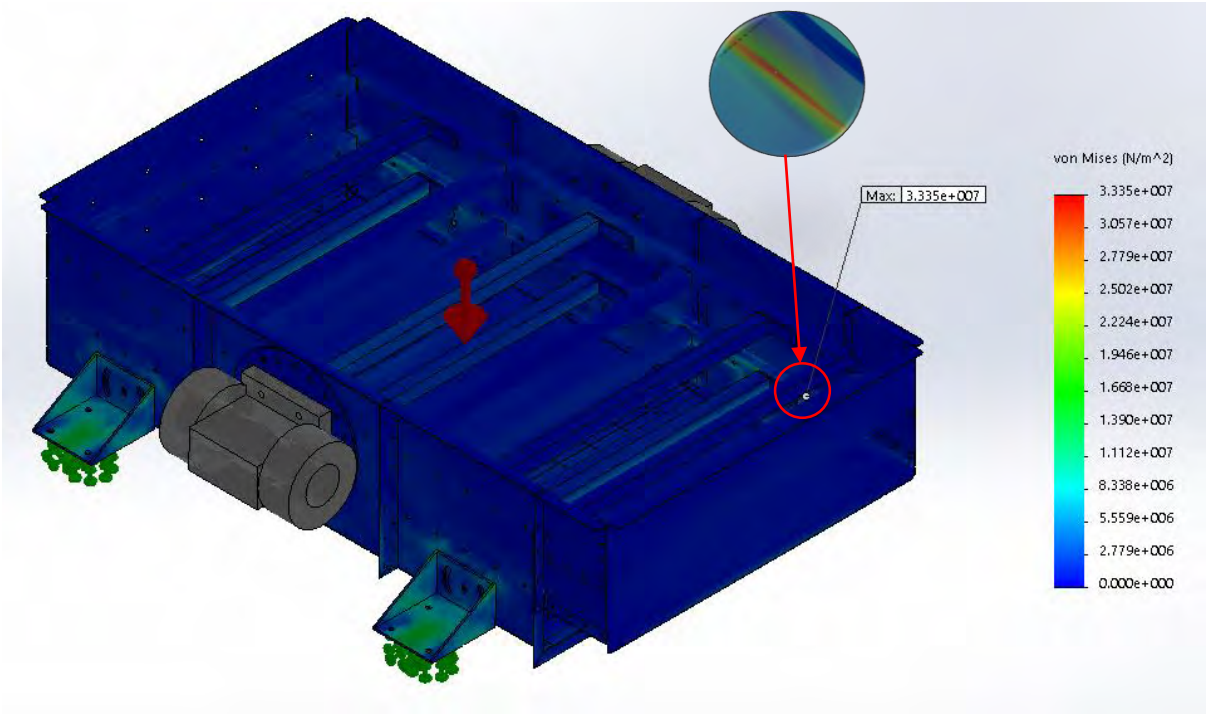

Figure 5.27 FEA midrange (static) stress plot for empty screen

The maximum midrange Von Mises stress was computed as 33.4 MPa as indicted in Figure 5.27. This maximum stress is located at the inner radius of one of the square tubing stiffener members. The midrange stress for the fully loaded screen was computed similarly, with an additional uniformly distributed load of 638 N (65 kg) applied to the screen model to provide for the mass of the maize as shown in Figure 5.28. The maximum midrange Von Mises stress computed for the fully loaded screen was 38.5 MPa as shown in Figure 5.29.

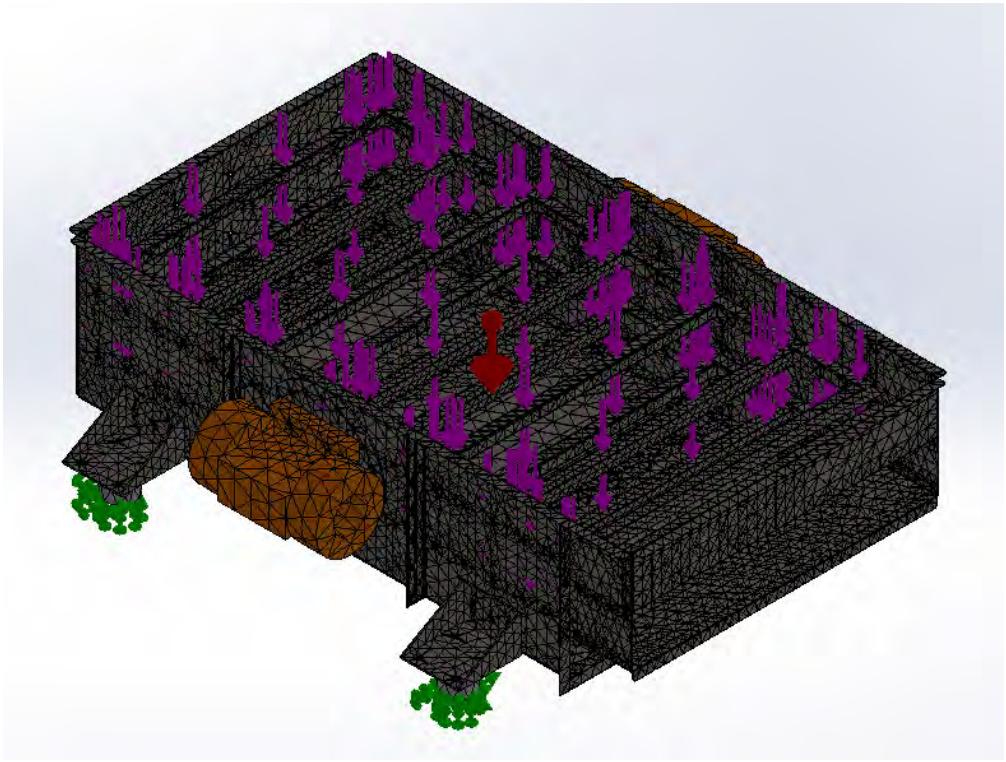

Figure 5.28: Vibration screen FEA mesh with static load for fully loaded screen

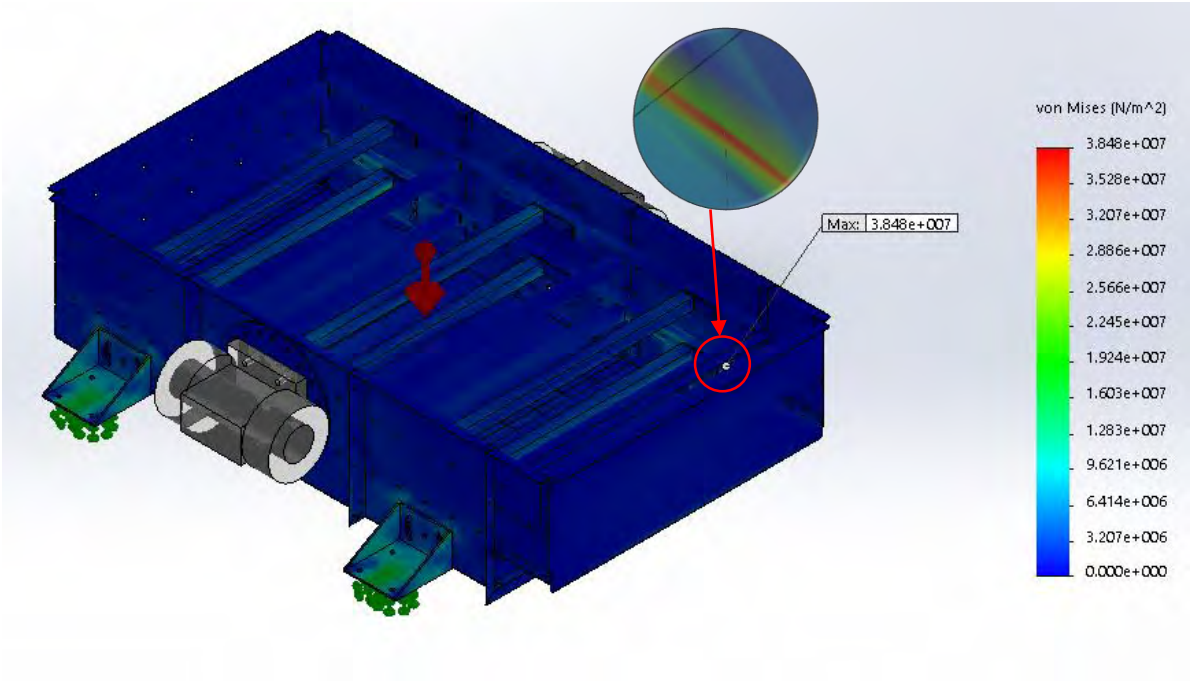

Figure 5.29: FEA midrange (static) stress plot for fully loaded screen

5.5.3.2 Alternating (dynamic) stress

The alternating stresses were also computed at the screen for both empty and fully loaded conditions respectively. This was done similar to the midrange stress, but new equivalent gravitational constants were determined to provide for the larger reaction forces during transient (starting and stopping) conditions. These largest transient mount reaction force magnitudes were obtained by computer simulation for the three degree of freedom screen system (see Figure 2.1, Paragraph 2.2 and Paragraph 3.2). These transient mount reaction force magnitudes were used to calculate the equivalent gravitational constants for the empty and fully loaded conditions respectively. For this analysis, it was necessary to calculate an equivalent gravitational constant for the horizontal direction as well. This was done to compensate for the dynamic reaction forces acting in the horizontal direction during transient conditions. The equivalent gravitational constants calculated for an empty vibration screen in the vertical and horizontal directions were $20.1\ m/s^2$ and $2.1\ m/s^2$ respectively. Figure 5.30 shows the vibration screen FEA model with the equivalent gravitational accelerations acting on the screen in the horizontal and vertical directions respectively. These equivalent accelerations provided the same transient mount reaction force magnitudes as simulated by the computer program.

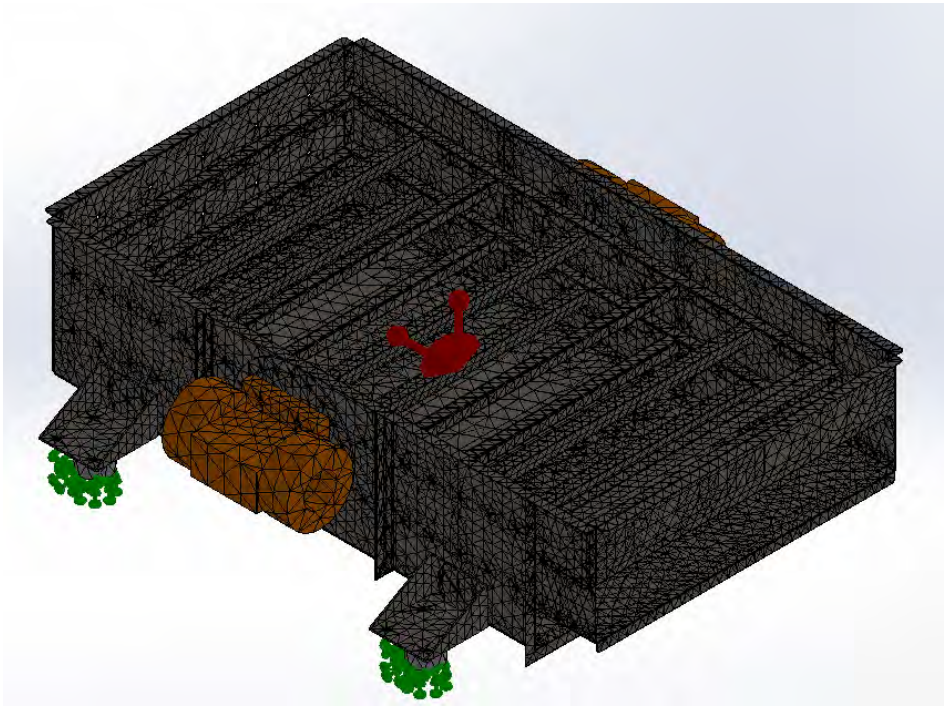

Figure 5.30: Vibration screen FEA mesh with dynamic load for empty screen

The maximum alternating Von Mises stress was computed as 54.8 MPa, and the FEA stress plot is shown in Figure 5.31. This maximum stress was obtained for an empty screen.

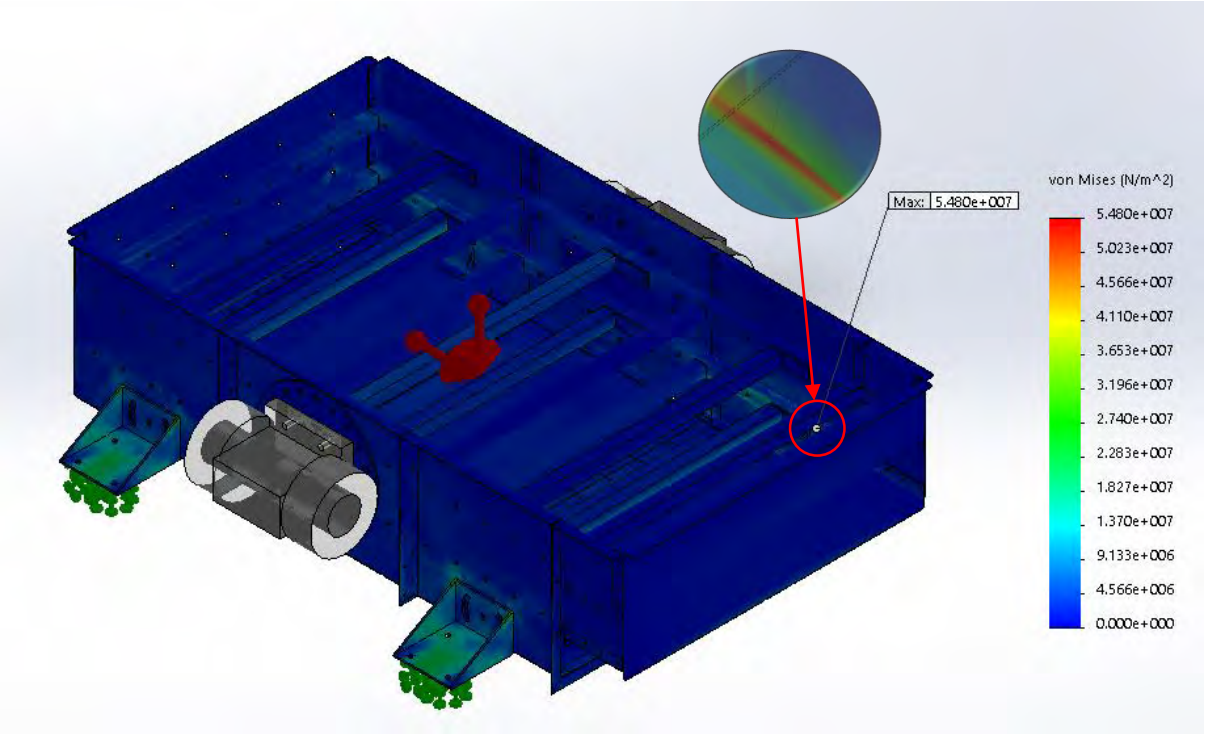

Figure 5.31: FEA alternating (dynamic) stress plot for empty screen

A similar analysis was done for a fully loaded grain vibration screen, but with the mass of the maize added as a uniformly distributed load. The equivalent acceleration constants for the fully loaded screen were calculated as $10\ m/s^2$ and $1.7\ m/s^2$ in the vertical and horizontal directions respectively. The maximum Von Mises alternating stress was computed as 31.2 MPa and is shown in Figure 5.32.

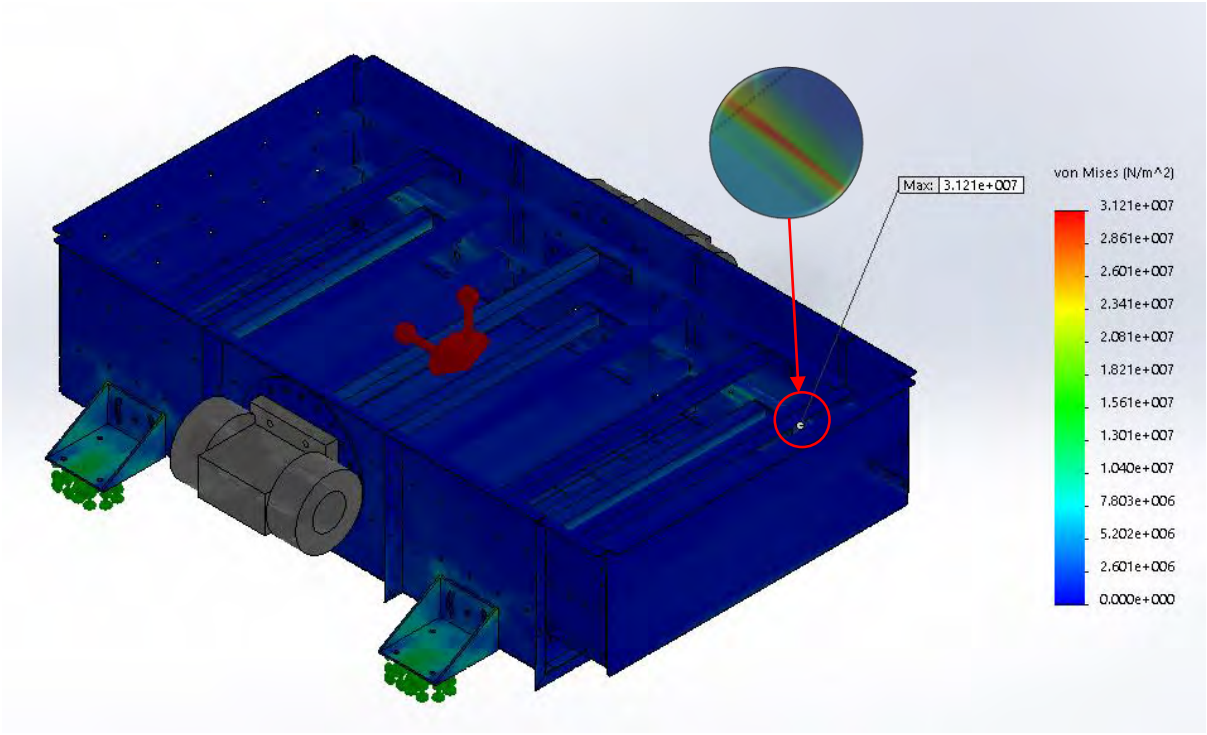

Figure 5.32: FEA alternating (dynamic) stress plot for fully loaded screen

5.5.3.3 Screen fatigue analysis according to EN 1993-1-9

Fatigue analysis was however also performed according to the EN 1993-1-9 code as developed for fatigue consideration in the standard design of steel structures. The material stresses in various critical areas were analysed and found to be the largest in one of the square tubing members. To ensure high fatigue strength, the screen structure was designed to have as little welded connections as possible. Although most connections are mechanically fastened by bolts and nuts, welded connections could not be avoided everywhere. The stresses in the few welded areas were also analysed and found to be very small, and thus of no concern regarding fatigue failure. To analyse the fatigue strength of the square tubing stiffener member, the EN 1993-1-9 code required that the maximum shear stress be computed with simple hand calculations. In this case however, a FEA model was available, and this model then used for computation of maximum shear stresses. Figures 5.33 and 5.35 show the maximum midrange (static) shear stresses computed for an empty and fully loaded screen respectively. Figures 5.34 and 5.36 show the maximum alternating (dynamic) shear stresses computed for an empty and fully loaded screen respectively. These

maximum shear stress magnitudes were then used to calculate the corresponding fatigue factors of safety related to the EN-1993-1-9 code, and indicated in Table 5.4.

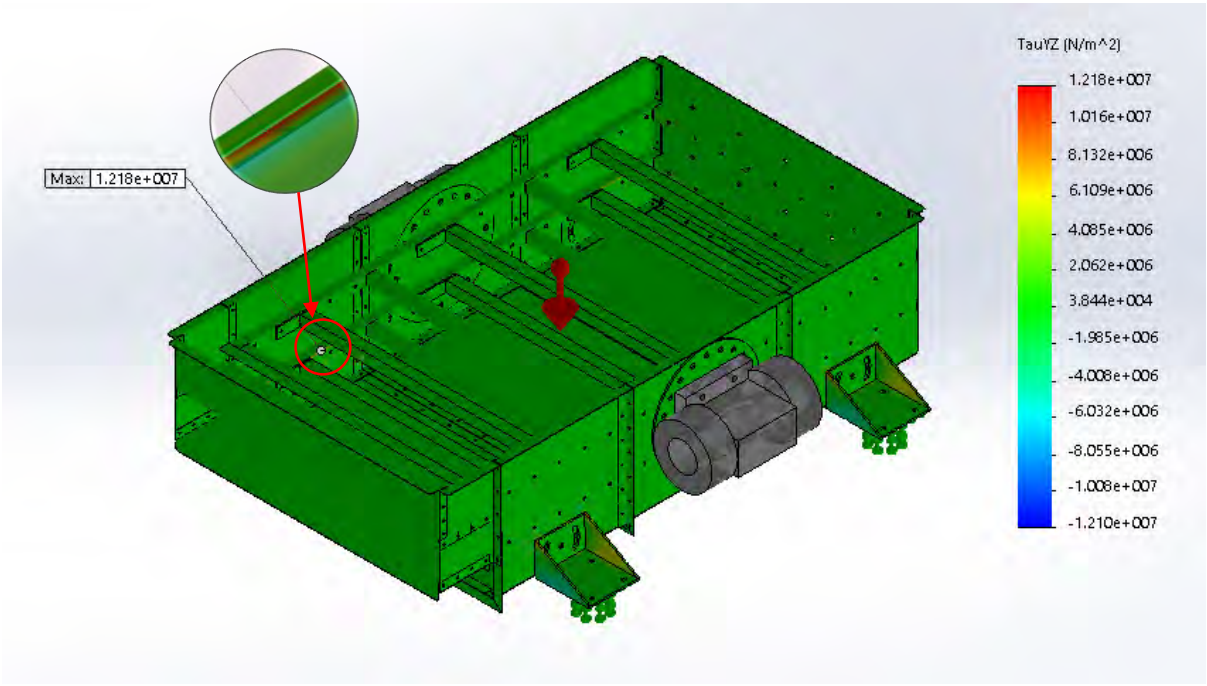

Figure 5.33: FEA midrange (static) shear stress plot for empty screen

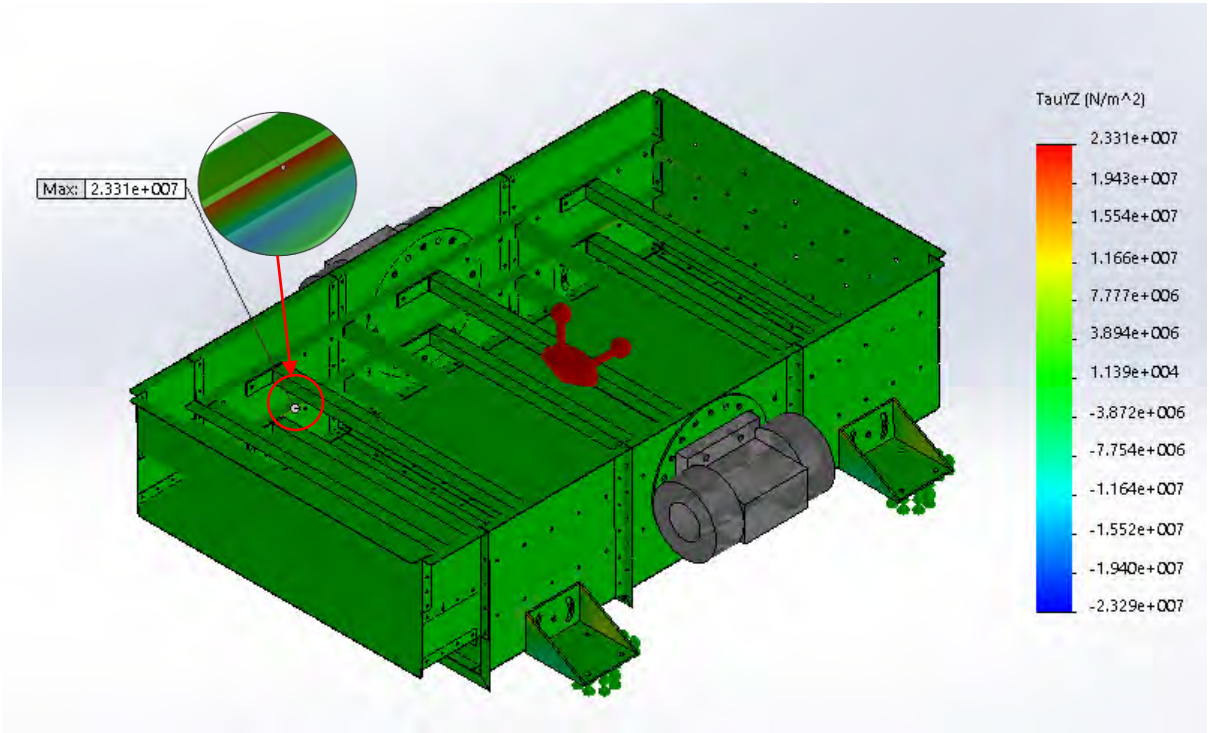

Figure 5.34: FEA alternating (dynamic) shear stress plot for empty screen

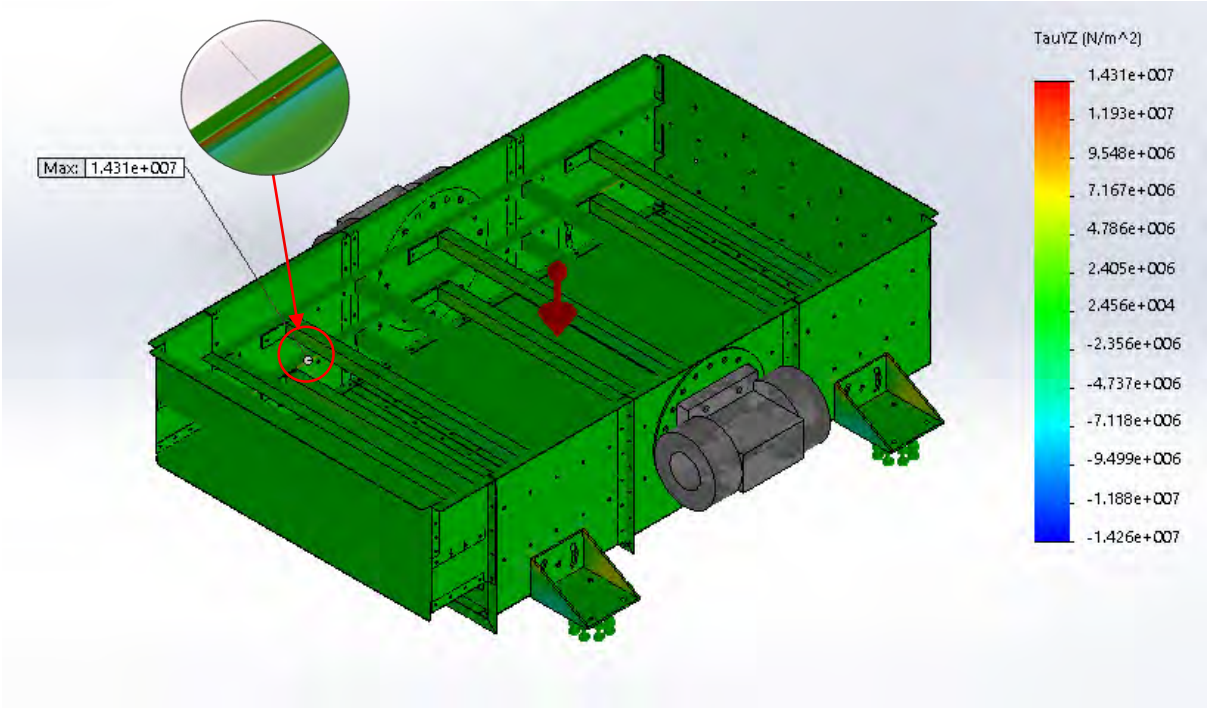

Figure 5.35: FEA midrange (static) shear stress plot for fully loaded screen

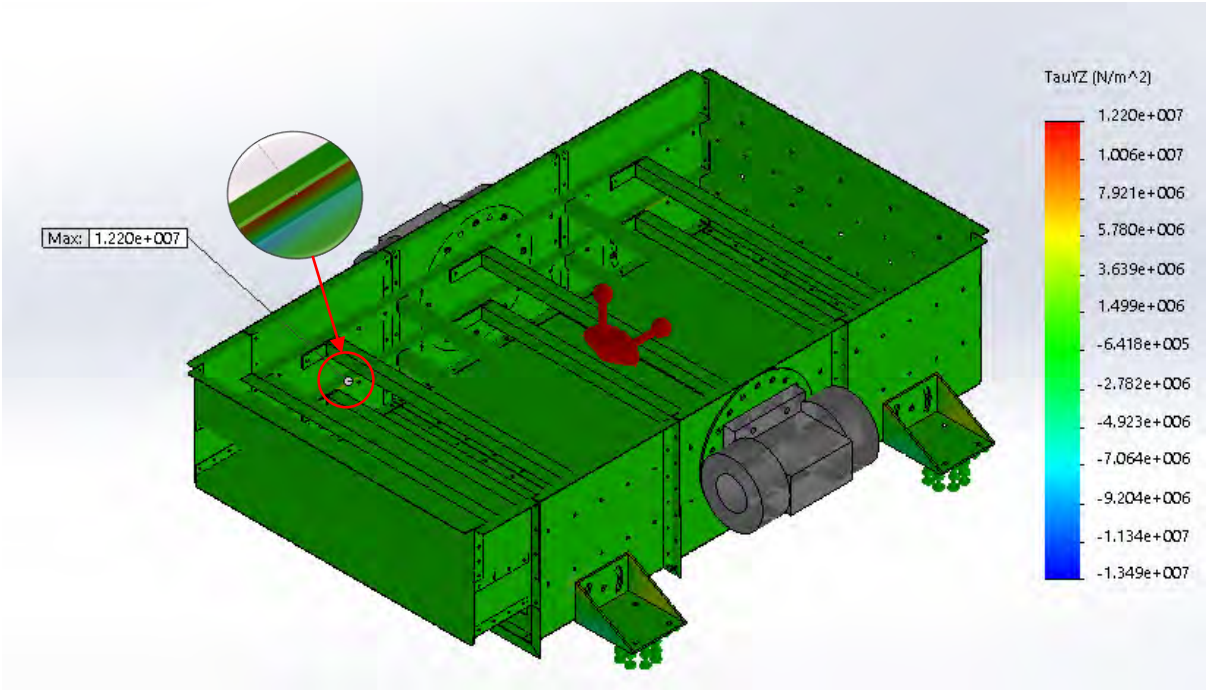

Figure 5.36: FEA alternating (dynamic) shear stress plot for fully loaded screen

5.5.3.4 Service life

The fatigue safety factors were compared for the two different approaches, namely for the Goodman criteria and also the alternative criteria described in the EN 1993-1-9 code as developed for fatigue consideration in the standard design of steel structures.

The Goodman criteria was used and safety factors then computed with the computer program as described in Paragraph 3.3. The input values for this program as indicated in Table 5.2 were used. These input values include certain endurance stress modification factors that were determined, and also the ultimate tensile strength of the screen material as described in Paragraph 2.3.

Table 5.2: Fatigue program input values

Factor	Value	Unit
S_{ut}	400	MPa
k_a	0.92	-
k_b	0.73	-
k_c	1	-
k_d	1	-
k_e	0.81	-
k_f	1	-

The data indicated in Table 5.2 and also the magnitudes for material stresses (midrange and alternating) obtained from the FEA described in Paragraph 5.5.3 were used as input values at the computer program for fatigue analysis. This was done in order to compute safety factors regarding fatigue failure (see Paragraph 2.3 and Paragraph 3.3), with the program code included in Appendix A. The computed stresses and corresponding safety factor regarding fatigue failure are indicated in Table 5.3 for the two loading conditions (empty and fully loaded) respectively.

Table 5.3: Summary of stress and fatigue safety factor according to Goodman's criteria

Loading condition	Midrange stress σ_m $[MPa]$	Alternating stress σ_a $[MPa]$	Modified endurance limit S_e $[MPa]$	Fatigue safety factor n_{sf}
Empty	33.35	54.80	108.80	1.7
Fully loaded	38.48	31.21	108.80	2.6

Table 5.3 indicates that the smallest safety factor regarding fatigue failure of 1.7 was obtained for an empty vibration screen. A fully loaded vibration screen experiences much less displacement during transient conditions, and hence the larger safety factor of 2.6. The risk regarding fatigue failure is eliminated for fatigue safety factor values larger than 1 (see Paragraph 2.3), and thus a grain vibration screen design with an infinite service life is expected according to the Goodman criteria.

The alternative criteria according to the EN 1993-1-9 code as developed for fatigue consideration in the standard design of steel structures was also used to compute fatigue safety factors. According to this code, fatigue strength curves for direct stress ranges should be used for a particular structural section, and its specific connection detail (bolted or welded). The manufacturing process for this critical screen structural section (square tubing stiffener in this case) identified also influence the particular fatigue strength curve and the corresponding direct stress range. The so called cut off limit stress should then be calculated as the product of a constant (0.549) and the direct stress range magnitude according to this code, and is then 45.7 MPa. This cut off limit stress could be seen as an equivalent endurance limit stress for this type of structural member of concern (square tubing stiffener). The maximum shear stresses described in Paragraph 5.5.3.2 was computed by FEA as shown in Figures 5.31 to 5.34. These computed midrange (static) and also alternating (dynamic) shear stress magnitudes for the square tubing stiffener are indicated in Table 5.4 for an empty and fully loaded screen respectively. The EN 1993-1-9 code specified a mathematical equation to be used for computation of a so called effective stress range, and the corresponding magnitudes obtained for an empty and fully loaded screen are also

indicated in Table 5.4. The fatigue safety factor magnitudes were calculated as the ratio between the cut off limit stress and the effective stress range, and indicated in Table 5.4. The smallest fatigue safety factor regarding fatigue failure is 1.08 as obtained for an empty vibration screen with the criteria of the EN 1993-1-9 code. As expected, the fatigue safety factor as obtained for a fully loaded screen is larger at 1.65 due to smaller dynamic forces transmitted. These safety factors indicates that an infinite service life for the screen can be expected. It should be kept in mind that the shear stress magnitudes used were obtained from FEA. These FEA stress magnitudes are more accurate, and also larger compared to the simplified hand calculations as suggested in the EN 1993-1-9 code. The corresponding factors of safety computed as indicated in Table 5.4 are thus smaller, and thus more conservative to evaluate fatigue service life.

Table 5.4: Summary of stress and fatigue safety factor according to EN 1993-1-9 criteria

Loading condition	Midrange shear stress $[\boldsymbol{MPa}]$	Alternating shear stress $[\boldsymbol{MPa}]$	Effective stress range $[\boldsymbol{MPa}]$	Cut off limit stress $[\boldsymbol{MPa}]$	Fatigue safety factor $\boldsymbol{n_{sf}}$
Empty	12.2	23.3	42.2	45.7	1.08
Fully loaded	14.3	12.2	27.8	45.7	1.65

5.6 Conclusions

Three different design goals for an optimisation approach were identified. Firstly, the criteria for vibration isolation an objective function based on the transmission of dynamic forces to the foundation were formulated. Secondly, two constraints that influenced vibration isolation were also formulated. These constraints were regarded as necessary to ensure enough movement for effective sieving, but also to limit the horizontal and vertical mount displacements typically during transient conditions. Three-dimensional graphic representations and contour plots were constructed in a Matlab environment, and used to determine mount vertical and horizontal stiffness

coefficients, chosen as design variables for an optimum design according to the criteria formulated.

A Finite Element Analysis (FEA) approach was followed to investigate possible structural resonance of the elastic screen, but the results revealed that the natural frequencies of the mode shapes mainly provided by the elasticity of the screen structure are above the exciter motor speed. Calculations also indicate that the natural frequencies at these mode shapes can be regarded as safe in spite of the larger magnitude in mass (actual screen structure mass and mass of maize, compared to mass used in FEA). The FEA approach was also used to evaluate the vertical stiffness of the screen. It was found that this vertical stiffness was large enough, and the assumption of a rigid body made in the three degree of freedom mathematical model thus regarded as valid (see also Chapter 2, Paragraph 2.2).

An FEA approach was also used to determine static and dynamic material stresses used for fatigue analysis of the screen structure. It was found that the risk regarding fatigue failure is eliminated for fatigue safety factor values larger than 1, thus an infinite service life is expected for this grain vibration screen for the larger safety factors obtained. This was obtained for two different fatigue analysis approaches, namely for the Goodman criteria and also the alternative criteria described in the EN 1993-1-9 code as developed for fatigue consideration in the standard design of steel structures.

6 Experimental evaluation

6.1 Introduction

The experimental evaluation entails vibration measurements at the vibration screen prototype. Feasible vibration screen and exciter motor angles were determined for maize, and the evaluation was performed at these fixed angles. Two accelerometers were attached at the two mount coordinates, and the vertical response and natural frequencies measured for different conditions (empty and fully loaded). The response was measured for multiple operational conditions which include start-up, shut-down and steady state. The dynamic forces transmitted to the support structure were determined with measured response and mount properties as experimentally characterised. This was done for the different operational conditions. The predicted responses, dynamic forces and also the natural frequencies were compared to the corresponding measured values respectively.

6.2 Vibration measurements at vibration screen

Accelerometers were placed at the two mount coordinates and coupled to a Diagnostics Instruments 2200 FFT Analyser and the measured time and frequency domain signals were then recorded. This was done for different operational conditions (empty, fully loaded, steady state and transient) of the vibration screen. The vibration screen angle was adjusted to 5 degrees relative to the horizontal (see Paragraph 4.10 and Figure 4.28). With the angle of the vibration screen set at 5 degrees downhill, a horizontal force component provided by the exciter motors and transmitted to the screen was obtained. For maize, this screen angle provided good material transport velocity (sufficient flow rate), as well as excellent screening efficiency as practically determined. The two exciter motor mass unbalances were set to 65 % each, as this allowed the desired dynamic force for efficient sieving. All the vibration measurements were done at these angles and with these exciter motor unbalanced settings.

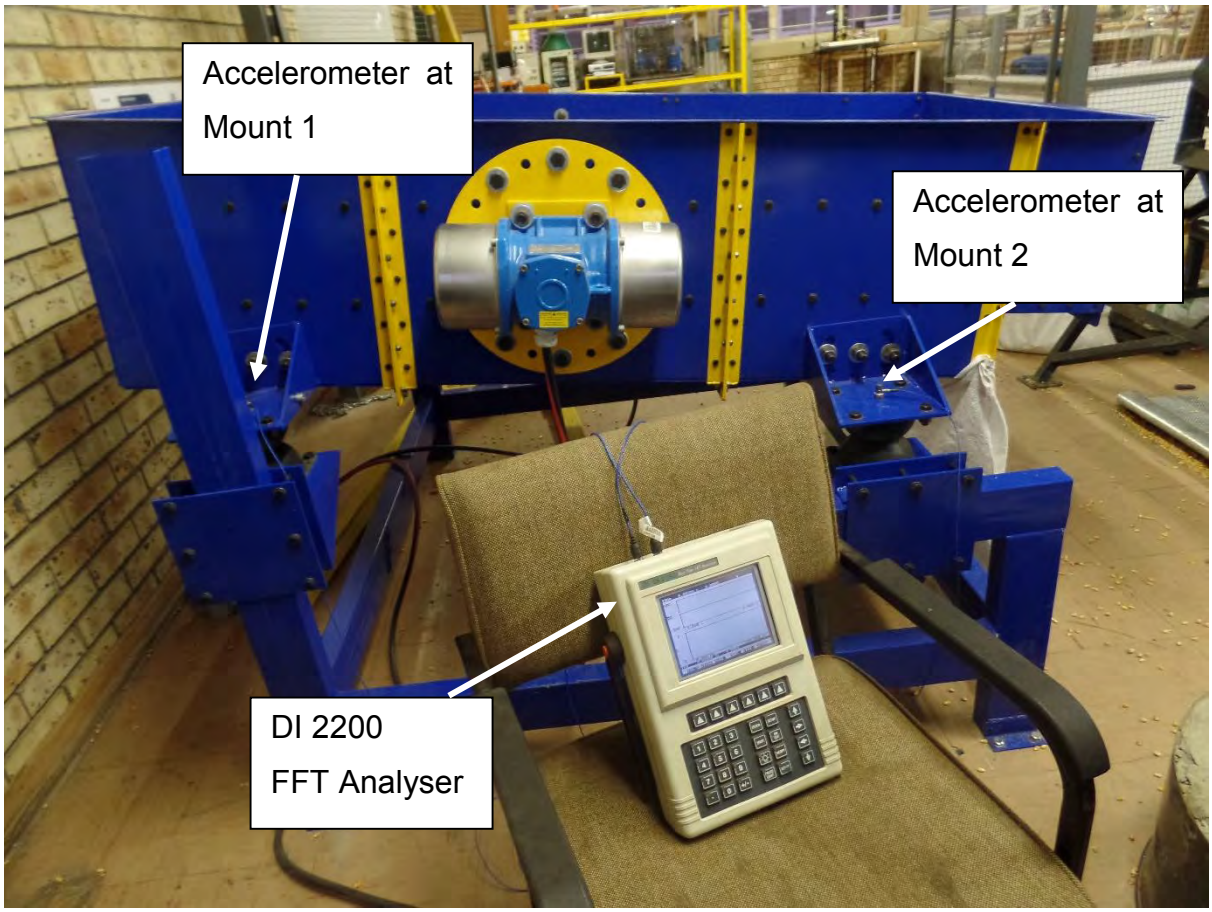

Figure 6.1: Vibration screen evaluation test setup

Figure 6.1 shows the vibration screen in the vibration Laboratory at the NWU with the accelerometers placed at the two mounts. The exciter motors were powered by a variable speed drive (VSD) unit which allowed that the rotational speed could be changed. All test were performed at 25 Hz, which is the normal running speed of the two exciter motors.

6.3 Empty vibration screen response

The responses at the empty vibration screen were measured at the two mounts, in both the vertical and horizontal directions respectively. Vibration measurements were taken during start-up, shut-down and also steady state (normal running speed) conditions. The computer program described in Chapter 3, Paragraph 3.2 was used to compute the predicted response signals. Some of the characteristics as characterised in Chapter 4 were used as input values to this computer program, with the program code included in Appendix A. The dynamic properties as characterised at the 1.4 mm excitation amplitude and a preload for an empty screen were used,

because this was close to the actual excitation amplitudes. These dynamic mount properties for each of the two screen mounts are 308.1 kN/m (stiffness coefficients k_{z1} and k_{z2}), and 0.084 kNs/m (damping coefficients c_{z1} and c_{z2}), as characterised and described in Chapter 4, Paragraph 4.6.4. The horizontal dynamic mount properties are 67.6 kN/m (stiffness coefficients k_{x1} and k_{x2}), and 0.11 kNs/m (damping coefficients c_{x1} and c_{x2}), as characterised and described in Chapter 4, Paragraph 4.6.6 were also used in the computer program. For transient conditions these mount properties were also used.

6.3.1 Steady state response for empty screen

Figures 6.2 to 6.5 show the predicted and also the measured steady state time and frequency domain signals at Mount 2 for an empty screen. The time domain acceleration signals were converted to frequency domain peak displacement signals. Table 6.1 indicates the comparison between corresponding predicted and measured amplitudes.

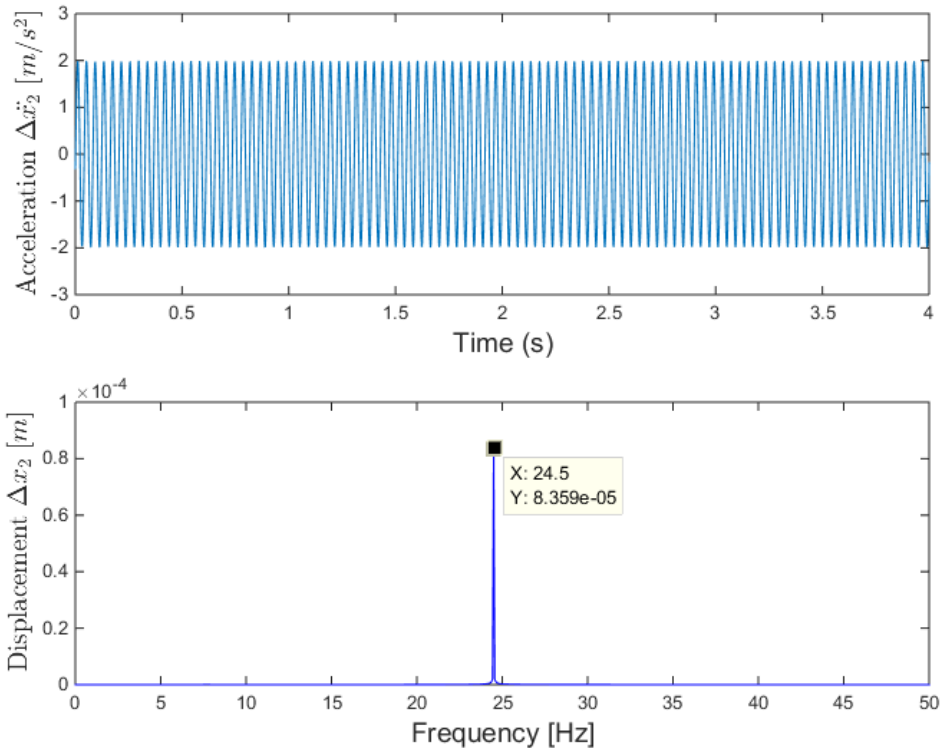

Figure 6.2: Predicted steady state horizontal response at Mount 2 for empty screen

top graph: time domain acceleration signal

bottom graph: frequency domain displacement signal

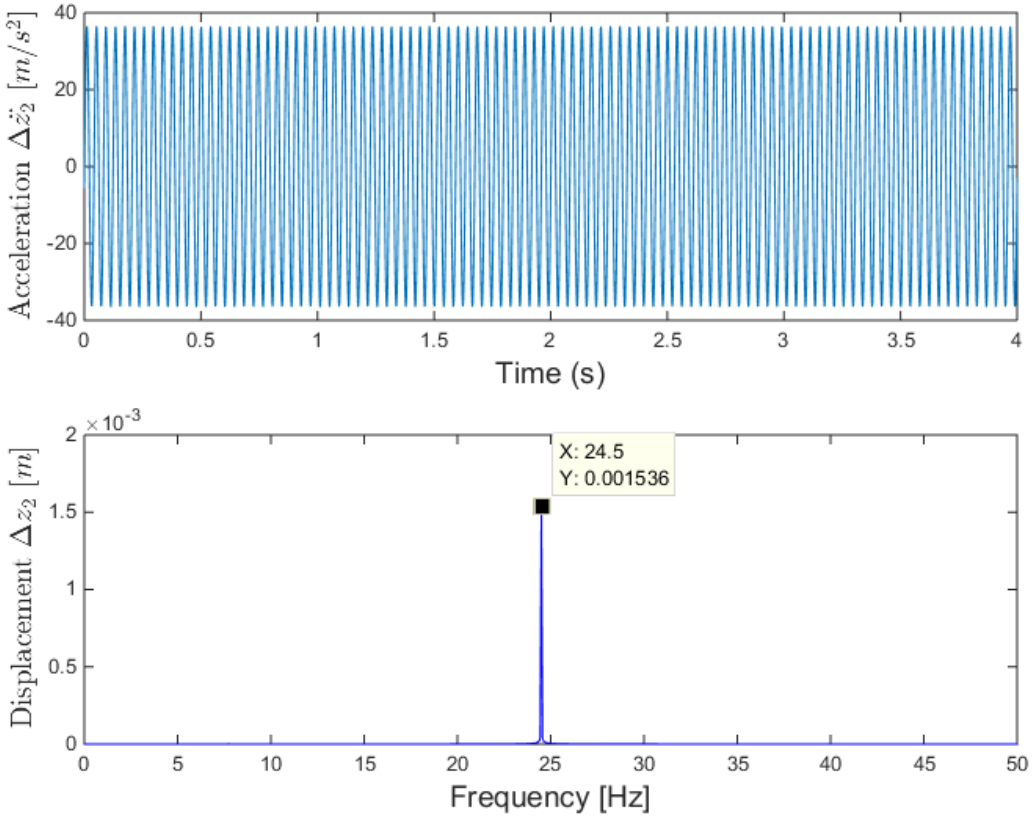

Figure 6.3: Predicted steady state vertical response at Mount 2 for empty screen

top graph: time domain acceleration signal

bottom graph: frequency domain displacement signal

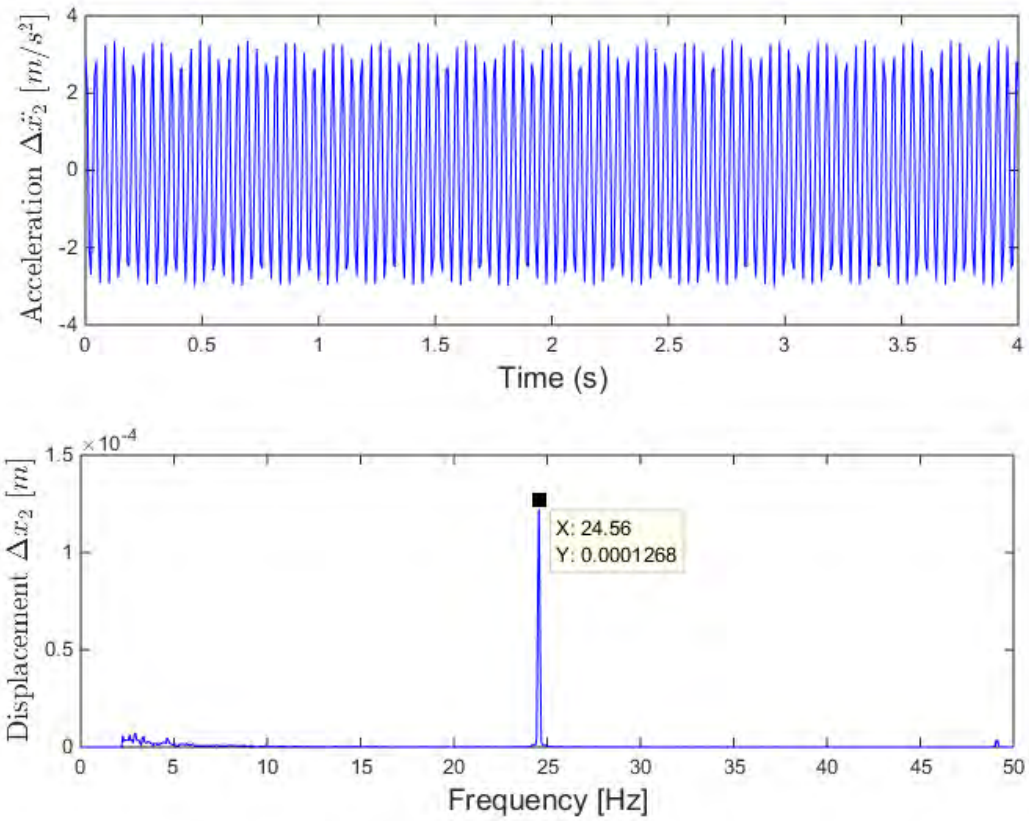

Figure 6.4: Measured steady state horizontal response at Mount 2 for empty screen

top graph: time domain acceleration signal

bottom graph: frequency domain displacement signal

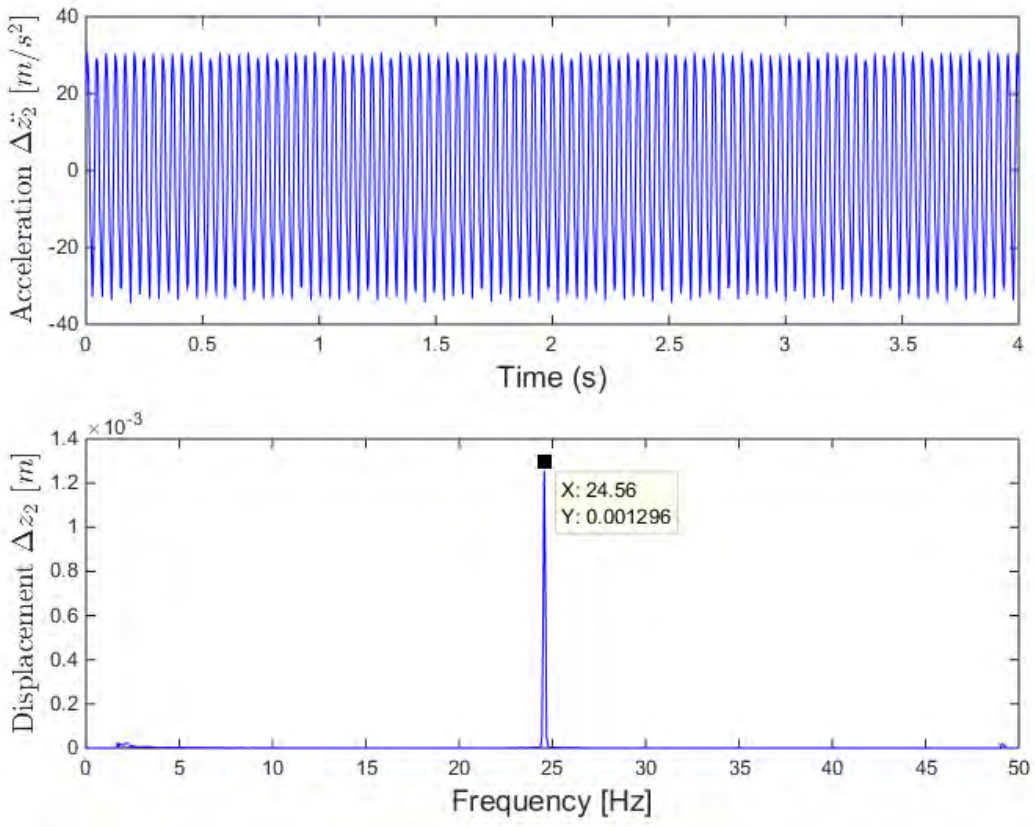

Figure 6.5: Measured steady state vertical response at Mount 2 for empty screen

top graph: time domain acceleration signal

bottom graph: frequency domain displacement signal

6.3.2 Transient response for empty screen

The transient responses were measured during start-up and shut-down respectively at the empty vibration screen. Transient response was simulated by solving the differential equations of motion described in Paragraph 2.1 in a computer program described in Paragraph 3.2 with numerical integration. The initial values used are that the response is zero at the beginning of time, for a certain excitation force then applied to simulate the start-up condition, until the steady state condition has been reached. To simulate the stopping (shut-down) condition, the forced frequency was then set to zero (see Appendix A). Figure 6.6 shows the predicted transient time domain signals in the horizontal direction at Mount 2, for start-up and shut-down conditions respectively. Figure 6.7 shows the predicted transient time domain signals in the vertical direction at Mount 2, for start-up and shut-down conditions respectively. Figure 6.8 shows the measured transient time domain signals in the horizontal direction at Mount 2, for start-up and shut-down conditions respectively. Figure 6.9 shows the measured transient time domain signals in the vertical direction at Mount 2, for start-up and shut-down conditions respectively.

Certain differences are observed regarding the corresponding predicted and measured time domain response signals for the shut-down condition with the empty screen. When the exciter motors were stopped, their rotors decelerated, and the screen response decreased as a result, until the speeds of these motors were very close to each of the system natural frequencies respectively. The response then increased when the exciter motor speeds coincided with each of the system natural frequencies sequentially. These differences were thus expected, because the deceleration of these rotors was neglected at these computer simulations, to simplify the mathematical model regarding the shut-down condition. The predicted and measured maximum acceleration amplitudes however corresponded well, when a natural frequency was exited during the screen shut-down condition.

Vibration measurements also indicated that maximum screen displacement was experienced during shut-down of the exciter motors. The analysis of these vibration signals revealed that the frequency for the cycle at the maximum response during shut-down as predicted was 8 Hz, and 8.3 Hz then measured, thus a very good

correlation was obtained. These frequencies were used for computation of the corresponding displacement amplitudes. Table 6.1 indicates the comparison between predicted and measured maximum amplitudes.

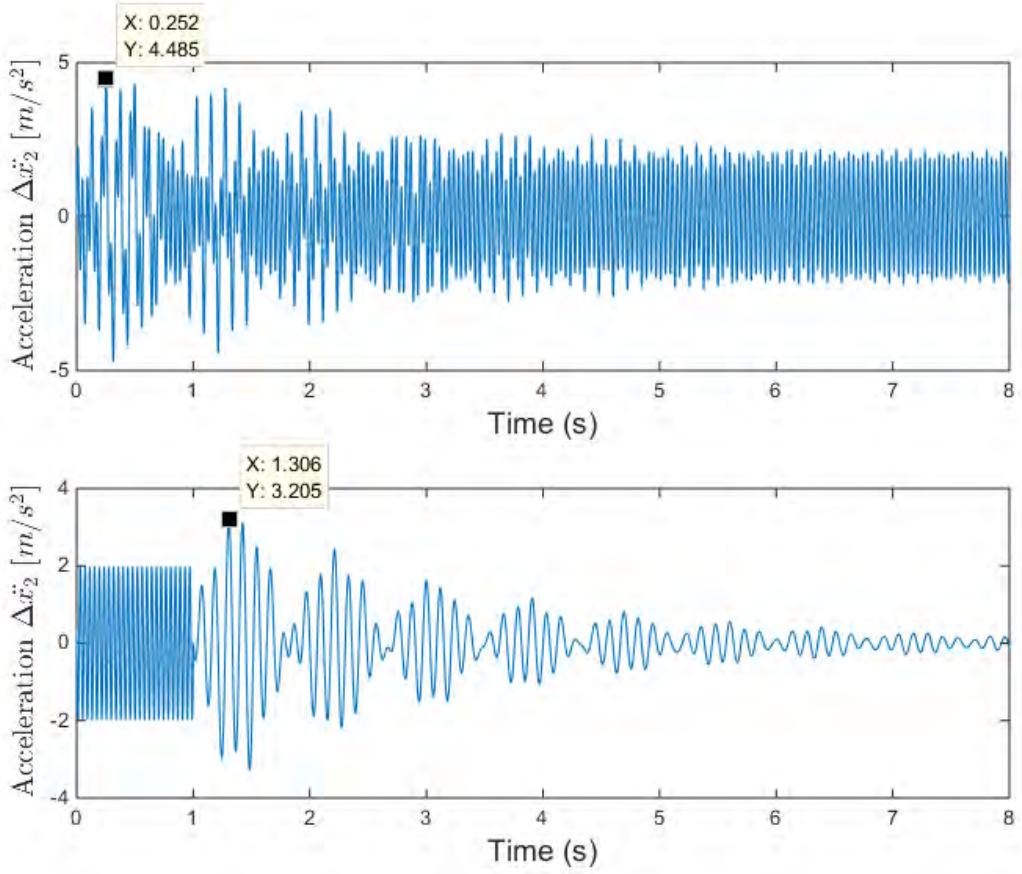

Figure 6.6: Predicted transient time domain horizontal acceleration response at Mount 2 for empty screen

top graph: start-up

bottom graph: shut-down

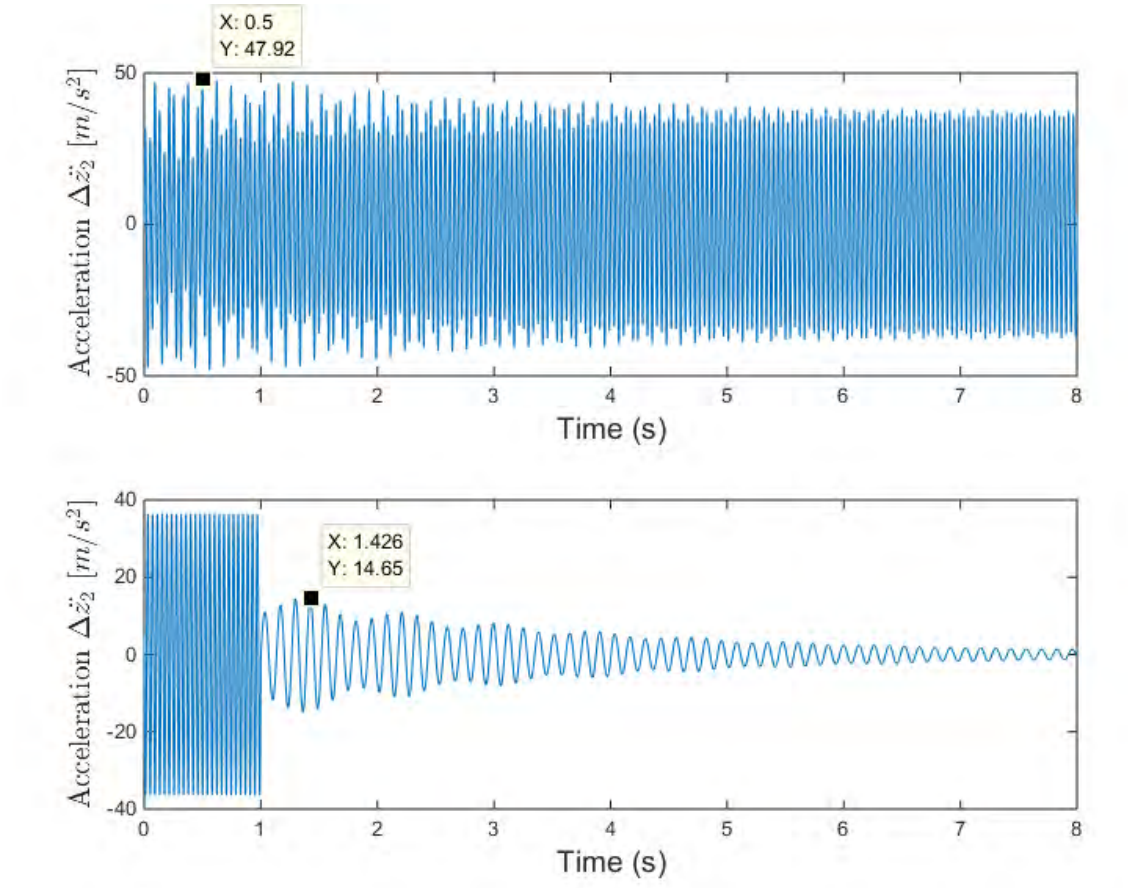

Figure 6.7: Predicted transient time domain vertical acceleration response at Mount 2 for empty screen

top graph: start-up

bottom graph: shut-down

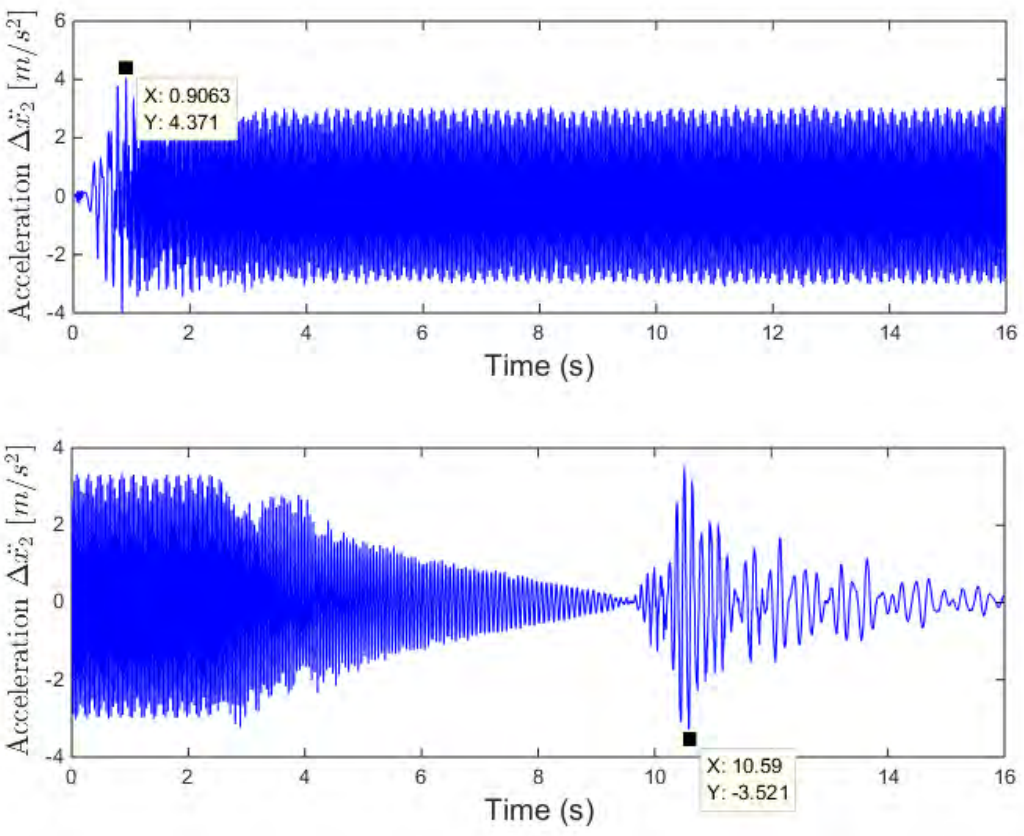

Figure 6.8: Measured transient time domain horizontal acceleration response at Mount 2 for empty screen

top graph: start-up

bottom graph: shut-down

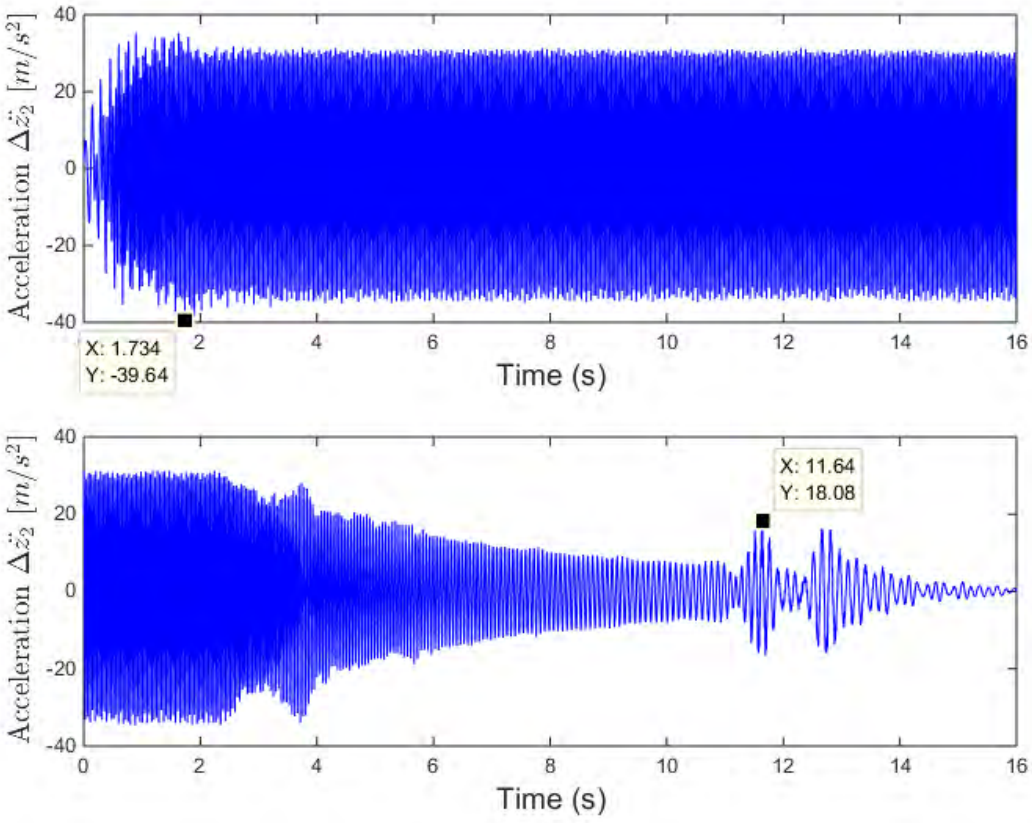

Figure 6.9: Measured transient time domain vertical acceleration response at Mount 2 for empty screen

top graph: start-up

bottom graph: shut-down

6.3.3 Comparison of predicted and measured response magnitudes for empty screen

Table 6.1 summarizes the predicted and measured response amplitudes at the different operational conditions for the empty vibration screen.

Table 6.1: Predicted and measured response amplitudes for empty vibration screen

Response parameter	Predicted displacement amplitude $[mm]$	Measured displacement amplitude $[mm]$
Steady state		
$\boldsymbol{\Delta X_1}$	0.10	0.14
$\boldsymbol{\Delta X_2}$	0.084	0.13
$\boldsymbol{\Delta Z_1}$	1.75	1.41
$\boldsymbol{\Delta Z_2}$	1.54	1.30
Transient (start-up)		
	Predicted acceleration amplitude $[m/s^2]$	Measured acceleration amplitude $[m/s^2]$
$\boldsymbol{\Delta \ddot{X}_1}$	4.17	4.54
$\boldsymbol{\Delta \ddot{X}_2}$	4.49	4.37
$\boldsymbol{\Delta \ddot{Z}_1}$	53.75	43.61
$\boldsymbol{\Delta \ddot{Z}_2}$	47.92	39.64
Transient (shut-down)		
	Predicted acceleration amplitude $[m/s^2]$	Measured acceleration amplitude $[m/s^2]$
$\boldsymbol{\Delta \ddot{X}_1}$	2.22	3.85
$\boldsymbol{\Delta \ddot{X}_2}$	3.21	3.52
$\boldsymbol{\Delta \ddot{Z}_1}$	13.20	18.42
$\boldsymbol{\Delta \ddot{Z}_2}$	14.65	18.08

6.4 Fully loaded vibration screen response

The vibration screen was fully loaded with a 65 kg mass of maize. The dynamic mount properties for each of the two screen mounts were 308.87 kN/m (stiffness coefficients k_{z1} and k_{z2}), and 0.044 kNs/m (damping coefficients c_{z1} and c_{z2}), as characterised and described in Chapter 4, Paragraph 4.6.4. The horizontal dynamic mount properties were 67.6 kN/m (stiffness coefficients k_{x1} and k_{x2}), and 0.13 kNs/m (damping coefficients c_{x1} and c_{x2}), as characterised and described in Chapter 4, Paragraph 4.6.6 were also used in the computer program. The small change in position of the centre of mass due to the maize on the screen was considered as negligible.

6.4.1 Steady state response for fully loaded screen

Figures 6.10 to 6.13 show the predicted and also the measured steady state time and frequency domain signals at Mount 2 for a fully loaded screen. The time domain acceleration signals were converted to frequency domain peak displacement signals. Table 6.2 indicates the comparison between corresponding predicted and measured amplitudes.

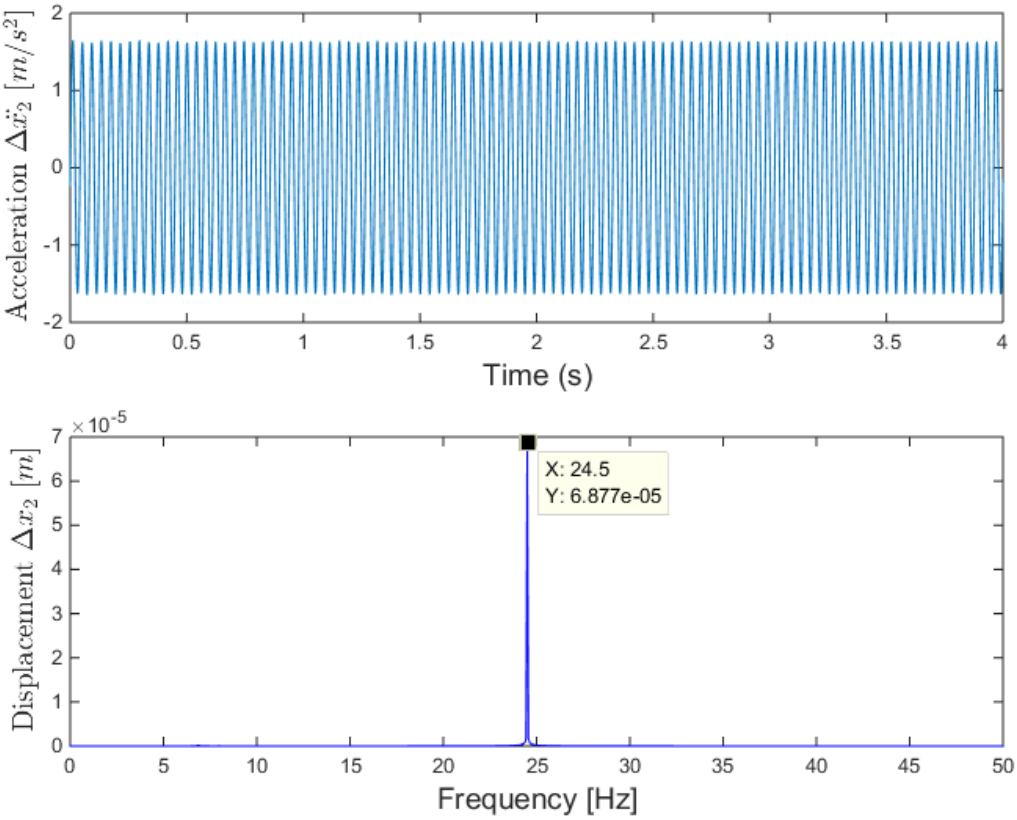

Figure 6.10: Predicted steady state horizontal response at Mount 2 for fully loaded screen

top graph: time domain acceleration signal

bottom graph: frequency domain displacement signal

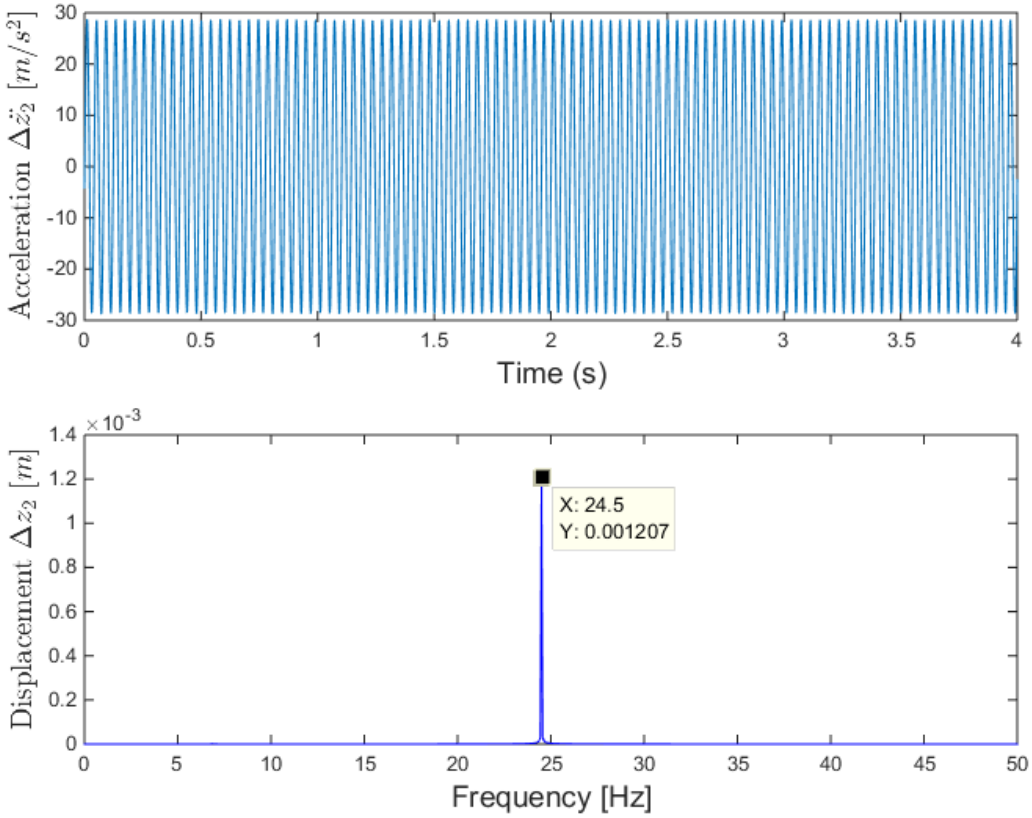

Figure 6.11: Predicted steady state vertical response at Mount 2 for fully loaded screen

top graph: time domain acceleration signal

bottom graph: frequency domain displacement signal

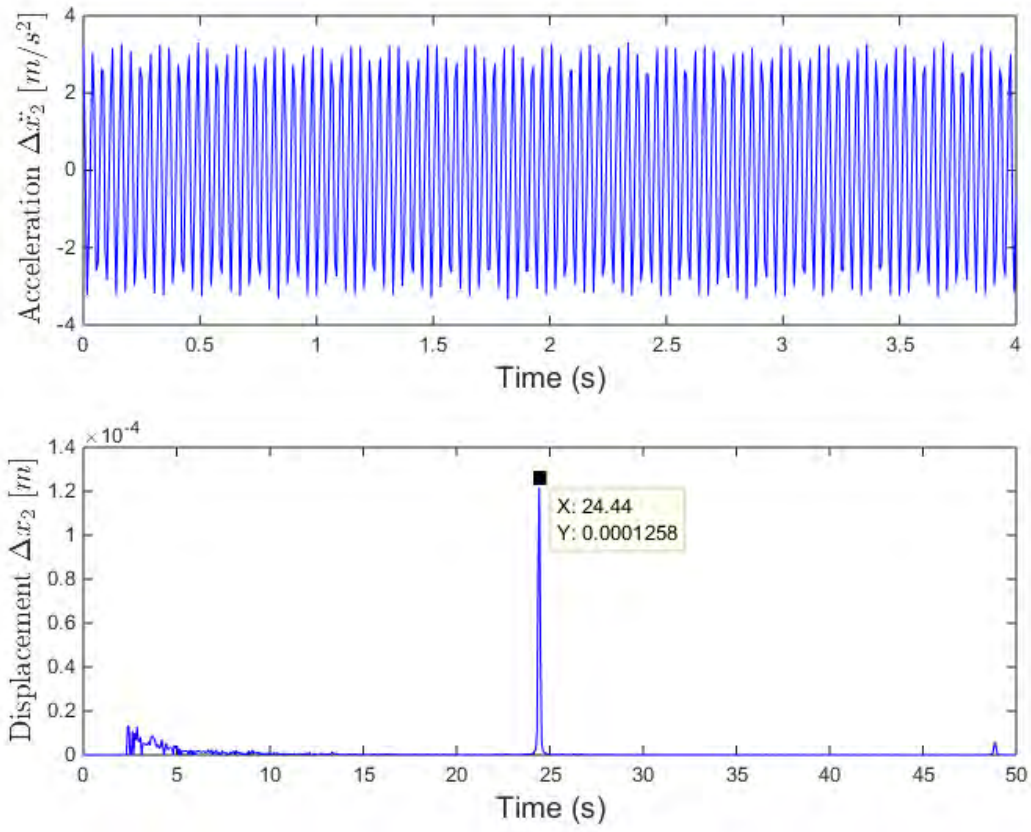

Figure 6.12: Measured steady state horizontal response at Mount 2 for fully loaded screen

top graph: time domain acceleration signal

bottom graph: frequency domain displacement signal

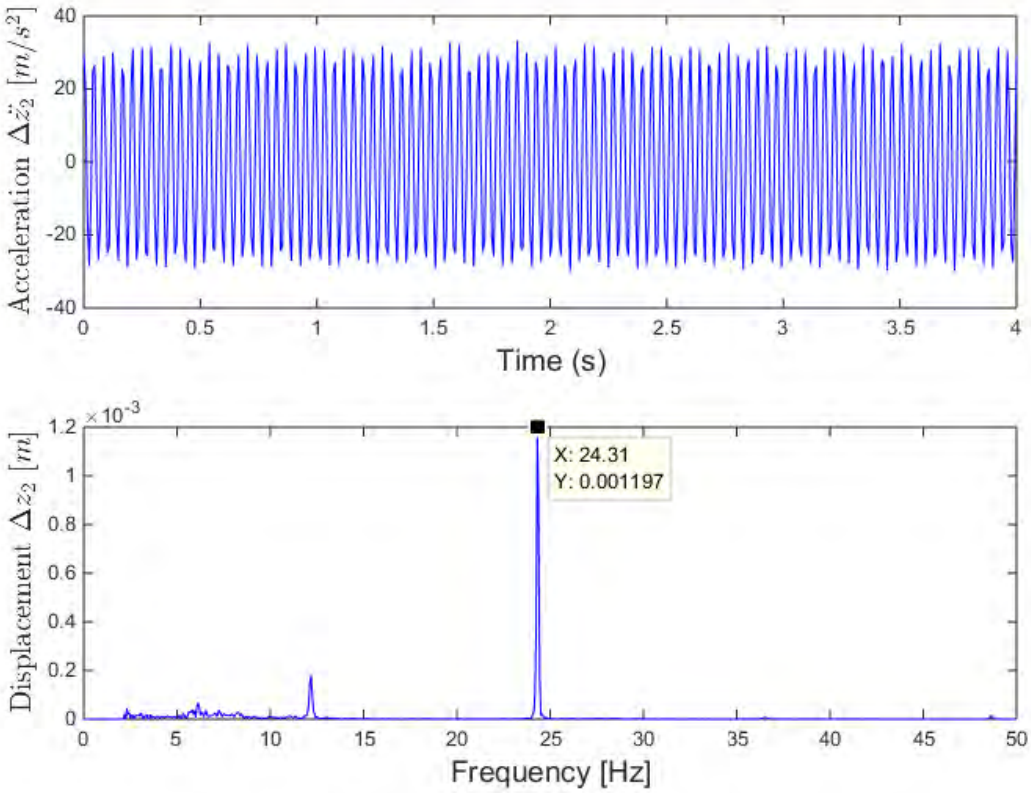

Figure 6.13: Measured steady state vertical response at Mount 2 for fully loaded screen

top graph: time domain acceleration signal

bottom graph: frequency domain displacement signal

6.4.2 Transient response for fully loaded screen

The transient responses were measured during start-up and shut-down respectively at the vibration fully loaded screen. The transient response for the empty vibration screen was simulated similarly to the empty screen. Figure 6.14 shows the predicted transient time domain signals in the horizontal direction at Mount 2, for start-up and shut-down conditions respectively. Figure 6.15 shows the predicted transient time domain signals in the vertical direction at Mount 2, for start-up and shut-down conditions respectively. Figure 6.16 shows the measured transient time domain signals in the horizontal direction at Mount 2, for start-up and shut-down conditions respectively. Figure 6.17 shows the measured transient time domain signals in the vertical direction at Mount 2, for start-up and shut-down conditions respectively.

Certain differences are observed regarding the corresponding predicted and measured time domain response signals for the shut-down condition with the fully loaded screen. When the exciter motors were stopped, their rotors decelerated, and the screen response decreased as a result, until the speeds of these motors were very close to each of the system natural frequencies respectively. The response then increased when the exciter motor speeds coincided with each of the system natural frequencies sequentially. These differences were thus expected, because the deceleration of these rotors was neglected at these computer simulations, to simplify the mathematical model regarding the shut-down condition. The predicted and measured maximum acceleration amplitudes, however, corresponded well when a natural frequency was exited during the screen shut-down condition.

Vibration measurements also indicated that maximum screen displacement was experienced during shut-down of the exciter motors. The analysis of these vibration signals revealed that the frequency for the cycle at the maximum response during shut-down as predicted was 7 Hz, and 7 Hz then also measured, thus an exact correlation was obtained. These frequencies were used for computation of the corresponding displacement amplitudes. Table 6.2 indicates the comparison between predicted and measured maximum amplitudes.

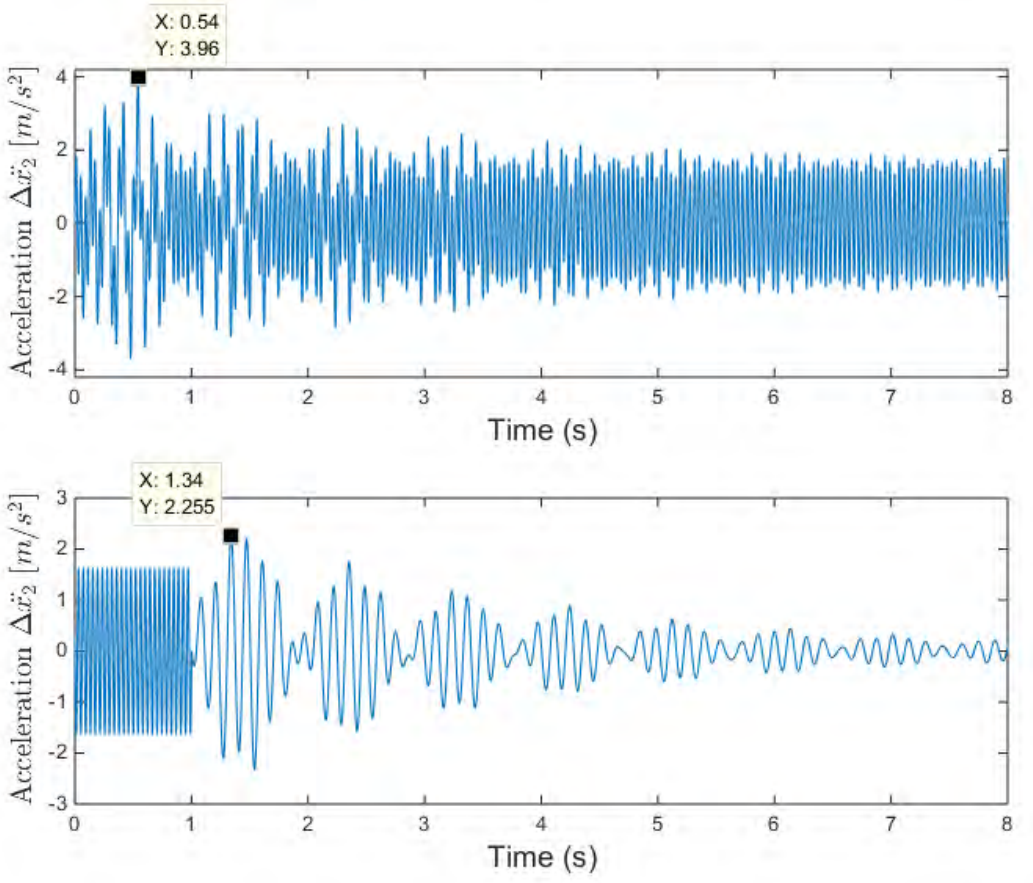

Figure 6.14: Predicted transient time domain horizontal acceleration response at Mount 2 for fully loaded screen

top graph: start-up

bottom graph: shut-down

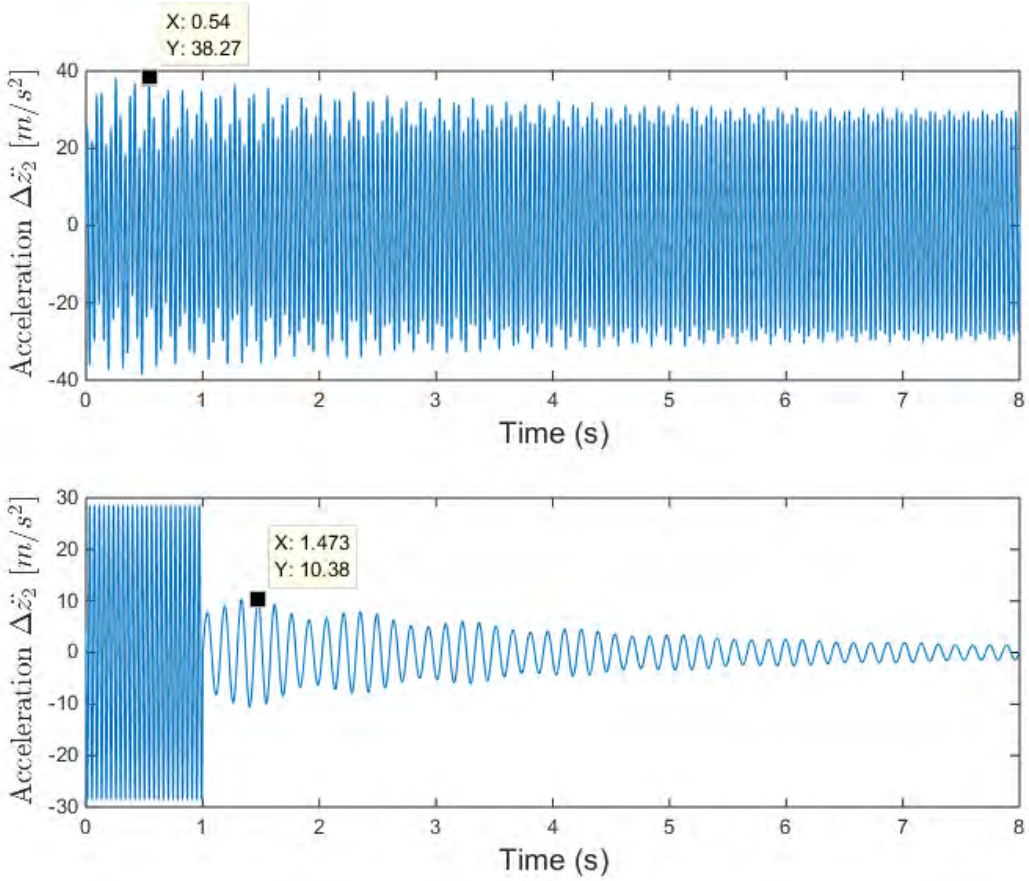

Figure 6.15: Predicted transient time domain vertical acceleration response at Mount 2 for fully loaded screen

top graph: start-up

bottom graph: shut-down

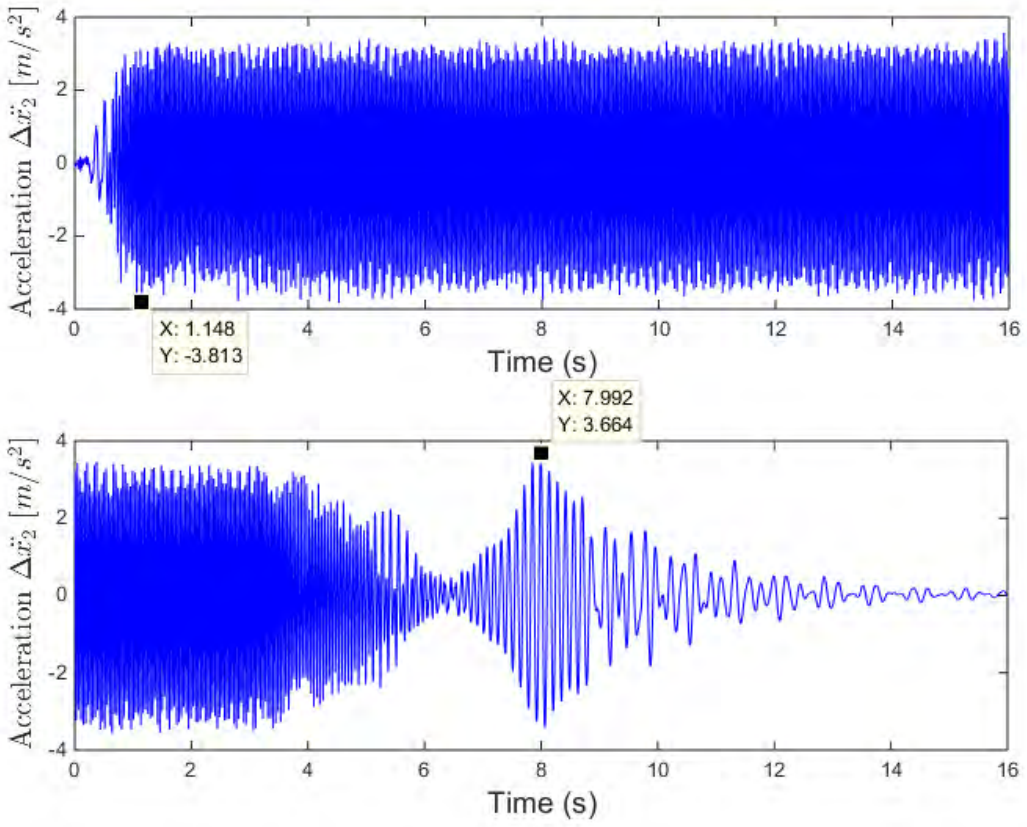

Figure 6.16: Measured transient time domain horizontal acceleration response at Mount 2 for fully loaded screen

top graph: start-up

bottom graph: shut-down

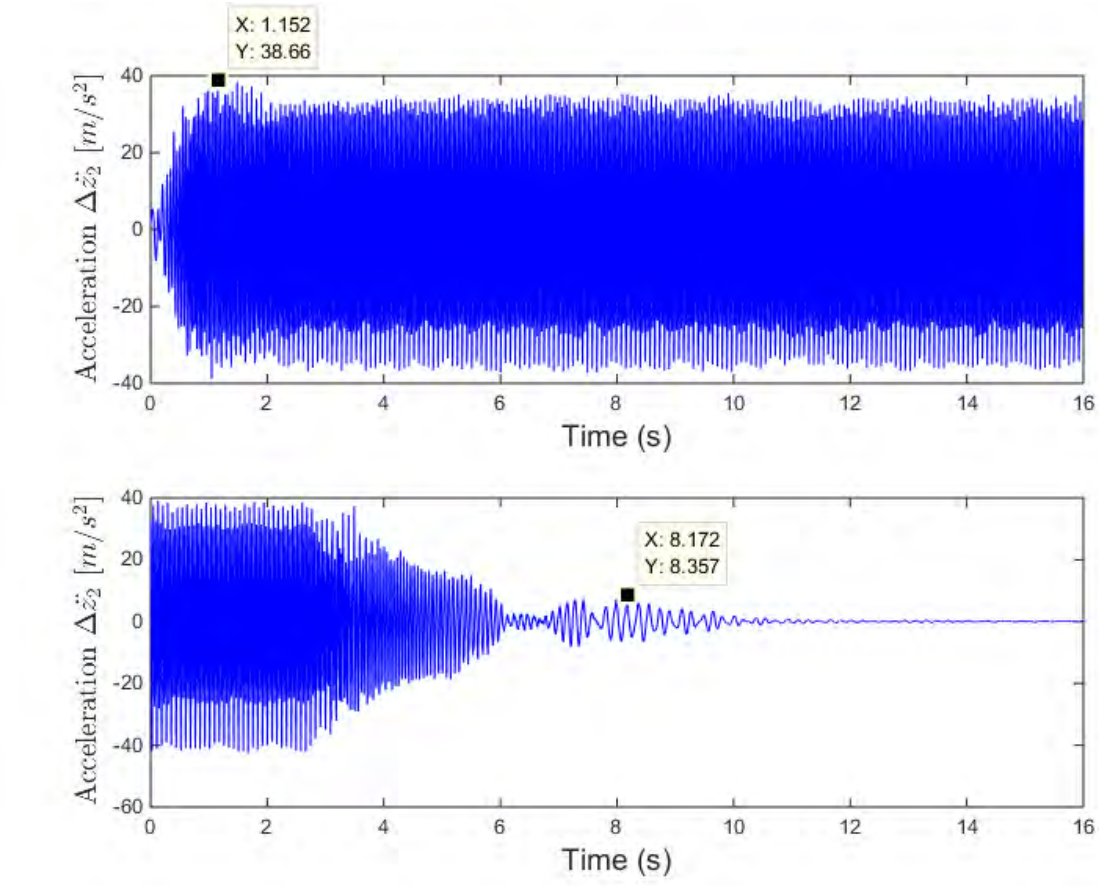

Figure 6.17: Measured transient time domain vertical acceleration response at Mount 2 for fully loaded screen

top graph: start-up

bottom graph: shut-down

6.4.3 Comparison of predicted and measured response magnitudes for fully loaded screen

Table 6.2 summarizes the predicted and measured response amplitudes at the different operational conditions for the fully-loaded vibration screen.

Table 6.2: Predicted and measured response amplitudes for fully-loaded screen

Response parameter	Predicted displacement amplitude $[mm]$	Measured displacement amplitude $[mm]$
Steady state		
$\boldsymbol{\Delta X_1}$	0.083	0.11
$\boldsymbol{\Delta X_2}$	0.069	0.12
$\boldsymbol{\Delta Z_1}$	1.37	1.36
$\boldsymbol{\Delta Z_2}$	1.21	1.2
Transient (start-up)		
	Predicted acceleration amplitude $[m/s^2]$	Measured acceleration amplitude $[m/s^2]$
$\boldsymbol{\Delta \ddot{X}_1}$	3.61	4.17
$\boldsymbol{\Delta \ddot{X}_2}$	3.97	3.81
$\boldsymbol{\Delta \ddot{Z}_1}$	40.14	40.38
$\boldsymbol{\Delta \ddot{Z}_2}$	38.27	38.66
Transient (shut-down)		
	Predicted acceleration amplitude $[m/s^2]$	Measured acceleration amplitude $[m/s^2]$
$\boldsymbol{\Delta \ddot{X}_1}$	1.53	2.63
$\boldsymbol{\Delta \ddot{X}_2}$	2.26	3.66
$\boldsymbol{\Delta \ddot{Z}_1}$	9.37	8.69
$\boldsymbol{\Delta \ddot{Z}_2}$	10.39	8.19

6.5 Empty vibration screen forces

The dynamic forces transmitted to the support structure were indirectly measured and determined with measured response and mount properties as experimentally characterised for an empty screen. This was done for the different operational conditions. The static forces at the screen mounts were determined.

6.5.1 Static forces for empty screen

The static reaction forces were computed based on the equations described in Paragraph 2.2.2, which were implemented in a computer program as described in Paragraph 3.2. The mount coordinates and magnitude of the mass as characterised in Chapter 4 were used as input values at this computer program. The computed reaction forces are indicated in the Table 6.3.

Table 6.3: Static reaction forces for empty screen

Reaction force Mount 1 $[N]$	Reaction force Mount 2 $[N]$
1 201.15	1 369.06

6.5.2 Steady state forces for empty screen

The steady state reaction forces are a combination of damping and spring forces. The reaction forces were computed at a fixed frequency of 24.5 Hz which is the steady state running speed of the exciter motors. The stiffness and damping mount properties for the empty vibration screen as characterised were used for the force computations (see Paragraph 4.6.4). The resultant force amplitude related to damping and stiffness force components was computed with the theorem of Pythagoras. The predicted and measured dynamic force amplitudes in the horizontal and vertical directions are indicated in Tables 6.4 and 6.5 respectively.

Table 6.4: Predicted and measured steady state horizontal force amplitudes for empty screen

Mount	Maximum displacement $[mm]$	Stiffness coefficient $[kN/m]$	Damping coefficient $[kNs/m]$	Spring force $[N]$	Damping force $[N]$	Resultant force $[N]$
Predicted						
1	0.10	67.6	0.11	6.76	1.69	6.97
2	0.084	67.6	0.11	5.68	1.42	5.85
Measured						
1	0.14	67.6	0.11	9.46	2.37	9.75
2	0.13	67.6	0.11	8.79	2.20	9.06

Table 6.5: Predicted and measured steady state vertical force amplitudes for empty screen

Mount	Maximum displacement $[mm]$	Stiffness coefficient $[kN/m]$	Damping coefficient $[kNs/m]$	Spring force $[N]$	Damping force $[N]$	Resultant force $[N]$
Predicted						
1	1.75	308.11	0.084	539.19	22.63	539.67
2	1.54	308.11	0.084	474.49	19.91	474.91
Measured						
1	1.41	308.11	0.084	434.44	18.23	434.82
2	1.30	308.11	0.084	400.54	16.81	400.90

6.5.3 Transient forces for empty screen

The transient force amplitudes were determined for shut-down at the empty vibration screen. The vibration screen experienced maximum displacement during this condition, and thus the maximum dynamic force amplitude. The analysis of the time signals revealed that the frequency for the cycle at the maximum response during shut-down as predicted was 8 Hz, and 8.3 Hz was measured. These frequencies were used for computation of the corresponding maximum displacement amplitudes. The stiffness and damping mount properties for the empty vibration screen as characterised were used for the corresponding force computations (see Paragraph 4.6.4). The resultant force amplitudes related to damping and stiffness force components were computed with the theorem of Pythagoras. These predicted and measured dynamic force amplitudes in the horizontal and vertical directions are indicated in Tables 6.6 and 6.7 respectively.

Table 6.6: Predicted and measured transient horizontal force amplitudes for empty screen

Mount	Maximum displacement $[mm]$	Stiffness coefficient $[kN/m]$	Damping coefficient $[kNs/m]$	Spring force $[N]$	Damping force $[N]$	Resultant force $[N]$
Predicted						
1	0.88	67.6	0.11	59.49	4.87	59.69
2	1.27	67.6	0.11	85.85	7.02	86.14
Measured						
1	1.42	67.6	0.11	95.99	8.15	96.34
2	1.29	67.6	0.11	87.20	7.40	87.51

Table 6.7: Predicted and measured transient vertical force amplitudes for empty screen

Mount	Maximum displacement $[mm]$	Stiffness coefficient $[kN/m]$	Damping coefficient $[kNs/m]$	Spring force $[N]$	Damping force $[N]$	Resultant force $[N]$
Predicted						
1	5.22	308.11	0.084	1 608.33	22.87	1 608.50
2	5.80	308.11	0.084	1 787.04	25.41	1 787.22
Measured						
1	6.77	308.11	0.084	2 085.90	29.66	2 086.12
2	6.65	308.11	0.084	2 048.93	29.13	2 049.14

6.5.4 Comparison of predicted and measured response magnitudes for empty screen

Table 6.8 summarizes the predicted and measured resultant force magnitudes for all operational conditions with the empty vibration screen.

Table 6.8: Predicted and measured resultant force amplitudes for empty screen

Force	Predicted resultant force amplitudes $[N]$	Measured resultant force amplitudes $[N]$
Steady State		
$\boldsymbol{F_{x1}}$	6.97	9.75
$\boldsymbol{F_{x2}}$	5.85	9.06
$\boldsymbol{F_{z1}}$	539.67	434.82
$\boldsymbol{F_{z2}}$	474.91	400.90
Transient		
$\boldsymbol{F_{x1}}$	59.69	96.34
$\boldsymbol{F_{x2}}$	86.14	87.51
$\boldsymbol{F_{z1}}$	1 608.50	2 086.12
$\boldsymbol{F_{z2}}$	1 787.22	2 049.14

6.6 Fully-loaded vibration screen forces

The same process as described in Paragraph 6.5 for the empty vibration screen was followed to compute the dynamic and static forces for a fully-loaded screen. Different mount and screen mass characteristics were used for these computations. The small change in position of the centre of mass due to the maize on the screen was neglected.

6.6.1 Static forces for fully-loaded screen

The static reaction forces were computed based on the equations described in Paragraph 2.2.2, which were implemented in a computer program as described in Paragraph 3.2. The mount coordinates and magnitude of the mass as characterised in Chapter 4 were used as input values at this computer program. The computed reaction forces are indicated in the Table 6.9.

Table 6.9: Static reaction forces for fully loaded screen

Reaction force Mount 1 $[N]$	Reaction force Mount 2 $[N]$
1 499.15	1 708.72

6.6.2 Steady state forces for fully-loaded screen

The stiffness and damping mount properties for the fully-loaded vibration screen as characterised were used for the force computations (see Paragraph 4.6.4). The resultant force amplitude related to damping and stiffness force components was computed with the theorem of Pythagoras. The predicted and measured dynamic force amplitudes in the horizontal and vertical directions are indicated in Tables 6.10 and 6.11 respectively.

Table 6.10: Predicted and measured steady state horizontal force amplitudes for fully-loaded screen

Mount	Maximum displacement $[mm]$	Stiffness coefficient $[kN/m]$	Damping coefficient $[kNs/m]$	Spring force $[N]$	Damping force $[N]$	Resultant force $[N]$
Predicted						
1	0.083	67.6	0.13	5.61	1.66	5.85
2	0.069	67.6	0.13	4.66	1.38	4.86
Measured						
1	0.11	67.6	0.13	7.44	2.20	7.76
2	0.12	67.6	0.13	8.11	2.40	8.46

Table 6.11: Predicted and measured steady state vertical force amplitudes for fully-loaded screen

Mount	Maximum displacement $[mm]$	Stiffness coefficient $[kN/m]$	Damping coefficient $[kNs/m]$	Spring force $[N]$	Damping force $[N]$	Resultant force $[N]$
Predicted						
1	1.37	308.87	0.044	423.15	9.28	423.25
2	1.21	308.87	0.044	373.73	8.2	373.82
Measured						
1	1.36	308.87	0.044	420.06	9.40	420.17
2	1.20	308.87	0.044	370.64	8.29	370.73

6.6.3 Transient forces for fully loaded screen

The transient forces of the loaded screen were computed similarly to the empty vibration screen as described in Paragraph 6.5.3. The analysis of the time signals revealed that the frequency for the cycle at the maximum response during shut-down as predicted was 7 Hz, and 7 Hz was also measured. These frequencies were used for computation of the corresponding maximum displacement amplitudes. The stiffness and damping mount properties for the fully-loaded vibration screen as characterised were used for the corresponding force computations (see Paragraph 4.6.4). The resultant force amplitudes related to damping and stiffness force components were computed with the theorem of Pythagoras. These predicted and measured dynamic force amplitudes in the horizontal and vertical directions are indicated in Tables 6.12 and 6.13 respectively.

Table 6.12: Predicted and measured transient horizontal force amplitudes for fully-loaded screen

Mount	Maximum displacement $[mm]$	Stiffness coefficient [kN/m]	Damping coefficient $[kNs/m]$	Spring force $[N]$	Damping force $[N]$	Resultant force $[N]$
Predicted						
1	0.79	67.6	0.13	53.4	4.52	53.59
2	1.17	67.6	0.13	79.09	6.69	79.37
Measured						
1	1.36	67.6	0.13	91.94	7.78	92.27
2	1.89	67.6	0.13	127.76	10.81	128.22

Table 6.13: Predicted and measured transient vertical force amplitudes for fully loaded screen

Mount	Maximum displacement $[mm]$	Stiffness coefficient $[kN/m]$	Damping coefficient $[kNs/m]$	Spring force $[N]$	Damping force $[N]$	Resultant force $[N]$
Predicted						
1	4.85	308.87	0.044	1498.02	9.39	1498.05
2	5.37	308.87	0.044	1658.63	10.39	1658.66
Measured						
1	4.49	308.87	0.044	1386.83	8.69	1386.85
2	4.23	308.87	0.044	1306.52	8.19	1306.55

6.6.4 Comparison of predicted and measured response magnitudes for fully-loaded screen

Table 6.14 summarizes the predicted and measured force magnitudes with all operational conditions with the loaded vibration screen.

Table 6.14: Predicted and measured resultant force amplitudes for fully-loaded screen

Force	Predicted resultant force amplitudes $[N]$	Measured resultant force amplitudes $[N]$
Steady State		
$\boldsymbol{F_{x1}}$	5.85	7.76
$\boldsymbol{F_{x2}}$	4.86	8.46
$\boldsymbol{F_{z1}}$	423.25	420.17
$\boldsymbol{F_{z2}}$	373.82	370.73
Transient		
$\boldsymbol{F_{x1}}$	53.59	92.27
$\boldsymbol{F_{x2}}$	79.37	128.22
$\boldsymbol{F_{z1}}$	1 498.05	1 386.85
$\boldsymbol{F_{z2}}$	1 658.66	1 306.55

6.7 Vibration screen natural frequencies

The natural frequencies of the vibration screen as a rigid body supported by elastic screen mounts were computed with the computer program as described in Paragraph 3.2 (see also Appendix A). These three natural frequencies were also measured with the accelerometer placed at Mount 2 and coupled to the DI 2200 FFT Analyser.

6.7.1 Empty vibration screen natural frequencies

The empty vibration screen was disturbed in the vertical z direction and the response then recorded. The measured time and frequency domain acceleration signals are shown in Figure 6.18.

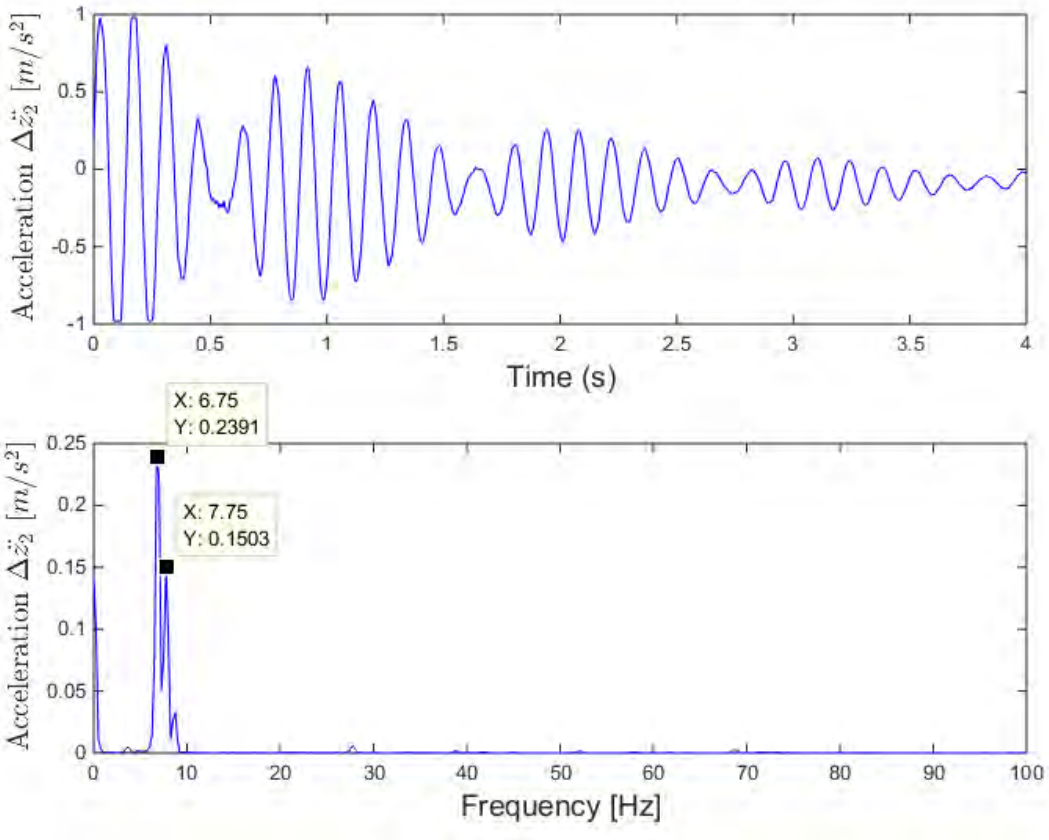

Figure 6.18: Measured vertical and rotational mode natural frequencies for empty screen

The empty vibration screen was also disturbed in the horizontal x direction and the response then recorded. The measured time and frequency domain response are shown in Figure 6.19.

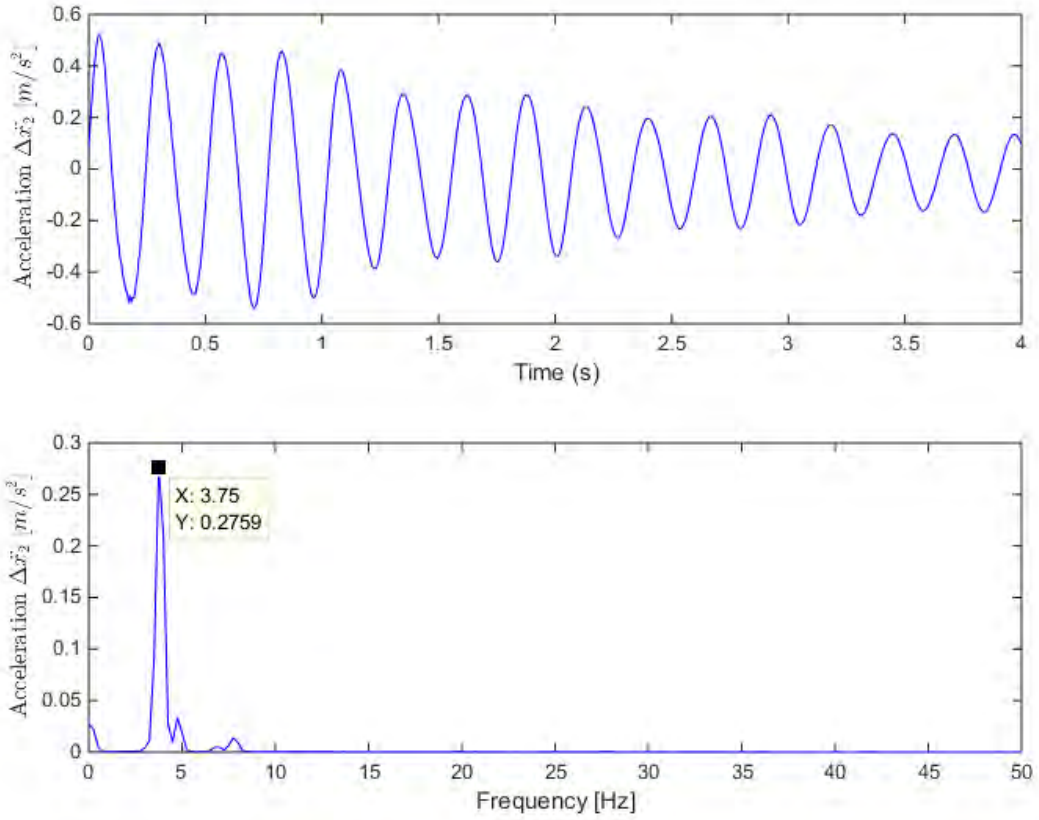

Figure 6.19: Measured horizontal mode natural frequency for empty screen

The magnitudes of these three natural frequencies for the fully loaded screen are indicated in Table 6.15

6.7.2 Fully-loaded vibration screen natural frequencies

The three natural frequencies were also measured with the screen then fully loaded with 65 kg of maize. The vibration screen was disturbed in the vertical z direction and the response then recorded. The measured time and frequency domain acceleration signals are shown in Figure 6.20.

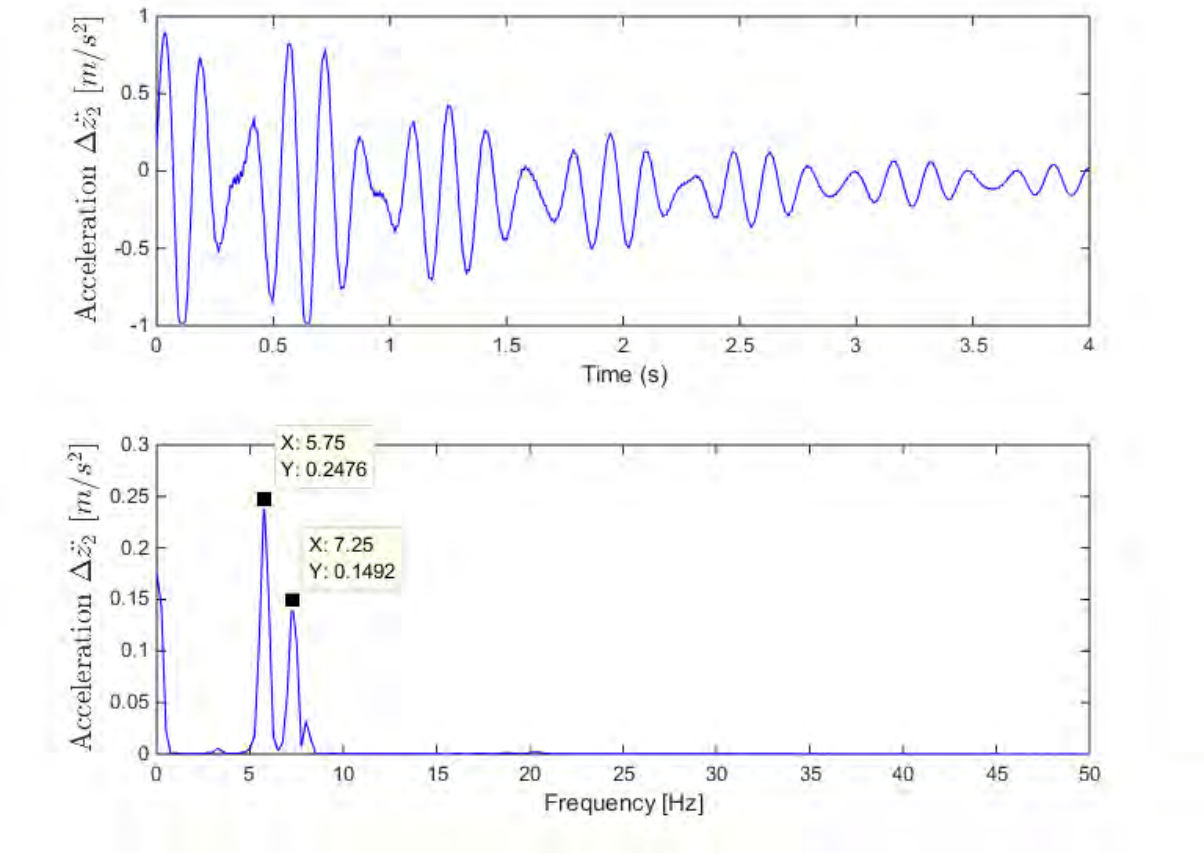

Figure 6.20: Measured vertical and rotational mode natural frequencies for fully loaded screen

Similar time and frequency domain signals were recorded as shown in Chapter 4, Figure 4.23 and previously used for the characterisation of the horizontal mount dynamic properties as described in Paragraph 4.6.6. This frequency domain signal also shows the natural frequency for the horizontal mode.

The magnitudes of these three natural frequencies for the fully-loaded screen are also indicated in Table 6.15.

6.7.3 Comparison of predicted and measured natural frequency magnitudes

The predicted and measured natural frequencies for the empty and fully-loaded vibration screens respectively are listed in Table 6.15. Good correlations were clearly obtained between corresponding predicted and measured magnitudes.

Table 6.15: Predicted and measured vibration screen natural frequencies

Empty vibration screen		
Mode	Predicted frequency $[Hz]$	Measured frequency $[Hz]$
$\boldsymbol{x}$	3.56	3.75
$\boldsymbol{z}$	7.85	6.75
$\boldsymbol{\theta_y}$	9.08	7.75
Fully-loaded vibration screen		
$\boldsymbol{x}$	3.19	3.25
$\boldsymbol{z}$	7.04	5.75
$\boldsymbol{\theta_y}$	8.14	7.25

6.8 Sieving process of vibration screen

The sieving process of the vibration screen was evaluated with harvested maize that typically contained weed seeds and other unwanted particles shown in Figure 6.21.

Figure 6.21: Maize kernels with unwanted particles on vibration screen

This unwanted material include Thorn Apple seeds, common cocklebur seeds, maize plant stems of various sizes, broken maize kernels, and small stone particles. Some of these particles are relatively smaller and other larger compared to the average maize kernel. The vibration screen was fitted with two sieves (large and small aperture sizes) which allowed both small and large particles to be removed simultaneously (see also Figure 6.22). A mass of 65 kg maize was used at the screen, and this resulted in a thickness layer of maize of approximately 50 mm on the screen. This ideal layer of maize was determined at the initial electrodynamic Shaker tests as described in Paragraph 4.2.

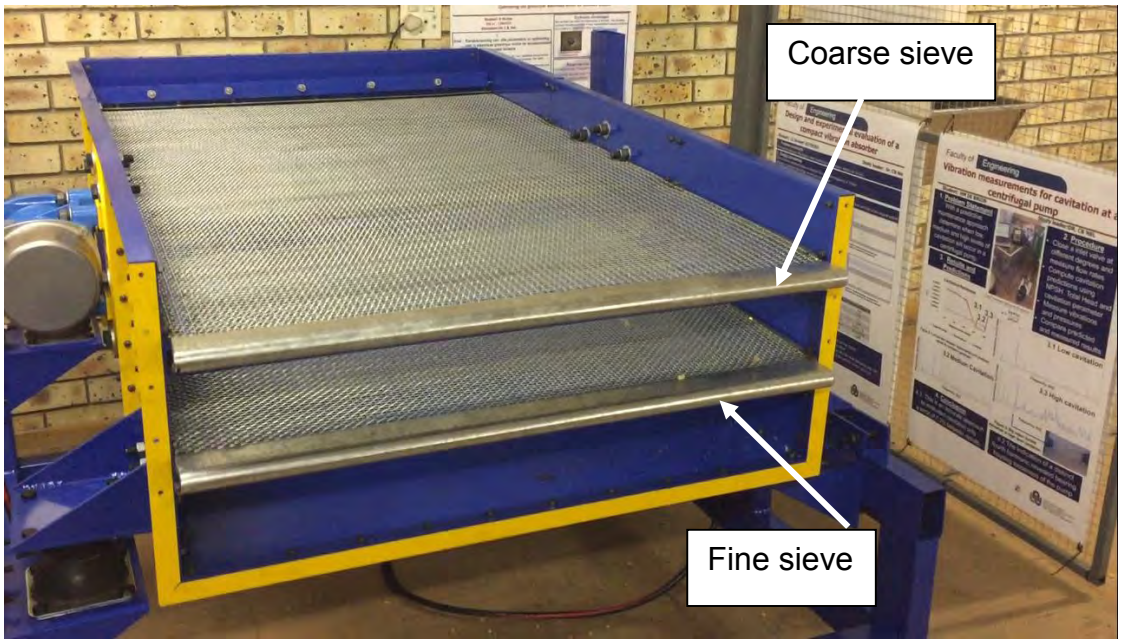

Figure 6.22: Two sieves fitted in vibration screen

Two bags were used at the discharge end of the vibration screen to collect the cleaned maize and also the finer unwanted particles. The screen with the bags attached is shown in the Figure 6.23.

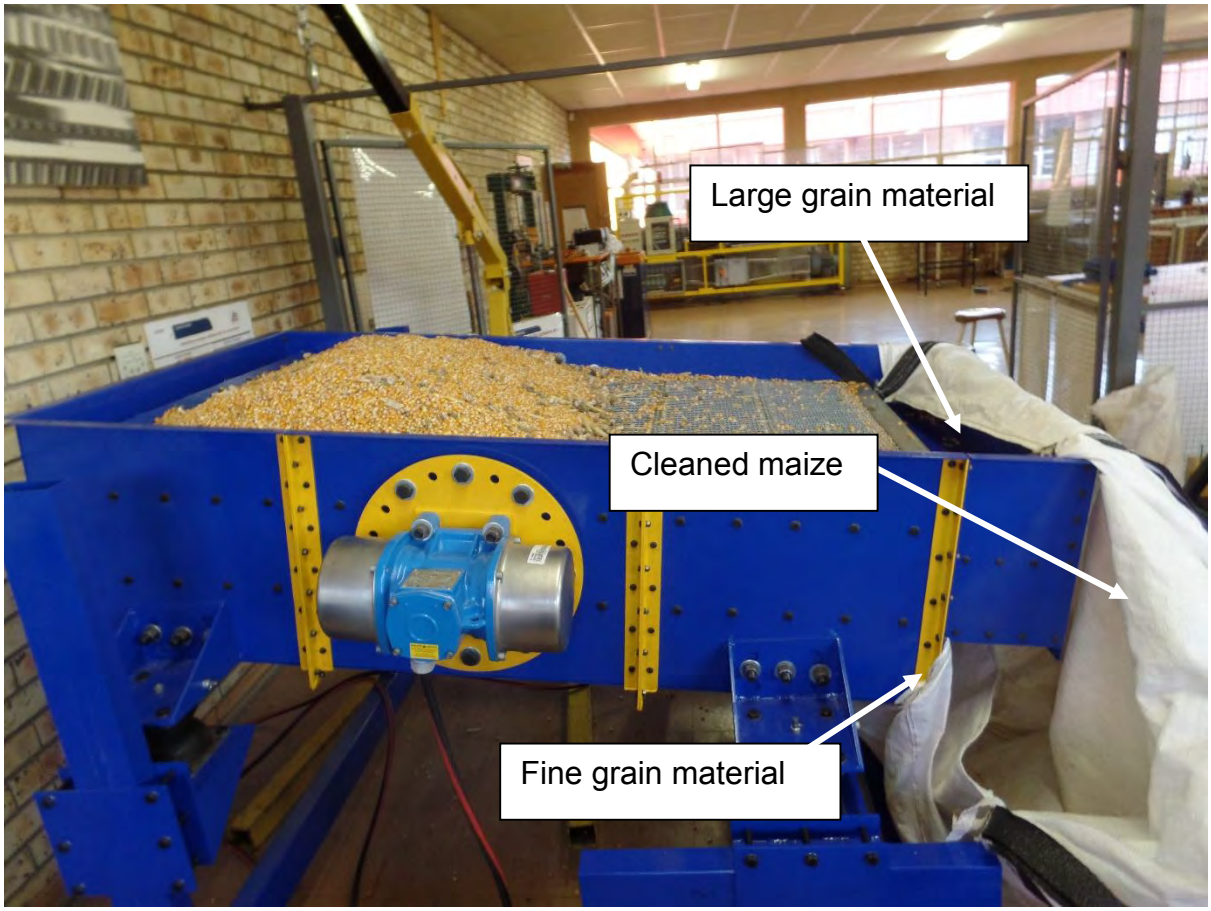

Figure 6.23: Vibration screen sieving of maize

The optimised design parameters were used to build and then test the vibration screen. The detailed design drawings are included in Appendix B. The vibration screen was successful in removing the smaller and larger unwanted particles from the maize. Different screen angles were tested, but the best angle at 5 degrees experimentally determined. Larger angles resulted in higher mass flow rates, but then poor sieving efficiency. Smaller angles resulted in poor mass flow rates, but then improved screening efficiency. With the 5 degree screen angle, a sufficient mass flow rate was determined as 2 tons per hour. Figures 6.24 and 6.25 show the unwanted fine and coarse material removed by the successful sieving process. Figure 6.26 shows the maize as cleaned by the vibration screen.

Figure 6.24: Fine unwanted particles successfully removed

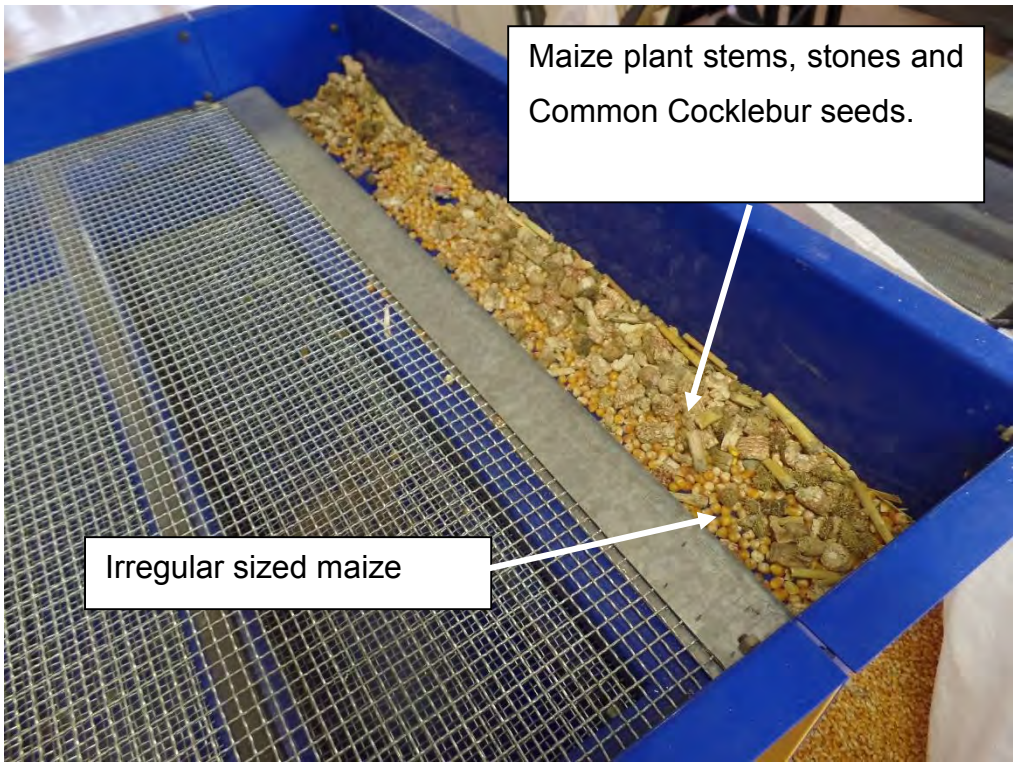

Figure 6.25: Coarse unwanted particles successfully removed

Figure 6.26: Cleaned maize

The two sieves used were 6x6 mm for the fine sieve, and 8x10 mm for the coarse sieve. The coarse sieve allowed the maize to pass, but any particles larger were then removed. A few relatively larger sized (irregular, round in shape) maize kernels were also removed, because they couldn't pass through the coarse sieve. All the material removed by the coarse sieve was captured at the discharge end at the top of the screen as shown in Figure 6.25. The fine grain material was collected at the bottom of the discharge end of the screen as shown in Figure 6.24. The unwanted particles that were removed by the fine sieve included Thorn apple seeds, small and broken pieces of maize, sand and fine plant material.

6.9 Conclusions

The underlying three degree of freedom mathematical model for the vibration screen was experimentally validated. The predicted responses, dynamic forces, and also the system natural frequencies were compared to the corresponding measured values respectively. This was done for several operational conditions (transient and steady state), at an empty and fully-loaded screen respectively. Transient conditions include start-up and shut-down of the screen. It was found that the predicted magnitudes for these parameters corresponded very well to the measured magnitudes. These measured parameters are related to the optimal design implemented, based on the optimisation criteria with mount stiffness coefficients chosen as design variables. The vibration screen was tested and the required measured response amplitude of 1.4 mm at 24.5 Hz also corresponded well to the predicted amplitude. This then resulted in the unwanted particles from the maize kernels being successfully and effectively removed. The experimental evaluation proved that all the underlying mathematical models are reliable.

An additional amplitude at exactly 50 % of the screen exciter motor speed was observed for vibration measurements taken at the fully loaded screen, which was not present for similar corresponding measurements taken at the empty screen. This amplitude is, however, significantly smaller, compared to the amplitude at running speed, and thus not of major concern. It is believed that the presence of this additional amplitude is caused by the fact that the maize did not stay in contact with sieve all the time during sieving. This also implied that the effective mass was then slightly changed, which might also explain the reason for small deviations in predicted and measured responses. This additional amplitude at this forced frequency could possibly also cause resonance, but for this design all three natural frequencies are significantly lower, and thus far away from resonance.

7 Conclusions

Mathematical models were developed and also implemented in computer programs used for design analysis of a vibration screen. This was regarded necessary to investigate effective screening of maize in order to remove unwanted particles, and also to provide acceptable service life from a fatigue point of view. A three degree of freedom mathematical model was developed and used for prediction of static and dynamic displacements, static and dynamic forces, and also system natural frequencies. Another mathematical model was formulated and implemented in a computer program and used for fatigue analysis.

The input parameters required for the computer programs were characterised. These parameters include screen rigid body mass, position of centre of gravity of screen, screen rigid body Mass Moment of Inertia, global coordinates of screen mounts, exciter motor speed and unbalance characteristics, global coordinates of two exciter motors, angle of attachment of the exciter motors, screen angle, and also rubber mount static and dynamic properties. In addition, the required amplitude and frequency for a certain layer of maize was also characterised with electrodynamic Shaker tests. Different feasible sieve apertures were identified for two sieves at the vibration screen.

A mathematical model was also developed for characterisation of the screen mount vertical stiffness and damping coefficients with an electrodynamic Shaker approach. This model was implemented in a computer program, and measured data used as input. The dynamic vertical properties of the rubber mounts were successfully characterised with the electrodynamic Shaker approach, and the values corresponded well to magnitudes obtained from the supplier. The Shaker tests showed that the mount dynamic properties are dependent on both amplitude and static preload, and this was then also taken into account in the screen design analysis. Another mathematical model was developed for characterisation of the screen mount horizontal stiffness and damping coefficients with a Bump test approach. This model was also implemented in a computer program, and measured data used as input. The horizontal dynamic properties of the rubber mounts were successfully characterised *in situ* with a Bump test approach and is in the same range compared to the magnitude obtained from the supplier. The static mount stiffness coefficients were also

experimentally determined and these magnitudes are different, compared to the dynamic stiffness properties as expected.

Three different design goals for an optimisation approach were identified. Firstly, the criteria for vibration isolation an objective function based on the transmission of dynamic forces to the foundation were formulated. Secondly, two constraints that influenced vibration isolation were also formulated. These constraints were regarded as necessary to ensure enough movement for effective sieving, but also to limit the horizontal and vertical mount displacements typically present during transient conditions. Three-dimensional graphical representations and contour plots were constructed in a Matlab environment, and used to determine vertical and horizontal mount stiffness coefficients, chosen as design variables for an optimal design according to the criteria formulated.

A Finite Element Analysis (FEA) approach was followed to investigate possible structural resonance of the elastic screen, but the results revealed that the natural frequencies of the mode shapes mainly provided by the elasticity of the screen structure are above the exciter motor speed. Calculations also indicate that the natural frequencies at these mode shapes can be regarded as safe in spite of the larger magnitude in mass (actual screen structure mass and mass of maize, compared to mass used in FEA). The FEA approach was also used to evaluate the vertical stiffness of the screen. It was found that this vertical stiffness was large enough, and the assumption of a rigid body made in the three degree of freedom mathematical model thus regarded as valid.

An FEA approach was also used to determine static and dynamic material stresses used for fatigue analysis of the screen structure. It was found that the risk regarding fatigue failure is eliminated for fatigue safety factor values larger than 1, thus an infinite service life is expected for this grain vibration screen for the larger safety factors obtained. This was obtained for two different fatigue analysis approaches, namely for the Goodman criteria and also the alternative criteria described in the EN 1993-1-9 code as developed for fatigue consideration in the standard design of steel structures.

The optimised design parameters were used to build and then test the vibration screen. The vibration screen was successful in removing the smaller and larger unwanted particles such as weed seeds, sand, small broken maize kernels, maize plant stems as typically present from harvested maize with the two different sieves simultaneously used. Different screen angles were tested, and the best angle at 5 degrees experimentally determined. Larger angles resulted in higher mass flow rates, but then poor sieving efficiency. Smaller angles resulted in poor mass flow rates, but then improved screening efficiency. For the 5 degree screen angle, a sufficient mass flow rate was determined at 2 tons per hour. This was regarded as a feasible maize flow rate through the screen.

The underlying three degree of freedom mathematical model for the vibration screen was experimentally validated. The predicted responses, dynamic forces, and also the system natural frequencies were compared to the corresponding measured values respectively. This was done for several operational conditions (transient and steady state), at an empty and fully loaded screen respectively. Transient conditions include start-up and shut-down of the screen. It was found that the predicted magnitudes for these parameters corresponded very well to the measured magnitudes. These measured parameters are related to the optimum design implemented, based on the optimisation criteria with mount stiffness coefficients chosen as design variables. The vibration screen was tested and the required measured response amplitude of 1.4 mm at 24.5 Hz also corresponded well to the predicted amplitude. This then resulted that the unwanted particles from the maize kernels were successfully and effectively removed. The experimental evaluation proved that all the underlying mathematical models are reliable.

An additional amplitude at exactly 50% of the screen exciter motor speed was observed for vibration measurements taken at the fully-loaded screen, which was not present for similar corresponding measurements taken at the empty screen. This amplitude is, however, significantly smaller, compared to the amplitude at running speed, and thus not of major concern. It is believed that the presence of this additional amplitude is caused by the fact that the maize did not stay in contact with sieve all the time during sieving. This also implied that the effective mass was then slightly changed, which might also explain the reason for small deviations in predicted and

measured responses. This additional amplitude at this forced frequency could possibly also cause resonance, but for this design all three natural frequencies are significantly lower, and thus far away from resonance.

The grain vibration screen was designed to mainly sieve maize, but other grain such as sunflower, soybean, canola, ground nuts, wheat, barley, oats and sorghum could also be sieved. The grain vibration screen was designed so that the angle of the vibration screen, and also the angle of attachment of the exciter motors were both adjustable. These adjustments could possibly then be changed for screening of different types of grain.

It was found that transient behaviour caused the larger maximum displacements defined as constraints and also used for optimisation. It is recommended that further research be done for the development of possible mechanisms such as for example hydraulic mounts with de-couplers to allow adjustment of damping properties, which could reduce mount displacements during transient conditions. This could then lead to softer screen mounts, with further improved vibration isolation and a smaller screen structure mass magnitude as a result.

References

BarryControls. 2014. Isolator Selection. http://www.hutchinsonai.com/engineering/shock.cfm Date of access: 7 November 2015.

Budynas, R.G. & Nisbett, J.K. 2011. Shigley's Mechanical Engineering Design: McGraw-Hill Education.

Chen, Y. & Tong, X. 2010. Modeling screening efficiency with vibrational parameters based on DEM 3D simulation. *Mining Science and Technology*, 20(4):615-620.

Cheng, L.L., Fan, H., Ying, Y.Z., Yang, G. & Peng, G. 2013. Failure analysis and structure improvement of beam of liner vibrating screen. *Advanced Materials Research,* 619, 69-70.

Dong, H., Liu, C., Zhao, Y. & Zhao, L. 2013. Influence of vibration mode on the screening process. *International Journal of Mining Science and Technology*, 23(1):95-98.

Du, X. 2012. Modal analysis and design on the base plate of large-scale linear vibration screen. *Applied Mechanics and Materials,* 155-156, 514-518.

Ewins, D.J. 1984. Modal Testing: Theory and practise: Research Studies Press.

Fletcher, R. & Reeves, C.M. 1964. Function minimization by conjugate gradients. *The computer journal*, 7(2):149-154.

Fuchs, C. 1984. UNBALANCE MOTORS - THE RELIABLE DRIVE FOR MODERN VIBRATORY SYSTEMS. *Bulk Solids Handling*, 4(1):149-151.

GKD. 2015. Overhook Screens. http://www.gkd.co.za/products/bu1-solidweave/category/overhook-screens Date of access: 17 March 2014.

GrainSA. 2014. Onkruidsaad in gewassaad: só versprei skadelike onkruide graag. http://www.grainsa.co.za/onkruidsaad-in-gewassaad:-soacute;-versprei-skadelike-onkruide-graag Date of access: 22 April 2014.

Harris, M.D. 1988. Locker vimec natural frequency conveyors. *Bulk Solids Handling*, 8(6):718-719.

He, X.m. & Liu, C.s. 2009. Dynamics and screening characteristics of a vibrating screen with variable elliptical trace. *Mining Science and Technology*, 19(4):508-513.

Heyns, P.S., Nel, C.B. & Snyman, J.A. 1994. Optimisation of engine mounting configurations. *International Seminar on Modal Analysis*.

Hota, S.P. & Karmakar, R. 1988. Optimisation studies on vibratory conveyors. *Bulk Solids Handling*, 8(6):715-717.

Hou, Y., Fang, P. & Zeng, L. 2012. Finite element analysis of dual-frequency vibrating screen. *Advanced Materials Research,* 479-481, 2124-2128.

Hurst, S. 2014. Plants Profile for Xanthium strumarium (rough cocklebur). http://luirig.altervista.org/photos-search/index2.php?rcn=23479 Date of access: 22 April 2014.

Ispot. 2014. Ispot. http://www.ispot.org.za/species_dictionary/Senecio%20ilicifolius Date of access: 22 April 2014 2014.

MGLEngineering. 2014. Featured Service: Screening. http://mglengineering.com/news/2014/3/3/featured-service-screening.html Date of access: 7 March 2014.

Nel, C.B. 2000. Optimisation of engine mount systems at front-wheel-drive vehicles for multiple operational conditions. *Proceedings. ISMA25*.

Nel, C.B. 2007. Design analysis of a rubber mount system for a push-type centrifuge. *Proceedings. ICSV14*.

Nel, C.B. 2009. Analysis of a vibration isolation system for a circulation pump. *International Conference on Integrity, Reliability and Failure*.

PATEL, B.P. & PRAJAPATI, H.R. 2013. Design of Vibratory Screen used in Coal Mining Industry to Prevent Failure – A Case Study. *International Journal of Research in Modern Engineering and Emerging Technology*, 1(1):14-23.

Peng, L.P., Liu, C.S., Song, B.C., Wu, J.D. & Wang, S. 2015. Improvement for design of beam structures in large vibrating screen considering bending and random vibration. *Journal of Central South University*, 22(9):3380-3388.

Rao, S.S., 2011. Mechanical Vibrations: Prentice Hall.

SAGIS. 2015. Introducing SAGIS. http://www.sagis.org.za/ Date of access: 16 September 2015.

Snyman, J.A. 1982. A new and dynamic method for unconstrained minimization. *Department of Applied Mathematics*, 6:449-462.

Steyn, J. 1995. Fatigue failure of deck support beams on a vibrating screen. *International Journal of Pressure Vessels and Piping*, 61(2-3):315-327.

Van Wyk, A.J., Snyman, J.A. & Heyns, P.S. 1994. Optimization of a vibratory conveyor for reduced support reaction forces. *R&D Journal*, 10(1):12-17.

von Beesten, F. 2014. Sklerotinia. http://www.sojafoerderring.de/anbauratgeber/krankheiten-und-schaedlinge/sklerotinia/ Date of access: 23 April 2014.

Winkler, G. 1979. Analysing the hopping conveyor. *International Journal of Mechanical Sciences*, 21(11):651-658.

Xiao, J. & Tong, X. 2012. Particle stratification and penetration of a linear vibrating screen by the discrete element method. *International Journal of Mining Science and Technology*, 22(3):357-362.

Xiao, J. & Tong, X. 2013. Characteristics and efficiency of a new vibrating screen with a swing trace. *Particuology*, 11(5):601-606.

Yue-min, Z., Chu-sheng, L., Xiao-mei, H., Cheng-yong, Z., Yi-bin, W. & Zi-ting, R. 2009. Dynamic design theory and application of large vibrating screen. (*In*. Procedia Earth and Planetary Science organised by. p. 776-784).

Zhang, L. & Zhong, L.W. 2009. Dynamics and fatigue analysis of linear vibrating screen. *Shanghai Ligong Daxue Xuebao/Journal of University of Shanghai for Science and Technology*, 31(3):299-302.

Zhang, Z. & Xu, J. 2013. Fatigue analysis of linear vibrating screen with different surface roughness. *Key Engineering Materials,* 561, 564-567.

Zhang, Z.R., Fan, Z.M. & Wang, Y.Y. 2014. Fatigue life and reliability analysis of large linear vibrating screen. *Meitan Xuebao/Journal of the China Coal Society*, 39(SUPPL.1):257-261.

Zhao, L., Liu, C. & Yan, J. 2010. A virtual experiment showing single particle motion on a linearly vibrating screen-deck. *Mining Science and Technology*, 20(2):276-280.

Zhou, N. 2015. Dynamic characteristics analysis and optimization for lateral plates of the vibration screen. *Journal of Vibroengineering*, 17(4):1593-1604.

Appendix A – Matlab computer programs

Three degree of freedom mathematical model

```
function response_single
global x1 x2 z3 x3 z1 z2 kx1 kx2 kz1 kz2 cx1 cx2 cz1 cz2 m alpha Jyy F0 r
omega beta

%Inputs
%=========================================================================
%Constants
g = 9.81;
%Integration time interval
t = 0:0.001:30;

%Initial values
x0 = [0.0 0.0 0.0 0.0 0.0 0.0];

%Coordinates
x1 = -0.5837;
x2 = 0.51211;
x3 = -0.02046;
z1 = -0.14969;
z2 = -0.24556;
z3 = 0.0377;

%Angles
alpha = 5*(pi/180);
beta = 85*(pi/180);

%Mass and mass moment of inertia
m = 262;
r = 0.490;

%Mount dynamic properties
kz1 = 290000;
kz2 = 290000;
kx1 = 80000;
kx2 = 80000;
zeta_z = 0.006129;
zeta_x = 0.0192;

%Mount static stiffness
k_s1 = kz1/1.45;
k_s2 = kz2/1.45;

%Exciter motor characteristics
M_u = 0.298*2*0.65;
f =  24.5; %Frequency [Hz]

%=========================================================================
%Calculations
%=========================================================================
%Viscous damping coefficients
Ccz = 2*sqrt((kz1+kz2)*(m));
Ccx = 2*sqrt((kx1+kx2)*(m));
cz1 = (zeta_z*Ccz)/2;
```

```
cz2 = cz1;
cx1 = (zeta_x*Ccx)/2;
cx2 = cx1;

%Masss moment of inertia
Jyy = m*r^2;

%Weight
W_s = m*g;

%Exciter motor force
omega = 2*pi*f;
F0 = M_u*omega^2;
clc
rungekutta
natfreq
    function rungekutta
    [t,y] = ode23('vibscreen',t,x0);

    %Dynamic displacements at mounts
    z1_dyn = y(:,2)-x1*y(:,6);
    z2_dyn = y(:,2)-x2*y(:,6);
    x1_dyn = y(:,4)+z1*y(:,6);
    x2_dyn = y(:,4)+z2*y(:,6);

    %Velocities at mounts
    Vz1 = y(:,1)-x1*y(:,5);
    Vz2 = y(:,1)-x2*y(:,5);
    Vx1 = y(:,3)+z1*y(:,5);
    Vx2 = y(:,3)+z2*y(:,5);

    %Dynamic forces at mounts
    Fz1_dyn = z1_dyn*kz1 + Vz1*cz1;
    Fz2_dyn = z2_dyn*kz2 +Vz2*cz2;
    Fx1_dyn = x1_dyn*kx1 + Vx1*cx1;
    Fx2_dyn = x2_dyn*kx2 +Vx2*cx2;

    %Static forces at mounts
    F_s1 = (W_s*-x2)/(x1-x2);
    F_s2 = W_s-(W_s*-x2)/(x1-x2);

    %Static displacements at mounts
    z_s1 = F_s1/k_s1;
    z_s2 = F_s2/k_s2;

    %Objective function

F_m=max(abs(Fz1_dyn))+max(abs(Fz2_dyn))+max(abs(Fx1_dyn))+max(abs(Fx2_dyn))

%=========================================================================
    %Acceleration vs Time signals
%=========================================================================
    F0 = vertcat((M_u*omega^2)*ones(32000,1),zeros(18001,1));
    xddt  =  ((-kx1-kx2).*y(:,4)  +  (-kx1*z1  -  kx2*z2).*y(:,6)  +  (-cx1-
cx2).*y(:,3)       +       (-cx1*z1       -       cx2*z2).*y(:,5)       +
F0.*cos(beta).*sin(omega.*t))./m;
    zddt   =   ((-kz1-kz2).*y(:,2)   +   (kz1*x1+kz2*x2).*y(:,6)   +   (-cz1-
cz2).*y(:,1) + (cz1*x1+cz2*x2).*y(:,5) + F0.*sin(beta).*sin(omega.*t))./m;
```

```
    thetaddt = ((-kx1*z1^2-kx2*z2^2-kz1*x1^2-kz2*x2^2).*y(:,6) + (-kx1*z1 -
kx2*z2).*y(:,4) + (kz1*x1 + kz2*x2).*y(:,2) + (-cx1*z1^2-cx2*z2^2-cz1*x1^2-
cz2*x2^2)*y(:,5) + (cx1*z1 - cx2*z2).*y(:,3) + (cz1*x1 + cz2*x2).*y(:,1) +
F0.*cos(beta).*z3.*sin(omega.*t) - F0.*sin(beta).*x3.*sin(omega.*t))./Jyy
    z1ddt = zddt-x1*thetaddt;
    z2ddt = zddt-x2*thetaddt;
    x1ddt = xddt+z1*thetaddt;
    x2ddt = xddt+z2*thetaddt;

    %Steady state signals
    z1ddt_ss = z1ddt(16000:32000);
    z2ddt_ss = z2ddt(16000:32000);
    x1ddt_ss = x1ddt(16000:32000);
    x2ddt_ss = x2ddt(16000:32000);

    tss = t(16000:32000)-t(16000);

    %Transient signals
    z1ddt_start = z1ddt(1:16001);
    z2ddt_start = z2ddt(1:16001);
    x1ddt_start = x1ddt(1:16001);
    x2ddt_start = x2ddt(1:16001);

    z1ddt_stop = z1ddt(31000:47000);
    z2ddt_stop = z2ddt(31000:47000);
    x1ddt_stop = x1ddt(31000:47000);
    x2ddt_stop = x2ddt(31000:47000);

    %Exciter motor start and stop times
    t_start = t(1:16001);
    t_stop = t(31000:47000)-t(31000);

    figure(1)
    subplot(2,1,1)
    plot (tss,x1ddt_ss)
    title('Horizontal acceleration at Mount 1','FontSize',16)
    xlabel('Time (s)','FontSize',12)
    ylabel('Acceleration                                    $\Delta\ddot{x_1}$
$[m/s^2]$','interpreter','latex','FontSize',14)

    subplot(2,1,2)
    plot(tss, x2ddt_ss)
    title('Horizontal acceleration at Mount 2','FontSize',16)
    xlabel('Time (s)','FontSize',12)
    ylabel('Acceleration                                    $\Delta\ddot{x_2}$
$[m/s^2]$','interpreter','latex','FontSize',14)



    figure(2)
    subplot(2,1,1)
    plot (tss,z1ddt_ss)
    title('Vertical acceleration at Mount 1','FontSize',16)
    xlabel('Time (s)','FontSize',12)
    ylabel('Acceleration                                    $\Delta\ddot{z_1}$
$[m/s^2]$','interpreter','latex','FontSize',14)

    subplot(2,1,2)
    plot(tss, z2ddt_ss)
    title('Vertical acceleration at Mount 2','FontSize',16)
```

```
    xlabel('Time (s)','FontSize',12)
    ylabel('Acceleration                                $\Delta\ddot{z_2}$
$[m/s^2]$','interpreter','latex','FontSize',14)

    %FFTs of steady state signals
    Ro = x1ddt_ss;
    Rt = x2ddt_ss;
    fs=1/tss(2);
    np=length(tss);
    ff=fs*(0:np-1)/np;

    FRo=fft(Ro);
    PRo=(abs(FRo)*2/np)/(f*2*pi)^2;


    FRt=fft(Rt);
    PRt=(abs(FRt)*2/np)/(f*2*pi)^2;

    npl=1:(length(tss)/10);

    figure(3)
    subplot(2,1,1);plot(ff(npl),PRo(npl),'b')
    title('Horizontal peak displacement at Mount 1','FontSize',16)
    ylabel('Peak Displacement \Deltax_1 [m]')
    xlabel('Frequency [Hz]')

    subplot(2,1,2);plot(ff(npl),PRt(npl),'b')
    title('Horizontal peak displacement at Mount 2','FontSize',16)
    ylabel('Peak Displacement \Deltax_2 [m]')
    xlabel('Frequency [Hz]')

    Ro = z1ddt_ss;
    Rt = z2ddt_ss;
    FRo=fft(Ro);
    PRo=(abs(FRo)*2/np)/(f*2*pi)^2;

    FRt=fft(Rt);
    PRt=(abs(FRt)*2/np)/(f*2*pi)^2;

    figure(4)
    subplot(2,1,1);plot(ff(npl),PRo(npl),'b')
    title('Vertical peak displacement at Mount 1','FontSize',16)
    ylabel('Peak Displacement \Deltax_1 [m]')
    xlabel('Frequency [Hz]')

    subplot(2,1,2);plot(ff(npl),PRt(npl),'b')
    title('Vertical peak displacement at Mount 2','FontSize',16)
    ylabel('Peak Displacement \Deltax_2 [m]')
    xlabel('Frequency [Hz]')

%=========================================================================
    %Transient signals
%=========================================================================

figure(5)
    subplot(2,1,1)
    plot (t_start,x1ddt_start)
    title('Horizontal acceleration at Mount 1','FontSize',16)
    xlabel('Time (s)','FontSize',12)
```

```
    ylabel('Acceleration                                    $\Delta\ddot{x_1}$
$[m/s^2]$','interpreter','latex','FontSize',14)

    subplot(2,1,2)
    plot(t_start, x2ddt_start)
    title('Horizontal acceleration at Mount 2','FontSize',16)
    xlabel('Time (s)','FontSize',12)
    ylabel('Acceleration                                    $\Delta\ddot{x_2}$
$[m/s^2]$','interpreter','latex','FontSize',14)

    figure(6)
    subplot(2,1,1)
    plot (t_start,z1ddt_start)
    title('Vertical acceleration at Mount 1','FontSize',16)
    xlabel('Time (s)','FontSize',12)
    ylabel('Acceleration                                    $\Delta\ddot{z_1}$
$[m/s^2]$','interpreter','latex','FontSize',14)

    subplot(2,1,2)
    plot(t_start, z2ddt_start)
    title('Vertical acceleration at Mount 2','FontSize',16)
    xlabel('Time (s)','FontSize',12)
    ylabel('Acceleration                                    $\Delta\ddot{z_2}$
$[m/s^2]$','interpreter','latex','FontSize',14)

    figure(7)
    subplot(2,1,1)
    plot (t_stop,x1ddt_stop)
    title('Horizontal acceleration at Mount 1','FontSize',16)
    xlabel('Time (s)','FontSize',12)
    ylabel('Acceleration                                    $\Delta\ddot{x_1}$
$[m/s^2]$','interpreter','latex','FontSize',14)

    subplot(2,1,2)
    plot(t_stop, x2ddt_stop)
    title('Horizontal acceleration at Mount 2','FontSize',16)
    xlabel('Time (s)','FontSize',12)
    ylabel('Acceleration                                    $\Delta\ddot{x_2}$
$[m/s^2]$','interpreter','latex','FontSize',14)

    figure(8)
    subplot(2,1,1)
    plot (t_stop,z1ddt_stop)
    title('Vertical acceleration at Mount 1','FontSize',16)
    xlabel('Time (s)','FontSize',12)
    ylabel('Acceleration                                    $\Delta\ddot{z_1}$
$[m/s^2]$','interpreter','latex','FontSize',14)

    subplot(2,1,2)
    plot(t_stop, z2ddt_stop)
    title('Vertical acceleration at Mount 2','FontSize',16)
    xlabel('Time (s)','FontSize',12)
    ylabel('Acceleration                                    $\Delta\ddot{z_2}$
$[m/s^2]$','interpreter','latex','FontSize',14)

% Display static forces, displacements and natural frequencies
    disp(' ')
    disp('Static forces and displacements')
    disp('==============================')
    disp(['Static displacement at mount 1 = ',num2str(z_s1),' [m]'])
```

```
    disp(['Static displacement at mount 2 = ',num2str(z_s2),' [m]'])
    disp(['Static force at mount 1 = ',num2str(F_s1),' [N]'])
    disp(['Static force at mount 2 = ',num2str(F_s2),' [N]'])

    end
end
```

Three degree of freedom mathematical model sub-routine with equations of motion

```
function zxthetadot = vibscreen(t,zxtheta)
global x1 x2 z3 x3 z1 z2 kx1 kx2 kz1 kz2 cx1 cx2 cz1 cz2 m Jyy F0 omega beta
%Simulate shut down
if t>32
  F0 =0;
end

%First order differential equations
zxthetadot = zeros(6,1);
zdot = zxtheta(1);
z = zxtheta(2);
xdot = zxtheta(3);
x = zxtheta(4);
thetaydot = zxtheta(5);
thetay = zxtheta(6);

zddot  =  ((-kz1-kz2)*z  +  (kz1*x1+kz2*x2)*thetay  +  (-cz1-cz2)*zdot  +
(cz1*x1+cz2*x2)*thetaydot + F0*sin(beta)*sin(omega*t))/m;
xddot = ((-kx1-kx2)*x + (-kx1*z1 - kx2*z2)*thetay + (-cx1-cx2)*xdot + (-
cx1*z1 - cx2*z2)*thetaydot + F0*cos(beta)*sin(omega*t))/m;
thetayddot  =  ((-kx1*z1^2-kx2*z2^2-kz1*x1^2-kz2*x2^2)*thetay  +  (-kx1*z1  -
kx2*z2)*x  +  (kz1*x1  +  kz2*x2)*z  +  (-cx1*z1^2-cx2*z2^2-cz1*x1^2-
cz2*x2^2)*thetaydot + (cx1*z1 - cx2*z2)*xdot + (cz1*x1 + cz2*x2)*zdot +
F0*cos(beta)*z3*sin(omega*t) - F0*sin(beta)*x3*sin(omega*t))/Jyy;
zxthetadot = [zddot;zdot;xddot;xdot;thetayddot;thetaydot];
end
```

Three degree of freedom mathematical model sub-program for natural frequencies

```
function
natfreq(m,x1,x2,z3,x3,z1,z2,kx1,kx2,kz1,kz2,r,Jyy,f_horisontal,f_vertical,f
_rotational)
global m x1 x2 z3 x3 z1 z2 kx1 kx2 kz1 kz2 r Jyy f_horisontal f_vertical
f_rotational
% Stiffness matrix
K = [(-kx1-kx2) 0 (-kx1*z1 - kx2*z2);
    0 (-kz1-kz2) (kz1*x1+kz2*x2);
    (-kx1*z1-kx2*z2)     (kz1*x1+kz2*x2)     (-kx1*z1^2-kx2*z2^2-kz1*x1^2-
kz2*x2^2)];

%Mass Matrix
M = -[m 0 0;0 m 0;0 0 Jyy];

%Compute eigenvalues and eigenvectors
[V,D] = eig(K,M);
eigenvectors = V;
f_n = sqrt(D)/(2*pi);
[val,horisontal] = max(abs(V(1,:)));
[val,vertical]   = max(abs(V(2,:)));
[val,rotational] = max(abs(V(3,:)));
f_horisontal = max(f_n(:,horisontal));
f_vertical = max(f_n(:,vertical));
f_rotational = max(f_n(:,rotational));

%Display Natural frequencies
disp('Natural frequencies')
disp('==================')
disp(['Vertical mode = ',num2str(f_vertical),' Hz'])
disp(['Horisontal mode = ',num2str(f_horisontal),' Hz'])
disp(['Rotational mode = ',num2str(f_rotational),' Hz'])
end
```

Three degree of freedom mathematical model used for optimisation

```
function response_opt
global x1 x2 z3 x3 z1 z2 kx1 kx2 kz1 kz2 cx1 cx2 cz1 cz2 m alpha Jyy F0 r
omega beta
%=========================================================================
%Inputs
%=========================================================================
%Constatnts
g = 9.81;
%Integration time interval
 t = 0:0.001:30;

%Initial values
x0 = [0.0 0.0 0.0 0.0 0.0 0.0];

%Coordinates
x1 = -0.5837;
x2 = 0.51211;
x3 = -0.02046;
z1 = -0.14969;
z2 = -0.24556;
z3 = 0.0377;

%Angles
alpha = 5*(pi/180);
beta = 85*(pi/180);

%Mass and mass moment of inertia
m = 262;
r = 0.490;

%Mount dynamic properties
k_min= 100000;
k_max = 15000000;
k_step = 100000;
k_num = 1+((k_max-k_min)/k_step);
k = [k_min:k_step:k_max];
k_1 = k(ones(1,k_num),:)';
k_2 = k(ones(1,k_num),:);

%Save stiffness matrix to text file
save('ks.dat','k_1','-ASCII')

zeta_z = 0.006622;
zeta_x = 0.0192;

%Exciter motor characteristics
M_u = 0.298*2*0.65;
f =  24.5; %Frequency [Hz]

%=========================================================================
%Calculations
%=========================================================================

%Viscous damping coefficients
Ccz = 2*sqrt((kz1+kz2)*(m));
```

```
Ccx = 2*sqrt((kx1+kx2)*(m));
cz1 = (zeta_z*Ccz)/2;
cz2 = cz1;
cx1 = (zeta_x*Ccx)/2;
cx2 = cx1;

%Masss moment of inertia
Jyy = m*r^2;

%Weight
W_s = m*g;

%Exciter motor force
omega = 2*pi*f;
F0 = M_u*omega^2;

%For loop for each stiffness coefficient
n = 1;
for i = 1:k_num
    for j = 1:k_num
kz1 = k_1(i,j)
kx1 = k_2(i,j)
kz2 = kz1;
kx2 = kx1;
k_s1 = kz1/1.45;
k_s2 = k_s1;

%Numerical integration
rungekutta
clc
    end

%Save computed data to text file
save(strcat('PlotData1','_',num2str(n),'.dat'),'F','-ASCII')
save(strcat('PlotData2','_',num2str(n),'.dat'),'X_d','-ASCII')
save(strcat('PlotData3','_',num2str(n),'.dat'),'X_s','-ASCII')
save(strcat('PlotData4','_',num2str(n),'.dat'),'F_m','-ASCII')
save(strcat('PlotData5','_',num2str(n),'.dat'),'X_m','-ASCII')
save(strcat('PlotData6','_',num2str(n),'.dat'),'X_m2','-ASCII')
end
    function rungekutta
    options = odeset('RelTol',1e-3,'AbsTol',1e-3);
    [t,y] = ode23('vibscreen',t,x0,options);

    %Dynamic displacements at mounts
    z1_dyn = y(:,2)-x1*y(:,6);
    z2_dyn = y(:,2)-x2*y(:,6);
    x1_dyn = y(:,4)+z1*y(:,6);
    x2_dyn = y(:,4)+z2*y(:,6);

    %Velocities at mounts
    Vz1 = y(:,1)-x1*y(:,5);
    Vz2 = y(:,1)-x2*y(:,5);
    Vx1 = y(:,3)+z1*y(:,5);
    Vx2 = y(:,3)+z2*y(:,5);


    %Dynamic forces at mounts
    Fz1_dyn = z1_dyn*kz1 + Vz1*cz1;
```

```
    Fz2_dyn = z2_dyn*kz2 +Vz2*cz2;
    Fx1_dyn = x1_dyn*kx1 + Vx1*cx1;
    Fx2_dyn = x2_dyn*kx2 +Vx2*cx2;

    %Static forces at mounts
    F_s1 = (W_s*-x2)/(x1-x2);
    F_s2 = W_s-(W_s*-x2)/(x1-x2);

    %Static displacements at mounts
    z_s1 = F_s1/k_s1;
    z_s2 = F_s2/k_s2;

    %Objective function steady state
    F(i,j)   =   max(abs(Fz1_dyn(tss:end)))+   max(abs(Fz2_dyn(tss:end)))+
max(abs(Fx1_dyn(tss:end)))+ max(abs(Fx2_dyn(tss:end)));

    %Average dynamic steady state displacement
    X_d1 = max(z1_dyn(tss:end));
    X_d2 = max(z2_dyn(tss:end));
    X_d(i,j) = (X_d1+X_d2)/2;

    %Maximum static displacement
    X_s(i,j) = max(z_s1,z_s2);

    %Objective function transient
    F_m(i,j)  =  max(abs(Fz1_dyn))  +  max(abs(Fz2_dyn))+  max(abs(Fx1_dyn))+
max(abs(Fx2_dyn));

    %Maximum vertical displacement
    Z_d1m = max(z1_dyn);
    Z_d2m = max(z2_dyn);
    Z_m1 = Z_d1m + z_s1;
    Z_m2 = Z_d2m + z_s2;
    X_m(i,j) = max(Z_m1,Z_m2);

    %Maximum horizontal displacement
    x_m1 = max(x1_dyn);
    x_m2 = max(x2_dyn);
    X_m2(i,j)= max(x_m1,x_m2);

    end
end
```

Matlab program code used for characterisation with electrodynamic Shaker

```
clear all;
clc;

%Frequency domain signals
freq = 97;
len = 1601;
nam1 = 'JB';

X = zeros(28,1);
Y = zeros(28,1);
phi = zeros(28,1);
omega = zeros(28,1);
c_veer = zeros(28,1);
k_veer = zeros(28,1);
fre = zeros(28,1);

%Mass Plates
m(1,1)   = 30.8819;
m(2,1)   = 30.8819;
m(3,1)   = 30.8819;
m(4,1)   = 30.8819;
m(5,1)   = 35.6505;
m(6,1)   = 35.6505;
m(7,1)   = 35.6505;
m(8,1)   = 35.6505;
m(9,1)   = 40.4074;
m(10,1)   = 40.4074;
m(11,1)   = 40.4074;
m(12,1)   = 40.4074;
m(13,1)   = 45.167;
m(14,1)   = 45.167;
m(15,1)   = 45.167;
m(16,1)   = 45.167;
m(17,1)   = 49.9388;
m(18,1)   = 49.9388;
m(19,1)   = 49.9388;
m(20,1)   = 49.9388;
m(21,1)   = 54.6796;
m(22,1)   = 54.6796;
m(23,1)   = 54.6796;
m(24,1)   = 54.6796;
m(25,1)   = 59.4539;
m(26,1)   = 59.4539;
m(27,1)   = 59.4539;
m(28,1)   = 59.4539;

%Test frequency
fre(1,1) = 45;
fre(2,1) = 45;
fre(3,1) = 45;
fre(4,1) = 45;
fre(5,1) = 45;
fre(6,1) = 45;
fre(7,1) = 45;
fre(8,1) = 45;
fre(9,1) = 45;
fre(10,1) = 45;
```

```
fre(11,1) = 45;
fre(12,1) = 45;
fre(13,1) = 45;
fre(14,1) = 45;
fre(15,1) = 45;
fre(16,1) = 45;
fre(17,1) = 45;
fre(18,1) = 45;
fre(19,1) = 45;
fre(20,1) = 45;
fre(21,1) = 45;
fre(22,1) = 45;
fre(23,1) = 45;
fre(24,1) = 45;
fre(25,1) = 45;
fre(26,1) = 45;
fre(27,1) = 45;
fre(28,1) = 45;

for i = 1:28
    %Load measured DI 2200 data
    filenam1 = [nam1 num2str((2*i)-1,'%02d') 'a' '.dat'];
    filenam2 = [nam1 num2str((2*i)-1,'%02d') 'b' '.dat'];
    filenam3 = [nam1 num2str((2*i),'%02d') 'a' '.dat'];
    filenam4 = [nam1 num2str((2*i),'%02d') 'b' '.dat'];

ff = load(filenam1);
f=ff(:,2);
af=9.81*ff(:,1);

ff1 = load(filenam2);
f1= ff1(:,2);
af1=9.81*ff1(:,1);

%%Lt= 256;
%%Lf= 101;
Lf=length(f);
Lf1=length(f1);


figure(1);
subplot(2,1,1);plot(f(1:Lf),af(1:Lf),'b')
ylabel('Mass Acceleration [m/s^2]')
xlabel('Frequency [Hz]')
subplot(2,1,2);plot(f1(1:Lf1),af1(1:Lf1),'b')
ylabel('Base Acceleration [m/s^2]')
xlabel('Frequency [Hz]')
pause;

%%%%%%%%%%%%%%%%%%%%%%%%%%%%%%%%%%%%%%%%%%%%%%%%%%%%%%%%%%%%%%%%%%%%%%%%%%%%%%%

%Time domain signals

tt = load(filenam3);
t=tt(:,2);
Ro=9.81*tt(:,1);

tt2 = load(filenam4);
t1=tt2(:,2);
```

```
Rt=9.81*tt2(:,1);


%%Lt= 256;
%%Lf= 101;
Lt=length(t);
Lt1=length(t1);

figure(2);

subplot(2,1,1);plot(t(1:Lt),Ro(1:Lt),'b')
ylabel('Mass Acceleration [m/s^2]')
xlabel('Time [sec]')
subplot(2,1,2);plot(t1(1:Lt1),Rt(1:Lt1),'b')
ylabel('Base Acceleration [m/s^2]')
xlabel('Time [sec]')
pause;

fs=1/t(2);

%========================================================================
% Load data
%========================================================================
% Determine FFTs on two time domain signals
%========================================================================

np=length(t);
f=fs*(0:np-1)/np;

FRo=fft(Ro);
PRo=abs(FRo)*2/np;
aRo=angle(FRo);

FRt=fft(Rt);
PRt=abs(FRt)*2/np;
aRt=angle(FRt);

%========================================================================
% Plot spectrum
%========================================================================

npl=1:(len);

figure(3)
subplot(2,1,1);plot(f(npl),PRo(npl),'b')
ylabel('Abs (Roe) [m/s^2]')
xlabel('Frequency [Hz]')

subplot(2,1,2);plot(f(npl),aRo(npl),'b')
ylabel('Phase (Roe) [rad]')
xlabel('Frequency   [Hz]')
pause;

figure(4)
subplot(2,1,1);plot(f(npl),PRt(npl),'b')
ylabel('Abs (Rte) [m/s^2]')
xlabel('Frequency [Hz]')
```

```
subplot(2,1,2);plot(f(npl),aRt(npl),'b')
ylabel('Phase (Rte) [rad]')
xlabel('Frequency   [Hz]')
pause;

%=========================================================================
% Fourier coefficients
%=========================================================================

datRo=[2*pi*f(npl); PRo(npl)'; aRo(npl)'];
datRt=[2*pi*f(npl); PRt(npl)'; aRt(npl)'];

%=========================================================================
% Reconstruct Time domain signals with noise
%=========================================================================

E=length(t);

for j=1:E;
Ros(j)=sum(datRo(2,:).*cos(datRo(1,:)*t(j)+datRo(3,:)));
Rts(j)=sum(datRt(2,:).*cos(datRt(1,:)*t(j)+datRt(3,:)));
end

%=========================================================================
% Store Fourier coefficients to folders
%=========================================================================

a=datRo(freq)';
b=datRt(freq)';

save Ro.dat a -ascii;
save Rt.dat b -ascii;

%=========================================================================
% Reconstruct Time domain signals without noise
%=========================================================================

for j=1:E;
Ros(j)=(datRo(2,freq).*cos(datRo(1,freq)*t(j)+datRo(3,freq)));
Rts(j)=(datRt(2,freq).*cos(datRt(1,freq)*t(j)+datRt(3,freq)));
end

%=========================================================================
% Plot Time domain signals with and without noise
%=========================================================================

figure(5)       %Time domain signals with and without noise.
subplot(2,1,1);plot(t,Ro,'r',t,Ros,'b')
ylabel('Ro [m/s^2]')
xlabel('Time [s]')

subplot(2,1,2);plot(t,Rt,'r',t,Rts,'b')
ylabel('Rt [m/s^2]')
xlabel('Time [s]')
pause;

figure(6)       %Time domain signals without noise.
subplot(2,1,1);plot(t,Ros,'b')
```

```
ylabel('Ros [m/s^2]')
xlabel('Time [s]')

subplot(2,1,2);plot(t,Rts,'b')
ylabel('Rts [m/s^2]')
xlabel('Time [s]')

pause;
% close all
phaseRorad = datRo(3,freq);
phaseRtrad = datRt(3,freq);
phasedifrad1 = phaseRtrad - phaseRorad

%=========================================================================
% Amplitudes at forced Frequency
%=========================================================================

AmplRo1 = datRo(2,freq)
AmplRt1 = datRt(2,freq)
%=========================================================================
%Compute mount dynamic properties
%=========================================================================
omega(i,1) = 2*pi*fre(i,1);

X(i,1) = AmplRo1;

Y(i,1) = AmplRt1;

phi(i,1) = phasedifrad1;

syms k c;

%Solve equations simulataneously
eq1                    =                    sqrt((k.^2+(c*omega(i,1)).^2)/((k-
m(i,1).*omega(i,1).^2).^2+(c.*omega(i,1)).^2))-(X(i,1)./Y(i,1));
eq2                    =                   (m(i,1).*c.*omega(i,1).^3.)/((k.*(k-
m(i,1).*omega(i,1).^2)+(omega(i,1).*c).^2))-tan(phi(i,1));

[c,k] = solve(eq1,eq2);

Styfheid1 = double(k);
Demping1 = double(c);

Styfheid = max(Styfheid1);
Demping = max(Demping1);

k_veer(i,1) = Styfheid; %Dynamic stiffness computed
c_veer(i,1) = Demping; %Damping coefficient computed

Cc(i,1) = 2*sqrt(k_veer(i,1)*m(i,1));

psi(i,1) = (c_veer(i,1)/Cc(i,1)); %Damping ratio computed

XY(i,1) = X(i,1)/Y(i,1);

grade(i,1) = phi(i,1)*((180)/pi);

end
```

Matlab program code used for *in situ* characterisation with Bump test

```
clc
syms zeta_x omega_n

m = 262+65; %mass of vibration screen
tau_d = 0.309; %Periodic time measured
x_dot1 = 0.5638; %Amplitude measured
x_dot2 = 0.4996; %Amplitude measured
omega_d = (1/tau_d)*2*pi; %Damped natural frequency

eq1 = exp(zeta_x*omega_n*tau_d)-(x_dot1/x_dot2);
eq2 = (omega_d/sqrt(1-zeta_x^2))-omega_n;

%Solve equations simultaneously
[omega_n,zeta_x] = solve(eq1,eq2);

zeta = max(double(zeta_x))
omega_nx = max(double(omega_n));

%Display natural frequency
f_nx = omega_nx/(2*pi)

%Display dynamic stiffness and damping coefficient
k_x1 = 0.5*m*omega_nx^2
c_x1 = zeta*2*sqrt(k_x1*(0.5*m))
```

Matlab program code used for fatigue analysis

```
%Input
S_ut = 400; %Ultimate tensile strength
k_a = 0.92; %Surface factor
k_b = 0.73; %Size factor
k_c = 1;    %Loading factor
k_d = 1;    %Temperature factor
k_e = 0.81; %Reliability factor
k_f = 1;    %Miscellaneous effects factor

s_e = 0.5*S_ut; %Material endurance limit

S_e = k_a*k_b*k_c*k_d*k_e*k_f*s_e; %Modified endurance limit

sigma_m = 26.4; %Midrange stress from FEA
sigma_a = 20.5; %Alternating stress from FEA

n_sf = ((sigma_a/S_e)+(sigma_m/S_ut))^-1 %Goodman criteria
```

Matlab program code used for load cell read out

```
function varargout = Weight(varargin)
gui_Singleton = 1;
gui_State = struct('gui_Name',       mfilename, ...
                   'gui_Singleton',  gui_Singleton, ...
                   'gui_OpeningFcn', @Weight_OpeningFcn, ...
                   'gui_OutputFcn',  @Weight_OutputFcn, ...
                   'gui_LayoutFcn',  [] , ...
                   'gui_Callback',   []);
if nargin && ischar(varargin{1})
    gui_State.gui_Callback = str2func(varargin{1});
end

if nargout
    [varargout{1:nargout}] = gui_mainfcn(gui_State, varargin{:});
else
    gui_mainfcn(gui_State, varargin{:});
end

function Weight_OpeningFcn(hObject, eventdata, handles, varargin)

handles.output = hObject;

guidata(hObject, handles);

function varargout = Weight_OutputFcn(hObject, eventdata, handles)

varargout{1} = handles.output;

%==========================================================================
% Connect to Amplifier via COM port
%==========================================================================
function pushbutton1_Callback(hObject, eventdata, handles)
global z E
prompt = {'Enter COM Port'};
dlg_title = 'COM';
num_lines = 1;
def = {'COM1','hsv'};
CP = inputdlg(prompt,dlg_title,num_lines,def);
delete(instrfindall);
s = serial(CP,'Tag','LoadCell');
set(handles.text1, 'String','Connecting.....');
drawnow;
fopen(s);
if strcmp(s.Status,'open') == 0
    h = msgbox('Unable to connect please check the COM port', 'Connection
Error','error');
else
    flushinput(s)
    pause(0.1)
    A = fscanf(s);
    A = fscanf(s);
    B = num2str(A);
    z = (str2num(B(3:7)));
while 1
    pause(0.1)
    A = fscanf(s);
    B = num2str(A);
```

```
    E = (str2num(B(3:7)));
    C = round(((z - E)*-0.00025)*1000)/1000;
    kg = C*250; % Load cell calibration constant (250)
    set(handles.text1, 'String',strcat(num2str(kg,'%0.2f'),' kg'));
    drawnow;
end
end

%==========================================================================
% Zero load cell reading
%==========================================================================
function pushbutton2_Callback(hObject, eventdata, handles)
global z E
    s1 = instrfind('Tag','LoadCell');
    z = E
    set(handles.text1, 'String','0.00 kg')
    drawnow
```

Appendix B – Detailed drawings

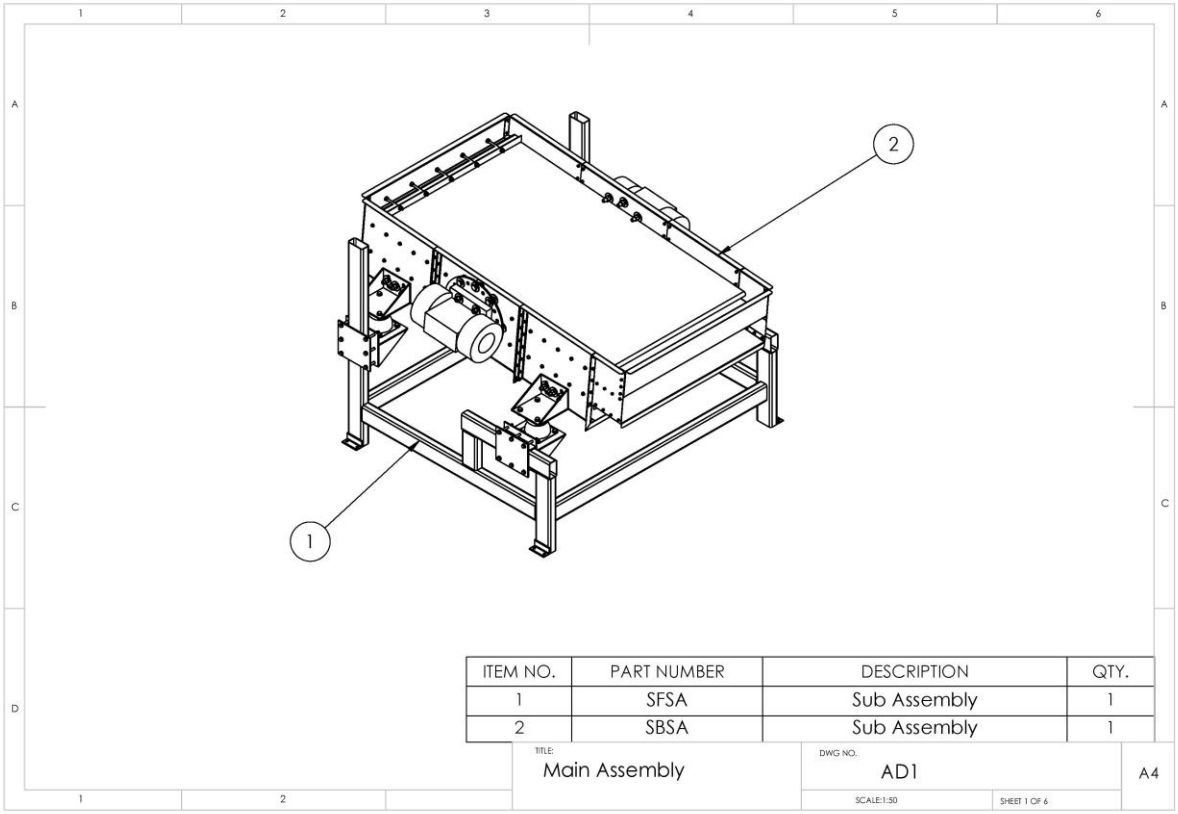

ITEM NO.	PART NUMBER	DESCRIPTION	QTY.
1	SFSA	Sub Assembly	1
2	SBSA	Sub Assembly	1

TITLE: Main Assembly | DWG NO. AD1 | A4 | SCALE:1:50 | SHEET 1 OF 6

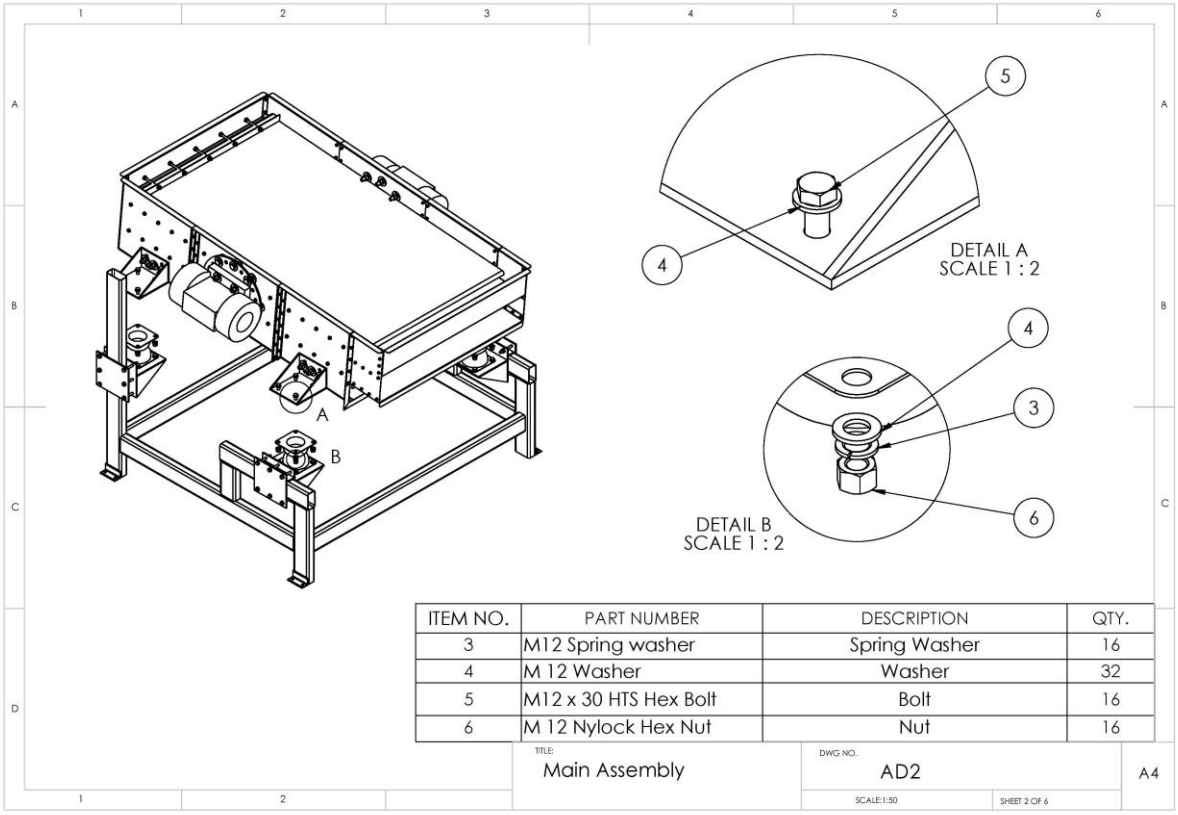

ITEM NO.	PART NUMBER	DESCRIPTION	QTY.
3	M12 Spring washer	Spring Washer	16
4	M 12 Washer	Washer	32
5	M12 x 30 HTS Hex Bolt	Bolt	16
6	M 12 Nylock Hex Nut	Nut	16

TITLE: Main Assembly | DWG NO. AD2 | A4 | SCALE:1:50 | SHEET 2 OF 6

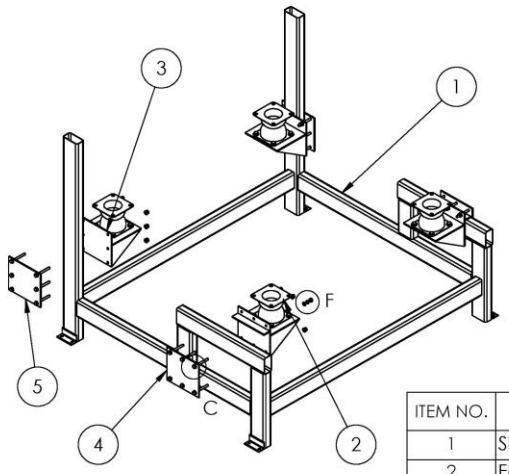

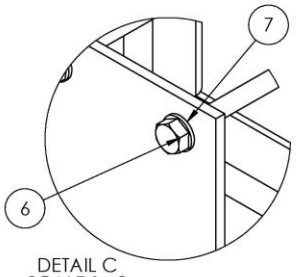

DETAIL C
SCALE 1 : 2

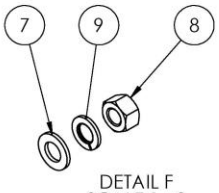

DETAIL F
SCALE 1 : 2

ITEM NO.	PART NUMBER	DESCRIPTION	QTY.
1	SF	Support Frame	1
2	FMBSA1	Sub Assembly	2
3	FMBSA2	Sub Assembly	2
4	FMBD2	Part	2
5	FMBF1	Part	2
6	M10 x 90 HTS Hex Bolt	Bolt	24
7	M10 Washer	Washer	48
8	M10 Nylock Hex Nut	Nut	24
9	M10 Spring Washer	Spring Washer	24

TITLE: SFSA | DWG NO. AD3 | A4 | SCALE:1:50 | SHEET 3 OF 6

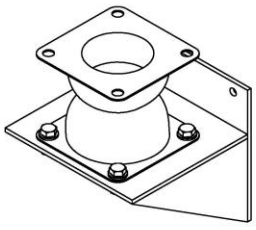

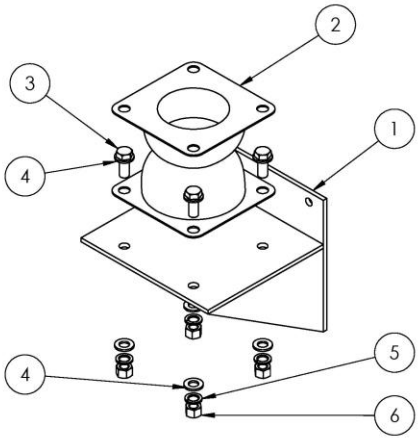

ITEM NO.	PART NUMBER	DESCRIPTION	QTY.
1	FMBF	Part	1
2	SM	Sub Assembly	1
3	M12 x 30 HTS Hex Bolt	Bolt	4
4	M12 Washer	Washer	8
5	M12 Spring Washer	Spring Washer	4
6	M12 Nylock Hex Nut	Nut	4

TITLE: FMBSA2 | DWG NO. AD4 | A4 | SCALE:1:50 | SHEET 4 OF 6

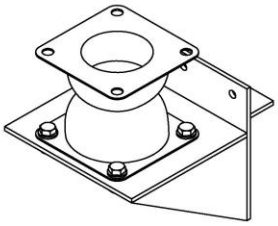

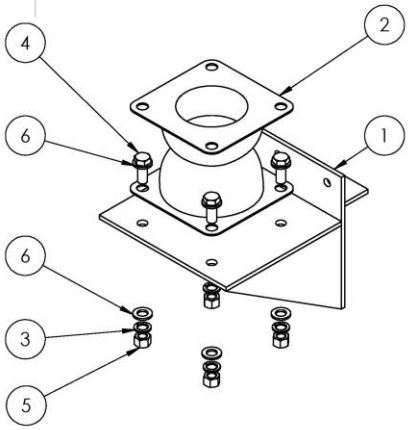

ITEM NO.	PART NUMBER	DESCRIPTION	QTY.
1	FMBD	Mount Bracket	1
2	SM	Sub Assembly	1
3	M12 Spring Washer	Spring Washer	4
4	M12 x 30 HTS Hex Bolt	Bolt	4
5	M12 Nylock Hex Nut	Nut	4
6	M12 Spring Washer	Spring Washer	8

TITLE: FMBSA1 DWG NO. AD5 A4

SCALE:1:50 SHEET 5 OF 6

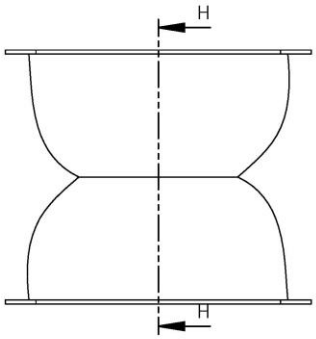

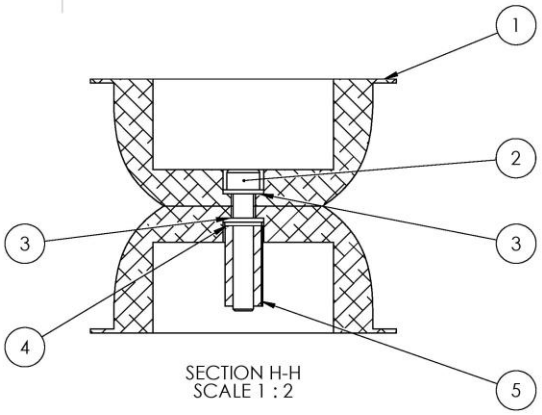

SECTION H-H
SCALE 1 : 2

ITEM NO.	PART NUMBER	DESCRIPTION	QTY.
1	M400-40	Novibra M400-40 Mounts	2
2	M10 x 60 Allen Cap	Allen Cap Screw	1
3	M10 Washer	Washer	2
4	M10 Spring Washer	Spring Washer	1
5	M10 Long Nut	Long Nut	1

TITLE: SM DWG NO. AD6 A4

SCALE:1:50 SHEET 6 OF 6

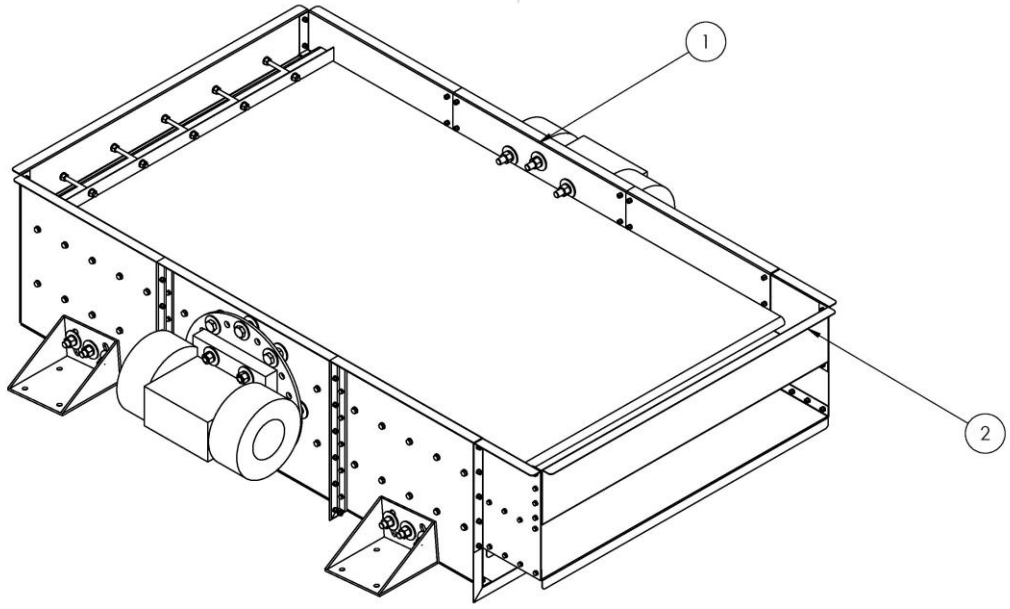

ITEM NO.	PART NUMBER	DESCRIPTION	QTY.
1	MBSA	Sub Assembly	1
2	SSB	Sub Assembly	1

TITLE: SBSA
DWG NO. AD7
A4
SCALE:1:50
SHEET 1 OF 3

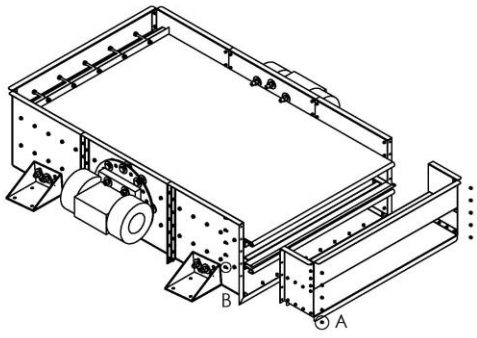

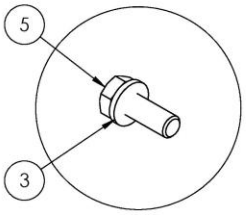

DETAIL B
SCALE 1 : 1

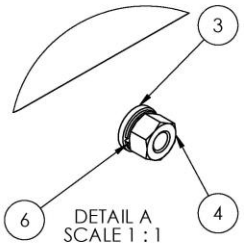

DETAIL A
SCALE 1 : 1

ITEM NO.	PART NUMBER	DESCRIPTION	QTY.
3	M6 Washer	Washer	20
4	M6 Nylock Hex Nut	Nut	10
5	M6 x 16 HTS Hex Bolt	Bolt	10
6	M6 Spring Washer	Spring Washer	10

TITLE: SBSA
DWG NO. AD8
A4
SCALE:1:50
SHEET 2 OF 3

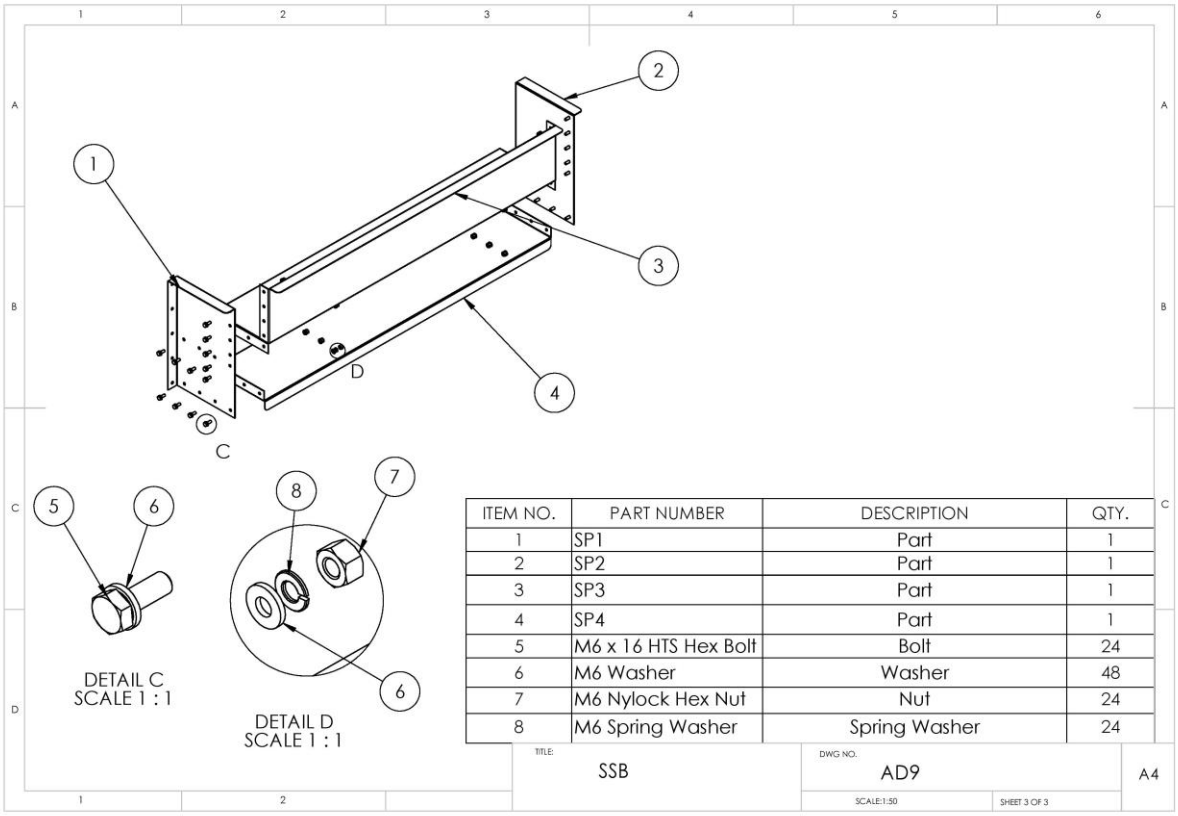

ITEM NO.	PART NUMBER	DESCRIPTION	QTY.
1	SP1	Part	1
2	SP2	Part	1
3	SP3	Part	1
4	SP4	Part	1
5	M6 x 16 HTS Hex Bolt	Bolt	24
6	M6 Washer	Washer	48
7	M6 Nylock Hex Nut	Nut	24
8	M6 Spring Washer	Spring Washer	24

TITLE: SSB | DWG NO. AD9 | A4 | SCALE:1:50 | SHEET 3 OF 3

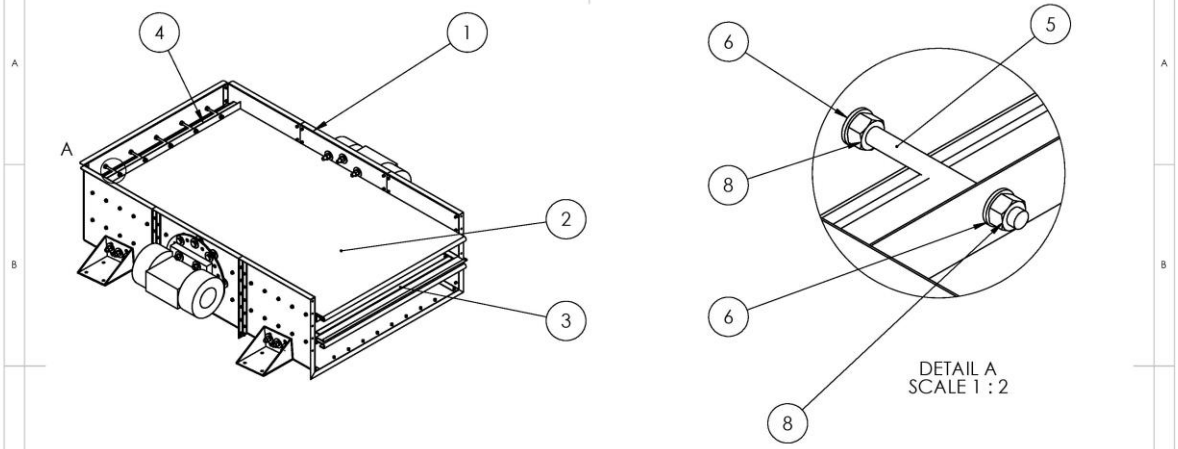

ITEM NO.	PART NUMBER	DESCRIPTION	QTY.
1	MBSA1	Sub Assembly	1
2	SS1	Sieve	1
3	SS2	Sieve	1
4	ST	Part	2
5	M10 x 150 TR	Threaded Rod	10
6	M10 Washer	Washer	26
8	M10 Nylock Hex Nut	Nut	26

TITLE: MBSA | DWG NO. AD10 | A4 | SCALE:1:50 | SHEET 1 OF 2

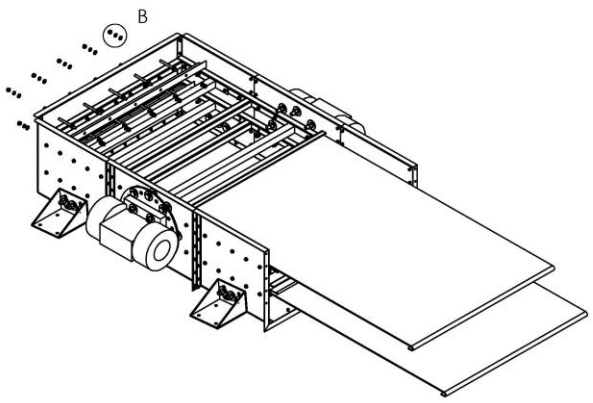

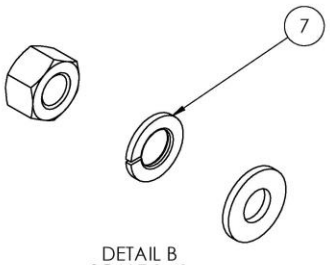

DETAIL B
SCALE 1 : 1

ITEM NO.	PART NUMBER	DESCRIPTION	QTY.
7	M10 Spring Washer	Spring Washer	10

TITLE: MBSA

DWG NO. AD11

A4

SCALE:1:50 SHEET 2 OF 2

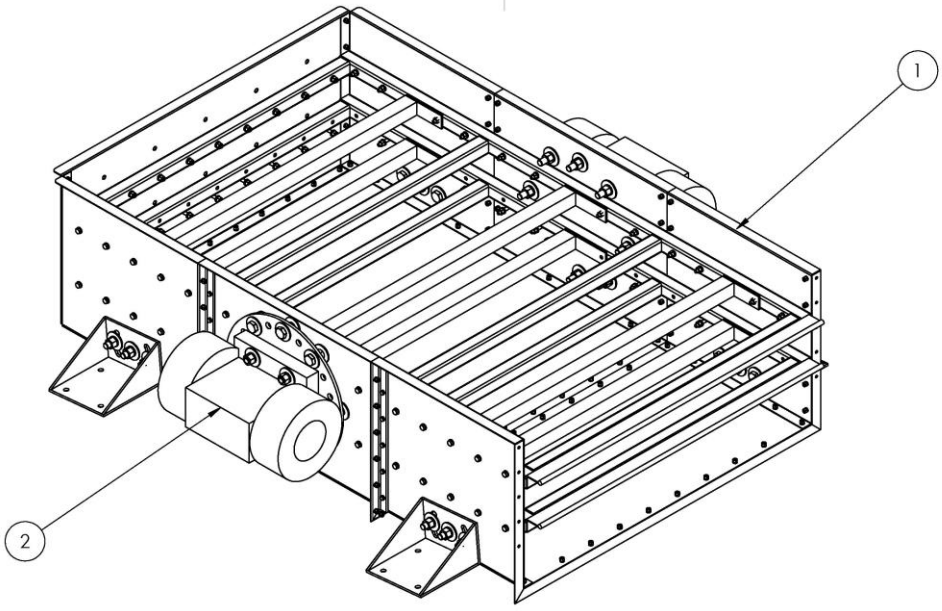

ITEM NO.	PART NUMBER	DESCRIPTION	QTY.
1	MBSA2	Sub Assembly	1
2	EMSA	Sub Assembly	2

TITLE: MBSA1

DWG NO. AD12

A4

SCALE:1:20 SHEET 1 OF 3

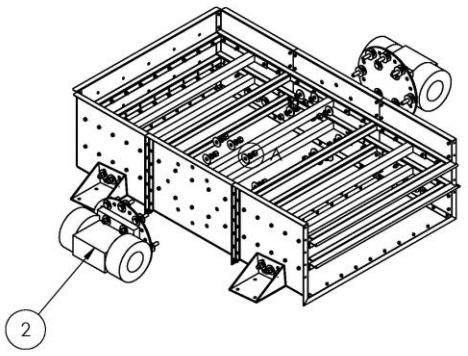

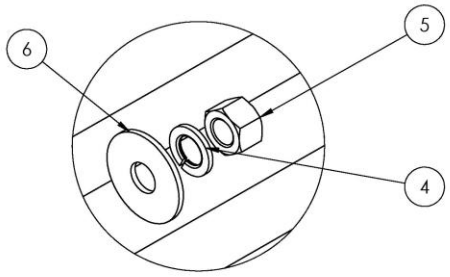

DETAIL A
SCALE 1 : 2

ITEM NO.	PART NUMBER	DESCRIPTION	QTY.
2	EMSA	Sub Assembly	2
3	M16 Washer	Washer	16
4	M16 Spring Washer	Spring Washer	16
5	M16 Nylock Hex Nut	Nut	16

TITLE: MBSA1 | DWG NO. AD13 | A4 | SCALE:1:20 | SHEET 2 OF 3

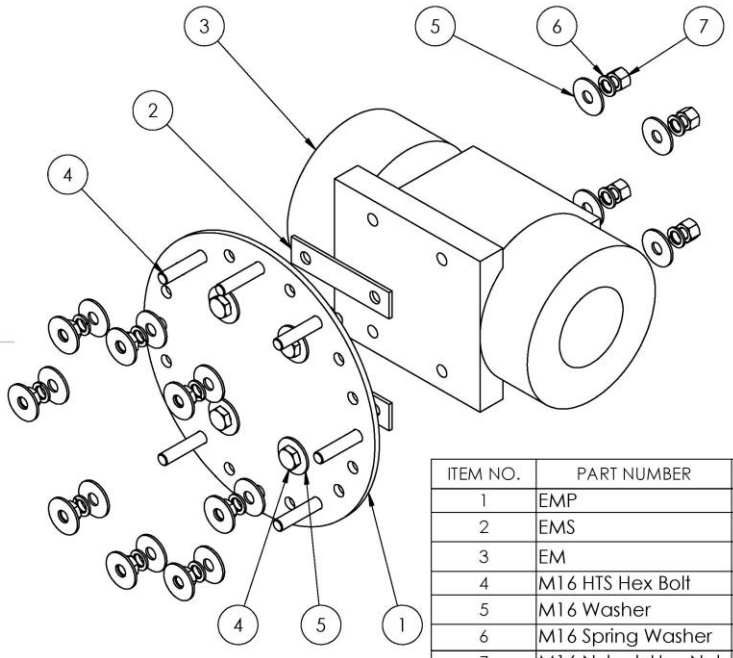

ITEM NO.	PART NUMBER	DESCRIPTION	QTY.
1	EMP	Part	1
2	EMS	Part	2
3	EM	Exciter Motor	1
4	M16 HTS Hex Bolt	Bolt	12
5	M16 Washer	Washer	32
6	M16 Spring Washer	Spring Washer	12
7	M16 Nylock Hex Nut	Nut	12

TITLE: EMSA | DWG NO. AD14 | A4 | SCALE:1:20 | SHEET 3 OF 3

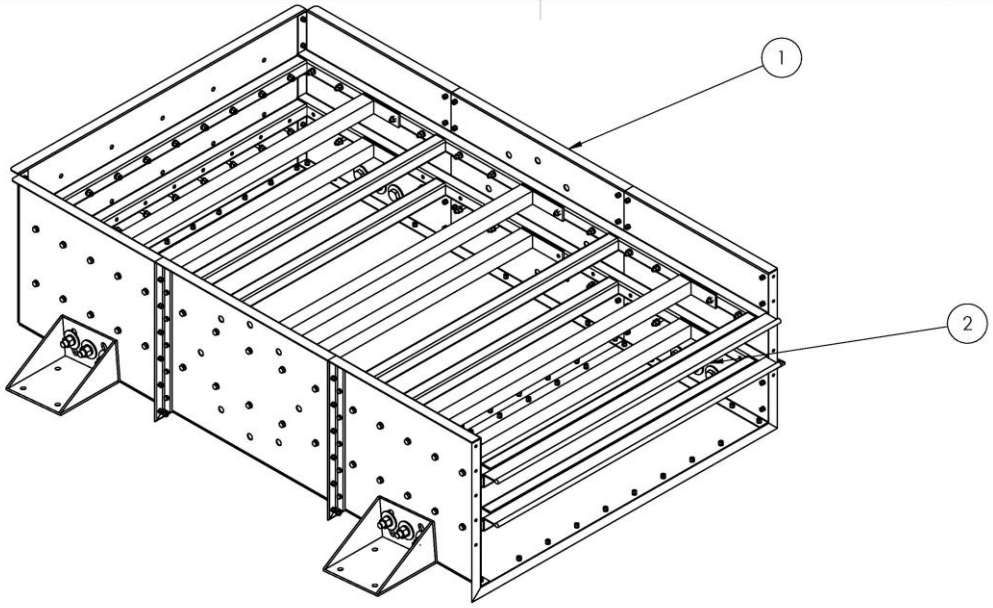

ITEM NO.	PART NUMBER	DESCRIPTION	QTY.
1	MBSA3	Sub Assembly	1
2	SSF	Sub Assembly	2

TITLE: MBSA2 | DWG NO. AD15 | A4 | SCALE:1:20 | SHEET 1 OF 3

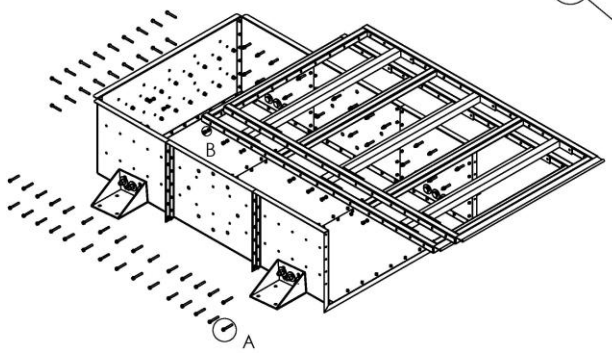

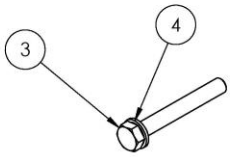

DETAIL A
SCALE 1 : 2

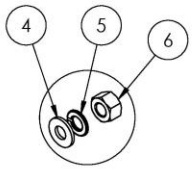

DETAIL B
SCALE 1 : 2

ITEM NO.	PART NUMBER	DESCRIPTION	QTY.
3	M8 x 60 HTS Hex Bolt	Bolt	78
4	M8 Washer	Washer	156
5	M8 Spring Washer	Spring Washer	78
6	M8 Nylock Hex Nut	Nut	78

TITLE: MBSA2 | DWG NO. AD16 | A4 | SCALE:1:20 | SHEET 2 OF 3

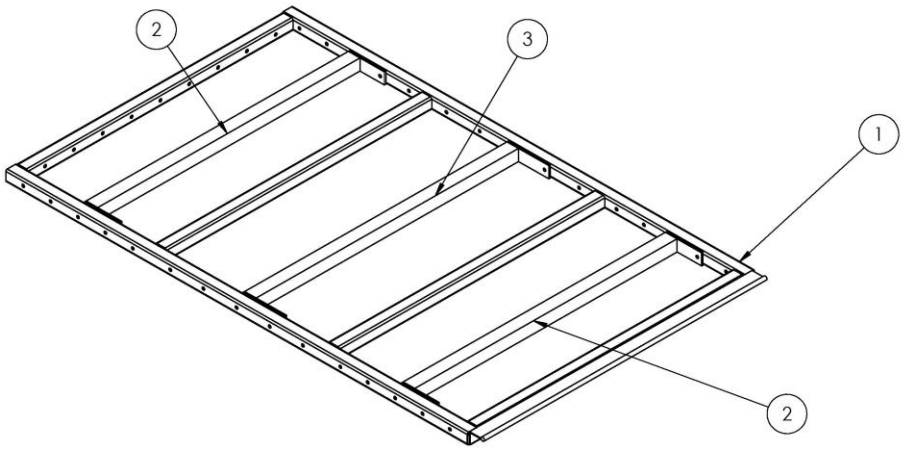

ITEM NO.	PART NUMBER	DESCRIPTION	QTY.
1	SSF1	Part	1
2	SSF2	Part	2
3	SSF3	Part	1

TITLE: SSF | DWG NO. AD17 | A4 | SCALE:1:20 | SHEET 3 OF 3

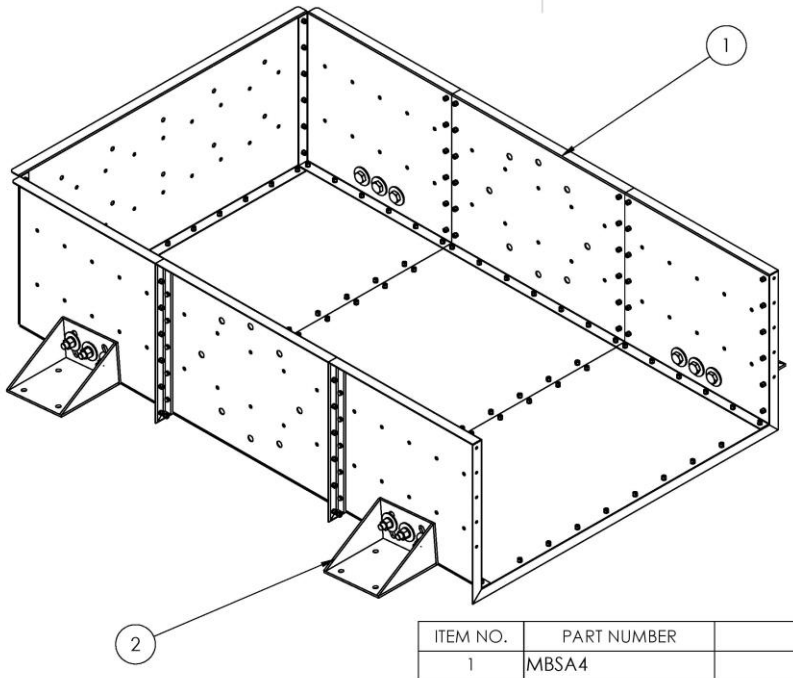

ITEM NO.	PART NUMBER	DESCRIPTION	QTY.
1	MBSA4	Sub Assembly	1
2	BMB	Part	4

TITLE: MBSA3 | DWG NO. AD16 | A4 | SCALE:1:20 | SHEET 1 OF 6

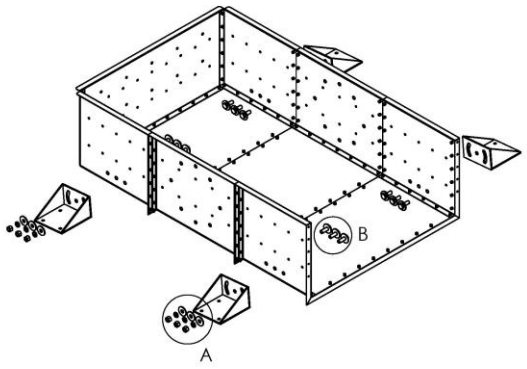

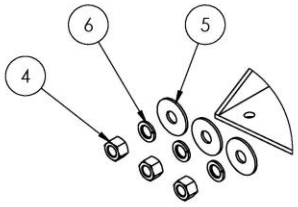

DETAIL A
SCALE 1 : 5

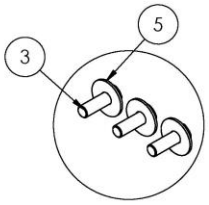

DETAIL B
SCALE 1 : 5

ITEM NO.	PART NUMBER	DESCRIPTION	QTY.
3	M16 x 45 HTS Hex Bolt	Bolt	12
4	M16 Nylock Hex Nut	Nut	12
5	M16 Washer	Washer	24
6	M16 Spring Washer	Spring Washer	12

TITLE: MBSA3 | DWG NO. AD17 | A4
SCALE:1:20 | SHEET 2 OF 6

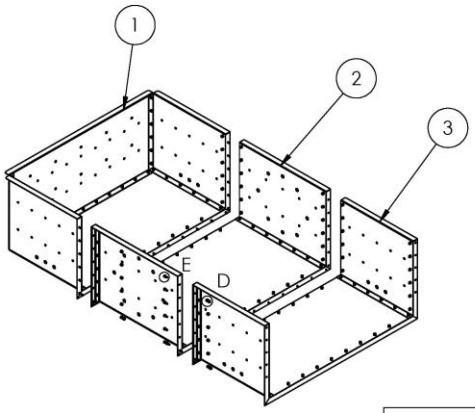

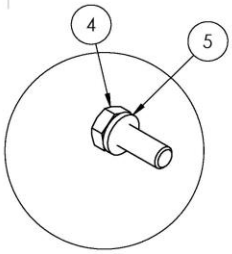

DETAIL E
SCALE 1 : 1

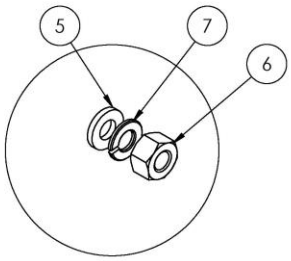

DETAIL D
SCALE 1 : 1

ITEM NO.	PART NUMBER	DESCRIPTION	QTY.
1	BB	Sub Assembly	1
2	MB	Sub Assembly	1
3	FB	Sub Assembly	1
4	M6 x 16 HTS Hex Bolt	Bolt	46
5	M6 Washer	Washer	92
6	M6 Nylock Hex Nut	Nut	46
7	M6 Spring Washer	Spring Washer	46

TITLE: MBSA4 | DWG NO. AD18 | A4
SCALE:1:20 | SHEET 3 OF 6

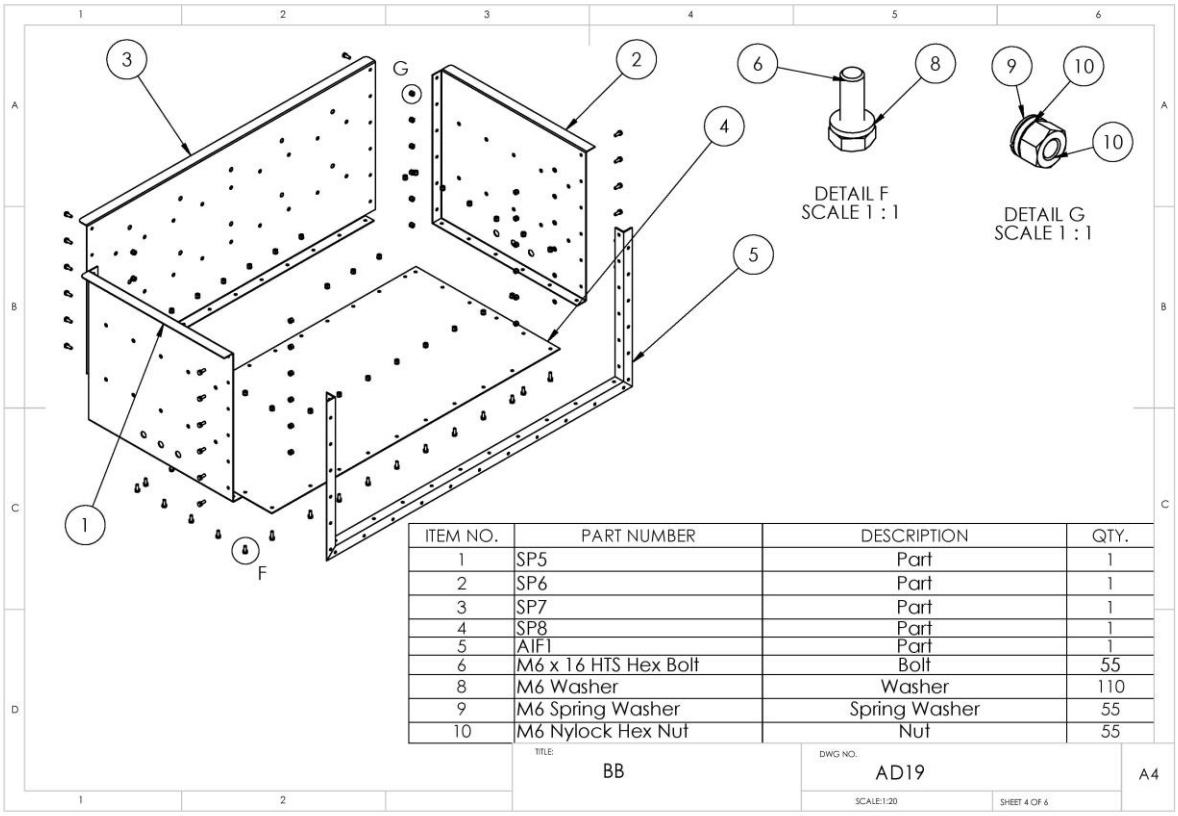

ITEM NO.	PART NUMBER	DESCRIPTION	QTY.
1	SP5	Part	1
2	SP6	Part	1
3	SP7	Part	1
4	SP8	Part	1
5	AIF1	Part	1
6	M6 x 16 HTS Hex Bolt	Bolt	55
8	M6 Washer	Washer	110
9	M6 Spring Washer	Spring Washer	55
10	M6 Nylock Hex Nut	Nut	55

TITLE: BB | DWG NO. AD19 | A4 | SCALE:1:20 | SHEET 4 OF 6

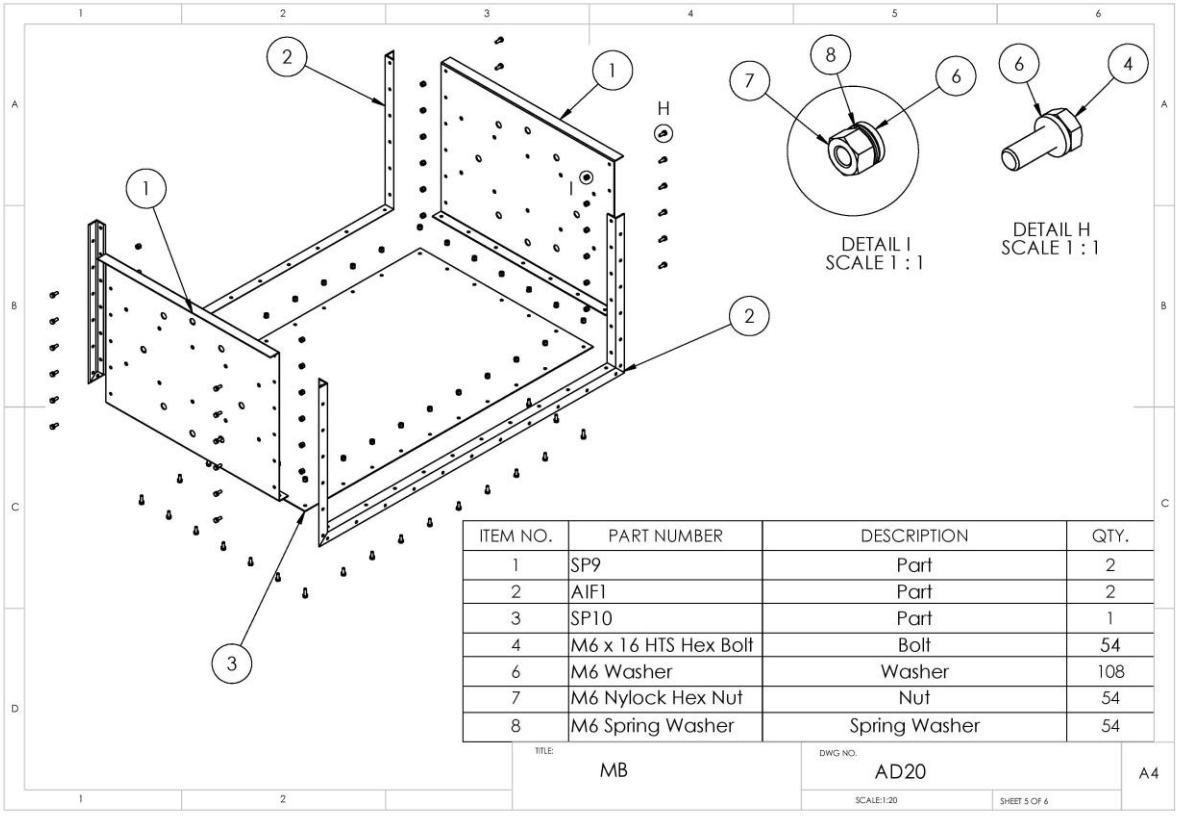

ITEM NO.	PART NUMBER	DESCRIPTION	QTY.
1	SP9	Part	2
2	AIF1	Part	2
3	SP10	Part	1
4	M6 x 16 HTS Hex Bolt	Bolt	54
6	M6 Washer	Washer	108
7	M6 Nylock Hex Nut	Nut	54
8	M6 Spring Washer	Spring Washer	54

TITLE: MB | DWG NO. AD20 | A4 | SCALE:1:20 | SHEET 5 OF 6

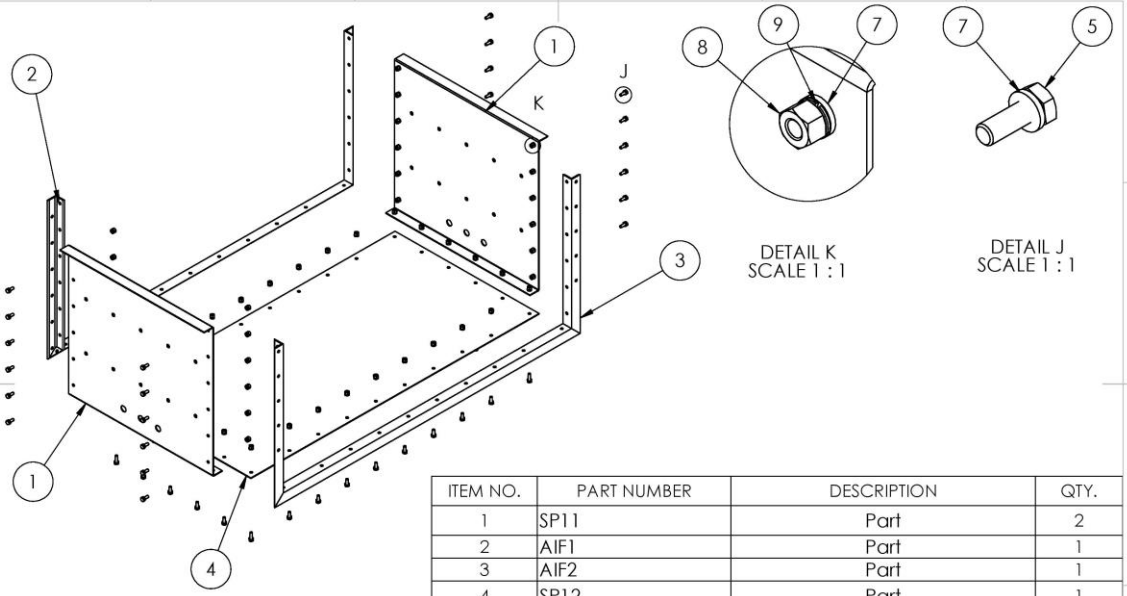

ITEM NO.	PART NUMBER	DESCRIPTION	QTY.
1	SP11	Part	2
2	AIF1	Part	1
3	AIF2	Part	1
4	SP12	Part	1
5	M6 x 16 HTS Hex Bolt	Bolt	52
7	M6 Washer	Washer	104
8	M6 Nylock Hex Nut	Nut	52
9	M6 Spring Washer	Spring Washer	52

TITLE: FB
DWG NO. AD21
A4
SCALE:1:20
SHEET 6 OF 6

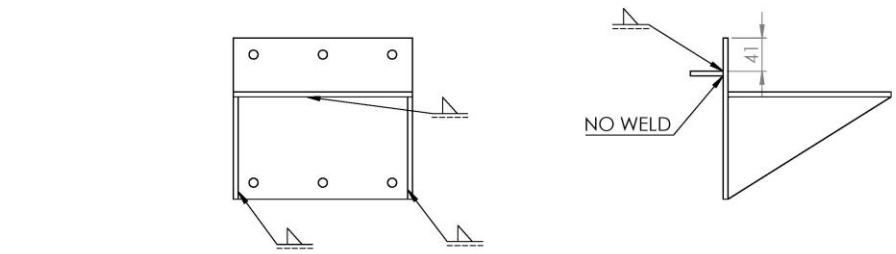

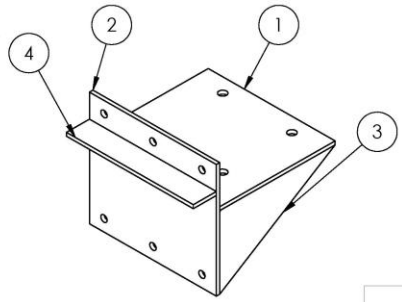

ITEM NO.	PART NUMBER	DESCRIPTION	QTY.
1	FMBD1	MILD STEEL SHEET	1
2	FMBD2	MILD STEEL SHEET	1
3	FMBD3	MILD STEEL SHEET	2
4	FMBD4	MILD STEEL SHEET	1

DEBUR AND BREAK SHARP EDGES
UNLESS OTHERWISE SPECIFIED:
DIMENSIONS ARE IN MILLIMETERS
SURFACE FINISH:
TOLERANCES:
LINEAR:
ANGULAR:
TITLE: FMBD
DO NOT SCALE DRAWING
MATERIAL: MILD STEEL
DWG NO. FMBD
A4
WEIGHT:
SCALE:1:5
SHEET 1 OF 5

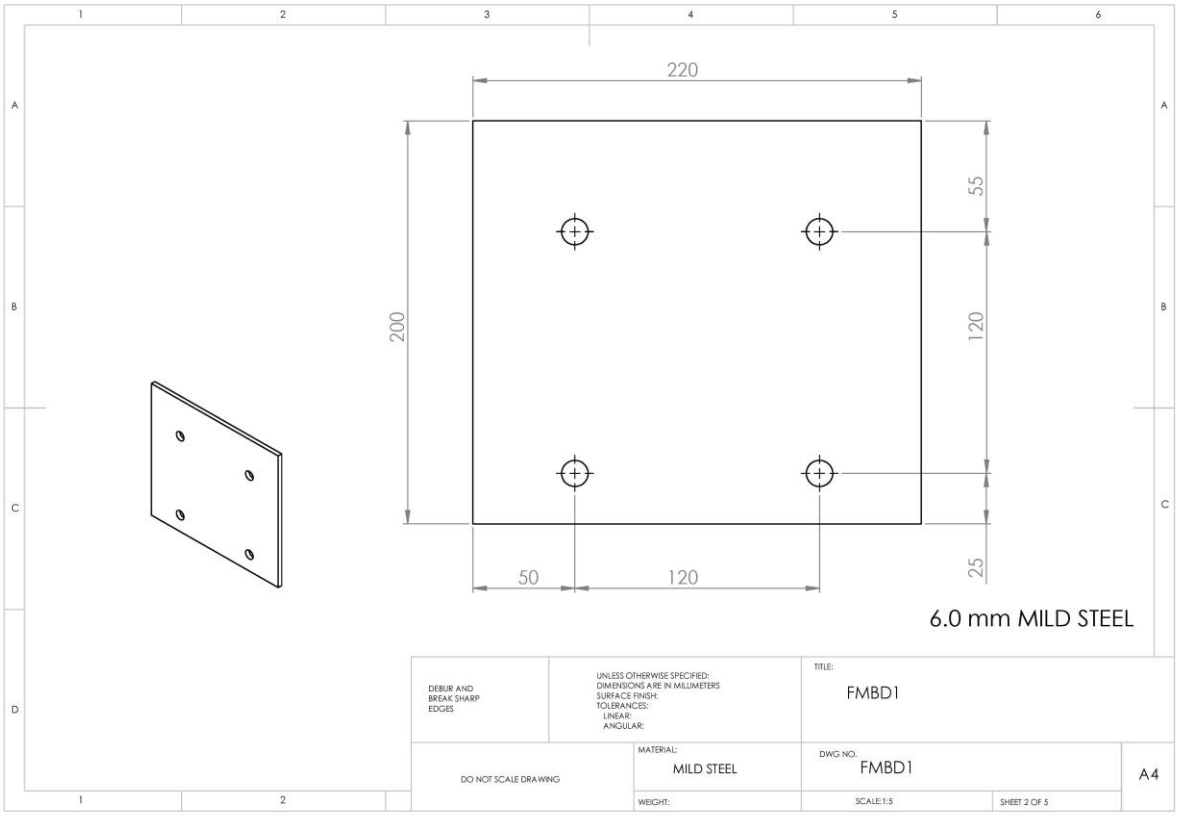
220
55
200
120
50
120
25
6.0 mm MILD STEEL
DEBUR AND
BREAK SHARP
EDGES
UNLESS OTHERWISE SPECIFIED:
DIMENSIONS ARE IN MILLIMETERS
SURFACE FINISH:
TOLERANCES:
LINEAR:
ANGULAR:
TITLE:
FMBD1
DO NOT SCALE DRAWING
MATERIAL:
MILD STEEL
DWG NO.
FMBD1
A4
WEIGHT:
SCALE:1:5
SHEET 2 OF 5

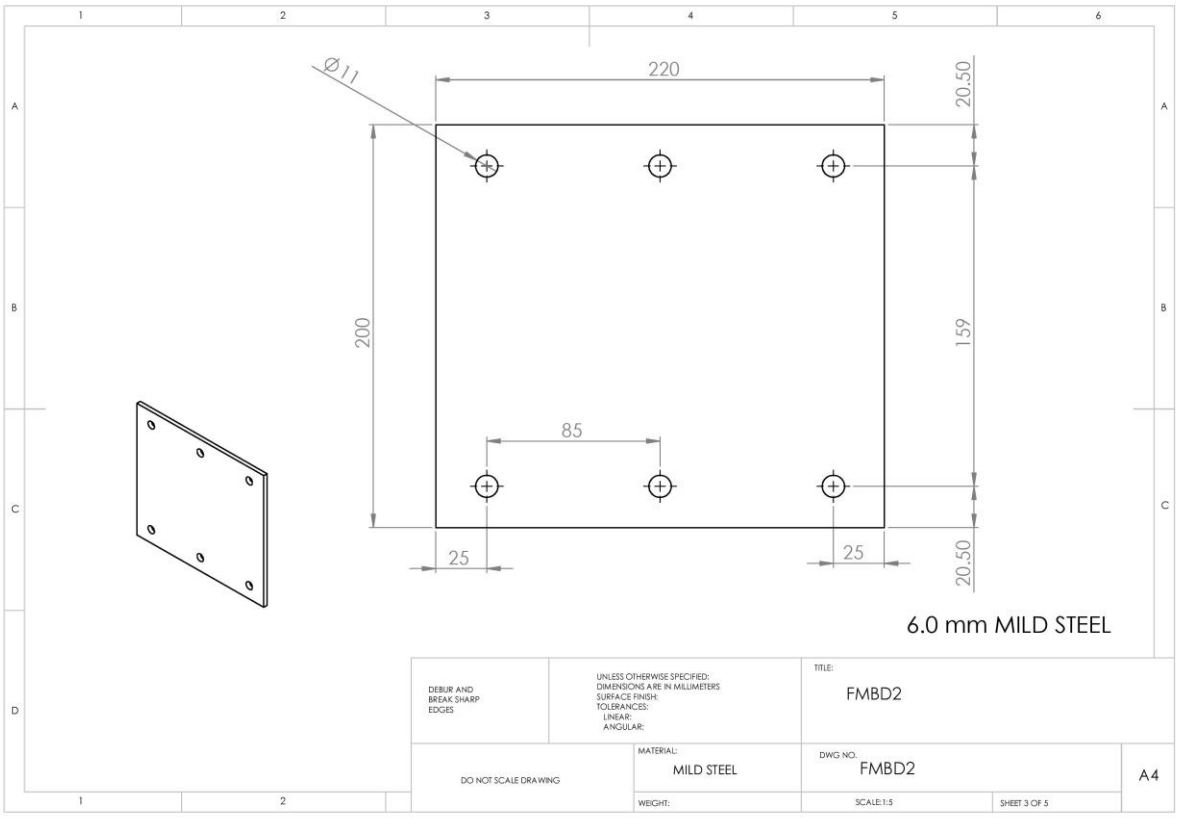
Ø11
220
20.50
200
159
85
25
25
20.50
6.0 mm MILD STEEL
DEBUR AND
BREAK SHARP
EDGES
UNLESS OTHERWISE SPECIFIED:
DIMENSIONS ARE IN MILLIMETERS
SURFACE FINISH:
TOLERANCES:
LINEAR:
ANGULAR:
TITLE:
FMBD2
DO NOT SCALE DRAWING
MATERIAL:
MILD STEEL
DWG NO.
FMBD2
A4
WEIGHT:
SCALE:1:5
SHEET 3 OF 5

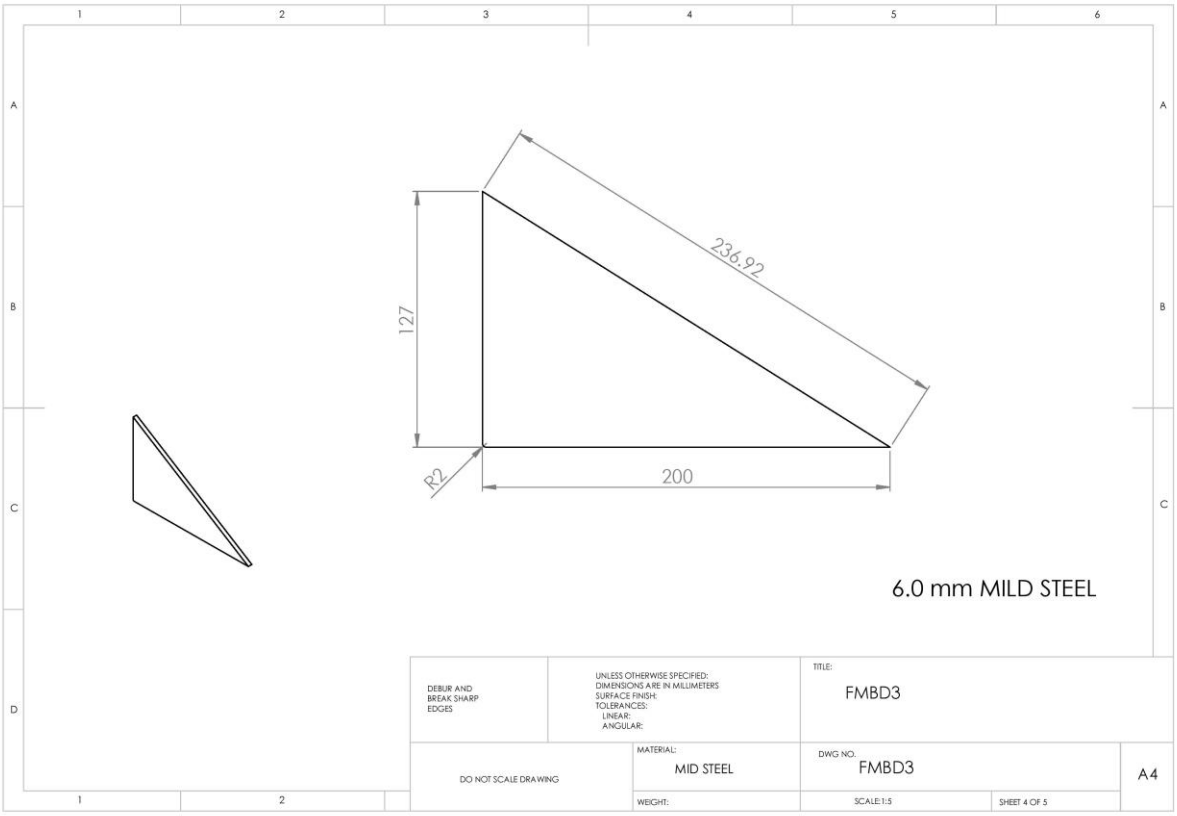
236.92
127
R2
200
6.0 mm MILD STEEL
DEBUR AND
BREAK SHARP
EDGES
UNLESS OTHERWISE SPECIFIED:
DIMENSIONS ARE IN MILLIMETERS
SURFACE FINISH:
TOLERANCES:
LINEAR:
ANGULAR:
TITLE:
FMBD3
DO NOT SCALE DRAWING
MATERIAL:
MID STEEL
DWG NO.
FMBD3
A4
WEIGHT:
SCALE:1:5
SHEET 4 OF 5

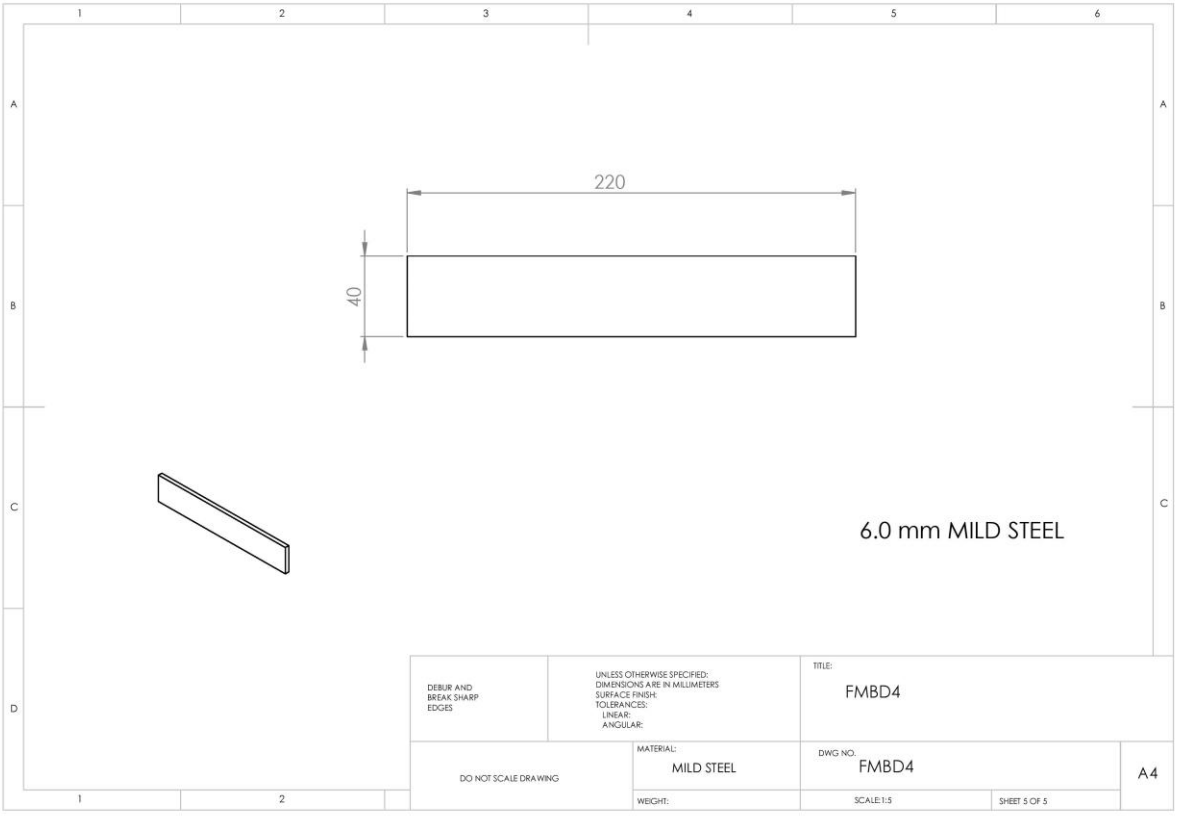
220
40
6.0 mm MILD STEEL
DEBUR AND
BREAK SHARP
EDGES
UNLESS OTHERWISE SPECIFIED:
DIMENSIONS ARE IN MILLIMETERS
SURFACE FINISH:
TOLERANCES:
LINEAR:
ANGULAR:
TITLE:
FMBD4
DO NOT SCALE DRAWING
MATERIAL:
MILD STEEL
DWG NO.
FMBD4
A4
WEIGHT:
SCALE:1:5
SHEET 5 OF 5

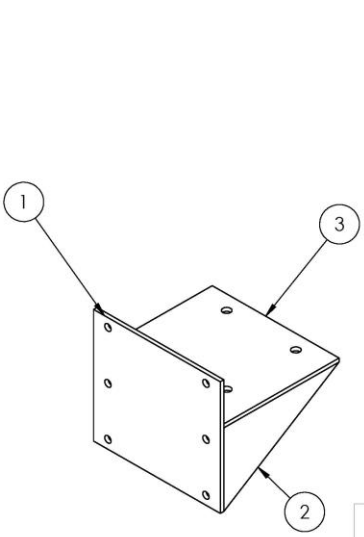

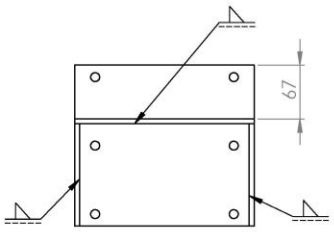

ITEM NO.	PART NUMBER	DESCRIPTION	QTY.
1	FMBF1	MILD STEEL SHEET	1
2	FMBD3	MILD STEEL SHEET	2
3	FMBF2	MILD STEEL SHEET	1

DEBUR AND BREAK SHARP EDGES

UNLESS OTHERWISE SPECIFIED:
DIMENSIONS ARE IN MILLIMETERS
SURFACE FINISH:
TOLERANCES:
LINEAR:
ANGULAR:

TITLE: FMBF

DO NOT SCALE DRAWING

MATERIAL: MILD STEEL

DWG NO. FMBF

A4

WEIGHT:

SCALE:1:5

SHEET 1 OF 3

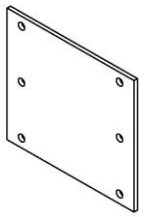

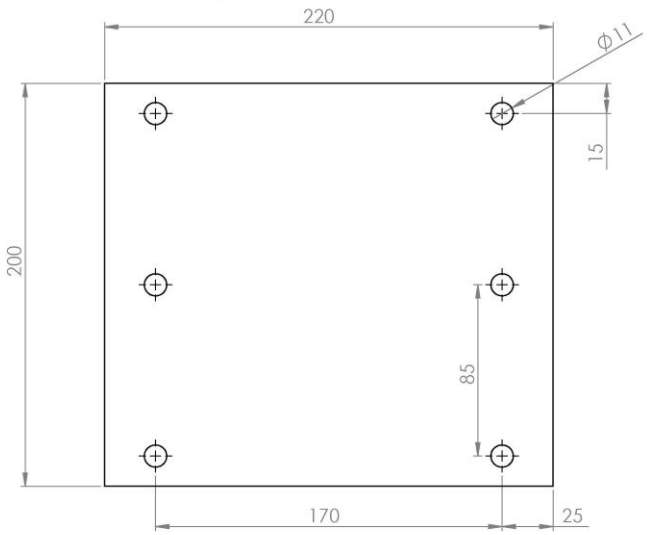

6.0 mm MILD STEEL

DEBUR AND BREAK SHARP EDGES

UNLESS OTHERWISE SPECIFIED:
DIMENSIONS ARE IN MILLIMETERS
SURFACE FINISH:
TOLERANCES:
LINEAR:
ANGULAR:

TITLE: FMBF1

DO NOT SCALE DRAWING

MATERIAL: MILD STEEL

DWG NO. FMBF1

A4

WEIGHT:

SCALE:1:5

SHEET 2 OF 3

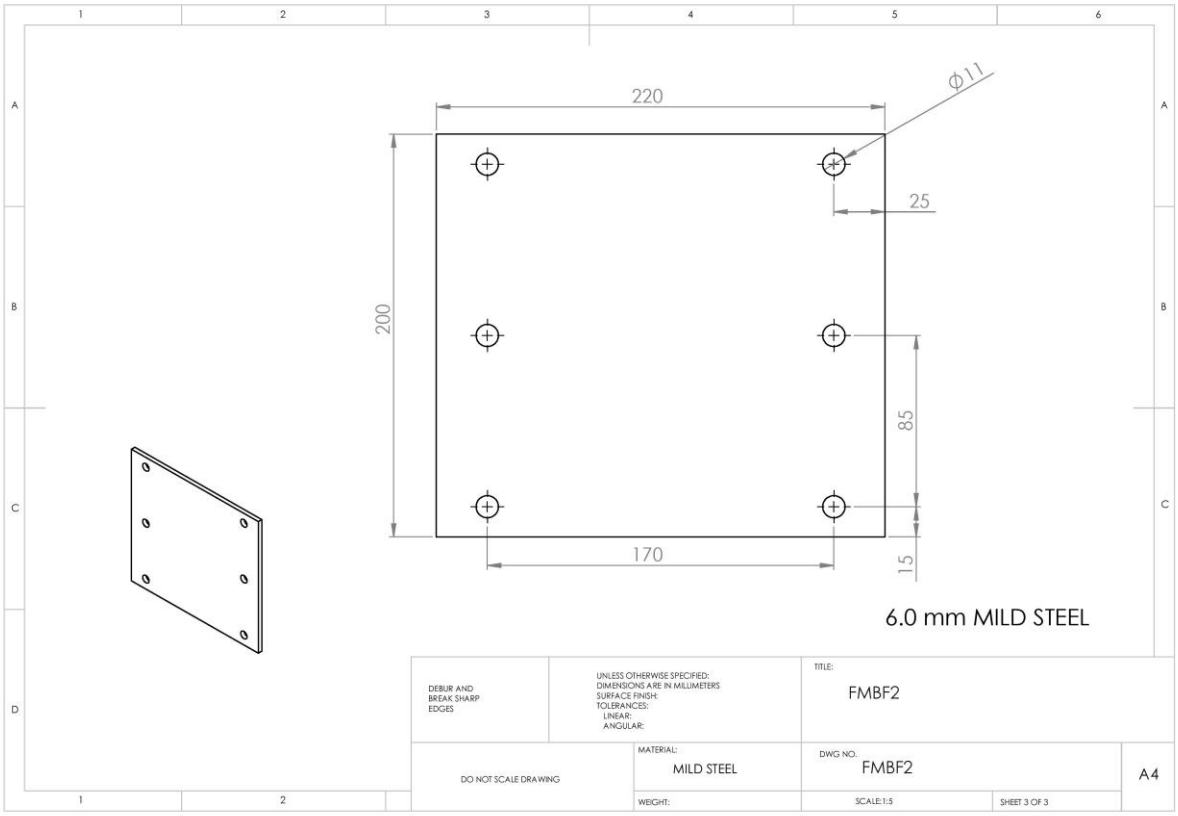
220
ϕ11
25
200
85
170
15
6.0 mm MILD STEEL
DEBUR AND BREAK SHARP EDGES
UNLESS OTHERWISE SPECIFIED:
DIMENSIONS ARE IN MILLIMETERS
SURFACE FINISH:
TOLERANCES:
LINEAR:
ANGULAR:
TITLE:
FMBF2
DO NOT SCALE DRAWING
MATERIAL:
MILD STEEL
DWG NO.
FMBF2
A4
WEIGHT:
SCALE:1:5
SHEET 3 OF 3

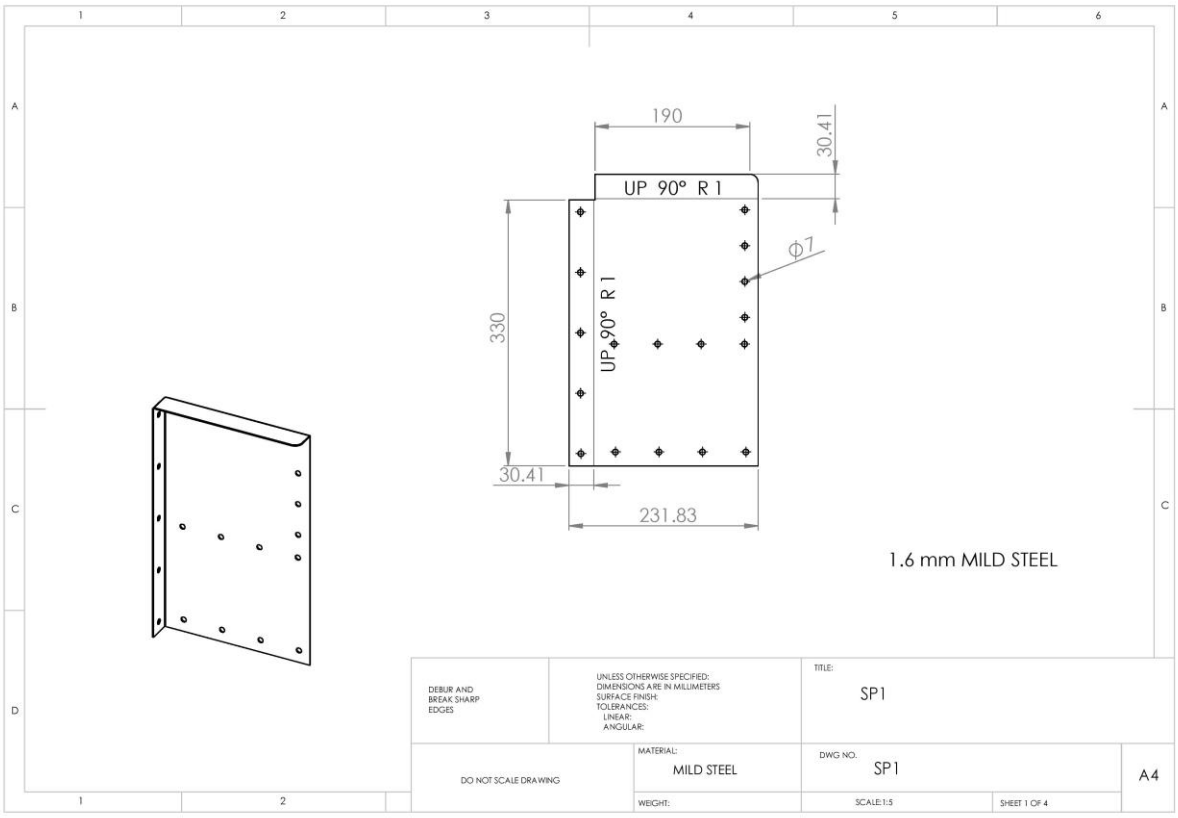
190
30.41
UP 90° R 1
ϕ7
UP 90° R 1
330
30.41
231.83
1.6 mm MILD STEEL
DEBUR AND BREAK SHARP EDGES
UNLESS OTHERWISE SPECIFIED:
DIMENSIONS ARE IN MILLIMETERS
SURFACE FINISH:
TOLERANCES:
LINEAR:
ANGULAR:
TITLE:
SP1
DO NOT SCALE DRAWING
MATERIAL:
MILD STEEL
DWG NO.
SP1
A4
WEIGHT:
SCALE:1:5
SHEET 1 OF 4

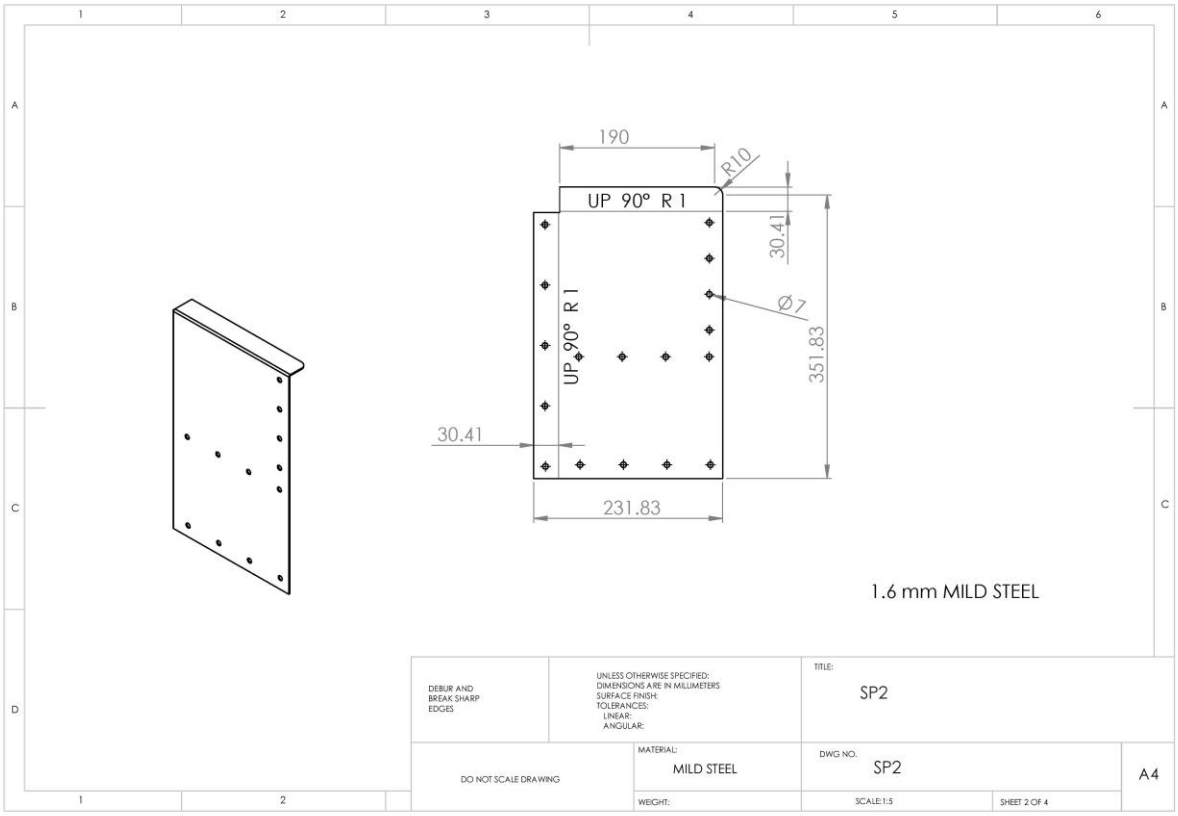
190
R10
UP 90° R 1
30.41
Ø7
UP 90° R 1
351.83
30.41
231.83
1.6 mm MILD STEEL
DEBUR AND BREAK SHARP EDGES
UNLESS OTHERWISE SPECIFIED:
DIMENSIONS ARE IN MILLIMETERS
SURFACE FINISH:
TOLERANCES:
LINEAR:
ANGULAR:
TITLE:
SP2
DO NOT SCALE DRAWING
MATERIAL:
MILD STEEL
DWG NO.
SP2
A4
WEIGHT:
SCALE:1:5
SHEET 2 OF 4

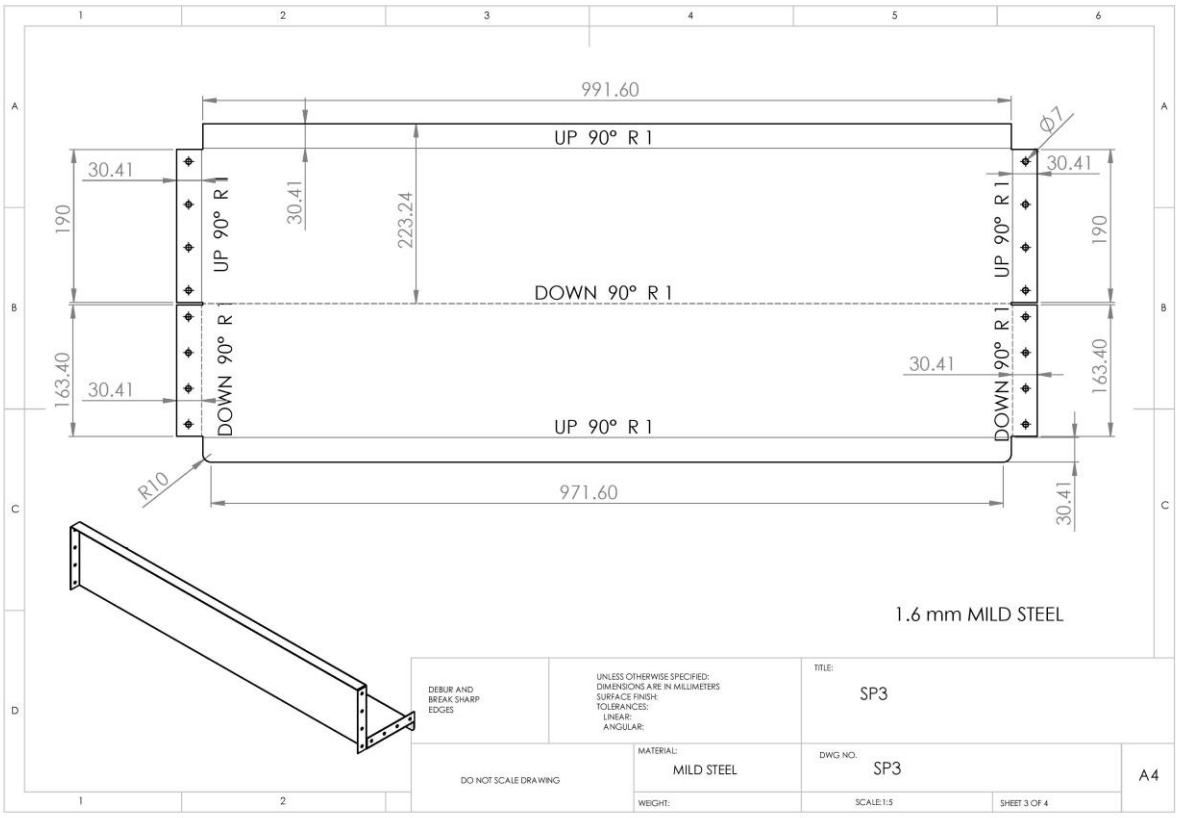
991.60
UP 90° R 1
Ø7
30.41
30.41
190
UP 90° R 1
30.41
223.24
UP 90° R 1
190
DOWN 90° R 1
163.40
30.41
DOWN 90° R 1
30.41
DOWN 90° R 1
163.40
UP 90° R 1
R10
971.60
30.41
1.6 mm MILD STEEL
DEBUR AND BREAK SHARP EDGES
UNLESS OTHERWISE SPECIFIED:
DIMENSIONS ARE IN MILLIMETERS
SURFACE FINISH:
TOLERANCES:
LINEAR:
ANGULAR:
TITLE:
SP3
DO NOT SCALE DRAWING
MATERIAL:
MILD STEEL
DWG NO.
SP3
A4
WEIGHT:
SCALE:1:5
SHEET 3 OF 4

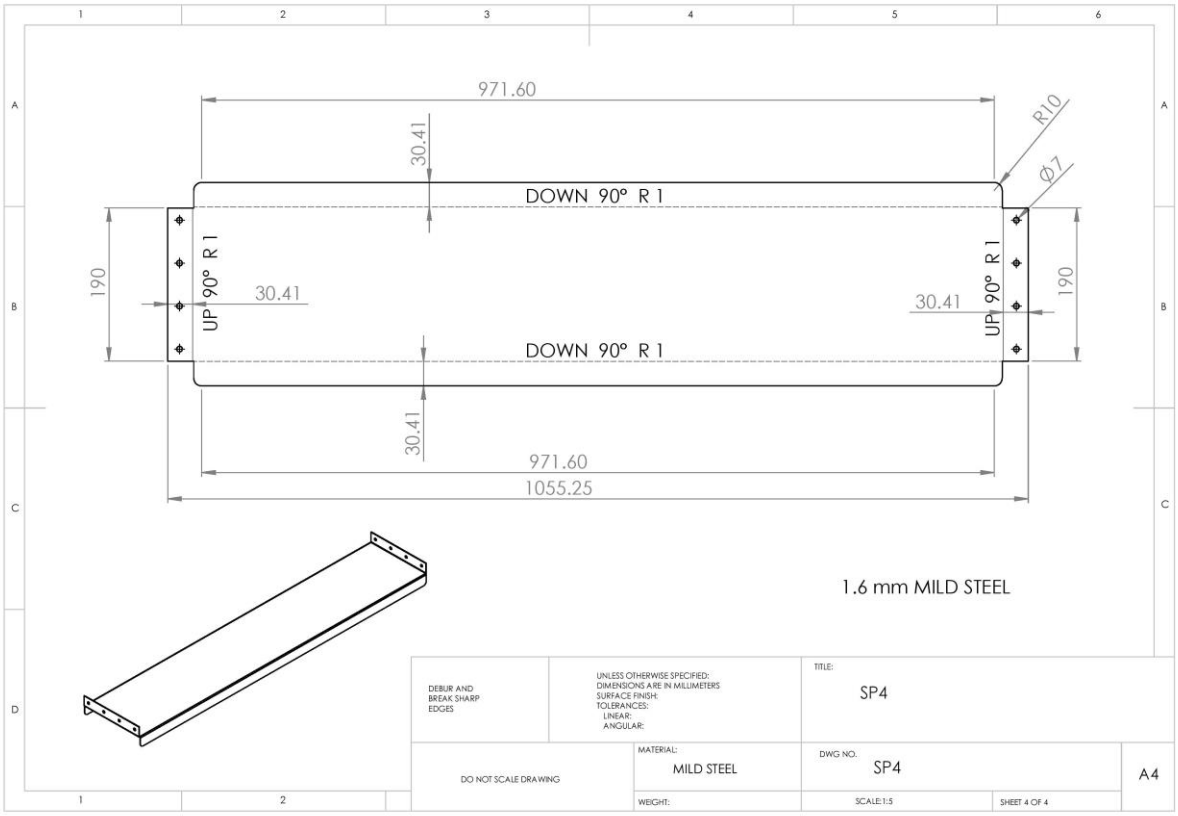

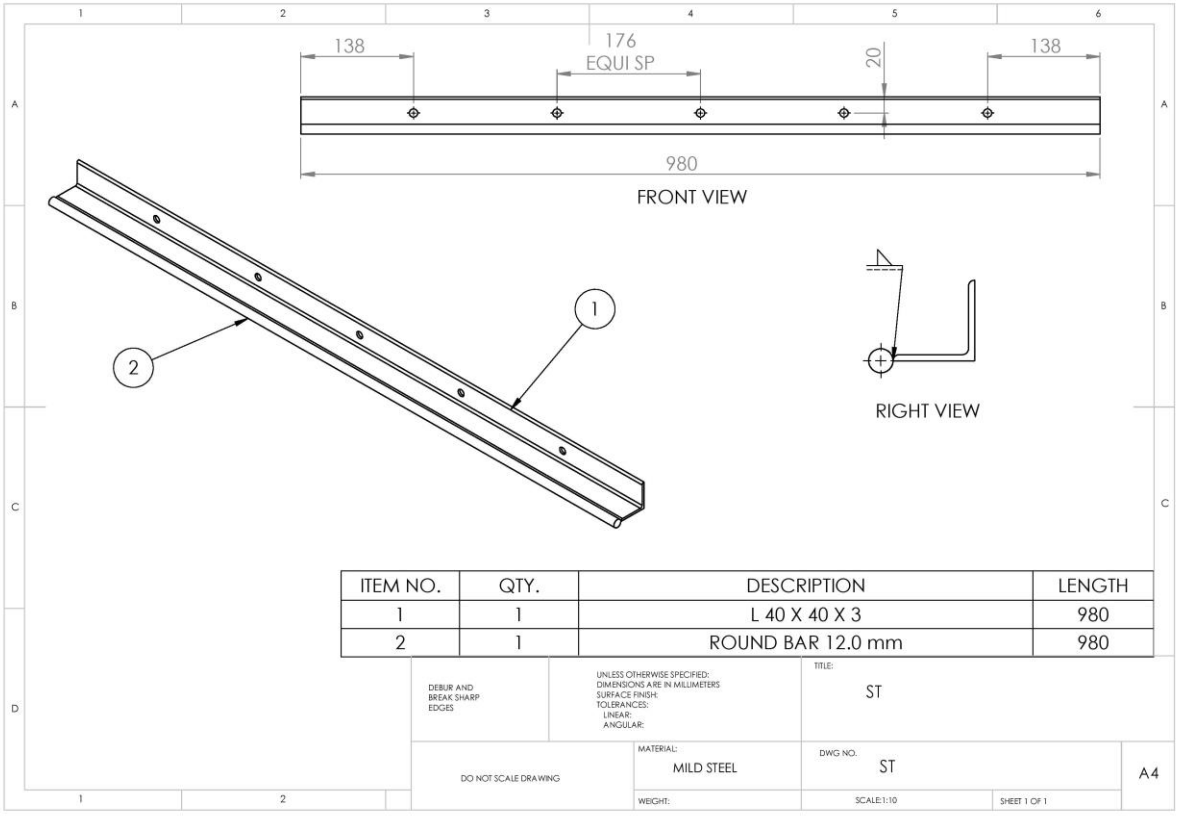

ITEM NO.	QTY.	DESCRIPTION	LENGTH
1	1	L 40 X 40 X 3	980
2	1	ROUND BAR 12.0 mm	980

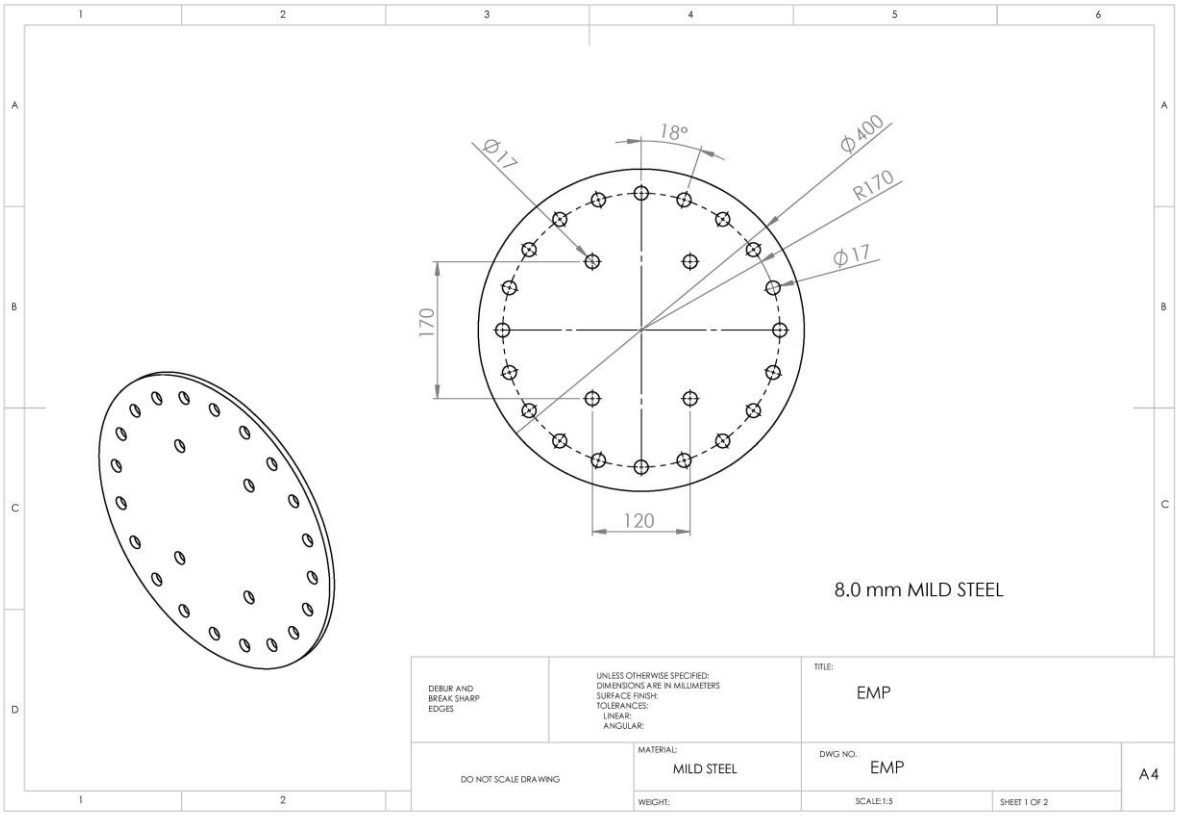
18°
Ø17
Ø400
R170
Ø17
170
120
8.0 mm MILD STEEL
DEBUR AND BREAK SHARP EDGES
UNLESS OTHERWISE SPECIFIED:
DIMENSIONS ARE IN MILLIMETERS
SURFACE FINISH:
TOLERANCES:
LINEAR:
ANGULAR:
TITLE:
EMP
DO NOT SCALE DRAWING
MATERIAL:
MILD STEEL
DWG NO.
EMP
A4
WEIGHT:
SCALE:1:5
SHEET 1 OF 2

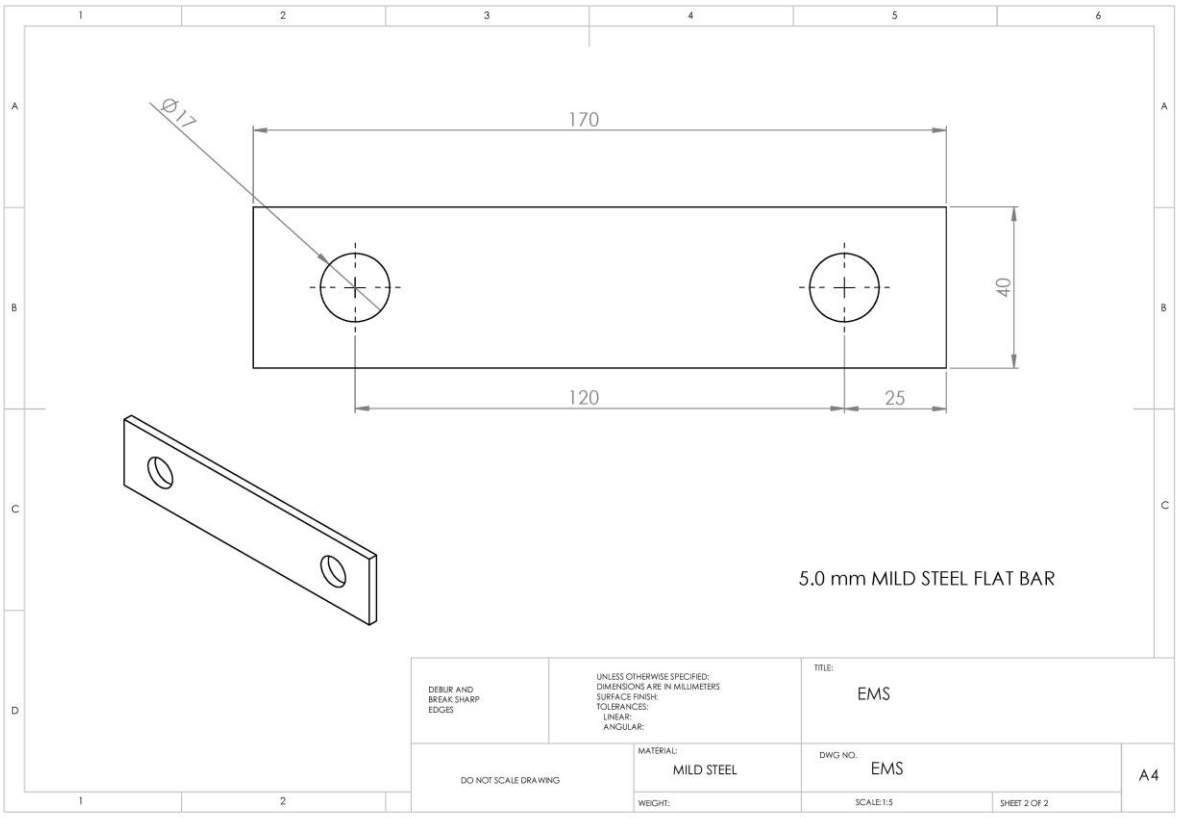
Ø17
170
40
120
25
5.0 mm MILD STEEL FLAT BAR
DEBUR AND BREAK SHARP EDGES
UNLESS OTHERWISE SPECIFIED:
DIMENSIONS ARE IN MILLIMETERS
SURFACE FINISH:
TOLERANCES:
LINEAR:
ANGULAR:
TITLE:
EMS
DO NOT SCALE DRAWING
MATERIAL:
MILD STEEL
DWG NO.
EMS
A4
WEIGHT:
SCALE:1:5
SHEET 2 OF 2

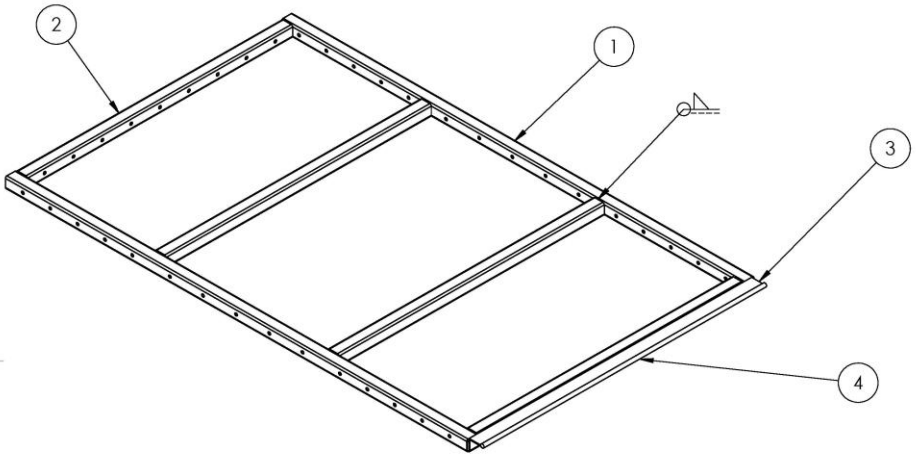

ITEM NO.	QTY.	DESCRIPTION	LENGTH
1	2	TUBE, SQUARE 38 X 38 X 1.60	1600
2	4	TUBE, SQUARE 38 X 38 X 1.60	920
3	1	L 40 X 40 X 3	980
4	1	12 MM ROUND BAR	980

ALL WELDS PERIPHERAL

DEBUR AND BREAK SHARP EDGES

UNLESS OTHERWISE SPECIFIED:
DIMENSIONS ARE IN MILLIMETERS
SURFACE FINISH:
TOLERANCES:
LINEAR:
ANGULAR:

TITLE: SSF

DO NOT SCALE DRAWING

MATERIAL: MILD STEEL

DWG NO. SSF

A4

WEIGHT:

SCALE:1:20

SHEET 1 OF 4

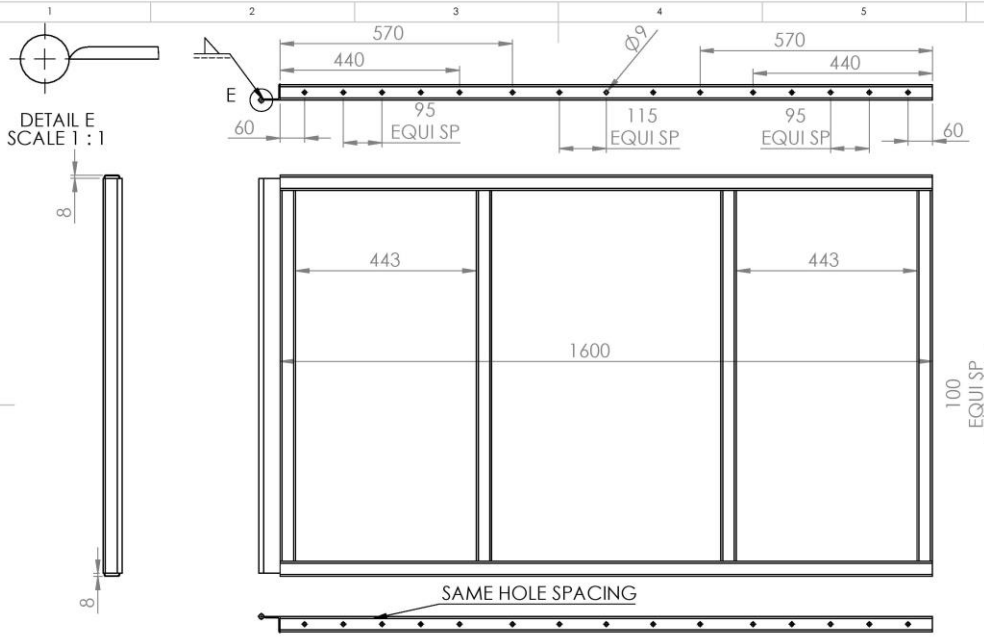

ALL HOLES 9.0 MM THRU AND CENTERED

DEBUR AND BREAK SHARP EDGES

UNLESS OTHERWISE SPECIFIED:
DIMENSIONS ARE IN MILLIMETERS
SURFACE FINISH:
TOLERANCES:
LINEAR:
ANGULAR:

TITLE: SSF1

DO NOT SCALE DRAWING

MATERIAL: MILD STEEL

DWG NO. SSF1

A4

WEIGHT:

SCALE:1:20

SHEET 2 OF 4

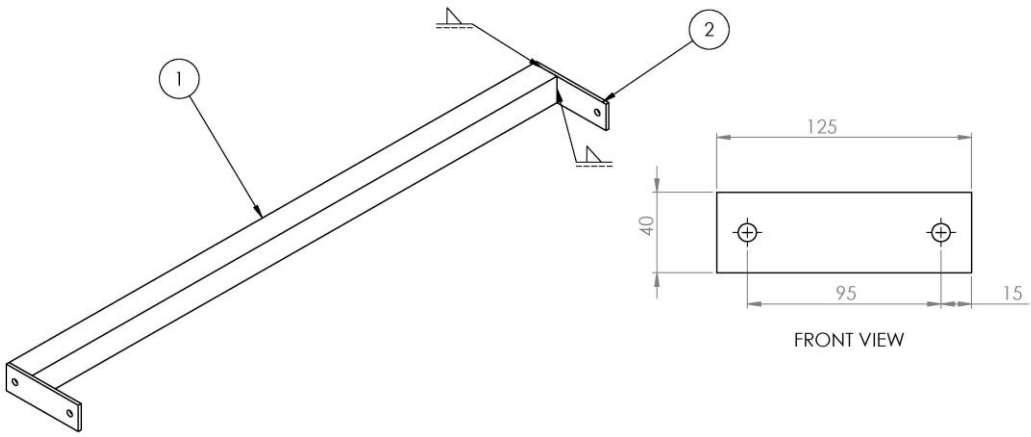

FRONT VIEW

ITEM NO.	QTY.	DESCRIPTION	LENGTH
1	1	L 40 X 40 X 3	910
2	2	40 X 5 FLAT BAR	125

DEBUR AND BREAK SHARP EDGES

UNLESS OTHERWISE SPECIFIED:
DIMENSIONS ARE IN MILLIMETERS
SURFACE FINISH:
TOLERANCES:
LINEAR:
ANGULAR:

TITLE: SSF2

DO NOT SCALE DRAWING

MATERIAL: MILD STEEL

DWG NO. SSF2

A4

WEIGHT:

SCALE:1:20

SHEET 3 OF 4

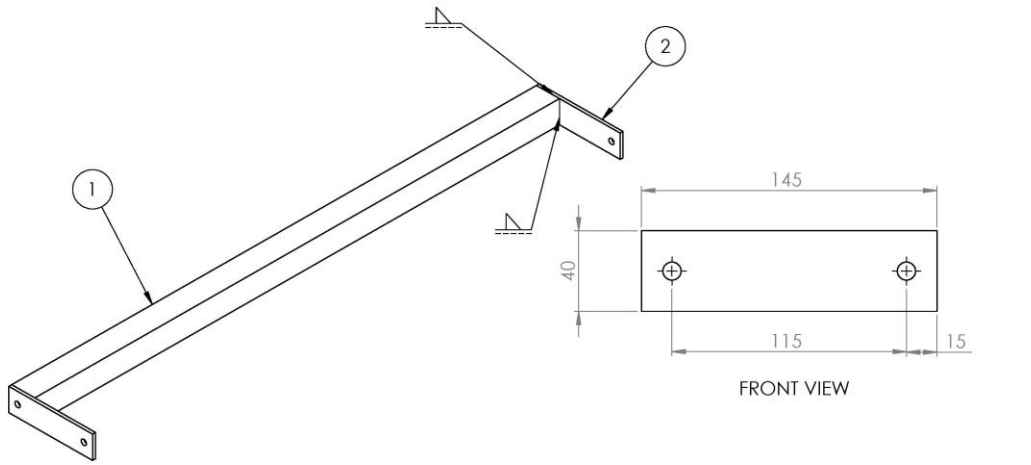

FRONT VIEW

ITEM NO.	QTY.	DESCRIPTION	LENGTH
1	1	L 40 X 40 X 3	910
2	2	40 X 5 FLAT BAR	145

DEBUR AND BREAK SHARP EDGES

UNLESS OTHERWISE SPECIFIED:
DIMENSIONS ARE IN MILLIMETERS
SURFACE FINISH:
TOLERANCES:
LINEAR:
ANGULAR:

TITLE: SSF3

DO NOT SCALE DRAWING

MATERIAL: MILD STEEL

DWG NO. SSF3

A4

WEIGHT:

SCALE:1:20

SHEET 4 OF 4

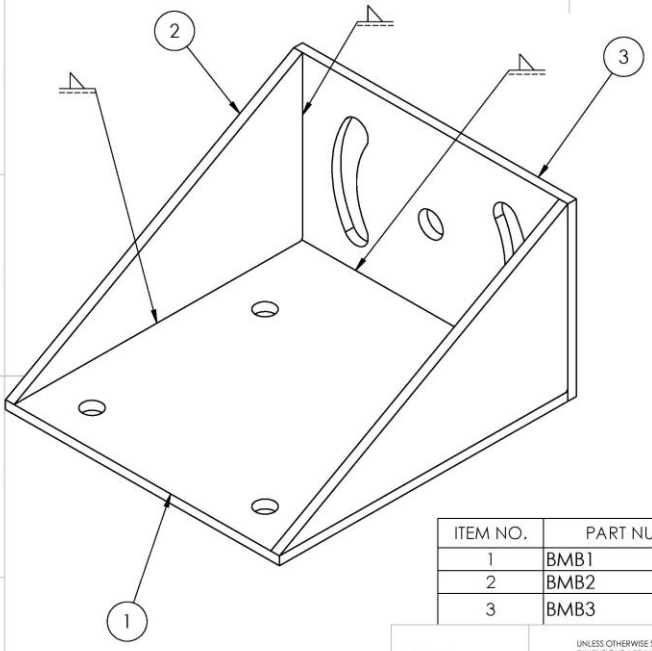

ITEM NO.	PART NUMBER	DESCRIPTION	QTY.
1	BMB1	MILD STEEL SHEET	1
2	BMB2	MILD STEEL SHEET	2
3	BMB3	MILD STEEL SHEET	1

DEBUR AND BREAK SHARP EDGES

UNLESS OTHERWISE SPECIFIED:
DIMENSIONS ARE IN MILLIMETERS
SURFACE FINISH:
TOLERANCES:
LINEAR:
ANGULAR:

TITLE: BMB

DO NOT SCALE DRAWING

MATERIAL: MILD STEEL

DWG NO. BMB

A4

WEIGHT:

SCALE:1:5

SHEET 1 OF 4

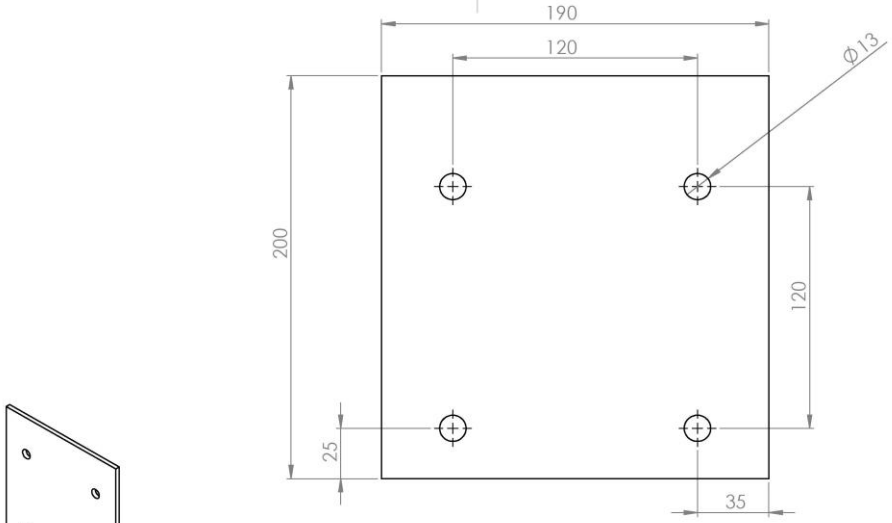

6.0 mm MILD STEEL

DEBUR AND BREAK SHARP EDGES

UNLESS OTHERWISE SPECIFIED:
DIMENSIONS ARE IN MILLIMETERS
SURFACE FINISH:
TOLERANCES:
LINEAR:
ANGULAR:

TITLE: BMB1

DO NOT SCALE DRAWING

MATERIAL: MILD STEEL

DWG NO. BMB1

A4

WEIGHT:

SCALE:1:5

SHEET 2 OF 4

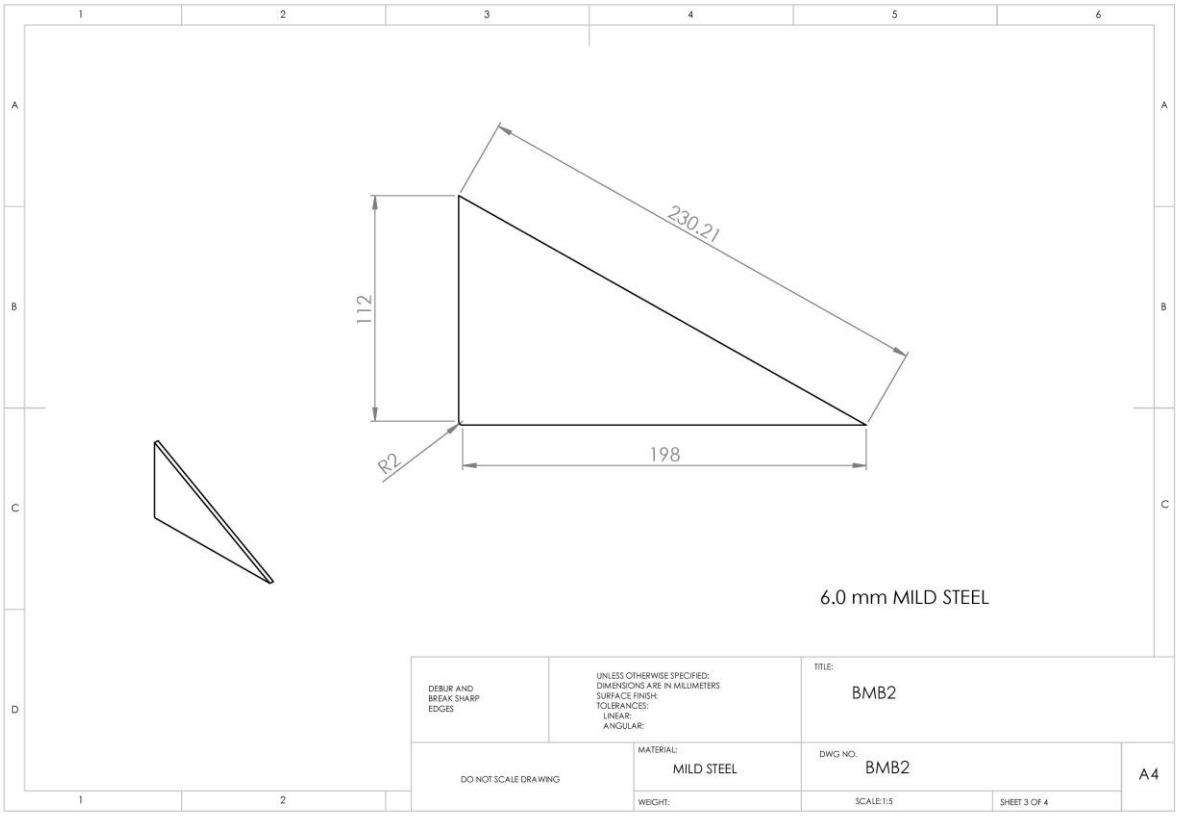
230.21
112
198
R2
6.0 mm MILD STEEL
DEBUR AND
BREAK SHARP
EDGES
UNLESS OTHERWISE SPECIFIED:
DIMENSIONS ARE IN MILLIMETERS
SURFACE FINISH:
TOLERANCES:
LINEAR:
ANGULAR:
TITLE:
BMB2
DO NOT SCALE DRAWING
MATERIAL:
MILD STEEL
DWG NO.
BMB2
A4
WEIGHT:
SCALE:1:5
SHEET 3 OF 4

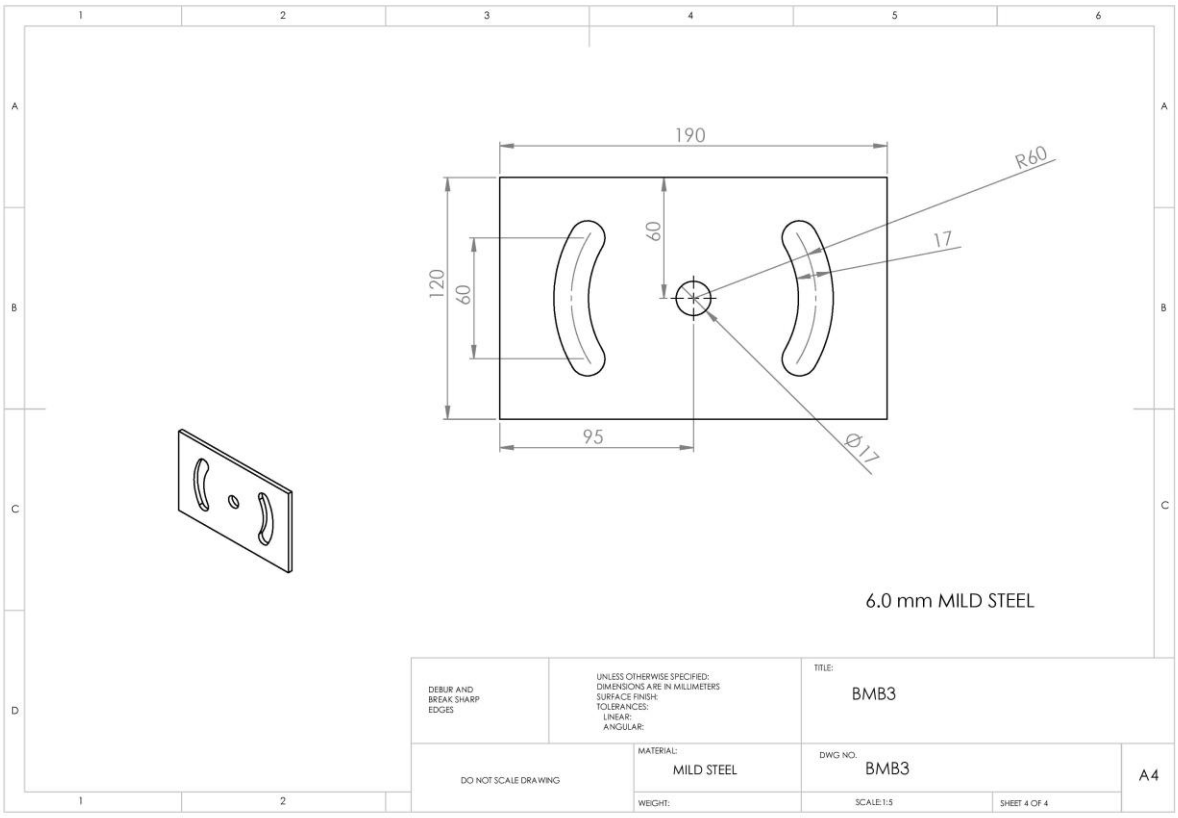
190
120
60
60
95
R60
17
Ø17
6.0 mm MILD STEEL
DEBUR AND
BREAK SHARP
EDGES
UNLESS OTHERWISE SPECIFIED:
DIMENSIONS ARE IN MILLIMETERS
SURFACE FINISH:
TOLERANCES:
LINEAR:
ANGULAR:
TITLE:
BMB3
DO NOT SCALE DRAWING
MATERIAL:
MILD STEEL
DWG NO.
BMB3
A4
WEIGHT:
SCALE:1:5
SHEET 4 OF 4

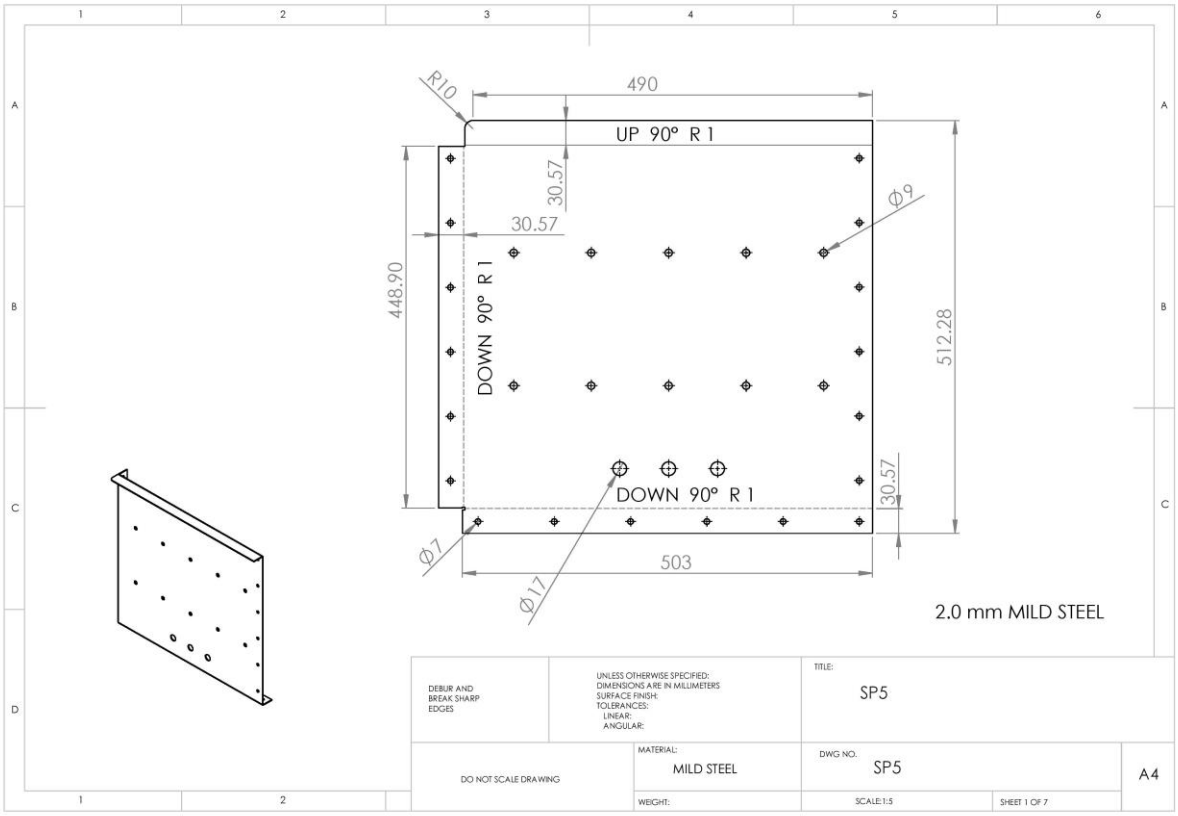
R10
490
UP 90° R 1
30.57
30.57
Ø9
448.90
DOWN 90° R 1
512.28
DOWN 90° R 1
30.57
Ø7
503
Ø17
2.0 mm MILD STEEL
DEBUR AND BREAK SHARP EDGES
UNLESS OTHERWISE SPECIFIED:
DIMENSIONS ARE IN MILLIMETERS
SURFACE FINISH:
TOLERANCES:
LINEAR:
ANGULAR:
TITLE:
SP5
DO NOT SCALE DRAWING
MATERIAL:
MILD STEEL
DWG NO.
SP5
A4
WEIGHT:
SCALE:1:5
SHEET 1 OF 7

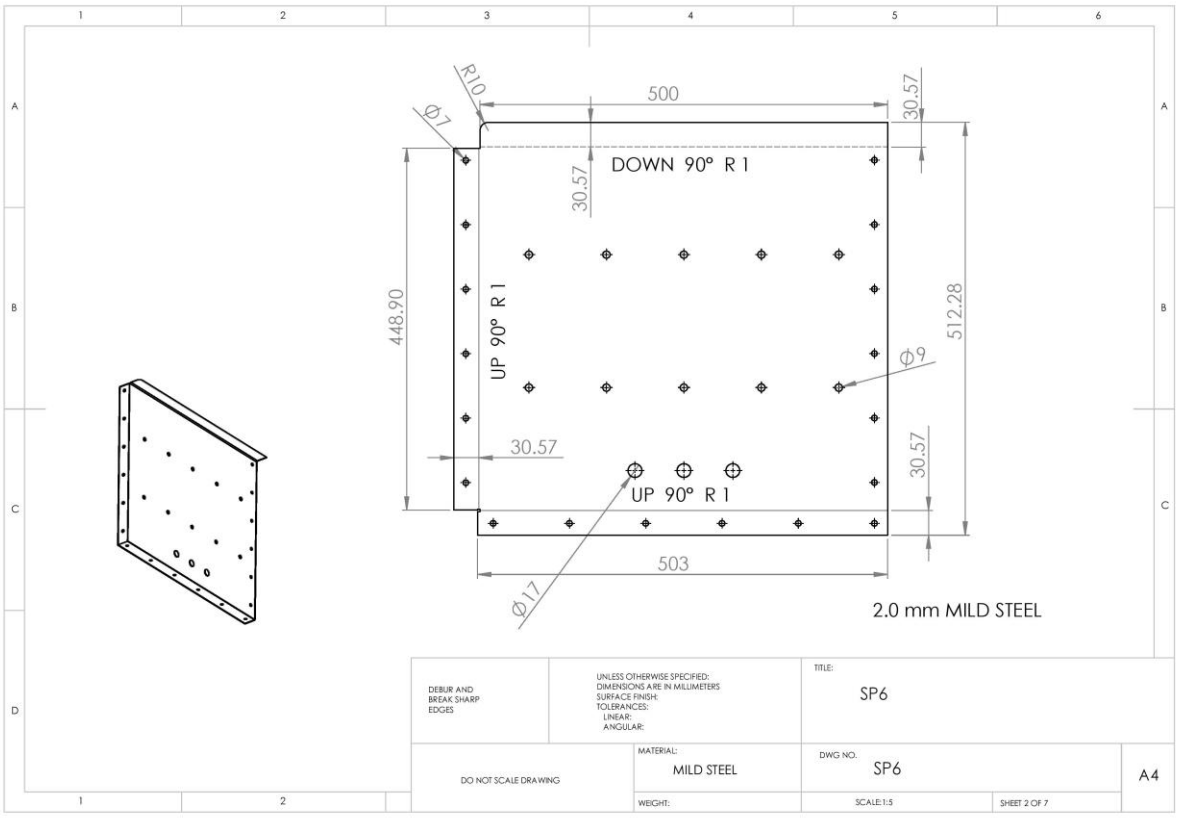
R10
Ø7
500
30.57
30.57
DOWN 90° R 1
448.90
UP 90° R 1
512.28
Ø9
30.57
30.57
UP 90° R 1
503
Ø17
2.0 mm MILD STEEL
DEBUR AND BREAK SHARP EDGES
UNLESS OTHERWISE SPECIFIED:
DIMENSIONS ARE IN MILLIMETERS
SURFACE FINISH:
TOLERANCES:
LINEAR:
ANGULAR:
TITLE:
SP6
DO NOT SCALE DRAWING
MATERIAL:
MILD STEEL
DWG NO.
SP6
A4
WEIGHT:
SCALE:1:5
SHEET 2 OF 7

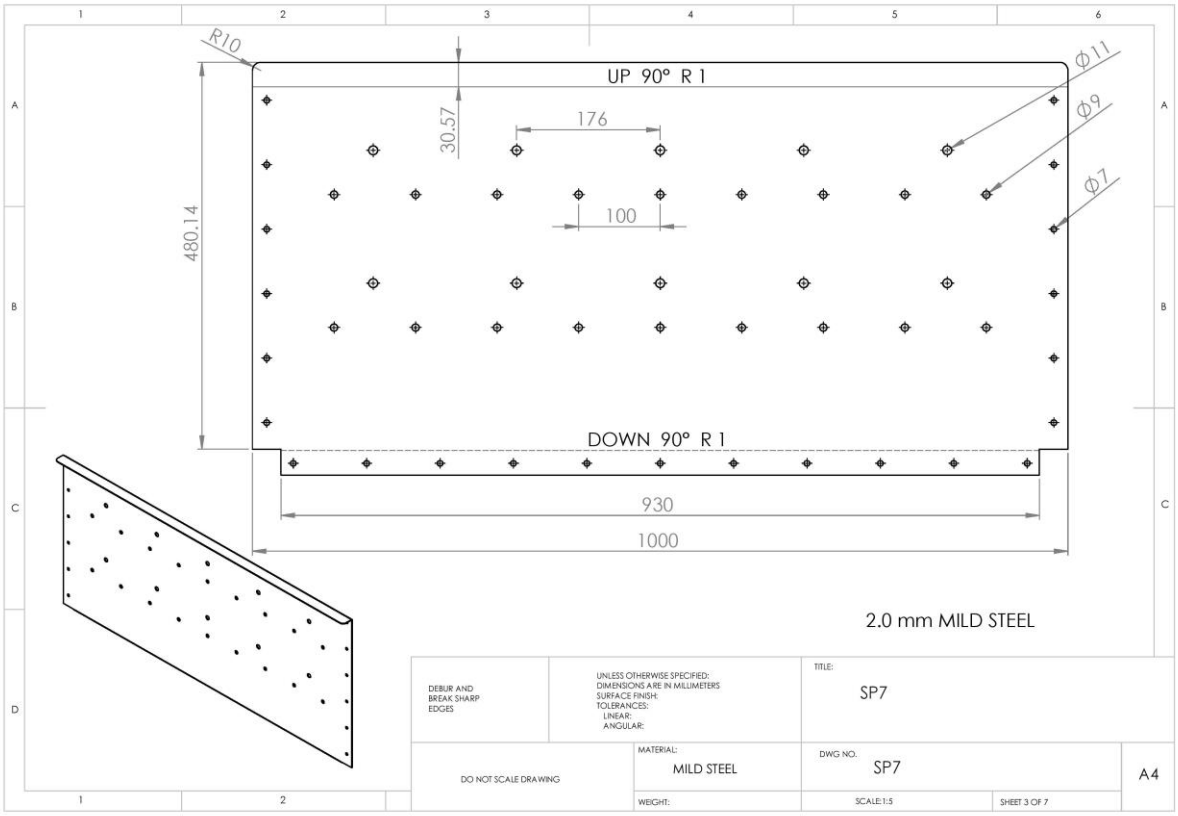
R10
UP 90° R 1
30.57
176
100
480.14
Ø11
Ø9
Ø7
DOWN 90° R 1
930
1000
2.0 mm MILD STEEL
DEBUR AND BREAK SHARP EDGES
UNLESS OTHERWISE SPECIFIED:
DIMENSIONS ARE IN MILLIMETERS
SURFACE FINISH:
TOLERANCES:
LINEAR:
ANGULAR:
TITLE:
SP7
DO NOT SCALE DRAWING
MATERIAL:
MILD STEEL
DWG NO.
SP7
A4
WEIGHT:
SCALE:1:5
SHEET 3 OF 7

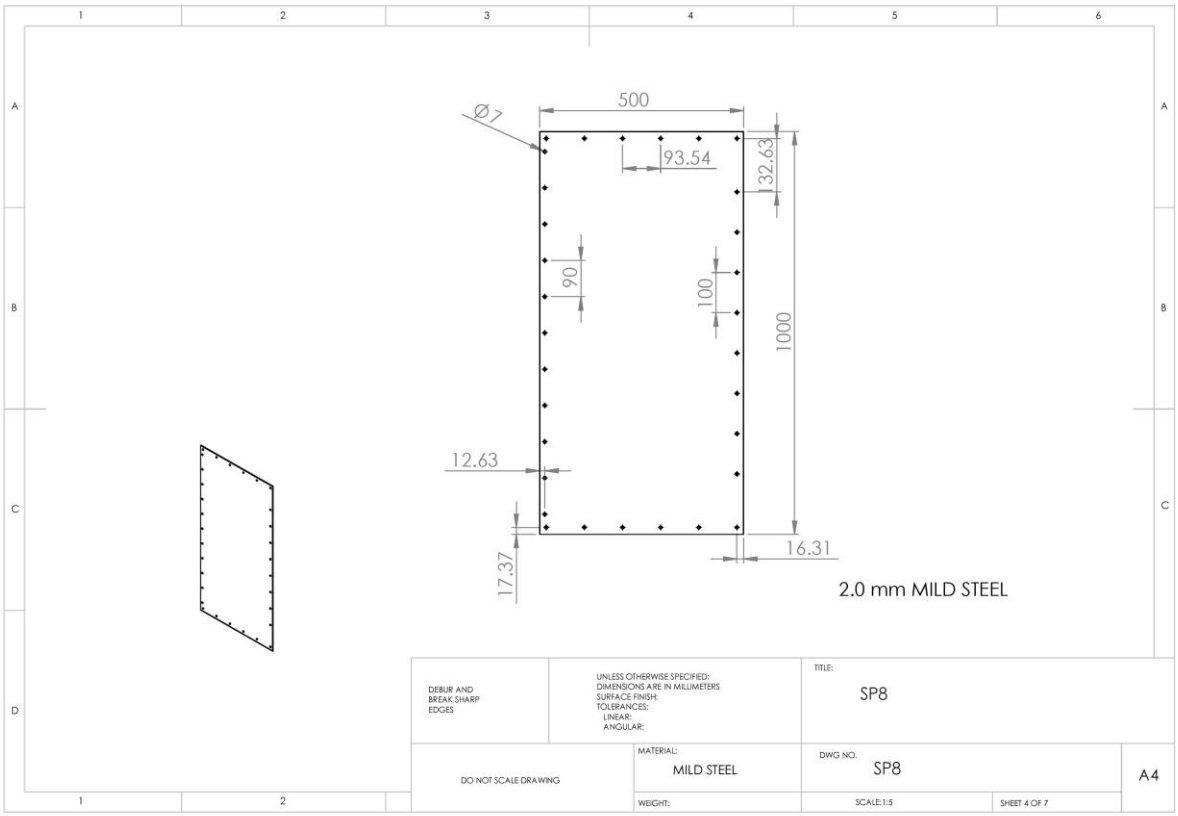
Ø7
500
93.54
32.63
90
100
1000
12.63
16.31
17.37
2.0 mm MILD STEEL
DEBUR AND BREAK SHARP EDGES
UNLESS OTHERWISE SPECIFIED:
DIMENSIONS ARE IN MILLIMETERS
SURFACE FINISH:
TOLERANCES:
LINEAR:
ANGULAR:
TITLE:
SP8
DO NOT SCALE DRAWING
MATERIAL:
MILD STEEL
DWG NO.
SP8
A4
WEIGHT:
SCALE:1:5
SHEET 4 OF 7

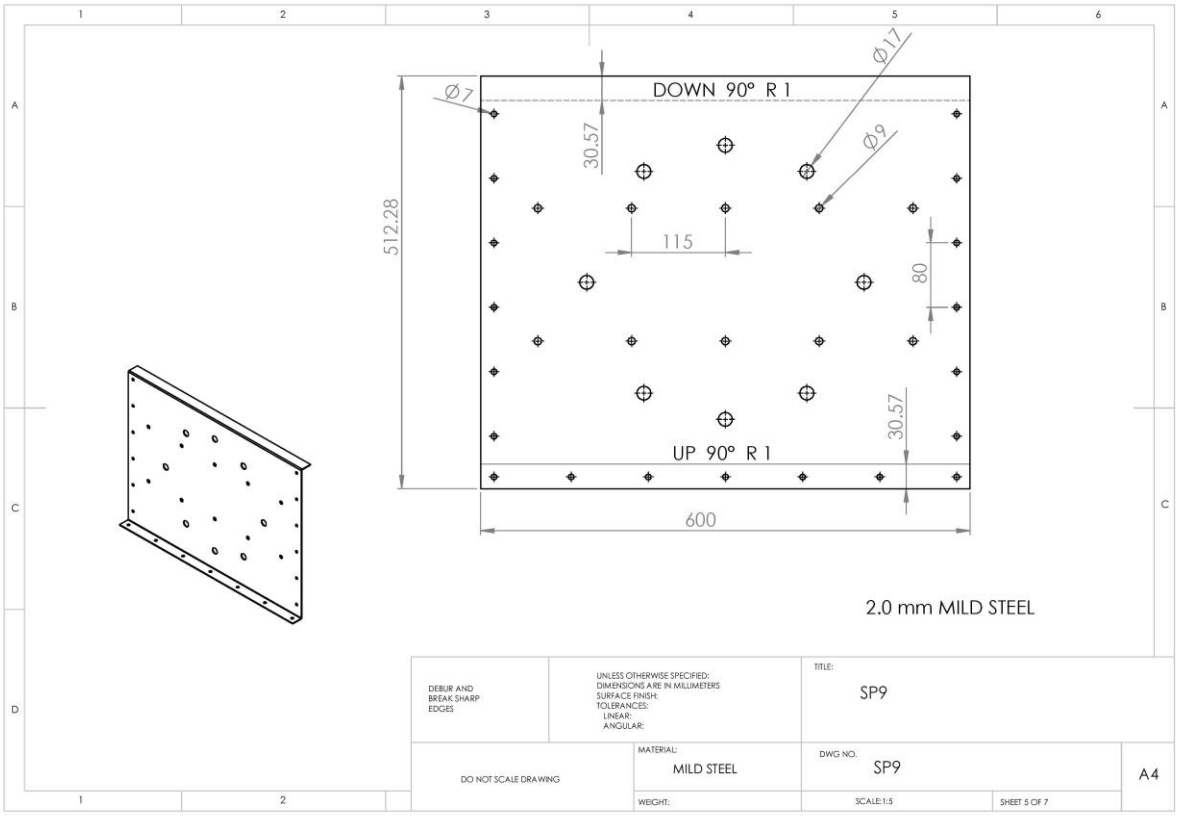
DOWN 90° R 1
UP 90° R 1
Ø17
Ø7
Ø9
30.57
512.28
115
80
30.57
600
2.0 mm MILD STEEL
DEBUR AND BREAK SHARP EDGES
UNLESS OTHERWISE SPECIFIED:
DIMENSIONS ARE IN MILLIMETERS
SURFACE FINISH:
TOLERANCES:
LINEAR:
ANGULAR:
TITLE:
SP9
DO NOT SCALE DRAWING
MATERIAL:
MILD STEEL
DWG NO.
SP9
A4
WEIGHT:
SCALE:1:5
SHEET 5 OF 7

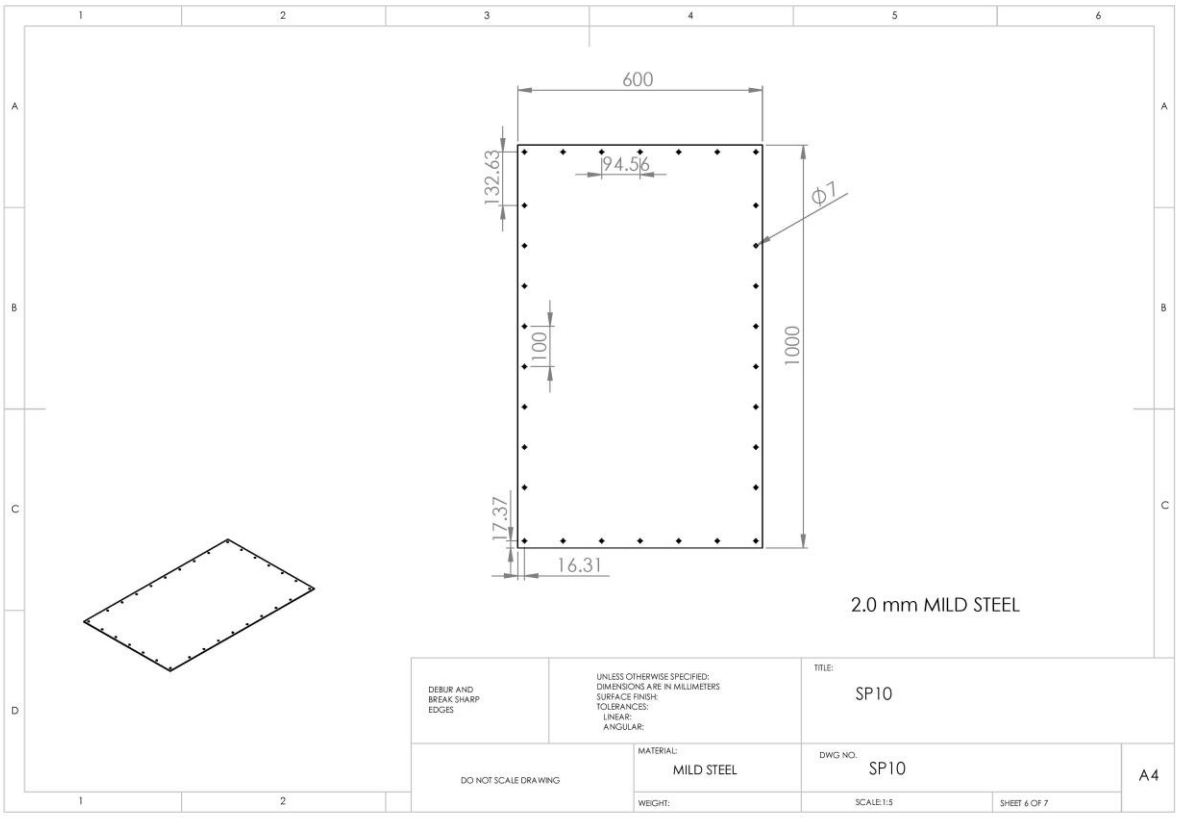
600
94.56
132.63
Ø7
1100
1000
17.37
16.31
2.0 mm MILD STEEL
DEBUR AND BREAK SHARP EDGES
UNLESS OTHERWISE SPECIFIED:
DIMENSIONS ARE IN MILLIMETERS
SURFACE FINISH:
TOLERANCES:
LINEAR:
ANGULAR:
TITLE:
SP10
DO NOT SCALE DRAWING
MATERIAL:
MILD STEEL
DWG NO.
SP10
A4
WEIGHT:
SCALE:1:5
SHEET 6 OF 7

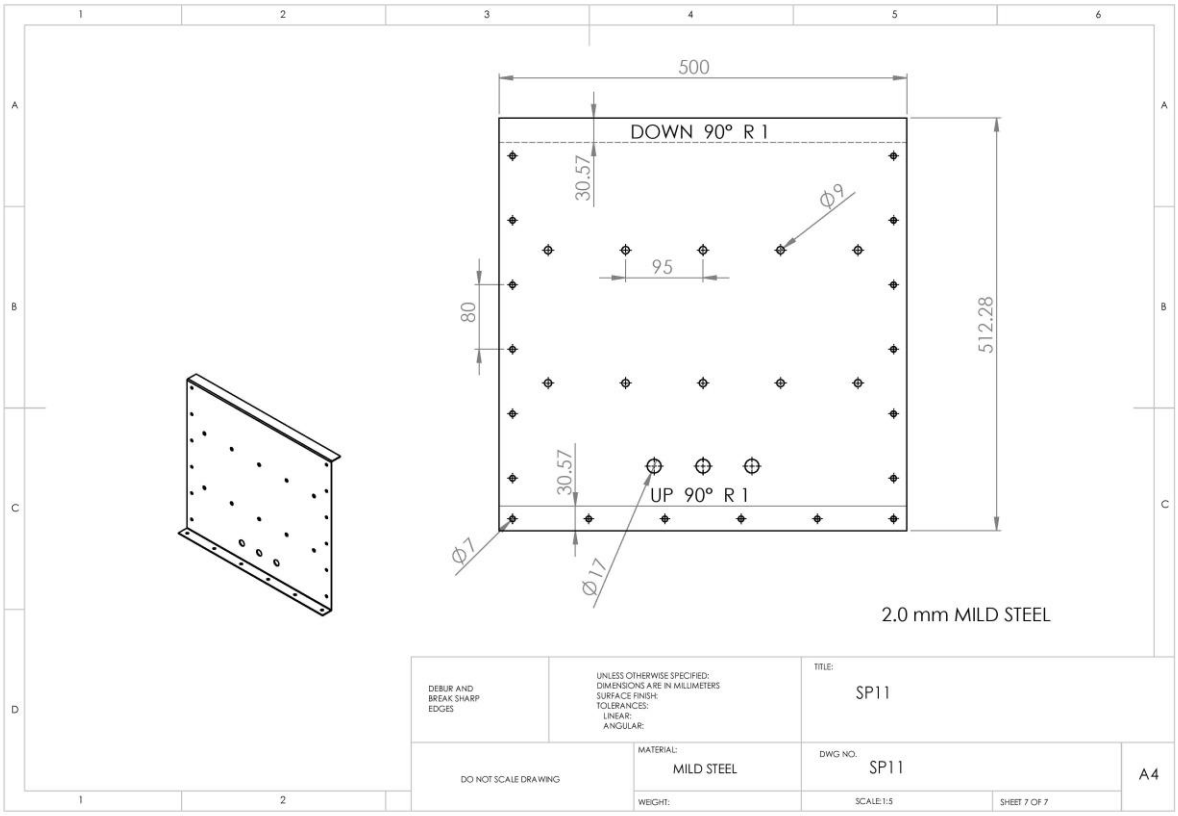

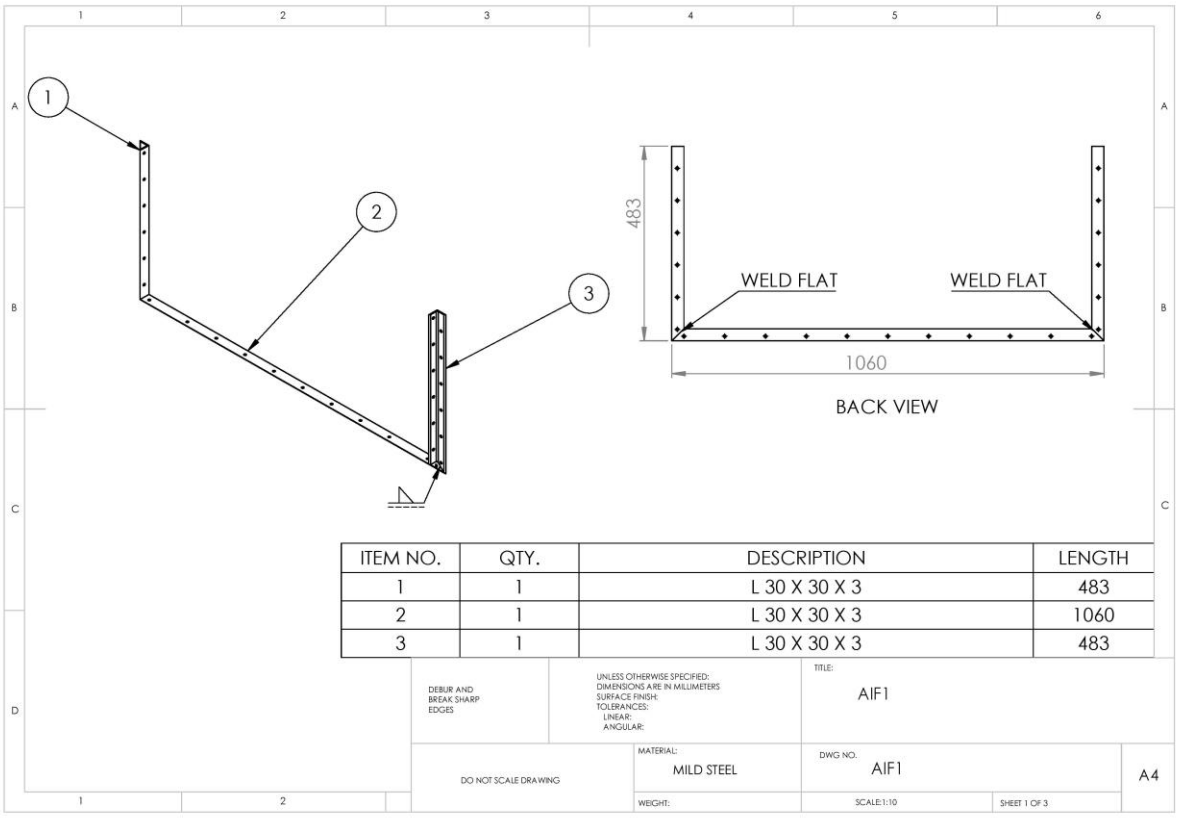

ITEM NO.	QTY.	DESCRIPTION	LENGTH
1	1	L 30 X 30 X 3	483
2	1	L 30 X 30 X 3	1060
3	1	L 30 X 30 X 3	483

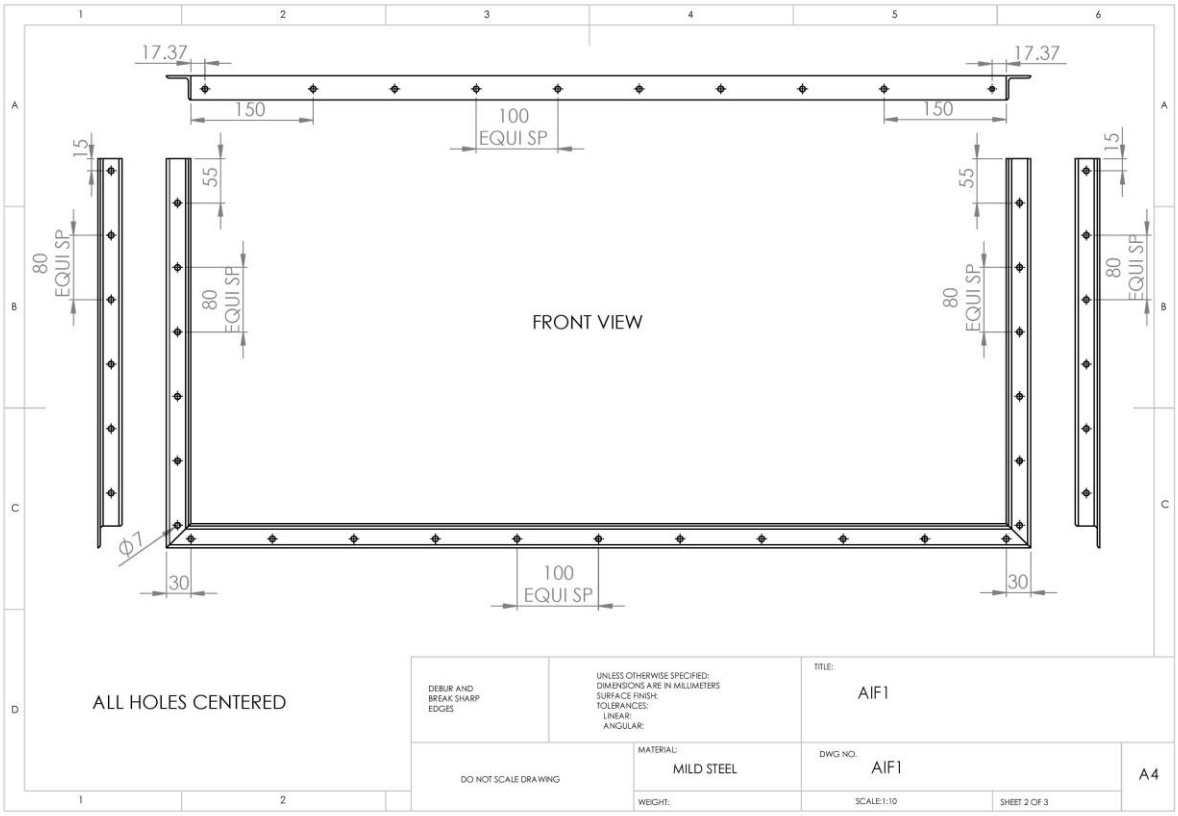
17.37
17.37
150
100
EQUI SP
150
15
55
80
EQUI SP
80
EQUI SP
FRONT VIEW
55
80
EQUI SP
15
80
EQUI SP
Φ7
30
100
EQUI SP
30
ALL HOLES CENTERED
DEBUR AND
BREAK SHARP
EDGES
UNLESS OTHERWISE SPECIFIED:
DIMENSIONS ARE IN MILLIMETERS
SURFACE FINISH:
TOLERANCES:
LINEAR:
ANGULAR:
TITLE:
AIF1
DO NOT SCALE DRAWING
MATERIAL:
MILD STEEL
DWG NO.
AIF1
A4
WEIGHT:
SCALE:1:10
SHEET 2 OF 3

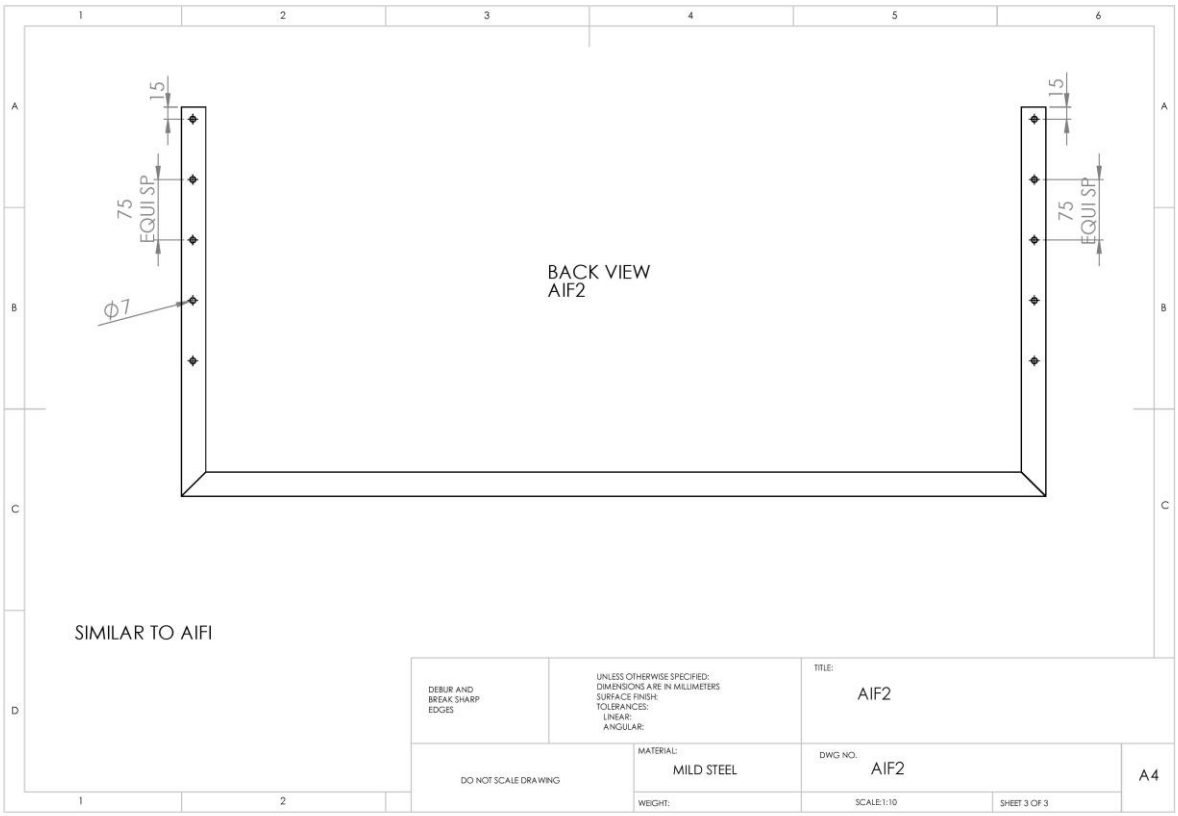
15
75
EQUI SP
Φ7
BACK VIEW
AIF2
15
75
EQUI SP
SIMILAR TO AIFI
DEBUR AND
BREAK SHARP
EDGES
UNLESS OTHERWISE SPECIFIED:
DIMENSIONS ARE IN MILLIMETERS
SURFACE FINISH:
TOLERANCES:
LINEAR:
ANGULAR:
TITLE:
AIF2
DO NOT SCALE DRAWING
MATERIAL:
MILD STEEL
DWG NO.
AIF2
A4
WEIGHT:
SCALE:1:10
SHEET 3 OF 3

Appendix C – Hardware specifications

Rubber mounts

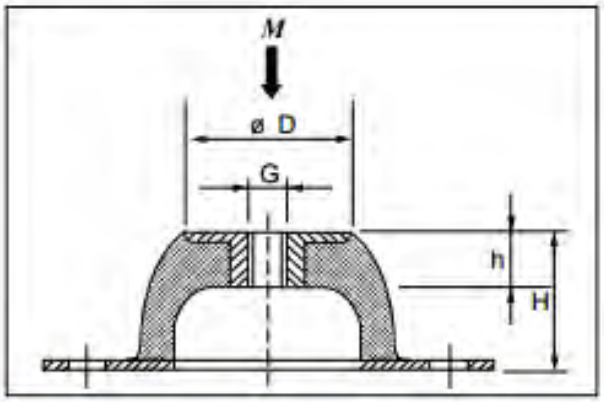

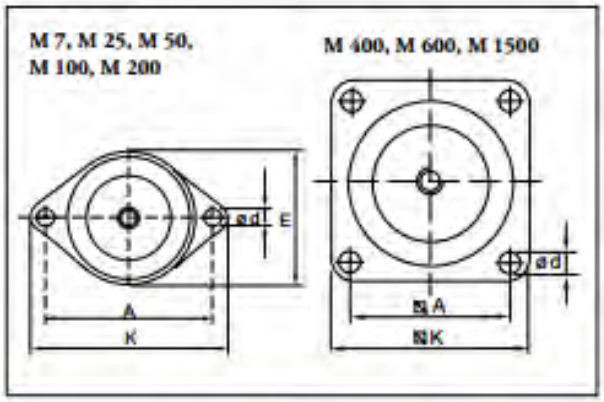

Type	Art.No. 40° IRH	Art.No. 60° IRH	Dimensions in mm D	E	A	K	H	h	d	G	Weight (kg)	M-Max (kg) 40° IRH	60° IRH
M 7	2255110	2255120	18	43	50	64	20	7	7.0	M 6	0.02	3.5	9
M 25	1861220	1861230	33	56	66	85	25	11	8.0	M 8	0.07	20	50
M 50	1861240	1861250	45	76	92	114	35	14	10.0	M 10	0.16	40	80
M 100	1861620	1861610	53	96	110	136	40	15	11.5	M 10	0.26	70	150
M 200	1861660	1861670	58	101	124	151	45	13	11.5	M 10	0.42	130	220
M 400	1861680	1861690	78		120	150	63	18	14.5	M 12	1.06	280	500
M 600	1533710	1533720	100		160	200	85	25	14.5	M 16	2.35	380	750
M 1500	1533730	1533740	186		250	310	160	43	18.0	M 24	9.43	1400	2500

4 poles Three-phase electric vibrators - 1500/1800 rpm

DESCRIPTION			MECHANICAL SPECIFICATIONS						ELECTRICAL SPEC.				DIMENSIONAL SPECIFICATIONS																
Code	Type	Size	STATIC MOMENT		CENTRIFUGAL FORCE				MAX. INPUT POWER (W)		MAX. INPUT CURRENT (A)		Weight (kg.)		Ref	Fixing distances					Fixing holes									
			kgmm		kg.f		kN				400V	460V				A	B	C	D	E	ØF	N°	G	H	I	L	M	N	O	Cable gland
			50Hz	60Hz	50Hz	60Hz	50Hz	60Hz	50Hz	60Hz	50Hz	60Hz	50Hz	60Hz															
V4000	VV03B/4	BA	14,0	11,6	35	42	0,343	0,412	80	90	0,20	0,19	6,0	6,0	2	62-74	106	216	125	30,5	9	4	24	23	93	154	129	64	50	PG13,5
V4001	VV05B/4	BA	32,0	22,1	80	80	0,785	0,785	80	90	0,20	0,19	6,6	6,4	2	62-74	106	216	125	30,5	9	4	24	23	93	154	129	64	50	PG13,5
V4002	VV10B/4	CA	87,0	60,8	220	220	2,16	2,16	160	160	0,38	0,38	12,5	11,5	2	90	125	295	152	28,5	13	4	28	30	93	178	144	73	80	PG13,5
V4003	VV20B/4	DA	167	116	420	420	4,12	4,12	280	330	0,57	0,57	19	18	2	105	140	340	167	32	13	4	28,5	30	111	204	163	80	96	PG16
V4004	VV30B/4	EA	298	215	750	780	7,36	7,65	500	620	0,88	0,93	28	26	2	120	170	376	205	38	17	4	40	33	111	214,5	191	91,5	97	PG16
V4005	VV35B/4	GA	437	276	1100	1000	10,8	9,81	520	640	0,90	0,90	45,5	41	2	120	170	436	210	60	17	4	22	47,5	111	243	223	115,5	118	PG16
V4006	VV38B/4	HA	556	387	1400	1400	13,7	13,7	850	1000	1,37	1,43	55	52	2	140	190	438	230	72	17	4	25	45	111	257	241	124,5	103	PG16
V4007	VV40B/4	IA	714	483	1800	1750	17,7	17,2	1100	1200	1,91	1,83	61	57	2	140	190	486	230	72	17	4	25	45	111	257	241	124,5	127	PG16
V4016	VV41B/4	IA	833	568	2100	2050	20,6	20,1	1300	1400	2,40	2,20	72	70	2	140	190	557	230	72	17	4	25	45	111	257	241	124,5	162,5	PG16
V4008	VV50B/4	LA	992	691	2500	2500	24,5	24,5	1500	1600	3,00	2,90	85	79	2	155	225	522	275	79,5	22	4	28	55	111	283	271	140	129,5	PG16
V4017	VV53B/4	LA	1250	870	3150	3150	30,9	30,9	1800	1900	3,60	3,30	95	92	2	155	225	600	275	79,5	22	4	28	55	111	283	271	140	168,5	PG16
V4009	VV55B/4	MA	1508	1050	3800	3800	37,3	37,3	2100	2400	3,80	3,70	118	113	2	155	255	590	310	103,5	23,5	4	30	60	155	335	309	160	140	PG16
V4018	VV57B/4	MA	1746	1188	4400	4300	43,2	42,2	2400	2700	4,60	4,40	125	120	2	155	255	658	310	103,5	23,5	4	30	60	155	335	309	160	174	PG21
V4010	VV60B/4	NA	1984	1367	5000	4950	49,1	48,6	3400	3200	5,70	4,80	174	166	2	180	280	638	340	106	26	4	30	65	155	369	336	173	154	PG21
V4011	VV67B/4	OA	2619	1823	6600	6600	64,7	64,7	5700	5700	10,0	8,60	212	200	2	200	320	662	390	111	28	4	32	75	155	381	384	189	151	PG21
V4012	VV71B/4	PA	3175	2210	8200	8200	80,4	80,4	6600	7600	11,0	10,9	228	213	2	200	320	624	392	111	28	4	35	75	155	403	402	199,5	132	PG21
V4013	VV81B/4	QA	3373	2486	8500	9000	83,4	88,3	7100	8000	11,5	11,3	319	305	3	125	380	862	460	70	39	6	35	95	170	434,5	439	215	230	PG21

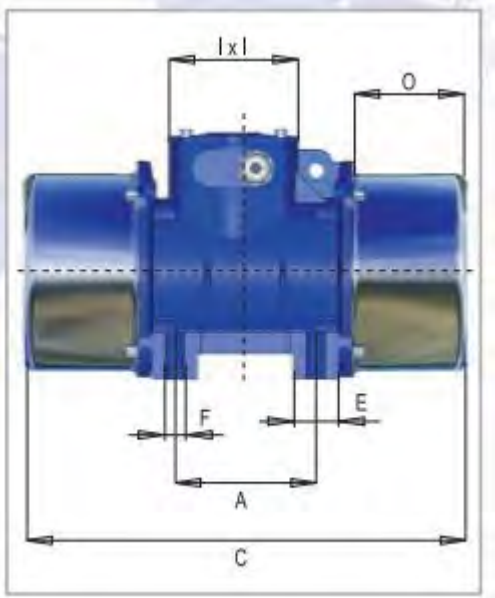

Exciter motor specifications

Appendix D – Contact details

Sieve supplier contact details

Declaration

This is to declare that I, Annette L Combrink, accredited language editor and translator of the South African Translators' Institute, have language-edited the dissertation by

J Bloem (22113657)

with the title

Design optimization and experimental evaluation of a grain vibration screen

Prof Annette L Combrink
Accredited translator and language editor
South African Translators' Institute
Membership No. 1000356
Date: 12 November 2015